THE UNIVERSITY OF HULL

New catalysts bearing chelate ligands for ring opening polymerisation studies

being a thesis submitted for the Degree of

Doctor of Philosophy

at the University of Hull

by

Xin Zhang

BSc. MSc.

Supervised by Professor Carl Redshaw

March 2023

Acknowledgements

I finally finished my final thesis! I would like to express my deepest gratitude to my supervisor, Professor Carl Redshaw, for his support, guidance and encouragement during my doctoral journey. I really appreciate the opportunity to learn from him, gaining not only experimental knowledge but also creative insights. I acknowledge the studentship from University of Hull that allows me to pursue the research.

I would like to appreciate Dr. Tim Prior for the support of the X-ray crystallography; Dr. Rob Lewis for the support of the NMR; Mr Dean A Moore for the support of the Mass spectrometry and GPC. I also thank the EPSRC National Crystallographic Service at Southampton for data collection. Moreover, I would like to thank my colleagues: Abdullah F. Alshamrani, Tian Xing, Kuiyuan Wang, Yi Gong and Orlando Santoro, for their assistance and support throughout the course of this work. I am grateful for the collegial and amicable environment.

Lastly, I would like to acknowledge the support and encouragement of my parents, Fukui Zhang and Gaihua Wu, and friends, who provided me with unwavering support and a listening ear throughout this journey.

Publications and Conferences

O. Santoro, X. Zhang and C. Redshaw, *Catalysts*, 2020, **10**, 800. https://doi.org/10.3390/catal10070800 (chapter 1)

X. Zhang, K. Chen, M. Chicoma, K. Goins, T. Prior, T. Nile and C. Redshaw, *Catalysts*, 2021, **11**, 1090. https://doi.org/10.3390/catal11091090 (chapter 2)

X. Zhang, T. J. Prior and C. Redshaw, *New J. Chem*, 2022, **46**, 14146-14154. https://doi.org/10.1039/D2NJ02527B (chapter 3)

X. Zhang, T. J. Prior, K. Chen, O. Santoro and C. Redshaw, *Catalysts*, 2022, **12**, 935. https://doi.org/10.3390/catal12090935 (chapter 4)

X. Zhang and C. Redshaw, Global Research and Innovation in Plastics Sustainability, 16th-18th March 2021, UK, Poster.

Abstract

Chapter 1: The accumulation of traditional polymer (plastic) pollution has led people to start looking for biodegradable plastics as alternatives. This first chapter provides information on the concept and the development of biodegradable polymers. It also highlights the development of efficient catalysts based on Sn/Al/Ti/Zn metals for producing biodegradable aliphatic polyester and the key ring-opening polymerization mechanisms, including coordination-insertion, cationic, anionic mechanisms. Moreover, this chapter delivers a comprehensive review of metal complexes bearing 2,2'-diphenylglycine or benzilic acid ligands, with particular focus on the binding modes of $Ph_2C(X)(CO_2H)$ ($X = NH_2$, OH) in these complexes. These complexes' application as catalysts for the ring-opening polymerisation of cyclic esters is summarised. Lastly, the characterisation methods used in this work are discussed.

Chapter 2: Here, the Schiff-base compounds 2,4-di-*tert*-butyl-6-(((3,4,5-trimethoxyphenyl)imino)methyl)phenol (L^1H), 2,4-di-*tert*-butyl-6-(((2,4,6-trimethoxyphenyl)imino)methyl)phenol (L^2H), 2,4-di-*tert*-butyl-6-(((2,4-dimethoxyphenyl)imino)methyl)phenol) (L^3H) derived from anilines bearing methoxy substituents have been employed in the preparation of alkylaluminium and zinc complexes. Molecular structure determinations reveal mono-chelate aluminium complexes of the type $[Al(L^n)(Me)_2]$ (L^1, **1**; L^2, **2;** L^3**, 3**), and bis(chelate) complexes for zinc, namely $[Zn(L^n)_2]$ (L^1, **5**; L^2, **6;** L^3**, 7**). All complexes have significant activity at 50 °C and higher activity at 100 °C for the ring-opening polymerisation (ROP) of ε-caprolactone (ε-CL) with good control over the molar mass distribution ($M_w/M_n < 2$) and molecular weight. Complex **1** was found to be the most active catalyst, achieving 99% conversion after 18 h at 50 °C and giving polycaprolactone with high molecular weight; results are compared against aniline-derived (*i.e.* non-methoxy containing) complexes (**4** and **8**). Aluminium or zinc complexes derived from L^1 exhibit higher activity as compared with complexes derived from L^2 and L^3. Complex **1** was also tested as an initiator for the copolymerisation of ε-CL and glycolide (GL). The CL-GL copolymers have various microstructures depending on the feed ratio. The crosslinker 4,4'-bioxepane-7,7'-dione was used in the polymerisation with ε-CL using **1**, and well-defined cross-linked PCL was afforded high molecular weight.

Chapter 3: This chapter focuses on niobium and tantalum complexes. In particular, reaction of benzilic acid, $Ph_2C(OH)(CO_2H)$ (L^4H_2), with equimolar amounts of $M(OR)_5$ (M = Nb, Ta) led, following work-up, to the tetranuclear complexes $[Nb_4(OEt)_8(L^4)_4(\mu\text{-}O)_2]$ (**9**) or $[Ta_4(OEt)_8(L^4)_4(\mu\text{-}O)_2]\cdot0.5MeCN$ (**10**·0.5MeCN), respectively. Similar use of 2,2'-diphenylglycine (L^5H_3), $Ph_2C(NH_2)(CO_2H)$ (L^5H_3), led to the isolation of the dinuclear complexes $[Nb_2(OEt)_4(L^5H_2)_4(\mu\text{-}O)]\cdot2MeCN$ (**11**·2MeCN) or $[Ta_2(OEt)_4(L^5H_2)_4(\mu\text{-}O)]\cdot2.25MeCN$ (**12**·2.25MeCN). The molecular structures of complexes **9**-**12** are reported. These complexes have been screened for their potential to act as catalysts for the ROP of ε-CL and *rac*-lactide (*r*-LA), with or without benzyl alcohol (BnOH) present. In the case of ε-CL, complex **9** displayed the best activity with >99 % conversion at 100 °C, whilst **10** and **11** were inactive under the same conditions. All complexes show moderate activities towards the ROP of *r*-LA at 160 °C, with **9**-**11** producing heterotactic enriched PLA while **12** afforded isotactic enriched PLA.

Chapter 4: The reactions of the titanium alkoxides $[Ti(OR)_4]$ (R = Me, *n*Pr, *i*Pr, *t*Bu) with the L^4H_2 or L^5H_3 have been investigated. Variation of the reaction stoichiometry allows for the isolation of mono-, bi-, tri or tetra-metallic products, the structures of which have been determined by X-ray crystallography. The ability of the resulting complexes to act as catalysts for the ROP of ε-CL and *r*-LA has been investigated. In the case of ε-CL, all catalysts except that derived from [Ti(O*n*Pr)$_4$] and L^5H_3 *i.e.* **19**, exhibited an induction period of between 60 and 285 min., with **19** exhibiting the best performance (>99% conversion within 6 min.). The PCL products are moderate to high molecular weight polymers. For *r*-LA, there was no induction period, and systems **13**, **15**, **16** and **19** afforded conversions of *ca*. 90% or more, with **16** exhibiting the fastest kinetics. The molecular weights for the PLA are somewhat higher than those of the PCL, with both cyclic and linear PLA products (end groups of OR/OH) identified. Comparative studies *versus* the $[Ti(OR)_4]$ starting materials were conducted and although high conversions were achieved, the control was poor.

Chapter 5: The better performing catalysts from chapters 2-4 are selected and compared with other reported catalysts with similar ligand systems. The evaluation of these catalysts is based on the ROP of ε-CL. Various factors, including polymerisation rate, molecular weight and distribution of polymer products, catalyst efficiency, and catalyst stability have been considered.

Contents

Lists of Figures

Lists of Tables

Abbreviations

β-PL	β-Propiolactone
γ-BL	γ-Butyrolactone
δ-VL	δ-Valerolactone
ε-CL	ε-Caprolactone
L-LA	*L*-Lactide
D-LA	*D*-Lactide
meso-LA	meso-Lactide
r-LA	racemic-Lactide
GL	Glycolide
PP	Polypropylene
PBAT	Poly(butylene-adipate-*co*-terephthalate)
PHAs	Polyhydroxyalkanoates
PDO	Poly(p-dioxanone)
PBS	Polybutylene succinate
PGA	Poly(glycolide acid)
PLA	Poly(lactide acid)
PCL	Poly(ε-caprolactone)
BnOH	Benzyl alcohol
$AlMe_3$	Trimethyl aluminium
$ZnEt_2$	Diethyl zinc
$Ti(OR)_4$	Titanium alkoxides

OMe	Methoxide
O*n*-Pr	*n*-Propoxide
O*i*-Pr	*iso*-Propoxide
O*t*-Bu	*tert*-Butoxide
Dpg	2,2’-Diphenylglycine
Benzilic acid	Diphenylglycolic acid
MeCN	Acetonitrile
THF	Tetrahydrofuran
CaH_2	Calcium hydride
BOD	4,4’-Bioxepane-7,7’-dione
FI	Phenoxyimine
ROP	Ring-opening polymerisation
NMR	Nuclear magnetic resonance
MS	Mass spectrometry
MALDI-TOF	Matrix-assisted laser desorption/ionization-time of flight
EI	Electron impact ionisation
ESI	Electrospray ionisation
SEC	Size exclusion chromatography
GPC	Gel permeation chromatography
IR	Infrared
M_n	Number-average molecular weight
M_w	Weight-average molecular weight
PDI	Polydispersity

s	Singlet
d	Doublet
δ	Chemical shift
J	coupling constant
k	Kappa convention
P_m	Probability of meso linkages
P_r	Probability of racemic linkages
P_i	Probability of *isi* dyad
k_obs	Observed rate constant
k_app	Apparent rate constant
Å	Ångstrom
°C	degrees Celsius
w	Weak
m	Medium
s	Strong

Chapter 1. Introduction

1.1 The status of biodegradable polymers

Biodegradable polymers are defined as polymers that are able to decompose into carbon dioxide, water, and biomass when they are placed in the nature environment.[1] Whereas, for non-degradable commodity polymers, such as polypropylene (PP) fabrics, the half-life in benign environments could be 500 years or more according to a study by the Federal Highway Administration (FHWA).

In January 2020, China's government released its new vision for a nationwide ban or restriction on the production or sale of single-use plastic bags and cutlery.[2] Moreover, the European Union launched "A European Strategy for Plastics in a Circular Economy" in 2018 (European Commission, 2018). One of the commitments is "by 2030, all plastic packaging placed on the EU market is either reusable or can be recycled in a cost-effective manner" (European Commission, 2018). The search for strategies and measures that boost the development of biodegradable polymers as alternatives to most traditional polymers is now very topical. Therefore, the market for biodegradable plastics has boomed during the last two decades. The total biodegradable polymers production globally in 2022 was around 1.1 million tonnes and is expected to increase to over 3.5 million in 2027.[3]

Biodegradable polymers are generally divided into two groups, biologically derived polymers and synthetic polymers. The common biologically derived polymers include starch, cellulose, chitosan, polylactic acid (PLA), and polyhydroxyalkanoates (PHAs) (Figure 1-1 (a-d, f)).[4] In industrial production, PLA and PHAs are produced by bacterial fermentation of sugars and lipids.[5] The other type, synthetic polymers, includes poly(glycolic acid) (PGA), poly(lactic acid) (PLA), poly(ε-caprolactone) (PCL), poly(*p*-dioxanone) (PDO), polybutylene succinate (PBS), poly(butylene-adipate-*co*-terephthalate) (PBAT), tyrosine-derived poly(amide carbonates), etc. It is noteworthy that PLA is produced commercially by both fermentation and a synthetic polymerisation method. Among the families of synthetic biodegradable polymers, polyesters (Figure 1-1 (d-k)) have attracted more attention from the industry because of their excellent properties for processing which are like conventional plastics. For example, PLA can be processed by all the methods used for processing and it is possible to produce film, fibre, packaging for food products and medical implants material.[6]

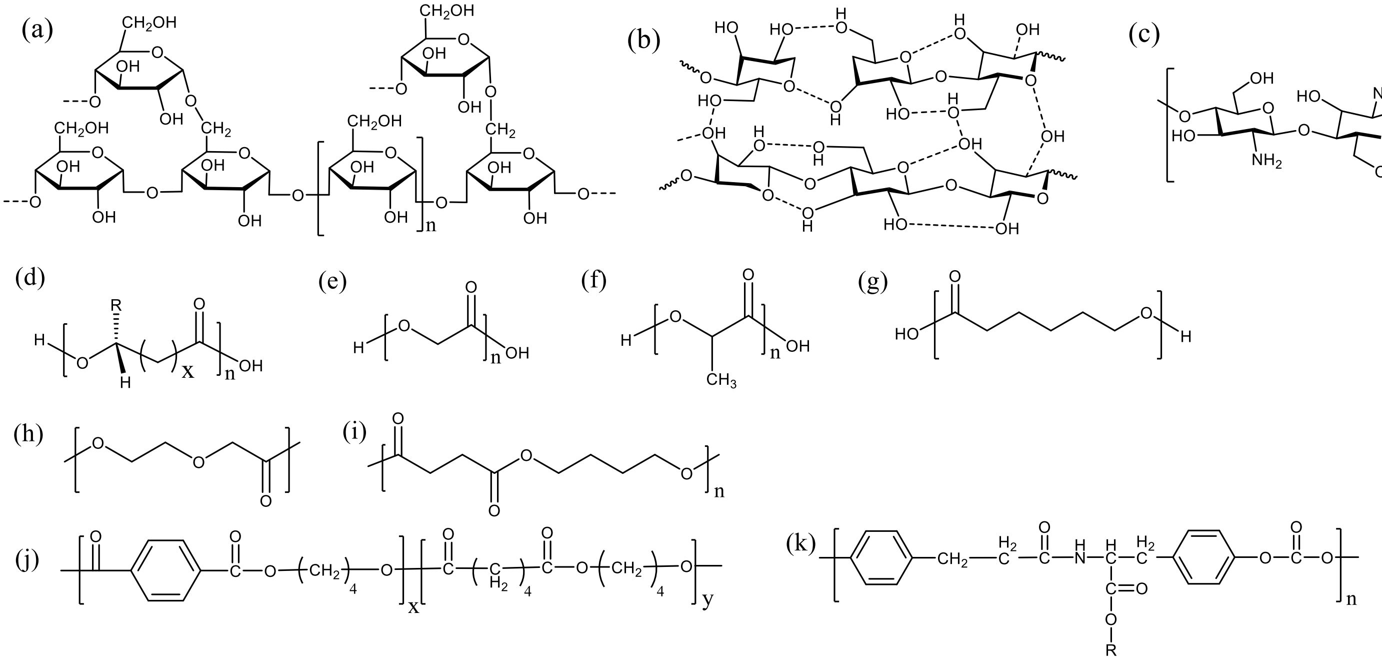

Figure 1-1. Chemical structure of (a) Starch; (b) Cellulose; (c) Chitosan; (d) PHAs; (e) PGA; (f) PLA; (g) PCL; (h) PDO;(i) PBS; (j) PBAT; (k) tyrosine-derived poly(amide carbonates).

1.2 Chemical synthesis of biodegradable aliphatic polyester

Chemical synthesis methods offer unparalleled advantages over fermentation methods for producing biodegradable polyesters. Through chemical polymerisation, large-scale production of biodegradable polyester can be achieved easily and efficiently, with greater control over molecular weight and crystallinity. Moreover, chemical synthesis methods could achieve the chemical modifications of biodegradable polyesters.[7] Currently, commercial biodegradable aliphatic polyesters, such as PCL, PLA, PGA, and PBS, are predominantly produced via chemical polymerisation.[8] Also, aliphatic polyesters appear as a class of promising materials in the packaging and medical implants industry have been extensively investigated. Therefore, this chapter aims to report on recent developments in the synthesis of biodegradable aliphatic polyesters. Furthermore, the more widely used metal-based catalysts are also introduced herein.

There are two distinct mechanisms for synthesising aliphatic polyesters: (i) the polycondensation, and (ii) the ring-opening polymerisation (ROP).[9]

1.2.1 Condensation polymerisation approach

The polycondensation aliphatic polyesters are synthesised by using equimolar amounts of aliphatic diacids with diols or hydroxy-acids directly, and catalysts in an organic solvent (Figure 1-2). To obtain high molecular weight polyesters, this reaction normally requires high temperatures, long reaction times, and high boiling point solvents.[10] Besides, the remaining water must be removed under high vacuum from the polymerisation medium to increase the conversion and the molecular weight. For example, Mitsui in Japan followed the condensation polymerisation approach using a tin-containing species as the catalyst to produce PLA. The flow diagram is shown in Figure 1-3. This process is quite costly and tedious. Also, high temperature will lead to discolouring of the final product. Although this approach has been known for a long time, its widespread use remains limited.[11]

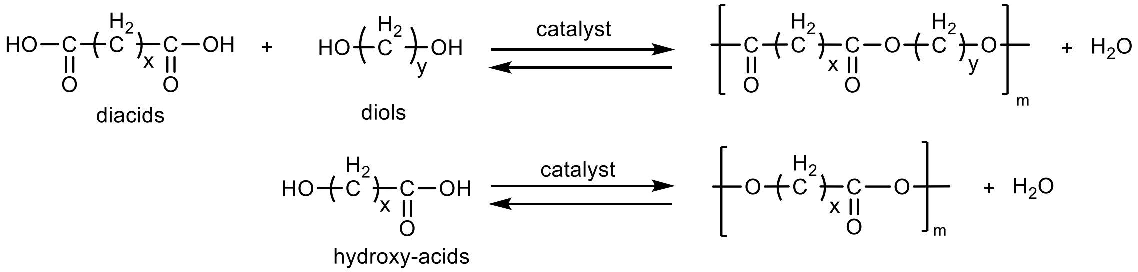

Figure 1-2. Preparation of aliphatic polyesters by polycondensation.

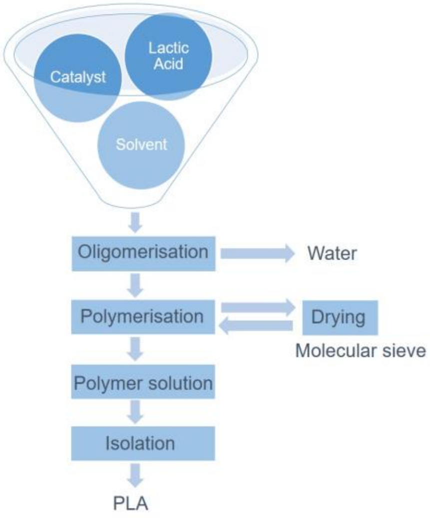

Figure 1-3. Flow diagram of the direct process when using polycondensation for lactic acid. [10]

1.2.2 Ring-opening polymerisation approach

The ring-opening polymerisation (ROP) of lactones and cyclic diesters is an alternative method to produce aliphatic polyesters (Figures 1-4), which has been successfully applied to produce high molecular weight polyesters under mild conditions in both academia and industry.[12]

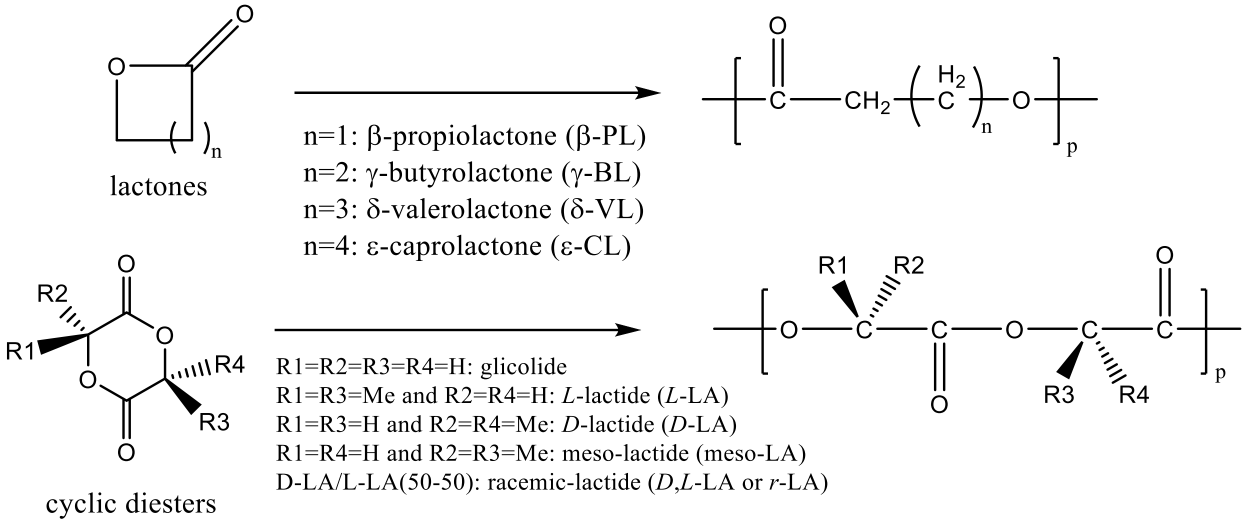

Figure 1-4. Ring-opening polymerisation of unsubstituted lactones and cyclic diesters.

Based on the type of metal catalysts used for the ROP reaction, the polymerisation mechanisms can be divided into four categories, coordination-insertion polymerisation, cationic polymerisation, anionic polymerisation, and monomer-activated ROP.[13] The following sections will report some representative metal-based catalysts used for the ROP reaction and various potential mechanisms are explained.

Coordination-Insertion Polymerisation

In 1962, Cherdron *et al.*[14] demonstrated the effectiveness of some Lewis acids, such as triethylaluminium/water (molar ratio of $[Al(C_2H_5)_3]/[H_2O] = 1.5$) or diethylaluminium ethoxide, as initiators for lactone polymerisation. This successful discovery promoted the investigation of other metal alkoxides[15] and metal carboxylates[16] used to initiate ROP of lactones and cyclic diesters, with numerous catalysts reported to date. Discrete metal catalysts are comprised of a Lewis acidic metal, an ancillary ligand, and a nucleophile as the initiating group.[17] The nucleophile is typically an alkoxide, alkyl, amido, or halide group bonded to the metal centre.[18,19] In 1971, Dittrich and Schulz [20] first proposed the coordination-insertion mechanism for cyclic ester polymerisation, which is the more prevalent mechanism invoked in metal-mediated for lactide polymerisation.[17] As shown in Figures 1-5, two major steps are involved. In the initial step, the electron rich carbonyl moiety of the lactide (electron pair donor) temporarily coordinates to the Lewis acidic metal centre (electron pair acceptor) of the metal alkoxide, which activates the carbonyl group towards nucleophilic attack and ring-opening; secondly, the alkoxide group performs a nucleophilic attack at the lactide carbonyl carbon. The acyl-oxygen bond of the lactide is broken (ring-opening) and simultaneously inserts into the metal alkoxide bond via nucleophilic attack, then a new metal-alkoxide bond forms. The propagating species will continuously insert lactide monomers. Finally, termination of the polymerisation reaction is performed by using a protic source such as water or alcohol.

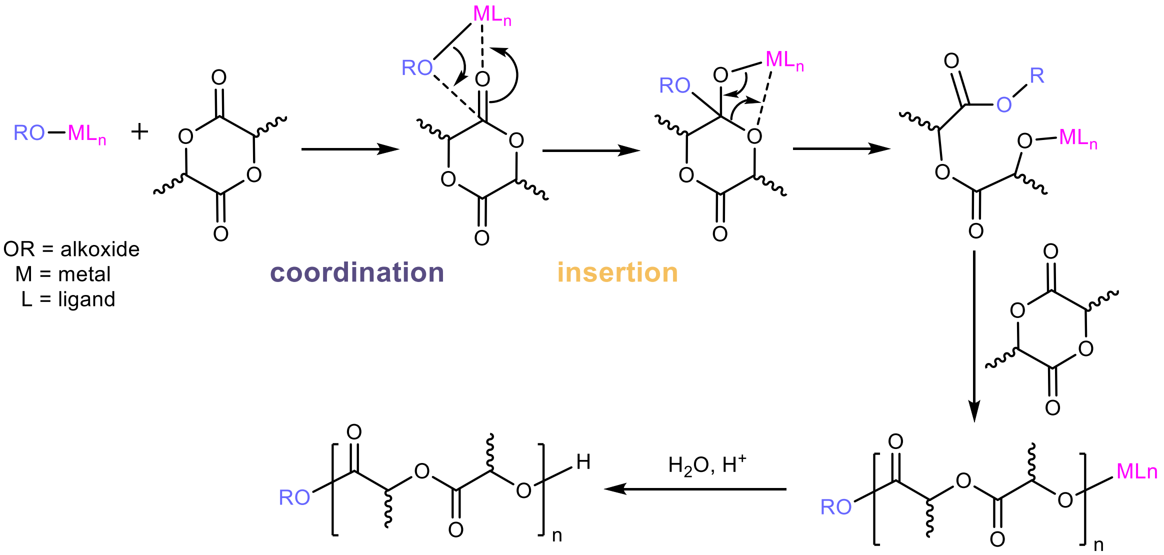

Figure 1-5. The speculated coordination-insertion mechanism in the ROP of lactide.[21]

The most popular Lewis acid catalyst for ROP of aliphatic polyesters is tin(II) bis-(2-ethylhexanoate) also referred as tin octoate.[22] For the metal centre of tin octoate, its electronic configuration is $5s^2 4d^{10}$, containing free *p*- orbitals. Typical Lewis acid metal catalysts most likely coordinate through unoccupied *p*, *d* or *f* orbitals with the carbonyl oxygen atom of the monomer.[23] For the nucleophile part of tin octoate, carboxylates exhibit lower nucleophilicity compared to alkoxides and act more like a catalyst rather than an initiator. As a result, tin octoate is often used alongside an active hydrogen compound (alcohol, or water) as a co-initiator.[13] It is generally accepted that tin octoate is converted into a tin(II) alkoxide when adding protic reagents in the initiation step and acts as the actual initiator (Figure 1-6).[21]

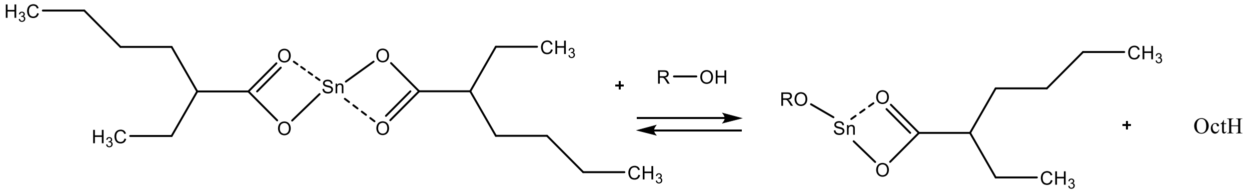

Figure 1-6. The formation of initiator when adding protic reagents to tin octoate.

One reason that tin octoate is the most used catalyst in the industry is because of its outstanding reactivity and the ability to produce high molecular weight polymers. Purnama *et al.*[24] investigated *D*-LA polymerisation using various catalysts under melt conditions (200 °C). The order of number molecular weight (M_n), molecular weight distribution, and conversion for the catalysts studied was $Sn(oct)_2$ (M_n = 56,979) > $La(OiPr)_3$ (M_n = 37,219) > $Al(OiPr)_3$ (M_n =32,365) > $Y_5O(OiPr)_{13}$ (M_n = 12,712). The results revealed that $Sn(oct)_2$ is a highly reactive catalyst and produces higher molecular weight polymer with good conversion. However, the molecular weight distribution of PDLA using $Sn(oct)_2$ is 1.75 which shows poor control for the polymerisation.

The tremendous growth in popularity of using aluminium alkoxides as initiators for ROP to synthesise aliphatic polyester has been driven by the demand of finding catalysts that can advantageously replace the tin(IV) or tin(II) alkoxides that have poorer control of the chain growth.[25,26] $Al(OiPr)_3$ was the first example that has been reported can achieve perfect control of polymerisation for high molecular weight PLA.[27] The excellent polymerisation control means the molecular weight can be predicted or manipulated by simply adjusting the monomer to catalyst ratio. Although it has relatively low polymerisation rate compared with tin-based catalysts, this type of compound still has been extensively employed. For example, a series of aluminium alkoxide complexes supported by non-chiral or chiral half salen-type tridentate ligands have been synthesised and investigated for the ROP of *r*-LA.[28] Polymerisation was conducted using toluene as solvent at 70 °C or 100 °C. Using complex **2** and **rac-3** (Figure 1-7) at 70 °C afforded the highest conversion of PLA after 96 h (100% and 80%, separately), whereas when using complex **4**, the conversion was only 28%, even raising the temperature to 100 °C. However, the P_m (probability of a diad being meso) value of PDLLA initiated by complex **4** (Figure 1-7) was > 0.9. These results suggest that complex **4** can provide stereoregulated polymerisation of *r*-LA. It should be noted another prominent feature of aluminium complexes is to initiate stereoregular polymerisation of lactide. Similar results have been reported in other literature. [29-32]

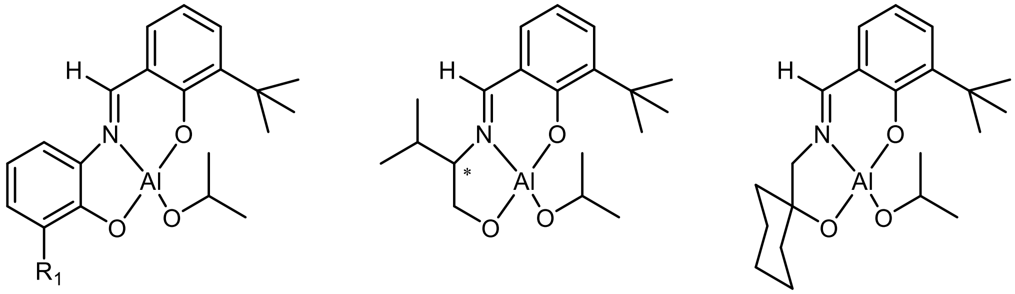

1: R_1 = H
2: R_1 = CH_3

(*rac*)-3

4

Figure 1-7. Schiff-base aluminium complexes of **1-4**.[28]

Titanium is nontoxic and its metal alkoxides have been reported as initiators for the ring-opening polymerisation. For instance, Meelua *et al*. [33] reported the bulk ROP of ε-CL using Ti(O*t*-Bu)$_4$ which was carried out under nitrogen at 120 °C for 72 h. Ti(O*t*-Bu)$_4$ gave high M_n (28,000) and conversion (92%). Compared with other metal alkoxide catalysts, the order of molecular weight and conversion of PCL follows the sequence Sn(O*t*-Bu)$_2$ > Ti(O*t*-Bu)$_4$ > Al(O*t*-Bu)$_3$ > Li(O*t*-Bu). This was thought to be due to the solubility of catalysts in the ε-CL monomer. Sn(O*t*-Bu)$_2$ and Ti(O*t*-Bu)$_4$ are completely soluble, whereas Al(O*t*-Bu)$_3$ is partially soluble and Li(O*t*-Bu) is completely insoluble. The results have shown the metal centre significantly affects the initiating efficiency. Cayuela *et al*. [34] using Ti(OPh)$_4$ and Ti(O*n*-Pr)$_4$ examined the influence of the nucleophile of some titanium alkoxides on the bulk ROP of ε-CL initiated by titanium derivatives. The apparent polymerisation rate (K_{app}) of Ti(O*n*-Pr)$_4$ is two times faster than Ti(OPh)$_4$. The superior reactivity of the catalyst Ti(O*n*-Pr)$_4$ compared to Ti(OPh)$_4$ is attributed to the increased nucleophilicity of the O*n*-Pr group *versus* the OPh group, which accelerates the nucleophilic attack. The successful use of titanium alkoxide initiators for the ROP of lactone under solvent-free conditions has raised industrial interest. It is noteworthy that melting polymerisation is the most common method to synthesis aliphatic polyesters with high molecular weight.

Gregson *et al*. [35] synthesised a family of bis(*iso*-propoxide) titanium (IV) complexes supported by tetradentate Schiff base (salen) ligands (shown as Figure 1-8). The influence of substituents attached to the phenoxy donors of the salen ligand on the ROP of *r*-LA was studied. The ROP of *r*-LA was carried out at 70 °C under nitrogen and toluene was used as solvent. The order of *r*-LA conversion after 24 h by using different initiators follows the sequence: *t*Bu-salen-OMe > *t*Bu-salen-H > *t*Bu-salen-*t*Bu > *t*Bu-salen-I > *t*Bu-salen-Cl. OMe is a strongly electron-donating group at the *para* position of the salen aryl rings. *t*Bu and H are weakly electron donating groups, whereas, –I and –Cl are electron withdrawing groups; –Cl is a stronger electron withdrawing group than –I. The results suggested the electron withdrawing substituents on the salen ligand have a detrimental influence, while the electron donating alkoxy groups achieved the highest conversion.

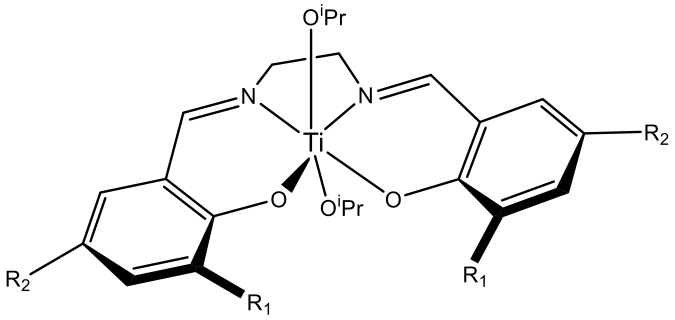

R_1 = *t*Bu, R_2 = OMe (*t*Bu-salen-OMe)
R_1 = *t*Bu, R_2 = H (*t*Bu-salen-H)
R_1 = *t*Bu, R_2 = *t*Bu (*t*Bu-salen-*t*Bu)
R_1 = *t*Bu, R_2 = I (*t*Bu-salen-I)
R_1 = *t*Bu, R_2 = Cl (*t*Bu-salen-Cl)

Figure 1-8. Proposed structures of the titanium initiators in solution.

Despite the nontoxicity and the decent performance of the titanium alkoxide as the Lewis acidic metal initiator for ROP, surprisingly not much attention has been paid to titanium initiators compared with Al, Zn or Sn (Figure 1-9). Indeed, there is significant potential for further investigation of Ti based catalysts for ROP of lactones and lactides.

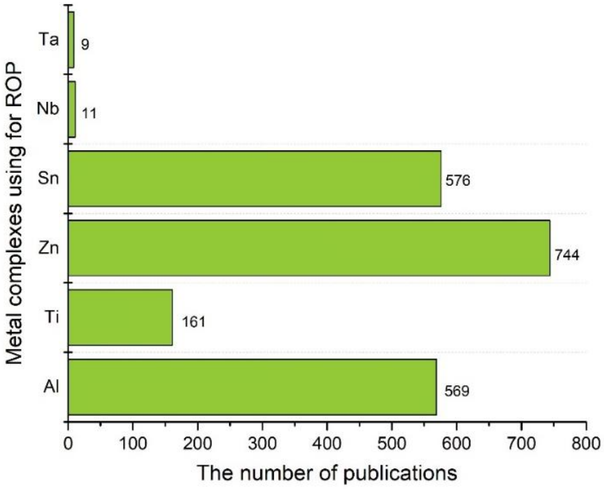

Figure 1-9. The number of publications about ROP by different metal initiators.[36]

Zinc is a divalent metal and the coordination number can be four, five or six. The electronic configuration of zinc is $3d^{10}4s^2$.[19] Within the same family, zinc complexes are intrinsically less active.[37] Zinc catalysts have been extensively exploited in the ROP chemistry, largely attributed to their biocompatibility and low cost.[38] From previous content, it is known that the ligand design is crucial to control the ROP activity of metal initiators supported by ancillary ligands. Monoanionic phenolate ligands containing nitrogen donors (Figures 1-10) have been commonly used in the synthesis of zinc complexes.[39] Very promising results have also been reported in polymerisation catalysis.

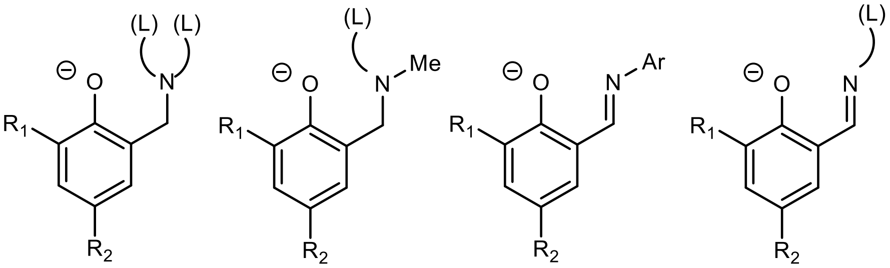

Figure 1-10. Chemical structures of phenoxy-amines or phenoxy-imines ligands.[39]

Williams *et al*.[38] reported a type of Zn(II) alkoxides complex bearing 2,4-di-*tert*-butyl-6-{[(2'-dimethylaminoethyl)methylamino]methyl}phenolate) ligand (Figure 1-11 left). The X-ray crystal structure of this complex shows that in the solid state, the complex exists as a dimer bridged by two ethoxides, the Zn1-Zn2 distance is 3.0835 (6) Å (Figure 1-11 (right)). It was surprising that this zinc complex was highly active for the ROP of *r*-LA in CH_2Cl_2 at ambient temperature. For example, even with a [LA]/[catalyst] ratio of 1500, a 93% conversion was achieved within 18 minutes. The molecular weight of PLA was as large as 130 kg mol^{-1}. The polydispersity (PDI) is relatively narrow at 1.34.

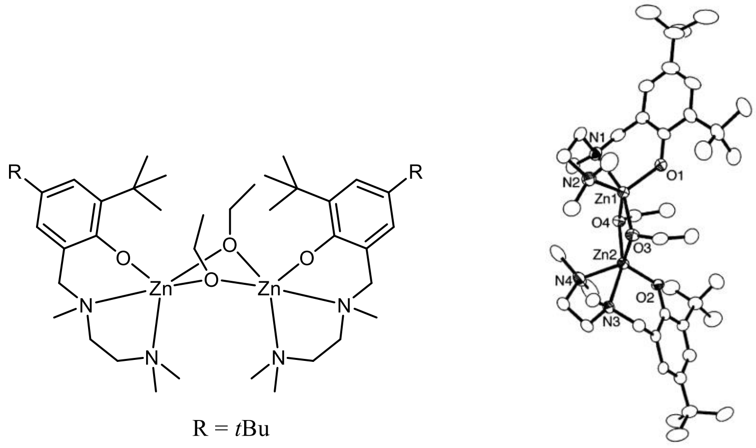

Figure 1-11. Structural formula of dimeric zinc alkoxides complex bearing 2,4-di-*tert*-butyl-6-{[(2'-dimethylaminoethyl)methylamino]methyl}phenolate) ligand (left); X-ray crystal structure of this complex (right).[37]

Poirier *et al.*[39] synthesised a centrosymmetric dimer ethyl-zinc complex bearing bis(morpholinomethyl)phenoxy ligand (Figure 1-12) for the large-scale immortal ROP of cyclic esters. This zinc complex was used in combination with *i*PrOH as a transfer agent for the immortal ROP of *L*-LA. It has been proved that this zinc-based complex is a highly active initiator for the ROP of *L*-LA, being able to convert up to 50,000 equiv. of monomer to PLA within 16 h at 60 ^{o}C with the [complex]/[*i*PrOH] molar ratio of 1/500.

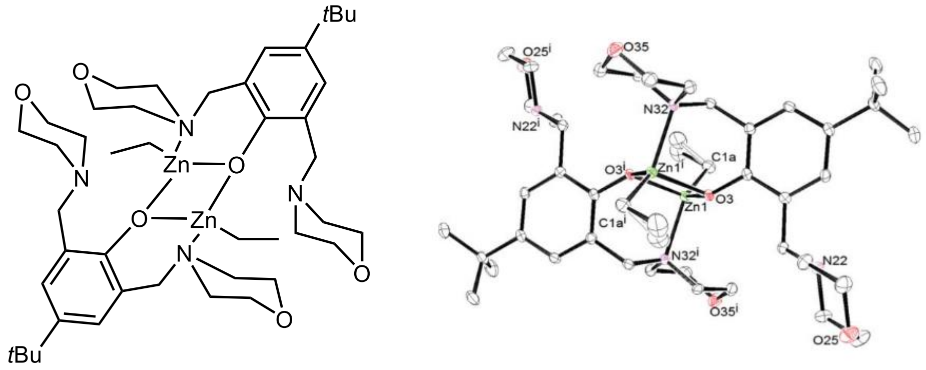

Figure 1-12. Dimeric ethyl-zinc (left); X-ray crystal structure of this zinc complex (right).[38]

Anionic Polymerisation

The ROP for lactides or lactones has also been reported in an anionic or coordinated anionic fashion. The effective initiators include alkali metals (*e.g.* Li, Na, K), alkali metal alkoxides, alkali metal hydroxides, alkali metal naphthalenide complexes with crown ethers, and alkaline earth metals, etc.[12] Anionic ROP takes place by the nucleophilic attack of a negatively charged initiator on the carbonyl carbon, resulting in the opening of the cyclic ring. The propagating species is negatively charged and counter-balance with a positive ion.[40,41] One interesting example of this research work is calcium hydride (CaH_2) which could act as an initiator for the ROP of ε-CL. It is common to use CaH_2 to dry ε-CL and distil it under reduced pressure before use. However, when increasing the temperature to boost the distillation, ε-CL started turning to solid which means polymerisation happened. Ca is alkaline earth metal which can promote an anionic-type polymerisation. The mechanism is possible like KH presented in Figure 1-13. The KH reacts with the monomer by addition to the carbonyl group or direct nucleophilic ring-opening in the acyl-oxygen position.[42] So many reports proved simple alkali salts give poorly controlled polymerisation affording low molecular weight polyesters with broad dispersities.[19] Both intra- and intermolecular transesterification reactions in anionic polymerisation have been observed.[12]

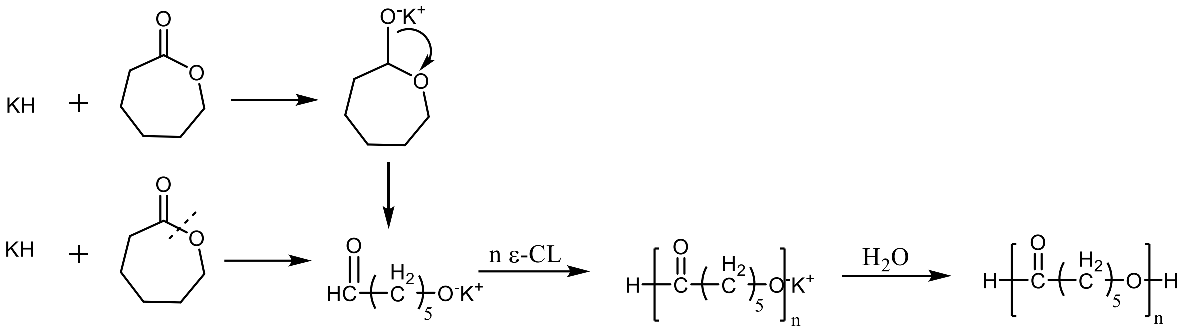

Figure 1-13. Proposed mechanism for anionic polymerisation of ε-CL initiated by KH.[42]

Cationic Polymerisation

Cationic ROP of lactides or lactones has been explored for a long time but its limited ability to regulate molecular parameters has resulted in a lack of popularity. The cationic initiators and catalysts include alkylating agents, acylating agents, Lewis acids, and organic Brønsted acids. Metal-based catalysts are rarely found successful in cationic polymerisation.[13] In 2006, Nomura *et al*.[43] reported an example of using scandium trifluoromethanesulfonate, Sc(OTf)$_3$, as an excellent catalyst to produce PCL with M_n = 260,000 and PDI =1.1 at 25 °C for 33 h in the presence of protic agent.[7]

1.3 Use of 2,2′-diphenylglycine and benzilic acid chelating ligands

1.3.1 Complexes derived from 2,2′-diphenylglycine or benzilic acid

The acid-containing ligands 2,2’-diphenylglycine (dpg) and diphenylglycolic acid (synonym: benzilic acid) have an identical structural moiety $Ph_2C(X)CO_2H$ (X= O^- or NH^-) (Figure 1-14) with multi-functional groups: carboxylate group and the amino group/hydroxy group. These multi-dentate ligand systems exhibit excellent coordinative flexibility. After searching the Cambridge Structural Database (CSD), it was found that 23 different metal ions are known to coordinate to dpg or benzilic acid (Figure 1-14). The binding modes of these ligands with metal ions are considerably different and include monodentate monoanion[44,45], monodentate bridging[46], bidentate monoanionic[47], bidentate dianion, bidentate bridging and also as a neutral molecule in the outer coordination sphere.[44]

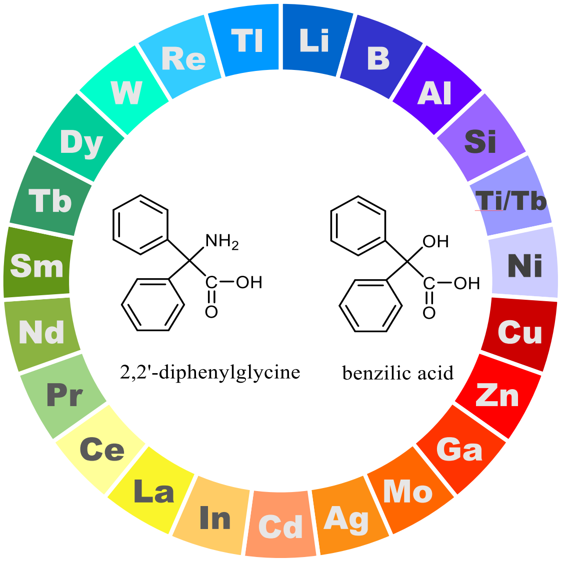

Figure 1-14. Chemical structures of dpg and benzilic acid; Metal ions that have been reported to coordinate with dpg or benzilic acid.

The functional groups of dpg or benzilic acid could also form intermolecular hydrogen bonds using oxygen or nitrogen atoms as donors. Furthermore, ligands bearing the moiety $Ph_2C(X)$ have proved to own the ability to promote highly crystalline samples.[48] On these grounds, the nature of the ligand allows the formation of supramolecular architectures.[44] A striking feature of the coordination chemistry of these "magic" acid ligands is that they allow the coordination of multiple metal ions in a great variety of arrangements. Given the merit of the $Ph_2C(X)$ containing ligand systems, Redshaw group has intensively investigated the reaction of different metal ions with these ligands. In this thesis, the use of dpg and benzilic acid chelating ligands with diverse metals and metalloids has been reviewed.

Monodentate coordination mode

For most complexes, $Ph_2C(X)$ acid ligands, their two donor groups, the carboxylate and hydroxyl/amino moieties, commonly act as bidentate chelating ligands.[49] By investigating the literature, the monodentate coordination mode of the $Ph_2C(X)$ acid ligands is frequently found in the mixed ligand system, especially when in the presence of *N*-chelating ancillary ligands such as 1,10-phenanthroline, imidazole and pyridine, etc. (Figure 1-15). For example, tris(pentafluorophenyl)boron(III) reacted with triethylamine and benzilic acid or dpg separately afforded similar mononuclear boron(III) complexes (Figure 1-15 (a) and (b)).[42] B(III) centre being monodentate coordinated to the deprotonated carboxylate acid moiety through the C-O oxygen rather than through the C=O carbonyl group.[50] In both (a) and (b) complexes, intermolecular hydrogen bonds N–H···O=C or O–H···O=C were formed between the ammonium/ hydroxyl group and carbonyl group.

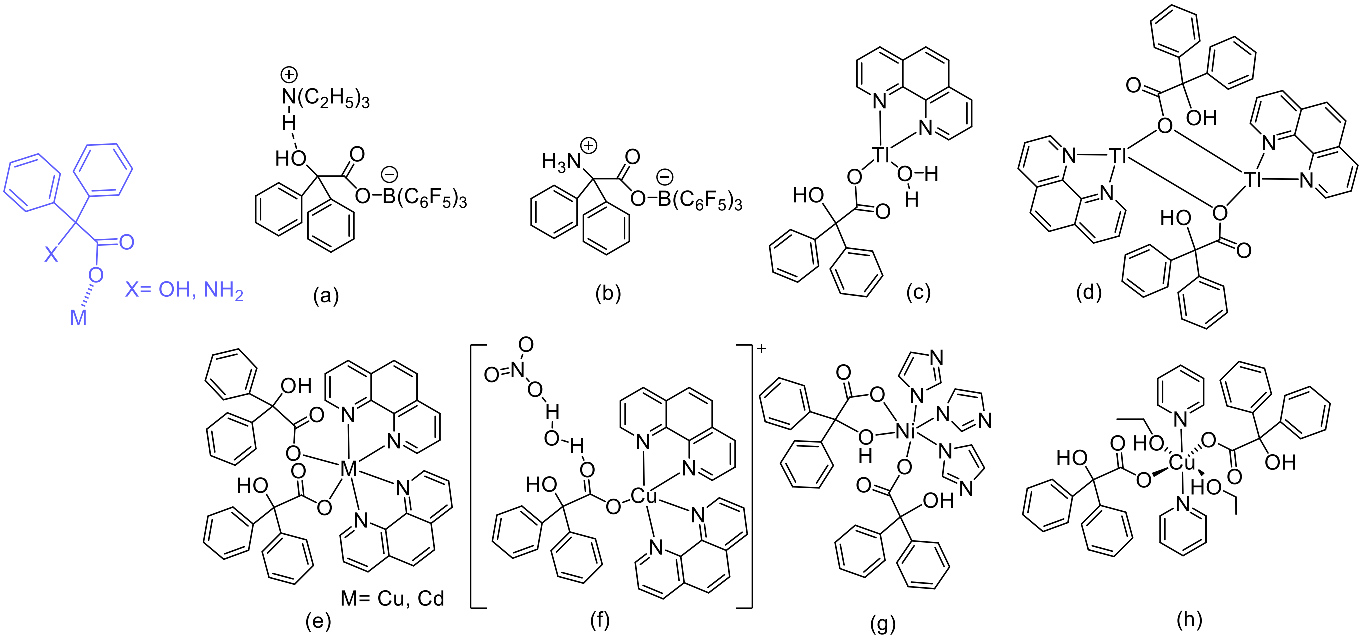

Figure 1-15. Monodentate $Ph_2C(X)$ acid ligands derived complexes (a-h).

For thallium metal ions, Halevas *et al*.[51] reported a neutral mononuclear complex that is illustrated in Figure 1-15 (c). The Tl(I) centre bounds to one carboxylate oxygen atom from a benzilato monodentate ligand, two nitrogen atoms from one 1,10-phenanthroline, and another oxygen atom from a neutral water molecule. In the same system, changing the stoichiometric ratio of $TlNO_3$, benzilic acid and 1,10-phenanthroline to 1:1:1, leads to the binuclear Tl(I) complex shown in Figure 1-15 (d). Each benzilato ligand provides bridging monodentate coordination mode that two Tl(I) ions are bridged through oxygen atom of carboxylate group. A similar reaction was conducted by Qiu *et al*.,[52] except that $TlNO_3$ was replaced by $CdCl_2\cdot 6H_2O$ or $Cu(NO_3)_2$. The Cu(II) or Cd(II) complexes have a mononuclear structure (Figure 1-15 (e)). The metal centre coordinates to two carboxylate oxygen atoms from two benzilato ligands and four nitrogen atoms from two bidentate 1,10-phenanthroline ligands. Complex (e) forms a 1D helical chain polymer structure through a hydrogen-bonds network and $\pi - \pi$ stacking interactions. It has been shown that the functional groups of benzilic acid play an important role in the formation of the supramolecular architecture. For complexes (f-h) [44,53,54], the presence of the mixed ligand imidazole or pyridine gives rise to a monodentate chelating fashion for benzilic acid.

Bidentate coordination mode

Three coordination modes have been observed in $Ph_2C(X)$ acid ligands that follow the bidentate coordination fashion. The first mode is when the metal ion chelates the ligands through carboxylato oxygen atom and the hydroxyl/amino group then forms five membered chelate ring. [55] Specifically, for complexes (a-f)[45,47,49,51,56] (Figure 1-16), the dpg or benzilic acid ligands are singly deprotonated at the acid. In most of their coordination compounds, dpg ligands are monoanionic, both hydrogen atoms were experimentally located on *N*, except complex (e) [57], one of the dpg ligands is dianionic chelating, where the hydrogens of the amino are lost, *i.e*. it is deprotonated. For complexes (e) and (f), the free carboxylato oxygen atom of the benzilato ligand is engaged in hydrogen bonding to two molecules of water and a neighbouring benzilato ligand. Because of such interactions, a two-dimensional crystal lattice was formed. For complexes (g-j)[45,58] (Figure 1-16), all the benzilato ligands were observed as bidentate doubly deprotonated benzilic acid ligands.

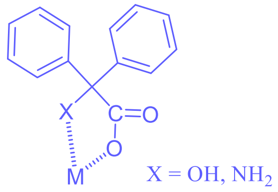

Bidentate coordination
singly deprotonated ligand

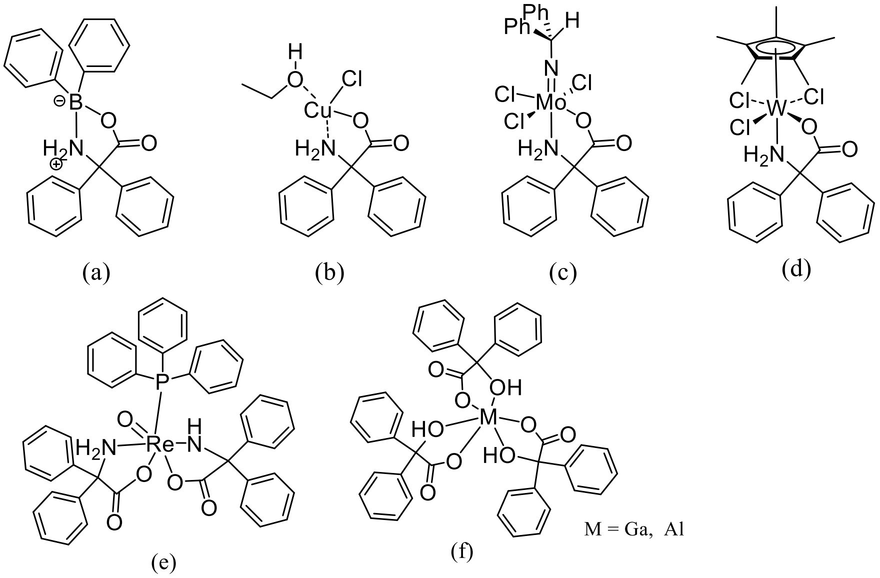

(a) (b) (c) (d)

(e) (f)

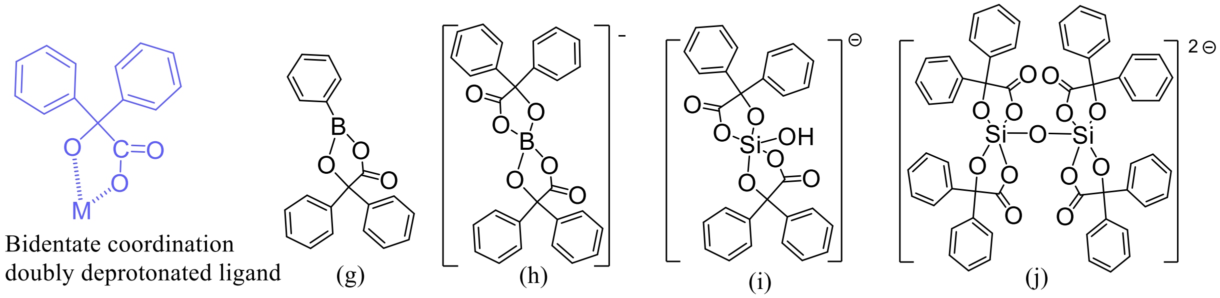

Figure 1-16. Bidentate singly deprotonated (a-f) and doubly deprotonated (g-j) $Ph_2C(X)$ acid ligands derived complexes.

The second type of bidentate coordination mode shows the metal centre binds to two oxygen atoms from the carboxylate group alone. This mode is rare; it has only been found in La(III) and Ce(III) compounds with dpg as ligand.[59] As shown in Figure 1-17 (k), the La centre is surrounded by three dpg moieties in their zwitterionic form. It is common that α-amino acids are normally present in solutions in their zwitterionic form.[60]

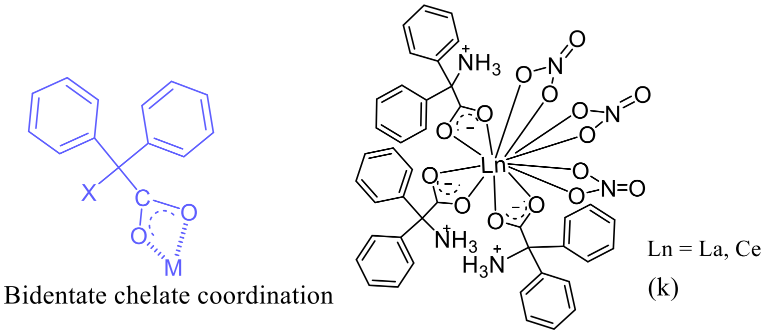

Figure 1-17. Bidentate chelate $Ph_2C(X)$ acid ligands derived complex (k).

The last type of mode is the bridging bidentate which means two oxygen atoms from carboxylato group bind to two metal ions separately (Figure 1-8 (m)).[51] This coordination mode easily leads to a chain structure for the complex. For example, a polymeric complex was obtained when thallium ions were coordinated with one oxygen atom of one benzilato anion and another oxygen atom from a neighbouring benzilato ligand.

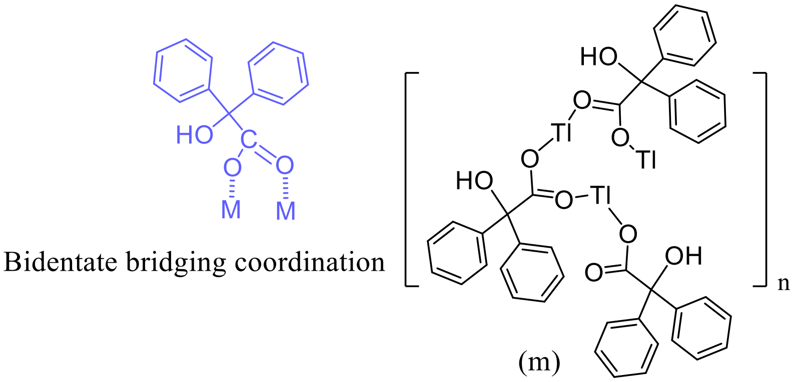

Bidentate bridging coordination

(m)

Figure 1-18. Bidentate bridging $Ph_2C(X)$ acid ligands derived complex (m).

Mixed coordination modes

In most cases, in which $Ph_2C(X)$ acid ligands react with metal alkyls directly without co-ligands, the coordination modes adopted by $Ph_2C(X)$ acid ligands are really complicated. For example, one dpg moiety could chelate to as many as five metal ions which indicates different coordination modes in the same compound.[61] Several polynuclear complexes supported by $Ph_2C(X)$ acid ligands have been reported. Herein, the kappa convention (κ) is used to specify the number of attached atoms in a multi-dentate ligand and which ligand atoms are bonding to the metal-binding site.[62,63]

The first type is κ^2N,O(1):κ^1O(2), which represents one metal chelated by a dpg moiety with the carbonyl oxygen of the carboxylate group and the nitrogen atom of the amino group, whilst the other metal ion binds to the hydroxyl oxygen of the carboxylate group. This mode has been observed in both polynuclear and polymeric 1D chain complexes. For example, a 16-membered ring zinc complex (Figure 1-19 (n))[61] adopts this mode, in which the carboxylates are all in *anti-syn* fashion. When the carboxylate group coordinates to a metal ion, if the dihedral angle of metal-O-C-O is around 0°, the coordination mode is denoted as *syn*. By contrast, if the angle is close to 180°, it is called *anti*.[64] Each zinc is four-coordinate with dpg moiety binding in *N,O* fashion. The other oxygen of this ligand binds to an adjacent zinc. This mode is also found in the chain structured complexes $[(CuBr_2)_2(Dpg)_2Cu(EtOH)_4]$ and heterometallic $[(CuCl_2)(Dpg)Li(THF)]\cdot THF$ (Figure 1-19 (o) and (p), separately).[49] For complex (o), the chain structure is formed by bridging Br atoms and chelating dpg units.

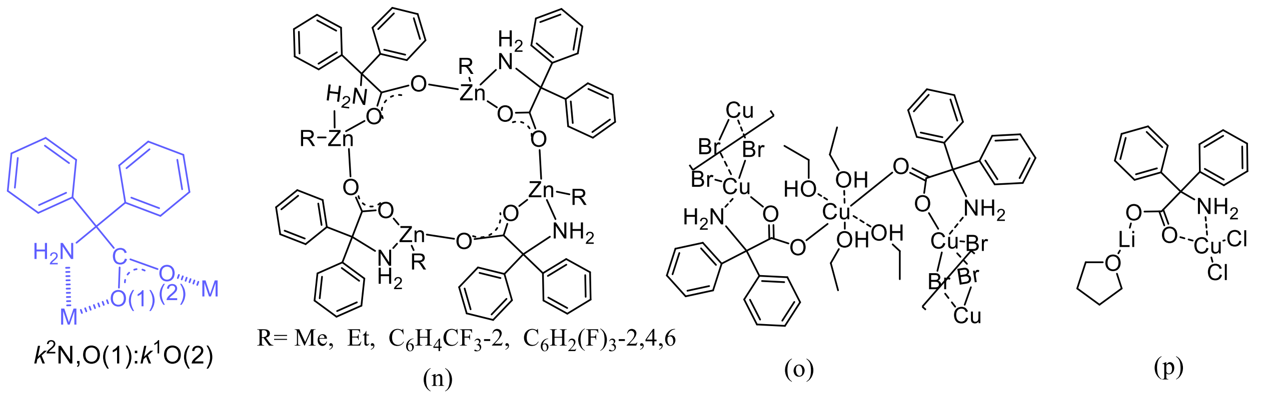

Figure 1-19. k^2N,O(1):k^1O(2) mode $Ph_2C(X)$ acid ligands derived complex (n-p).

The second type of mode is κ^2O(1),O(3):κ^1O(1). This mode is like the previous one that $Ph_2C(X)$ acid ligand chelates two metals except two metal ions are coordinated by the same oxygen atom from the carboxylate group. It has been found in a heterometallic complex [TbTi(μ_3-O)(benzi)$_3$(H_2O)$_4$] (Figure 1-20 (q)).[65] Two benzilato ligands coordinate Ti ion through hydroxyl and carboxylate groups. The same oxygen atom of the carboxylate additionally coordinates to the Tb ion. This mode is also displayed in a lithium [Li(benzi)]·THF complex[46] in which one benzilic acid is bidentate to a Li through hydroxy oxygen atom and oxygen atom of the carboxylate. The same oxygen atom of the carboxylate also coordinates to a second Li (Figure 1-20 (r)).

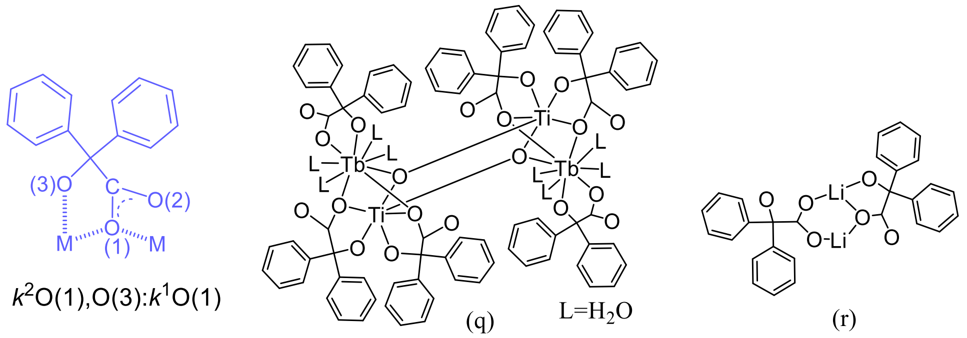

Figure 1-20. k^2O(1),O(3):k^1O(1) mode $Ph_2C(X)$ acid ligands derived complex (q-r).

The use of 1.5 molar equivalents of Me_3Al to react with dpg or benzilic acid results in a 16-membered macrocyclic structure. This hexanuclear complex (s)[66] consists of a building block (Figure 1-21 (s), within the red frame) that follows the coordination mode of κ^2X,O(1):κ^1X:κ^1(O2) (X=NH, or O(3)). Throughout the mode, the hydroxy/amino and carboxylate moiety chelates one aluminium, the hydroxy/amino group additionally coordinates another aluminium, and the third metal ion is coordinated by another oxygen of the carboxylate group. The carboxylate groups bind in an *anti/syn* fashion.

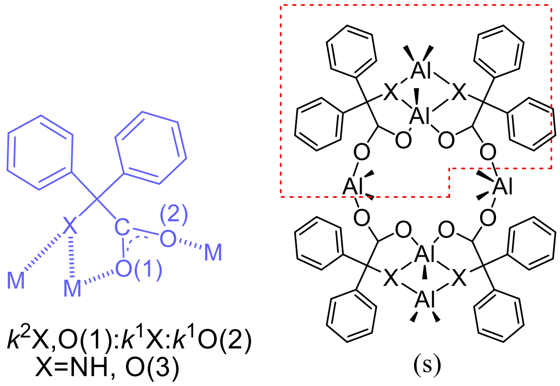

Figure 1-21. k^2X,O(1): k^1X:k^1O(2) mode Ph$_2$C(X) acid ligands derived complex (s).

The fourth type of mode is κ^2O(1),O(2):κ^1O(1):κ^1(O2):κ^1(O3). This mode represents the case where each benzilic acid moiety chelates to four metals, in which three metal ions are monodentate coordinated to three oxygen atoms (one hydroxy, two carboxylate), whilst the fourth metal is bidentate coordinated to two oxygen atoms (one hydroxyl, one carboxylate). Two zinc complexes[67] have been reported following this mode. For instance, the use of benzilic acid with 2 molar equivalents of Et$_2$Zn afforded a hexanuclear zinc complex (Figure 1-22 (t)). There are three benzilic acid ligands, and each follows this coordination mode. The binding of the carboxylate groups with the three zinc centres is anti/syn/syn. When changing Et$_2$Zn to (C$_6$F$_5$)$_2$Zn to react with benzilic acid, an octanuclear complex was obtained (Figure 1-22 (u)). The coordination mode resembles complex (t).

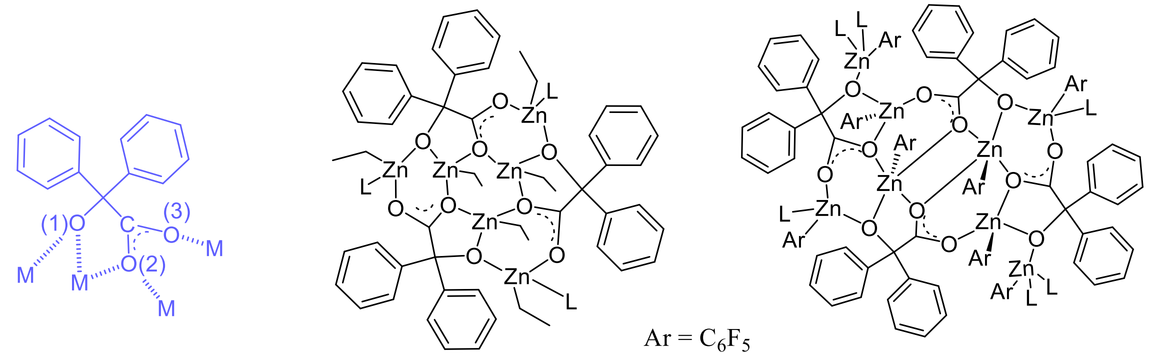

$k^2O(1),O(2):k^1O(1):k^1O(2):k^1O(3)$

(t)

(u)

Figure 1-22. $k^2O(1),O(2)$: $k^1O(1):k^1O(2):k^1O(3)$ mode $Ph_2C(X)$ acid ligands derived complex (t) and (u).

When adding 4.1 molar equivalents of *t*BuLi to complex (n) (Figure 1-19), a heterobimetallic cage complex is formed (Figure 1-23 (v)).[67] The dpg ligands that coordinate with two Zn and three Li centres are followed the coordination mode $\kappa^2N,O(1):\kappa^1O(N):\kappa^1O(1):\kappa^1(O2):\kappa^1(O2)$. Each Zn is bidentate bound by one nitrogen and one oxygen atom of dpg ligand.

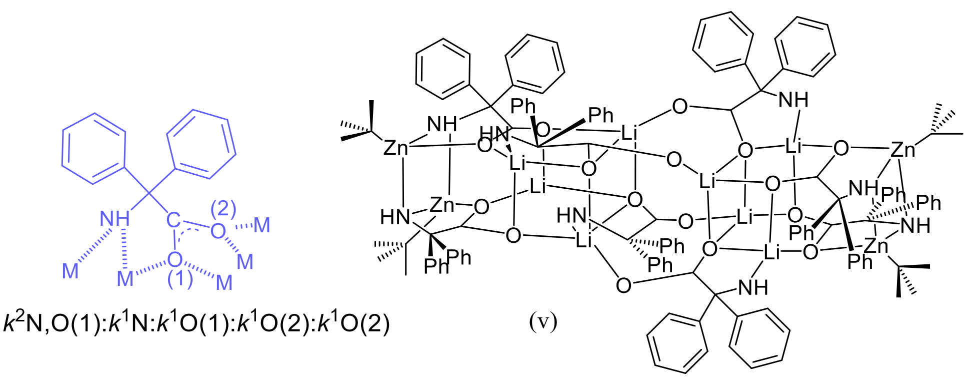

$k^2N,O(1):k^1N:k^1O(1):k^1O(2):k^1O(2)$

(v)

Figure 1-23. $k^2N,O(1):k^1N:k^1O(1):k^1O(2):k^1O(2)$ mode $Ph_2C(X)$ acid ligands derived complex (v).

In conclusion, the multi-dentate $Ph_2C(X)$ acid ligands, where X = OH, NH_2, have been shown to display great coordination versatility, forming single and multi-nuclear metal complexes with fascinating structures and different bonding modes. The monodentate coordination mode of the $Ph_2C(X)$ acid ligands is frequently found in the mixed ligand system, especially when the presence of *N*-chelating ancillary ligands such as 1,10-phenanthroline, imidazole and pyridine, etc. Bidentate coordination is more common to see in the complexes, in which carboxyl/amino and alcoholic hydroxyl coordinate to metal ions to form a five-membered chelate ring. When Ph$_2$C(X) acid ligands react with metal ions directly without the presence of co-ligands, macrocycles, ladders and cages complexes are obtained. The coordination flexibility of these chelating ligands depends on the nature of the metal ion, various aryl or alkyl groups of organometallics compounds, the metal-to-ligand stoichiometry, co-ligands, the synthetic method, and the solvent used for recrystallisation. Overall, the ability of these Ph$_2$C(X) acid ligands to promote the complexes with versatile structures is now well documented.

1.3.2 Complexes bearing 2,2′-diphenylglycine or benzilic acid ligand as catalysts for ring-opening polymerisation

Several copper, lithium, zinc, and lanthanum complexes incorporating the Ph$_2$C(X) moiety (as mentioned above) have been reported for their ability to act as catalysts to initiate the ROP of cyclic esters (Figure 1-24). This chapter now reviews the catalytic performance of these complexes and the type of coordination sites and various ligands present. All complexes have a general formula of *L*$_n$MR, where M is a central metal atom surrounded by an ancillary ligand *L*$_n$, and R (OR) is the initiating group.[21] The different combinations of *L*$_n$ with M and R(OR) will dramatically influence the polymerisation activity of the complexes.

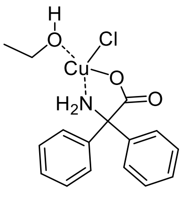

(Cu1)

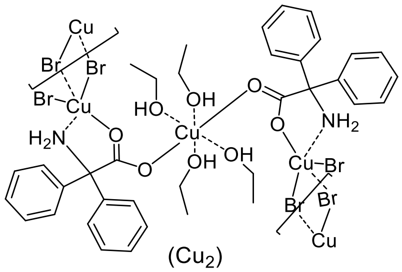

(Cu$_2$)

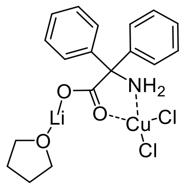

(Cu$_3$)

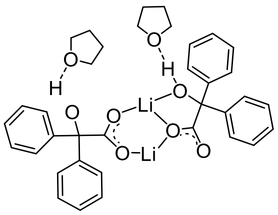

(Li$_1$)

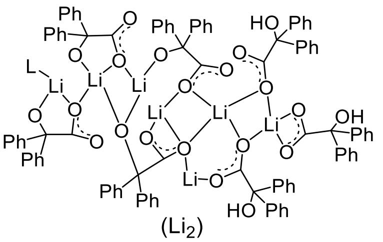

(Li$_2$)

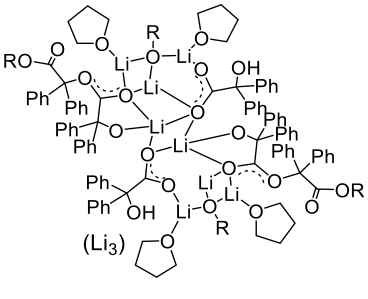

(Li$_3$)

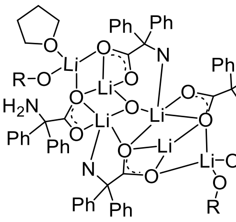

(Li$_4$)

L=MeCN
R=tBu

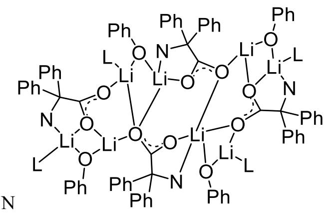

(Li$_5$)

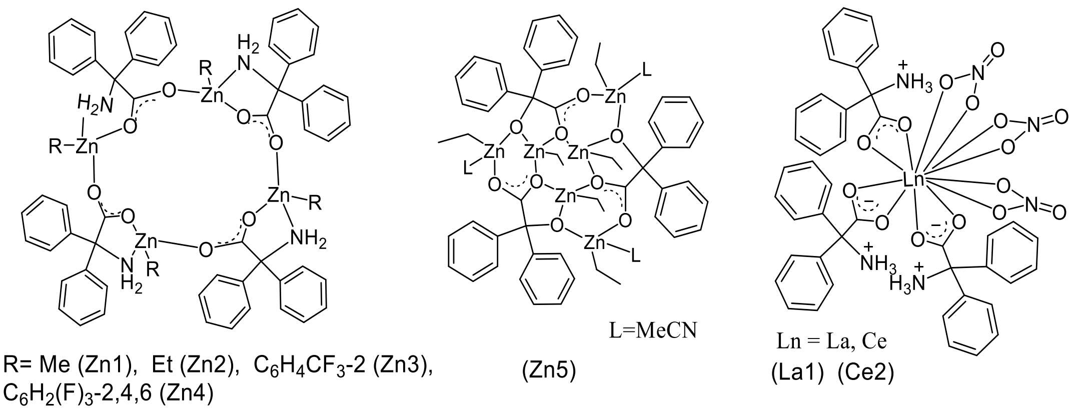

R= Me (Zn1), Et (Zn2), $C_6H_4CF_3$-2 (Zn3), $C_6H_2(F)_3$-2,4,6 (Zn4)

L=MeCN

(Zn5)

Ln = La, Ce

(La1) (Ce2)

Figure 1-24. Copper, lithium, zinc, and lanthanum complexes for ROP application.

Table 1-1 presents all compounds that were tested as catalysts in the ROP of ε-CL or LA with different reaction conditions. Firstly, benzilic acid and dpg ligands with carboxylic acid group are potential organocatalysts for ROP reaction. Under the same reaction conditions, when dpg was applied for the ROP of ε-CL, only 5% conversion was achieved, whereas a better conversion of 14% was achieved when using benzilic acid (Table 1-1, run 1-2). Overall, using organic ligands $Ph_2C(X)$ moiety itself has limited ability as catalysts to provide high activity. The activity of Li-based complexes followed the trend **Li3** > **Li4** > **Li5** > **Li1 > Li2**. Complexes **Li1** and **Li2** lack a typical initiating group: lithium alkoxide (OR). So **Li1** has poor activity when in the absence of BnOH as the co-initiator (Table 1-1, run 3-4). For **Li3** and **Li4**, the presence of O-*t*Bu and/or THF ligation at lithium is beneficial. The better performance of **Li3** compared with **Li4** maybe due to the effect of benzilic acid moieties binding to lithium. For Cu-based complexes, no matter the presence of co-initiator, none of the complexes proved to be active in the ROP of ε-CL (Table 1-1, run 9-11). The reactivity trend of zinc-based complexes was found to be **Zn4** > **Zn3** > **Zn5** > **Zn2** > **Zn1**, suggesting that R groups dramatically influence the catalytic performance. The fluorinated aryl group led to an improvement in the catalytic performance (Table1-1, run 12-16). In the case of lanthanum and cerium-based complexes, both reached high conversion (>90%) of ε-CL, while only traces (8%) were obtained for LA upon using **Ce2** and its corresponding metal precursor (Table1-1, run 17-18, 31). In conclusion, a zinc complex bearing dpg ligand (**Zn4**) has been demonstrated to be a highly active catalyst for the ROP of ε-CL, regardless of the desired molecular weight of the resulting PCL and the level of conversion (>90%).

In terms of catalysts in the ROP of *r*-LA, lithium complex bearing dpg ligand (**Li4**) is better performing than Zn complexes.

Table 1-1. ROP screening using copper, lithium, zinc, or lanthanum-based catalysts

run	**Cat.**	**ligand**	**OR/R group**	**monomer:Cat:BnOH**	**T ℃**	**Time (h)**	**Conversion (%)**	**M_n (Da)**	**PDI**	**Solvent**	**Atmosphere**
ε-CL											
1	**dpg**[59]	/	/	250:1:0	150	24	none	-	-	-	air
2	**benzi**[59]	/	/	250:1:0	150	24	14	-	-	-	air
3	**Li1**[46]	benzi	-	150:1:1	110	1	83	3500	1.59	-	N_2
4	**Li1**[46]	benzi	-	150:1:0	110	3	-	-	-	-	N_2
5	**Li2**[46]	benzi	-	150:1:1	110	2	-	-	-	-	N_2
6	**Li3**[46]	benzi	O*t*Bu	150:1:0	110	0.4	93	8250	1.56	-	N_2
7	**Li4**[46]	dpg	O*t*Bu	150:1:0	110	0.5	91	6750	2.01	-	N_2
8	**Li5**[46]	dpg	OPh	150:1:0	110	0.58	87	4880	1.21	-	N_2
9	**Cu1**[49]	dpg	-	100:1:0	130	24	-	-	-	-	N_2
10	**Cu2**[49]	dpg	-	100:1:0	130	24	-	-	-	-	N_2
11	**Cu3**[49]	dpg	-	100:1:0	130	24	-	-	-	-	N_2
12	**Zn1**[61]	dpg	Me	150:1:0	110	1	74	9600	1.37	toluene	N_2
13	**Zn2**[61]	dpg	Et	150:1:0	110	1	82	10600	1.31	toluene	N_2
14	**Zn3**[61]	dpg	$C_6H_4CF_3$-2	150:1:0	110	1	90	12800	1.40	toluene	N_2
15	**Zn4**[61]	dpg	$C_6H_2(F)_3$-2,4,6	150:1:0	110	1	92	12900	1.31	toluene	N_2
16	**Zn5**[61]	benzi	Et	150:1:0	110	1	84	10800	1.10	toluene	N_2
17	**La1**[59]	dpg	-	250:1:0	150	24	94	3200	1.57	-	air
18	**Ce2**[59]	dpg	-	250:1:0	150	24	93	2800	1.56	-	air
***r*-LA**											
19	**Benzi**	/	/	20:1:0	150	24	-	-	-	-	air
20	**Li1**	benzi	-	100:1:1	110	12	63	4360	1.09	toluene	N_2
21	**Li2**	benzi	-	100:1:1	110	12	-	-	-	toluene	N_2
22	**Li3**	benzi	O*t*Bu	100:1:0	110	12	61	4000	1.14	toluene	N_2
23	**Li4**	dpg	O*t*Bu	100:1:0	110	12	69	7000	1.15	toluene	N_2
24	**Li5**	dpg	OPh	100:1:0	110	12	65	4700	1.18	toluene	N_2
25	**Zn1**	dpg	Me	100:1:0	110	12	55	4600	1.88	toluene	N_2
26	**Zn2**	dpg	Et	100:1:0	110	12	57	5000	1.25	toluene	N_2
27	**Zn3**	dpg	$C_6H_4CF_3$-2	100:1:0	110	12	66	7000	1.51	toluene	N_2
28	**Zn4**	dpg	$C_6H_2(F)_3$-2,4,6	100:1:0	110	12	67	6200	1.23	toluene	N_2
29	**Zn5**	benzi	Et	100:1:0	110	12	61	6000	1.27	toluene	N_2
30	**La1**	dpg	-	250:1:0	150	24	-	-	-	-	air
31	**Ce2**	dpg	-	250:1:0	150	24	8	-	-	-	air

1.4 Characterisation methods

1.4.1 NMR spectroscopy

The atom is the basic building block of all matter. It is composed of a nucleus and one or more electrons surrounding the nucleus within a molecule. The nucleus consists of protons and neutrons.[68] Protons are electrically positive charged and both protons and neutrons have spin. The proton can be pictured as a magnetic dipole. In the presence of an external magnetic field, the nucleus takes an orientation corresponding to the direction of the applied field. A transition of a nucleus from one spin state to an adjacent state may occur by the absorption or emission of an appropriate quantum of energy. The absorption of energy during this transition is the principle of the nuclear magnetic resonance spectroscopy (NMR) method.[69,70] In 1963, Eugene Paul Wigner, Maria Goeppert Mayer, and J. Hans D. Jensen won the Nobel Prize in physics for their contributions to the nuclear shell model.[71] The shell model tells us that the nucleon is analogue to electrons, filling orbitals. The spin of nucleons can pair up when the orbitals are being filled and reach an energy level. The nuclear spin follows certain rules: If the number of neutrons and the number of protons are both even, the nucleus has no spin. If the number of neutrons plus the number of protons is odd, then the nucleus has a half-integer spin (*i.e.* 1/2, 3/2, 5/2). If the number of neutrons and the number of protons is both odd, then the nucleus has an integer spin (*i.e.* 1, 2, 3). All nuclei with non-zero spins exhibit NMR phenomena. One of the most common solvents used for ^{1}H NMR is $CDCl_3$ in which D represents an isotope of hydrogen. Deuterium has an even mass number (2) and an odd number of protons (1) and neutrons (1). The spin is equal to 1, unlike hydrogen (proton), which has spin = 1/2. Although deuterium has a nuclear spin, it requires greatly different operating frequencies at a given magnetic field strength compared with the proton NMR. Therefore, $CDCl_3$ cannot be detected under the conditions used for proton NMR which is beneficial to identify the chemical shift of target chemicals other than solvents.[72] However, there is still a residual small peak at 7.26 ppm, which is corresponding to incompletely deuterated $CHCl_3$. Similarly, for ^{13}C NMR, 1.1% of $CDCl_3$ has a ^{13}C isotope,[73] and this is the reason why we need to prepare a more concentrated solution for target chemical samples when testing ^{13}C NMR. In this work, ^{1}H and ^{13}C NMR spectroscopy has been applied for determining the structure of ligands and coordinated complexes in this work. Chemical shift, absorption intensity and spin-spin coupling are the most important information from NMR spectrometry. Particularly, the spin-spin coupling shows the multiple splits of one peak due to the presence of neighbouring magnetic nucleus. The chemical shift differences of adjacent lines in the multiples are denoted as coupling constant (*J*). It is a powerful tool to recognize fine structures. ^{13}Carbon and two-dimensional ^{1}H *J*-resolved (2D *J*-resolved) NMR were used to analyse the stereo-sequence of polylactide here.

1.4.2 Mass spectrometry

Mass spectrometry (MS) is the technique used for generating gas-phase ions, separating them according to mass-to-charge ratio, and detecting in proportion to their abundance.[74,75] This is a powerful analytical technique that provides structural information and molecular weight. According to the ionization techniques, MS is classified as matrix-assisted laser desorption/ionisation (MALDI), electron ionisation (EI), electrospray ionisation (ESI), chemical ionisation (CI), and atmospheric pressure chemical ionisation (APCI), etc. In the next step, the ions are separated by the mass analyser. The common types of mass analysers include sector, quadrupole, ion trap, and TOF. MS can be applied to characterise the structure information of coordination complexes. For example, the molecular mass, the number of ligands around the metal, and the binding stoichiometry.[76] To obtain this information, the detection of intact parent ions with relatively great abundances is crucial, whilst the occurrence of decomposition of complexes or only fragmentation ions observed in the spectrum is undesirable. ESI is a kind of “gentle” ionisation method that causes little or no fragmentation of the sample with the help of using a sample solution.[77] The analyte for the ESI ionisation method should dissolve in the solvent. Then the solution is transferred to the fine aerosol of highly charged ion droplets (*e.g.* 2.5 - 6.0 kV) with the assistance of electrical energy which is the process of generating electrospray. [78] The charged droplets are desolvated by a warm continuous nitrogen gas flow as a result the charge density increases and bare ions go to the mass analyser region.[79] In this work, acetonitrile was selected to dissolve all the coordination complexes for MS analysis. Acetonitrile is a type of polar solvent with a moderate boiling point (82 ^{o}C).

Interpretation of a coordination complex’s mass spectrum is challenging which requires the researcher to understand the fragmentation processes. However, there are still some fundamental rules that can be applied: The molecular ions in the mass spectrum are mostly metal-containing species; The ligand commonly departs as a radical; Fragmentation of ligand backbones while the ligand is still bound to the metal often occurs.[80] For example, the novel Schiff base ligand 2-(4-

(dimethylamino)benzylidene)-*N*-(4-phenylthiazol-2-yl)hydrazinecarboxamide cobalt(II) complexes undergo the fragmentation by loss of coordinated chloride radical and 2-amino-4-phenylthiazole molecule, giving a base ion peak at *m/z* 437 (100%) (Figure 1-25).[81] The ESI-MS spectra showed that fragments are metal-containing species. Besides, the fragmentation started with the ligand itself instead of dissociating the entire ligand. This is because the cobalt(II) complex contains a bidentate ligand and the ligand itself is not stable. ESI behaviour strongly depends on the ligand type and the charge.

In this work, another mass spectrometry application used was MALDI-TOF MS to deal with the polymer chain structure, which includes the repeating units, end group compositions, the number average molecular weight (M_n), and the weight averaged molecular weight (M_W).[82] The key feature of the ionisation method is using a pulsed laser beam to irradiate a mixture of matrix and polymer.[83] Then, polymers are ionized by deprotonation or protonation with the help of a matrix. Finally, molecular ions can be accelerated into the mass analyser. The TOF mass analyser is ideally compatible with MALDI pulsed ionisation method and exhibits a broad mass range which is up to 100,000 Da. [82,84] The matrix used for this work is 2,5-dihydroxybenzoic acid along with THF as solvent and sodium chloride as cationising agent.

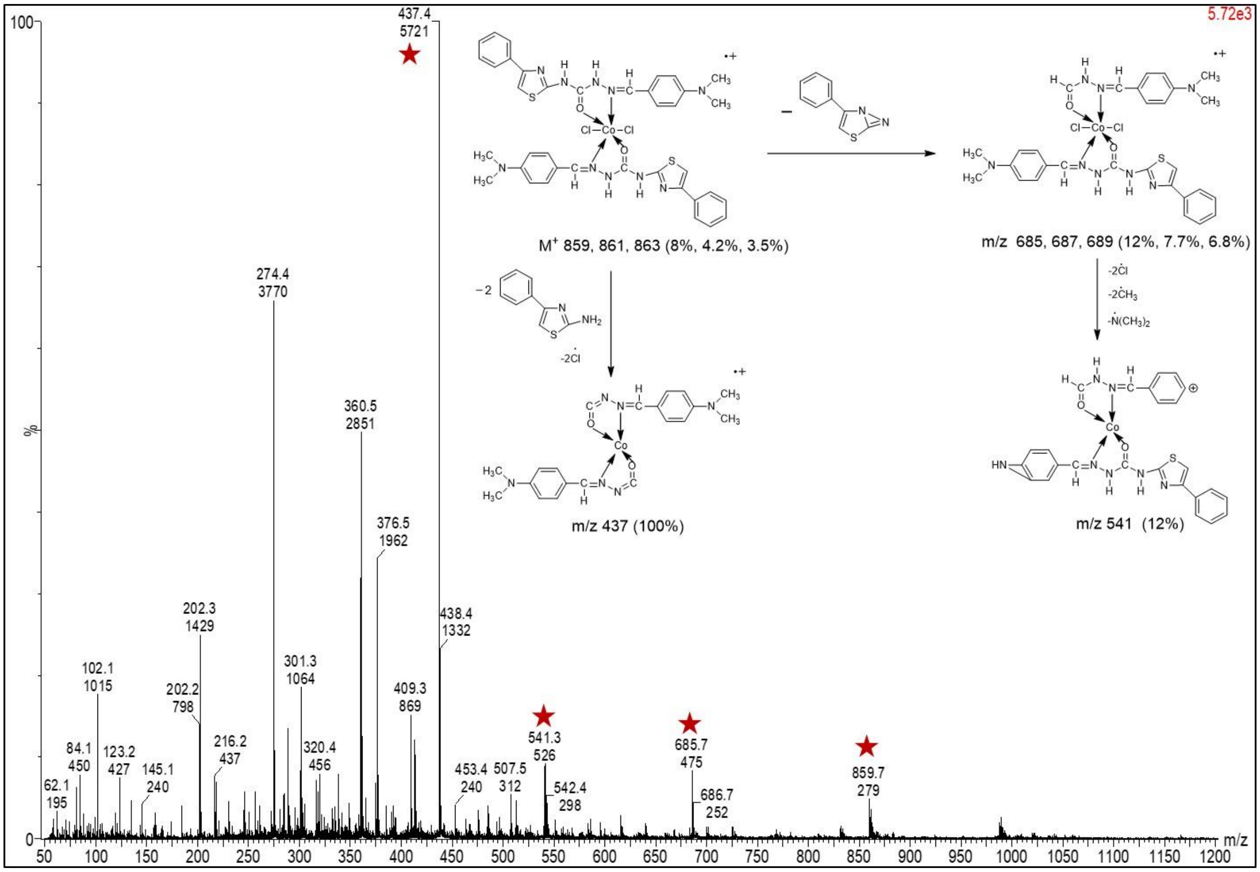

Figure 1-25. ESI mass spectrum of Co(II) complex

1.4.3 Infrared spectroscopy

Infrared (IR) spectroscopy is a supportive analytical technique for studying the structure of coordination complexes. It affords valuable information that includes chelating donors of coordination sites[85-87], number of binding sites of ligands[88] and linkage isomerism coordination modes.[86] The advantages of the IR technique are fast, simple, and cheap. A common way to prepare coordination samples for IR analysis is Nujol mulling. This method requires grinding the particles with agate mortar and suspending those particles with Nujol. Once prepared the mull is added to the middle of two potassium bromide plates, like preparing a sandwich.[86]

The general approach to analysing the structure of coordination complexes using IR involves obtaining background information about the infrared absorption bands associated with ligands and metal salts. Then, using this information to explore the differences of peak position, intensity, and new emerging peaks compared with the coordination complexes. Significant differences in the ligand binding modes lead to distinct absorption frequency. For example, the zinc(II) carboxylate binding modes vary from ionic, bridging (*syn-syn*, *syn-anti*, *monatomic*), and chelating to monodentate (Figure 1-26).[89] The asymmetric and symmetric stretching vibration of COO^{-} for complex $[Zn(C_6H_5CHCHCOO)_2(H_2O)_2]$ with chelating carboxylate group were 1523 and 1411 cm^{-1}, respectively (Figure 1-27 (a and c)). For the compound $[Zn(C_6H_5CHCHCOO)_2(mpcm)]_n$ (mpcm = methyl-3-pyridylcarbamate), two asymmetric (1561 and 1523 cm^{-1}) and two symmetric (1418 and 1376 cm^{-1}) carboxylate stretches were observed indicating the existence of two different modes of carboxylate binding which are monodentate and bidentate (Figure 1-27 (b and d)).[85]

Regarding Schiff-base complexes, the main interest has been the investigation of the imine bond vibration. Jenisha[90] reported the C=N stretching frequency of the complexes furfural(A)-ethylenediamine(B) cobalt(II)/zin(II)/copper(II) were lower than those of ligands. Other studies on bis(salicylaldehyde)ethylenediamine Ni(II) complex[91] and salicylidene aniline copper (II) complex [92] are in agreement with this phenomenon. Gluvchinsky also carried out the analysis on the metal-oxygen and metal-nitrogen stretching vibration for Schiff base complexes in the far infrared region. New peaks appeared at 415 and 292 cm^{-1} and were assigned to νNi-N and νNi-O mode.[91]

The IR spectra for the chelation of amino acids exhibited significant features in νN–H and νCOO– regions. Many previous investigations have shown that the coordination of amino groups with metal ions decreases the frequencies of the N–H stretching vibration of these groups.[93] The absence of a band at ~3440 cm^{-1} which is assigned to the O–H stretching vibration in the spectra of the complexes, in comparison to the free ligand, confirms the deprotonation and coordination through the COOH group.[94]

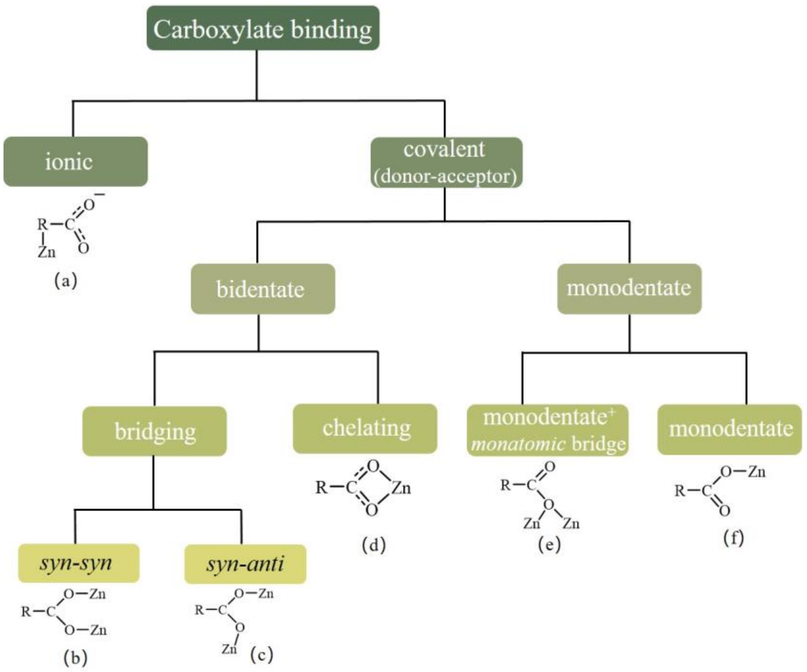

Figure 1-26. Versatile coordination behaviour of the carboxylate group.[89]

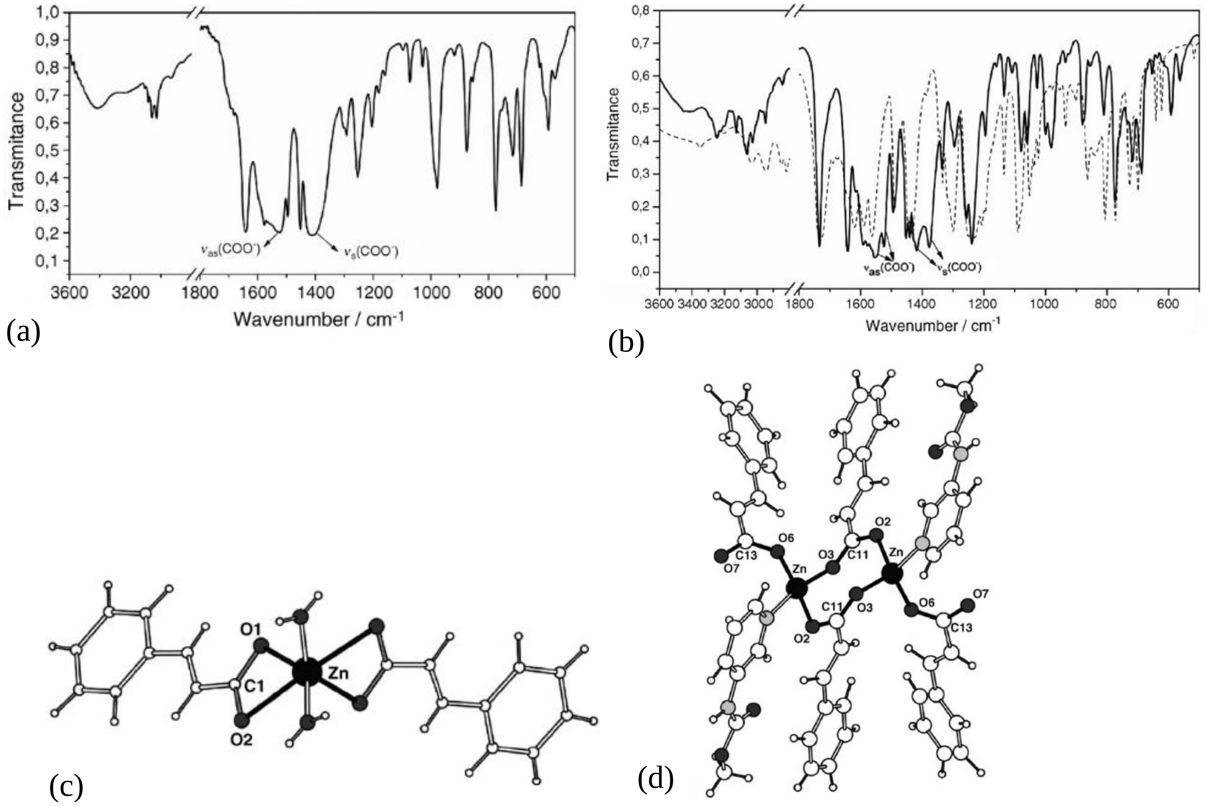

Figure 1-27. (a) IR spectrum of the complex [$Zn(C_6H_5CHCHCOO)_2(H_2O)_2$] with chelating carboxylate group; (b) IR spectrum of the complex [$Zn(C_6H_5CHCHCOO)_2(mpcm)$]$_n$ with *syn-anti*

carboxylate bridges and monodentate carboxylate; (c) the structure of the complex $[Zn(C_6H_5CHCHCOO)_2(H_2O)_2]$; (d) the structure of the complex $[Zn(C_6H_5CHCHCOO)_2(mpcm)]_n$.[89]

1.4.4 Elemental analysis

Elemental analysis (EA) is a reliable method to obtain information about an unknown substance's elemental composition and assess a compound's purity.[95,96]. The elements typically include carbon, hydrogen, nitrogen, and heteroatoms (X). X contains halogens and sulfur.[97] The principle of EA is using flash combustion to pyrolyse samples in a high purity oxygen rich environment and then converting the unknown substance to simple, known compounds containing only the element to be quantified. The compounds are in gaseous form state, which includes carbon dioxide, water, nitrogen gas, carbon monoxide, and sulfur dioxide. The gas mixtures are separated by a gas chromatography column and identified by a thermal conductivity detector to examine the mass percentage of C, H, N and S elements. Helium is used as the mobile phase.

The accepted allowed deviation of elemental analysis results from the calculated is $\pm$ 0.50%. The EA method has been used extensively in the analysis of coordination complexes. However, EA is a crude technique that supplies limited information, only an empirical formula.[98] When the measured values show significant deviations, it is difficult to identify the trace impurities. The common impurities that cause the deviation could be water, organic solvents and residual ligands. It was observed that the carbon levels of some complexes in this research work were consistently lower than the calculated value even after several times recrystallisation or preparing new products. Unfortunately, no similar problem or explanation has been found in the literature after examination. There are most perfectly fitting data from other publications. The possible explanation for the lower carbon level is water contaminates the air-sensitive complexes during the shipment. Small amounts of water could dramatically influence the EA results. For example, when 1 eq. of H_2O coordinates with complex **3** (structure shown in chapter 2), the deviations for C, H and N are 2.86%, 0.11%, and 0.13%, respectively. It clearly shows that carbon more easily fails.

Overall, EA is an auxiliary tool that should combine with data from X-ray diffraction, IR, MS and NMR to confirm the molecular composition, structure and geometry of coordination complexes.

1.4.5 Gel permeation chromatography

Gel permeation chromatography (GPC) is also known as size exclusion chromatography (SEC), which is the most widely used method to determine the molecular weight and molecular weight distribution of polymers.[99] The component parts of a GPC system include a degasser, pump, sample injector, column, detector, and data analyser. GPC is a type of liquid chromatography that uses liquid as the mobile phase. The typical stationary phase that fills inside the columns is cross-linked polystyrene/divinylbenzene copolymer (PLgel) and silica, designed to have porous beads with well-defined pore sizes. The function of the column is to separate the polymer coils with different sizes. The size of the polymer coils (spheres) is based on the molecular weight. When the solvent contained the polymers flushing the porous column, with the driving force of a high-pressure pump, the big size polymer coils pass quickly without penetrating the pores or accessing very few pores. Thus, the bigger size polymers exit the column faster and reach the detector earlier. In contrast, the small polymer coils could occupy all pores in the stationary phase and take a long time to travel down the column. The mechanism of GPC is physically separating polymers according to their size.[100]

The conventional GPC is only equipped with a differential reflective index detector that determines the amount of concentration eluting from the column as a function of retention time.[101] This is a comparative technique that determines the molecular weight by using the polymer's eluting time from the column. Then, the eluting time will convert to molecular weight by comparing it with the standard calibration curve. However, based on the column separation mechanism, the eluting time depends on the size of the polymer coils. It requires the testing sample should have a similar structure to the standard polymer used for calibration. If a polymer has the same molecular weight as the standard polymer but bigger size of polymer coils, the resulting molecular weight from this GPC detector will be higher than the real molecular weight. The limitation of the conventional GPC propelled the popularity of the multi-detector. The multi-detector is, without doubt, the dominant GPC analytical tool, which usually consists of a reflective index detector (concentration detector), viscometer detector and light scattering detector (shown in Figure 1-28). In this approach, molecular weight is calculated with light scattering, combined with determining the intrinsic viscosity.[99] The advantage of measuring the viscosity of the polymer is it permits calculating the accurate molecular weight no matter the type of standard polymer. In other words, it builds a direct relationship between molecular weight with viscosity, which is the Mark-Houwink plot.[102] In the equation, η is intrinsic viscosity, M is molecular weight, a and K are the Mark-Houwink constants.

$$\log\,[\eta] = \log \mathrm{K} + a\log \mathrm{M}$$

The light scattering detector collects the scattered light after the laser beam irradiates the sample. Similar to the measurement of viscosity, the intensity of scattered light is directly proportional to the molecular weight. Thus, it is ideal to obtain the accurate molecular weight of the polymer.

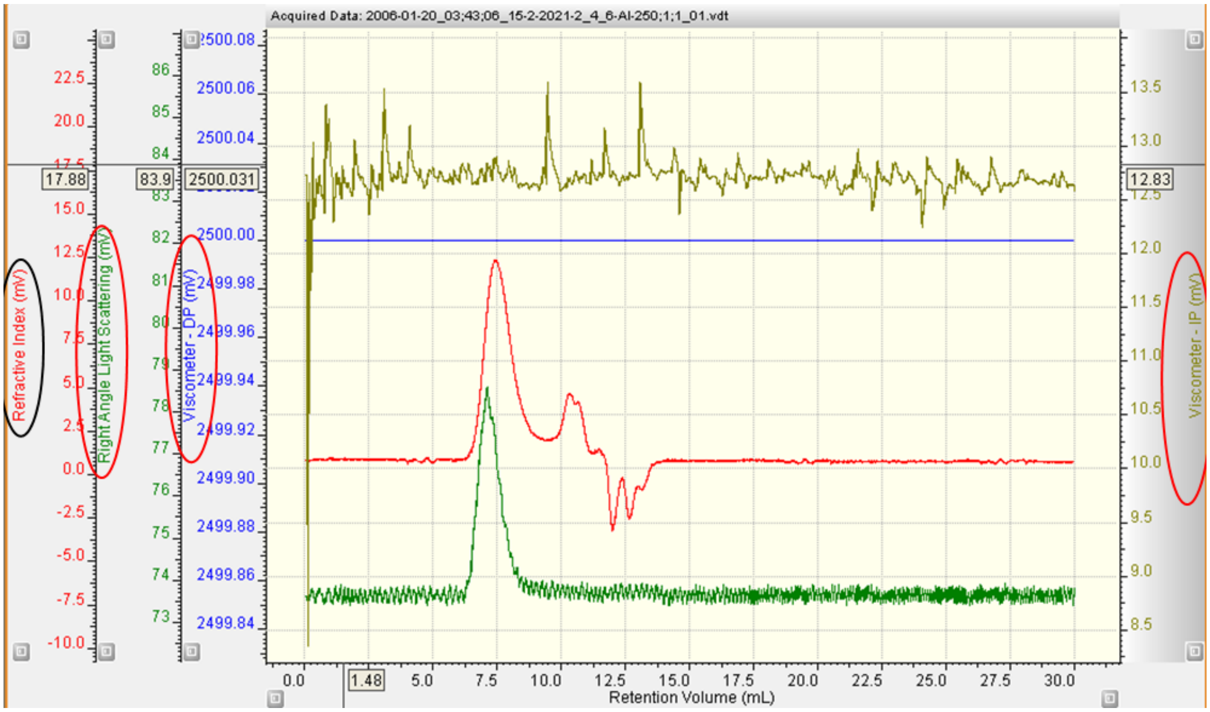

Figure 1-28. Overlaid multi-detector: refractive index, light scattering and viscometer chromatogram for an example of polycaprolactone.

Overall, GPC is a technique that supplies comprehensive information. In addition, it is a good technique to separate different sizes of molecules and it takes a short time for measurement.[103] It normally takes 15 minutes to test PLA or PCL.

1.4.6 X-ray crystallography

X-ray crystallography is the most direct technique to determine the arrangement of atoms of a crystalline solid in three-dimensional.[104,105] It provides ultimate and uncompromising results to the crystal structures. The most commonly used X-ray resource is an X-ray tube where the anode material is copper (Cu) or molybdenum (Mo), which give the X-ray wavelengths 1.54184 and 0.71073 Å, respectively.[106] The wavelength of X-ray is comparable to the interatomic distances occurring in the molecules[107], which are useful tools to explore within crystals. When the X-ray beams interact with electrons in the molecule that the atomic arrangement shows the long-range order, the diffracted X-rays are scattered by the crystal at a certain angle. This phenomenon is denoted as Thomson scattering.[108] The nucleus cannot scatter the X-rays since it is too heavy compared with an X-ray photo. Measurement of the X-ray scattering pattern provides unit cell structure information (symmetry, geometry and positions of the atoms). Bragg law. Equation demonstrated a relationship of the interplanar spacing d with incident light angle θ (Figure 1-29). hkl are three integers to define a space with respect to the orientation of three unit cell edges. The wavelength is λ.

$$2d_{hkl}\sin\theta = \lambda$$

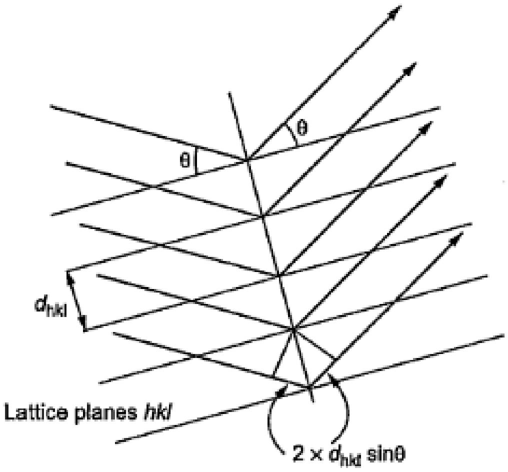

Figure 1-29. The Bragg construction for diffraction by a three-dimensional crystal structure.[106]

X-ray crystallography requires that the samples must be crystalline solid because of the principle of diffraction.[109] The most challenging step for characterising a coordination complex is growing a crystal via recrystallisation. The process includes dissolving the solid product in a suitable solvent and reaching saturation when temperature increases, then decreasing the solution temperature. The complex product will grow into a crystal, leaving impurities in the solution. The principle is straightforward. However, growing a crystal suitable for X-ray crystallography is not easy and sometimes is referred to as "black magic" in the laboratory. Researchers tend to rely on trial and error. Based on research experience, to initially confirm if the sample is crystalline, which is suitable for X-ray crystallography, use a microscope to examine the morphology of the sample crudely. Crystals tend to grow flat surfaces and present facets. It may be needles or plates shaped in macroscopic form due to the arrangements at the atomic or molecular level.[109] However, this method is not reliable. The observed needles or plate forms could be the aggregates of ligand crystals other than metal complex crystals.

Once finishing the X-ray analysis, the data obtained should be processed by the structural analysis program. The final file is named CIF, defined by the International Union of Crystallography (IUCR), shows the molecular structure on the computer screen. Most of the structure files have been submitted and recorded in the Cambridge Structural Database (CSD) or Inorganic Crystal Structure Database (ICSD), where they are evaluated for suitability before publication.[98] By using the CSD software, researchers who are new to some areas could directly search the structure or name of the ligand or metal complex. The results contain structures of all related complexes that have been published. This is a necessary tool for all the researchers who focused on the metal complex area.

1.5 Aims and Objectives

Two main aims are pursued in this thesis: (1) investigating the effect of coordination complexes' metal centres/structures/ancillary ligands/initiating groups on the ROP behaviour of lactides and lactones (*i.e.*, initiator selectivity and activity). (2) developing novel metal catalysts which are easily synthesised and exhibit high activity and good polymerisation control.

Concerning the design of a coordination complex for ROP catalysis, the choice of central metal atom is undoubtedly a highly significant factor. In this thesis, the objective is to study earth-abundant metals: Zn, Al, Ti and less explored group V elements (Nb and Ta) complexes. For this purpose, precursors such as aluminium trimethyl, diethyl zinc, titanium alkoxides, niobium ethoxide, and tantalum ethoxide were utilised to synthesise the aimed novel coordination complexes catalysts.

The approach for determining the structure/reactivity dependence is based on fine-tuning the ancillary ligand and study of the effect on the catalytic reactivity. For this purpose, the applicability and performance of *N,O*-donor and *O,O'*-donor ligands system were investigated, where *N,O*-

donors are Schiff-base ligand and 2,2’-diphenylglycine ligand; *O,O’*-donor ligand is a benzilic acid ligand. Furthermore, a systematic study of the steric and electronic effect of methoxy substituents at the aniline derived ring in a series of Schiff-base organoaluminium and zinc complexes is studied. By comparing ortho or meta substituents on the aniline moiety, *i.e.* 2,4,6- and 3,4,5-substituted anilines, and by varying the number of substituents on the ring, *i.e.* 2,4- versus 2,4,6- or with no methoxy substituent group.

Polymerisation behaviour was found to be influenced by both the ligand environment and the initiating group.[110] Thus, the objective of this thesis is to evaluate the effect of different titanium alkoxide initiating groups to initiate the polymerization, such as $Ti(OMe)_4$, $Ti(O\textit{n}Pr)_4$, $Ti(O\textit{i}Pr)_4$, and $Ti(O\textit{t}Bu)_4$.

The high activity in this thesis refers to the catalysts being capable to convert high monomer loadings (>1000 equiv.) to polymer with high polymer conversion (>95%) on minute timescales. Good polymerisation control requires polymers to have predictable molecular weights with less transesterification, and narrow polydispersity (PDI $\leqslant 2$).

The innovative catalyst design strategies afford new complexes of interest in the ROP of lactides and lactones and give valuable guidance about the potential factors that influence their catalytic behaviour for future research and advancements in this field.

References

1. T. P. Haider, C. Völker, J. Kramm, K. Landfester and F. R. Wurm, *Angew.Chem. Int. Ed*, 2019, **58**, 50-62.
2. China dialogue online, https://chinadialogue.net/en/pollution/china-cools-on-biodegradable-plastic/, (accessed March 2023)
3. European bioplastics online, https://www.european-bioplastics.org/market/, (accessed March 2023)
4. Z. Zhang, O. Ortiz, R. Goyal and J. Kohn, in *Handbook of Polymer Applications in Medicine and Medical Devices*, Elsevier, 2014, pp. 303-335.
5. S. V. G. Kumari, K. Pakshirajan and G. Pugazhenthi, *Int. J. Biol. Macromol.*, 2022, **221**, 163-182.
6. V. Fomin and V. Guzeev, *Int. Polym. Sci. Technol.*, 2001, **28**, 76-84.
7. M. Okada, *Prog. Polym. Sci.*, 2002, **27**, 87-133.
8. Y. Tokiwa and B. P. Calabia, *Appl. Microbiol. Biotechnol.*, 2006, **72**, 244-251.
9. C. Jerome and P. Lecomte, *Adv. Drug Deliv Rev.*, 2008, **60**, 1056-1076.
10. M. Ajioka, K. Enomoto, K. Suzuki and A. Yamaguchi, *Bull. Chem. Soc. Jpn.*, 1995, **68**, 2125-2131.
11. A. Löfgren, A. C. Albertsson, P. Dubois and R. Jérôme, *J. Macromol. Sci., Part C: Polym. Rev.*, 1995, **35**, 379-418.
12. A. C. Albertsson and I. K. Varma, in *Degradable aliphatic polyesters*, Springer, Berlin, 2002, vol. 157, 1-40.
13. P. Lecomte and C. Jérôme, in *Synthetic Biodegradable Polymers*, Springer, Berlin, 2012, vol. 245, pp. 173-217.
14. V. H. Cherdron, H. Ohse and F. Korte, *Macromol. Chem. Phys*, 1962, **56**, 179-186.
15. J. Baran, A. Duda, A. Kowalski, R. Szymanski and S. Penczek, *Macromol. Symp.*, 1997, **123**, 93-101.
16. S. Penczek, A. Duda, A. Kowalski, J. Libiszowski, K. Majerska and T. Biela, *Macromol. Symp.*, 2000, 157, 61-70.
17. A. B. Kremer and P. Mehrkhodavandi, *Coord. Chem. Rev.*, 2019, **380**, 35-57.
18. W. Gruszka and J. A. Garden, *Nat. Commun.*, 2021, **12**, 3252.
19. E. Fazekas, P. A. Lowy, M. Abdul Rahman, A. Lykkeberg, Y. Zhou, R. Chambenahalli and J. A. Garden, *Chem Soc Rev*, 2022, **51**, 8793-8814.
20. W. Dittrich and R. Schulz, *Angew. Makromol. Chem.*, 1971, **15**, 109.
21. P. J. Dijkstra, H. Du and J. Feijen, *Polym. Chem.*, 2011, **2**, 520-527.
22. A. Stjerndahl, A. F. Wistrand and A. C. Albertsson, *Biomacromolecules*, 2007, **8**, 937-940.
23. P. J. A. In't Veld, E. M. Velner, P. Van De Witte, J. Hamhuis, P. J. Dijkstra and J. Feijen, *J. Polym. Sci., Part A: Polym. Chem.*, 1997, **35**, 219-226.
24. P. Purnama, Y. Jung, C. H. Hong, D. S. Han and S. H. Kim, *Macromol. Res.*, 2012, **20**, 515-519.
25. P. Lecomte, F. Stassin and R. Jérôme, *Macromol. Symp.*, 2004, **215**, 325-338.26. S. I. Moon and Y. Kimura, *Polym. Int.*, 2003, **52**, 299-303.
27. P. Degée, P. Dubois and R. Jérôme, *Macromol. Chem. and Phys.*, 1997, **198**, 1973-1984.

28. K. Matsubara, C. Terata, H. Sekine, K. Yamatani, T. Harada, K. Eda, M. Dan, Y. Koga and M. Yasuniwa, *J. Polym. Sci., Part A: Polym. Chem.*, 2012, **50**, 957-966.
29. H.-L. Chen, S. Dutta, P.-Y. Huang and C.-C. Lin, *Organometallics*, 2012, **31**, 2016-2025.
30. T. M. Ovitt and G. W. Coates, *J. Polym. Sci., Part A: Polym. Chem.*, 2000, **38**, 4686-4692.
31. N. Spassky, M. Wisniewski, C. Pluta and A. Le Borgne, *Macromol. Chem. Phys*, 1996, **197**, 2627-2637.
32. T. M. Ovitt and G. W. Coates, *J. Am. Chem. Soc.*, 2002, **124**, 1316-1326.
33. W. Meelua, V. Bua-Own, R. Molloy and W. Punyodom, *Adv. Mater. Res.*, 2012, **506**, 142-145.
34. J. Cayuela, V. Bounor-Legaré, P. Cassagnau and A. Michel, *Macromolecules*, 2006, **39**, 1338-1346.
35. C. K. Gregson, I. J. Blackmore, V. C. Gibson, N. J. Long, E. L. Marshall and A. J. White, *Dalton Trans*, 2006, **25**, 3134-3140.
36. The SCiFinder Scholar, search for "metal+ ring-opening polyemerisation", (accessed March, 2023).
37. O. Dechy-Cabaret, B. Martin-Vaca and D. Bourissou, *Chem. Rev.*, 2004, **104**, 6147-6176.
38. C. K. Williams, L. E. Breyfogle, S. K. Choi, W. Nam, V. G. Young, M. A. Hillmyer and W. B. Tolman, *J. Am. Chem. Soc*, 2003, **125**, 11350-11359.
39. V. Poirier, T. Roisnel, J. F. Carpentier and Y. Sarazin, *Dalton Trans*, 2009, DOI: 10.1039/b917799j, 9820-9827.
40. A. Hofman, S. Slomkowski and S. Penczek, *Makromol. Chem., Rapid Commun.*, 1987, **8**, 387.
41. A. Hofman, S. Słomkowski and S. Penczek, *Die Makromol. Chemie: Macromol Chem Phys*, 1984, **185**, 91-101.
42. Z. Grobelny, S. Golba and J. Jurek-Suliga, *Polym. Bull.*, 2018, **76**, 3501-3515.
43. N. Nomura, A. Taira, T. Tomioka and M. Okada, *Macromolecules*, 2000, **33**, 1497-1499.
44. R. Carballo, A. Castiñeiras, B. Covelo, E. García-Martínez, J. Niclós and E. M. Vázquez-López, *Polyhedron*, 2004, **23**, 1505-1518.
45. A. Arbaoui, C. Redshaw, D. L. Hughes and M. R. J. Elsegood, *Inorg. Chim. Acta*, 2009, **362**, 509-514.
46. Y. F. Al-Khafaji, T. J. Prior, L. Horsburgh, M. R. J. Elsegood and C. Redshaw, *ChemistrySelect*, 2017, **2**, 759-768.
47. V. Gibson and A. Edwards, *J. Chem. Soc., Dalton Trans.*, 1997, 3343-3348.
48. M. Braun, *Angew. Chem., Int. Ed. Engl.*, 1996, **35**, 519-522.
49. A. F. A. Alshamrani, O. Santoro, S. Ounsworth, T. J. Prior, G. J. Stasiuk and C. Redshaw, *Polyhedron*, 2021, **195**.
50. S. Mitu and M. C. Baird, *Organometallics*, 2006, **25**, 4888-4896.
51. E. Halevas, A. Hatzidimitriou, M. Bertmer, A. A. Vangelis, A. Antzara, C. Mateescu and A. Salifoglou, *Cryst. Growth Des.*, 2014, **14**, 4041-4059.
52. Y. Qiu, K. Wang, Y. Liu, H. Deng, F. Sun and Y. Cai, *Inorg. Chim. Acta*, 2007, **360**, 1819-1824.

53. L.N. Zhu, S. Gao, L.H. Huo and H. Zhao, *Acta Crystallogr., Sect. E: Struct. Rep. Online*, 2005, **61**, m2646-m2648.
54. D.-Y. Ma, *Inorg. Chim. Acta*, 2012, **392**, 440-445.
55. R. Tapscott, R. Belford and I. Paul, *Coord. Chem. Rev.*, 1969, **4**, 323-359.
56. V. Gibson and M. J. Elsegood, *J. Chem. Soc., Dalton Trans.*,, 1997, 3207-3212.
57. A. F. Alshamrani, T. J. Prior, B. P. Burke, D. P. Roberts, S. J. Archibald, L. J. Higham, G. Stasiuk and C. Redshaw, *Inorg. Chem.*, 2020, **59**, 2367-2378.
58. R. Tacke, C. Burschka, I. Richter, B. Wagner and R. Willeke, *J. Am. Chem. Soc*, 2000, **122**, 8480-8485.
59. J. Collins, O. Santoro, T. J. Prior, K. Chen and C. Redshaw, *J. Mol. Struct.*, 2021, **1224**.
60. H. Howard-Lock, C. Lock and M. Martins, *Can. J. Chem.*, 1991, **69**, 1721-1727.
61. Y. F. Al-Khafaji, M. R. J. Elsegood, J. W. A. Frese and C. Redshaw, *RSC Adv.*, 2017, **7**, 4510-4517.
62. A. G. Blackman, *C. R. Chim.*, 2005, **8**, 107-119.
63. T. Schwarz, D. Hess and P. Klufers, *Dalton Trans*, 2010, **39**, 5544-5555.
64. U. Ryde, *Biophys. J.*, 1999, **77**, 2777-2787.
65. Z. Chen, B. Chen and J. Cheng, *Chin. J. Struct. Chem.*, 2021, **40**, 182-186.
66. C. Redshaw, M. R. Elsegood and K. E. Holmes, *Angew Chem Int Ed Engl*, 2005, **44**, 1850-1853.
67. C. Redshaw and M. R. J. Elsegood, *Angew. Chem.*, 2007, **119**, 7597-7601.
68. D. A. Haynes and M. A. Blackie, *HTS Theological Studies*, 2021, **77**, 1-8.
69. Process NMR Associates LLC online, http://www.process-nmr.com/pdfs/NMR%20Overview.pdf, (accessed September 2022).
70. L. M. Jackman and S. Sternhell, *Application of Nuclear Magnetic Resonance Spectroscopy in Organic Chemistry: International Series in Organic Chemistry*, Elsevier, 2013.
71. K. E. Johnson, *Phys. Perspect.*, 2004, **6**, 295-309.
72. R. C. Hewitt, S. Meiboom and L. C. Snyder, *J. Chem. Phys.*, 1973, **58**, 5089-5095.
73. H. Duddeck and M. Kaiser, *Org. Magn. Reson.*, 1982, **20**, 55-72.
74. W. Henderson and J. S. McIndoe, *Mass Spectrometry of Inorganic and Organometallic Compounds: Tools-Techniques-Tips*, Wiley, New Jersey, 2005.
75. E. De Hoffmann and V. Stroobant, *Mass spectrometry: principles and applications*, Wiley, New Jersey, 2007.
76. M. Y. Combariza and R. W. Vachet, *Anal. Chim. Acta*, 2003, **496**, 233-248.
77. W. Henderson and J. S. McIndoe, in Mass Spectrometry of Inorganic and Organometallic Compounds: Tools-Techniques-Tips, Wiley, New Jersey, 2005, ch. 5, pp. 153-173.
78. C. S. Ho, C. Lam, M. H. Chan, R. Cheung, L. Law, L. Lit, K. Ng, M. Suen and H. Tai, *Clin. Biochem. Rev.*, 2003, **24**, 3.
79. S. Nguyen and J. B. Fenn, *Proc. Natl. Acad. Sci.*, 2007, **104**, 1111-1117.
80. J. S. McIndoe and K. L. Vikse, *J Mass Spectrom*, 2019, **54**, 466-479.
81. G. Y. Nagesh, K. Mahendra Raj and B. H. M. Mruthyunjayaswamy, *J. Mol. Struct.*, 2015, **1079**, 423-432.
82. H. Räder and W. Schrepp, *Acta Polym.*, 1998, **49**, 272-293.
83. K. Okamoto, *R&D Review of Toyota CRDL*, 2006, **41**, 29-34.

84. Wikipedia Online, https://en.wikipedia.org/wiki/Matrix-assisted_laser_desorption/ionization, (accessed October 2022).
85. R. P. Paitandi, R. K. Gupta, R. S. Singh, G. Sharma, B. Koch and D. S. Pandey, *Eur. J. Med. Chem.*, 2014, **84**, 17-29.
86. LibreTexts chemistry online, https://chem.libretexts.org/Bookshelves/Analytical_Chemistry/Physical_Methods_in_Chemistry_and_Nano_Science_(Barron)/04%3A_Chemical_Speciation/4.02%3A_IR_Spectroscopy, (accessed September 2022).
87. K. Nakamoto, J. Fujita, S. Tanaka and M. Kobayashi, *J. Am. Chem. Soc*, 1957, **79**, 4904-4908.
88. L. C. Nathan, *J. Chem. Educ.*, 1974, **51**, 285.
89. V. Zelenak, Z. Vargova and K. Gyoryova, *Spectrochim. Acta, Part A*, 2007, **66**, 262-272.
90. Jenisha, S. T. David and J. P. Priyadharsini, *Int. J. Appl. Eng. Res.*, 2015, **9**, 1-4.
91. P. Gluvchinsky, G. M. Mockler and E. Sinn, *Spectrochim. Acta, Part A*, 1977, **33**, 1073-1077.
92. J. Kovacic, *Spectrochim. Acta, Part A*, 1967, **23**, 183-187.
93. I. Nakagawa, R. Hooper, J. Walter and T. Lane, *Spectrochim. Acta*, 1965, **21**, 1-14.
94. V. S. Shivankar, R. B. Vaidya, S. R. Dharwadkar and N. V. Thakkar, *Synth. React. Inorg. Met.-Org. Chem.*, 2003, **33**, 1597-1622.
95. D. A. Skoog, D. M. West and F. J. Holler, *Fundamentals of analytical chemistry*, cengage learning 1992.
96. F. Kasler, *Anal Biochemistry*, 1980, **103**, 435.
97. AZomaterials Online, https://www.azom.com/article.aspx?ArticleID=20385, (accessed March 2023).
98. W. Kandioller, J. Theiner, B. K. Keppler and C. R. Kowol, *Inorg. Chem. Front.*, 2022, **9**, 412-416.
99. Jordi Labs online, https://jordilabs.com/wp-content/uploads/filebase/White_Paper_GPC_Conventional_v_Light_Scattering.pdf, (accessed December 2022).
100. M. Nikookar, M. R. Omidkhah, G. R. Pazuki and A. H. Mohammadi, *J. Mol. Liq.*, 2022, **362**.
101. G. Saunders and B. Maccreath, A Guide to Multi-Detector Gel Permeation Chromatography Contents. Agil. GPC Backgr 2012 online, https://www.agilent.com/cs/library/primers/Public/5990-7196EN.pdf (accessed on March 2023).
102. M. Ambler, *J. Polym. Sci., Polym. Chem. Ed.*, 1973, **11**, 191-201.
103. M. Nikookar, M. R. Omidkhah, G. R. Pazuki and A. H. Mohammadi, *Journal of Molecular Liquids*, 2022, **362**, 119736.
104. K. Hasegawa, *Rigaku J.*, 2012, **28**, 14-18.
105. LibreTexts chemistry online, https://chem.libretexts.org/Bookshelves/Organic_Chemistry/Map%3A_Organic_Chemistry_(Bruice)/14%3A_NMR_Spectroscopy/14.23%3A_X-Ray_Crystallography, (accessed March 2023).
106. W. Clegg, *X-ray Crystallography*, Oxford University Press, USA, 2015.

107. CSIC online, https://www.xtal.iqfr.csic.es/Cristalografia/parte_02-en.html, (accessed March 2023).
108. Y. Waseda, E. Matsubara and K. Shinoda, *X-ray diffraction crystallography: introduction, examples and solved problems*, Springer Science & Business Media, 2011.
109. L. Ooi, *Principles of X-ray Crystallography*, Oxford University Press, 2010.
110. M. H. Chisholm and E. E. Delbridge, *New J Chem*, 2003, **27**, 1177-1183.

Chapter 2. Alkoxy-functionalized Schiff-base ligation at aluminium and zinc for ring-opening polymerisation

2.1 Introduction

The use of Schiff-base or as it is sometimes called phenoxyimine (FI) ligation in metal-based catalysis has seen some notable successes in recent years. For example, in α-olefin polymerisation, researchers at the Mitsui Chemical Corp. achieved both increased thermal stability and very high activity for vanadium-based systems of the type $[VO(FI)_2]$.[1] The use of pendant functionality has also proved to be an area of promise.[2] As catalysis researchers have turned their attention to more potentially environmental polymers, the use of Schiff-base ligation has remained a central theme. In particular, their use in the ROP of cyclic esters has led to catalysts employing the metals aluminium and zinc.[3-7] Given the sterics and electronics associated with the coordination geometry at the metal allow for the manipulation of the ROP process, numerous combinations of different Schiff-base ligands have been studied. However, the use of Schiff-base ligands bearing multiple alkoxy substituents is limited, despite the ready availability of suitable precursors. In other catalytic studies, Guo[8] previously reported iron(II) 2,6-bis(imino)pyridyl complexes bearing bulky *para* substituents (R = CH_3, OCH_3) at the aniline and their catalytic properties in ethylene polymerisation. It was found that the electron-donating methoxy substituent resulted in a slight decrease in catalytic activity, but a significant increase in molecular weight compared with the methyl analogue. Ghaffari[9] has also investigated the position effects (*ortho*, *meta*, *para)* of methoxy substituents for nickel(II) complexes and utilized such complexes for the epoxidation of cyclooctene. It is noted that in salen-based nickel chemistry, the presence of the methoxy substituents has led to enhanced activity and increased selectivity for epoxidations. Thus, in this chapter, a program has been initiated to screen Schiff-base ligands derived from anilines bearing alkoxy substituents. The effect on the catalytic activity of the ROP of cyclic esters of different substitution patterns for the electron-donating methoxy substituent groups at the aniline derived moiety of bidentate *N*,*O*-Schiff base is investigated. It is desirable that the catalyst is cheap and readily accessible and so this work has focused on the earth abundant metals aluminium and zinc. The use of main-group metal ROP catalysts has been reviewed[3,5], and other reviews have focused on the use of aluminium[4,6] and more recently Schiff-base ligation.[7]

In this chapter, a systematic study of the steric and electronic effect of methoxy substituents at the aniline derived ring in a series of Schiff-base organoaluminium and zinc complexes has been conducted. By comparing *ortho* or *meta* substituents on the aniline moiety, *i.e.* 2,4,6- and 3,4,5-

substituted anilines, and by varying the number of substituents on the ring, *i.e.* 2,4- *versus* 2,4,6- or with no methoxy substituent group, as shown in Figure 2-1. All Schiff-base complexes were applied to the ring opening polymerisation of ε-CL. One of the complexes was further investigated for the copolymerisation of ε-CL and glycolide (GL), as well as forming cross-linked PCL in the presence of 4,4’-bioxepane-7,7’-dione.

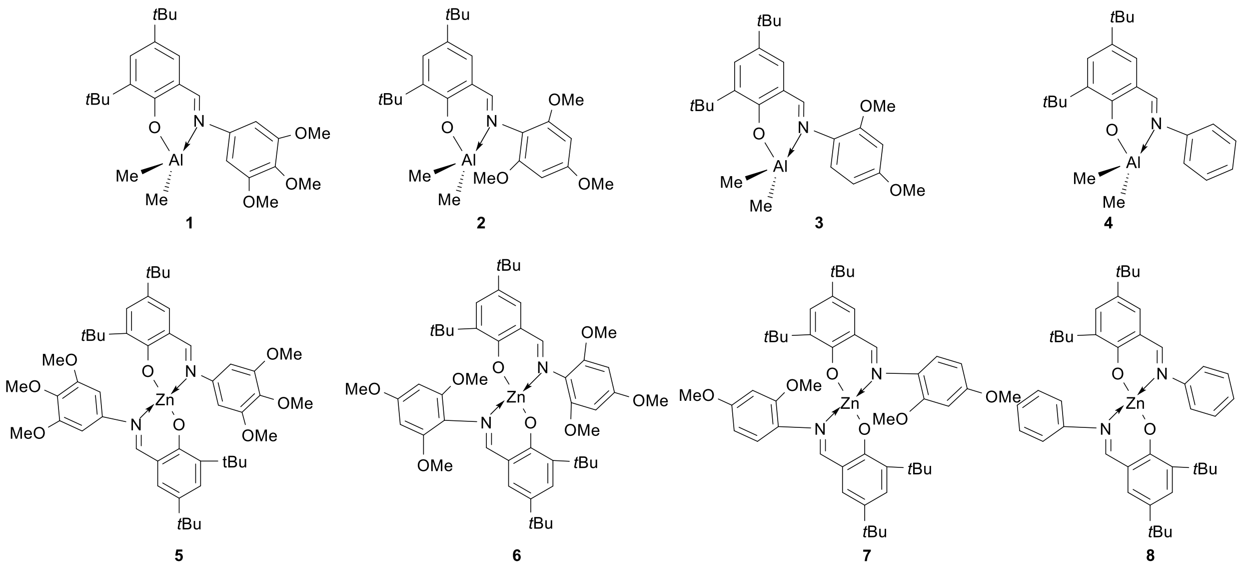

Figure 2-1. Structures of the aluminium and zinc complexes **1**–**8** prepared herein.

2.2 Results and discussion

2.2.1 Synthesis and characterisation of Schiff-base aluminium complexes

The organoaluminium complexes **1**, **2** and **3**, bearing the phenoxy-imines L^1, L^2 and L^3 respectively, were prepared by reaction of $AlMe_3$ with one equivalent of the parent phenoxyimine (L^1H = 2,4-di-*tert*-butyl-6-(((3,4,5-trimethoxyphenyl)imino)methyl)phenol, L^2H = 2,4-di-*tert*-butyl-6-(((2,4,6-trimethoxyphenyl)imino)methyl)phenol) and L^3H = dimethoxyphenyl)imino)methyl)phenol) in toluene. These reactions took place along with the evolution of methane[10], and following work-up, analytically pure yellow needle-shaped crystals were collected from the saturated solution of acetonitrile at 5 ^{o}C in 52% (**1**), 34% (**2**), 64% (**3**) yields, respectively. In the ^{1}H NMR spectra of **1**-**3** (Figures 2-2, 2-3, 2-4), the disappearance of the peak corresponding to the hydroxyl proton of ligand was observed; and a sharp single resonance is ascribed to the Al-Me$_2$ protons at -0.79, -1.00, -0.93 ppm, respectively; a resonance is ascribed to the C*H*=N proton at δ: 8.82 ppm for **1**, 8.58 ppm for **2**, or 8.58 ppm for **3**, respectively. All evidence proved the formation of the aluminium complexes was successful. In the aromatic region for complexes **1**-**3**, doublet peaks are observed for proton H$_g$ and H$_h$, with J_{gh} coupling constants in the range 2.5-2.8 Hz which is consistent with coupling across *meta* positions.[11] For complexes **1** and **2**, the two protons of H$_f$ have the same chemical shift, and no splitting is observed. However, for complexes **3**, H$_f$, H$_j$ and H$_k$ have different chemical environments.

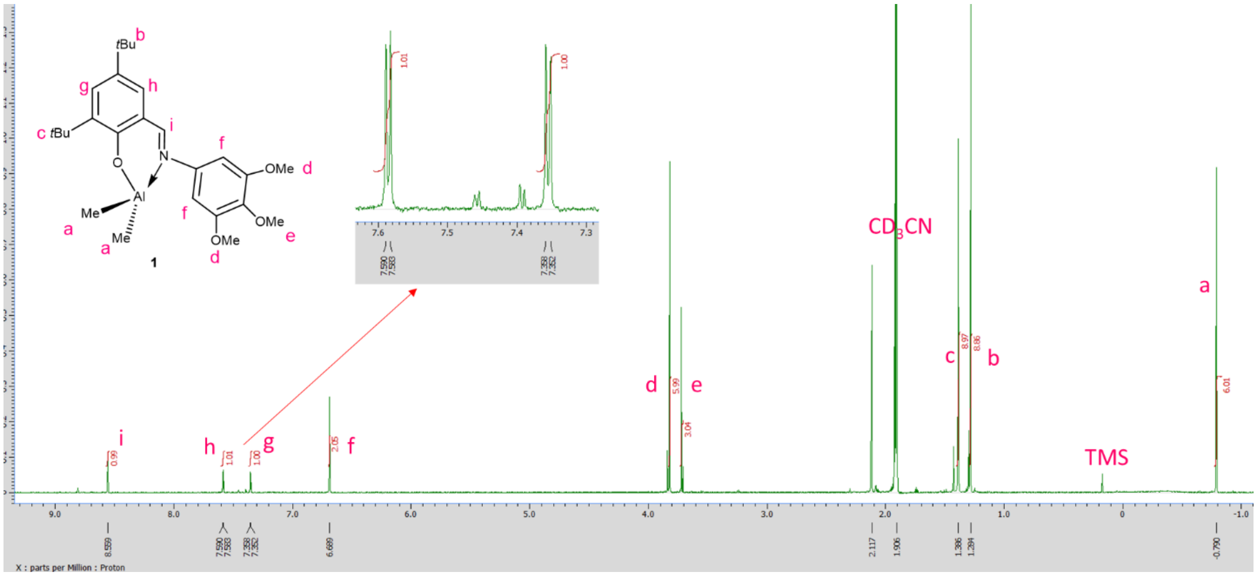

Figure 2-2. ^{1}H NMR spectrum (400 MHz, CD$_3$CN) of **1**.

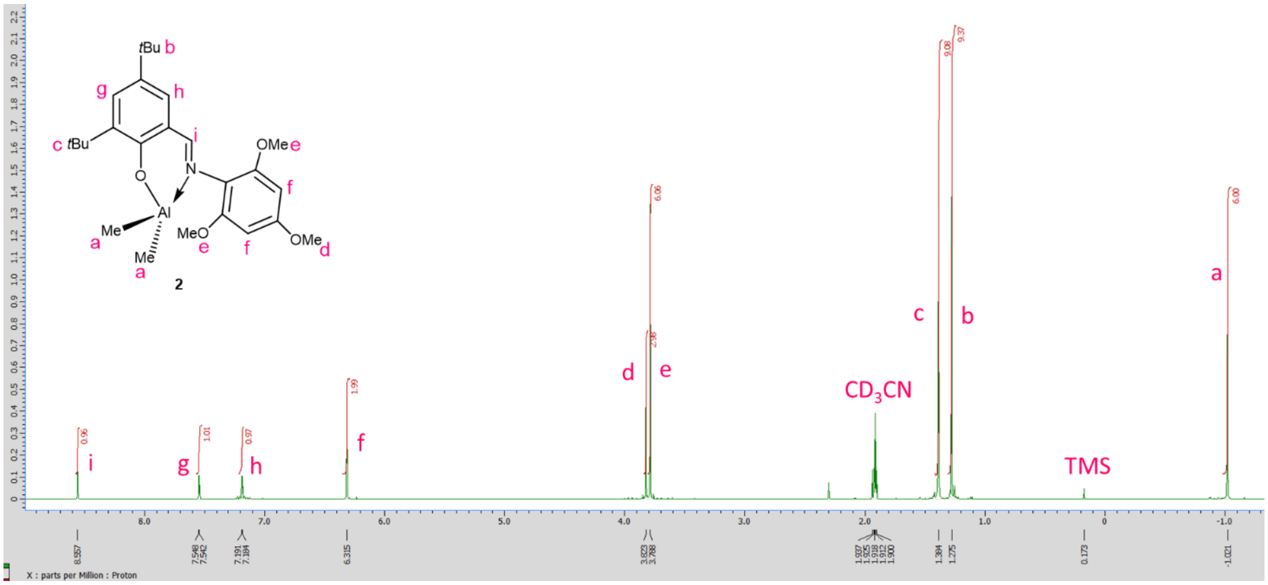

Figure 2-3. ^{1}H NMR spectrum (400 MHz, CD_3CN) of **2**.

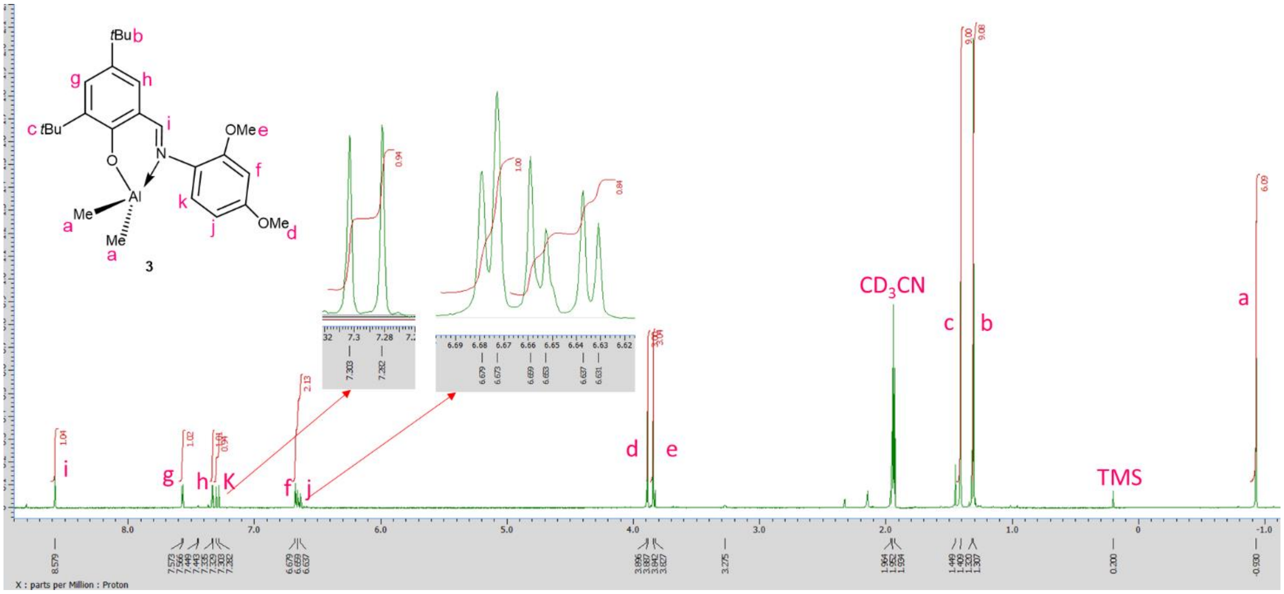

Figure 2-4. ^{1}H NMR spectrum (400 MHz, CD_3CN) of **3**.

The IR spectrum of **1** (Figure 1, appendix) contains an absorption band at 1613 cm^{-1} assigned to C=N. The C=N stretching frequency of the parent L^{1}H (Figure 4, appendix) is found at 1614 cm^{-1}, which is consistent with the observation of Sarma and Bailar[12] who reported no shift in

C=N band frequency even after complexation. The coordination of the azomethine nitrogen is further supported by the appearance of a new band at 587 cm^{-1} due to the Al–N band. The stretching vibration observed at 1249 cm^{-1} is attributed to the phenolic C–O vibration of L^1.[13] [14] For **1**, the shift of this band to a lower frequency at 1237 cm^{-1} indicates the bonding of the ligand to the metal atom through oxygen. The formation of the Al–O bond is supported by the appearance of medium bands in the region of 708 cm^{-1}. The absorption at 609 cm^{-1} is assigned to Al–C band.[14] The IR spectra of **2** and **3** (Figures 2 and 3, appendix) are similar to **1**. The strong absorption at 1614 cm^{-1} is assigned to the C=N stretching band. Compared to the free ligand (1619 cm^{-1}), the C=N stretching band of **2** is slightly shifted to a lower frequency. The important IR bands are summarized in Table 2-1. The solid-state structures of the aluminium complexes **1**–**3** are consistent with their ^{1}H NMR spectra, elemental analysis and mass spectrometry data. Strong absorption peaks observed around 2956-2853, 1465-1450, and 1377-1378 cm^{-1} are due to Nujol.[15] In this research work, the Nujol mull method was applied to protect air sensitive complexes during the acquisition of their IR spectrum.

Table 2-1. Some relevant IR spectral data of complexes **1-3, 5-7** and L$^{1\text{-}3}$H (cm^{-1})

Compound:	***v*C=N**	***v*C-O**	***v*M-O**	***v*M-N**	***v*Al-C**
1	1613	1237	708	587	609
2	1614	1230	705	575	604
3	1615	1240	755	579	676
5	1612	1237	661	598	–
6	1614	1227	687	571	–
7	1616	1258	–	–	–
L^{1}H	1614	1249	–	–	–
L^{2}H	1619	1230	–	–	–
L^{3}H	1616	1250	–	–	–

The molecular structures of **1**, **2** and **3** were further verified by single crystal X-ray analysis (Figure 2-5 and Table 2-2). The Al centres in **1**, **2** and **3** are four-coordinate with a bidentate *N*,*O*-chelate and two methyl ligands. Complex **1** crystallises in space group $P4_2/n$ with coordination geometry around the metal centre described as distorted tetrahedral; angles range from 94.59(10) to 119.12(16)°. The most "acute" angle is associated with the bite angle of the chelate ligand [94.59(10)°], which is close to those previously reported for [L$^{\text{ClBu}}$-AlMe$_2$(5)] [93.32(6)°][16] (L$^{\text{ClBu}}$ = 4-ClC$_6$H$_4$CH=NN=CHC$_6$H$_2$-2-(O)-3,5-*t*Bu) and Me$_2$Al[O-2-Me-6-(R$_2$N=CH)C$_6$H$_3$] [R$_2$=2,6-

i$Pr_2C_6H_3$] [93.68(7)^{o}][17], [Me_2AlL^{hyd}] ($L^{hyd}H$ = 2,4-di-*tert*-butyl-6-(2,6-dibenzylhydryl-4-isopropylphenylimino)methyl)phenol) [94.14(8)^{o}][18]. The Al–C bond distances in **1** [Al(1)–C(22) 1.955(4) Å, Al(1)–C(23) 1.961(3) Å] are typical, while the Al(1)–O(1) bond length is [1.765(2) Å], indicative of a σ-bond.[18] The Al(1)–N(1) bond distance in **1** [1.980(3) Å] is longer than those in [$Me_2NC(N$*i*$Pr)_2AlCl_2$] [1.872(3) Å][19], consistent with dative type bonding.

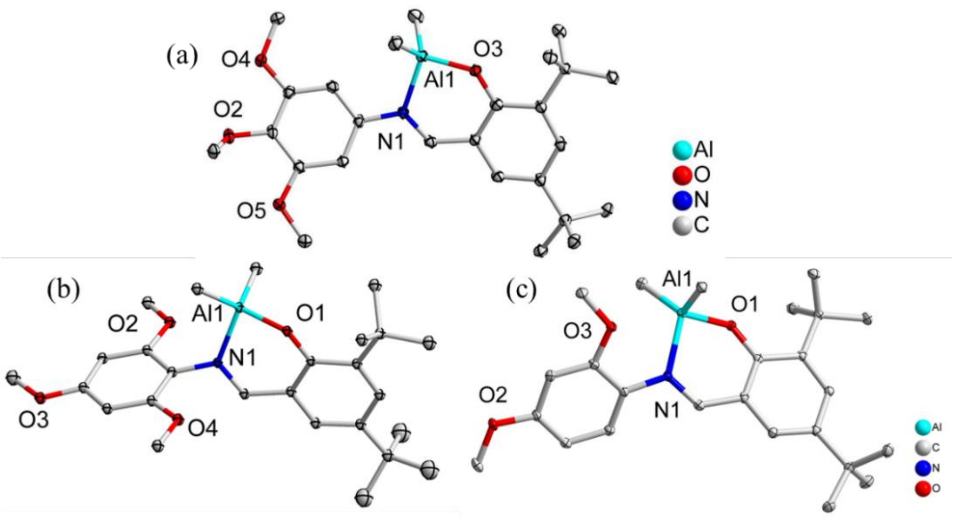

Figure 2-5. ORTEP drawing (20% probability) of complexes (**a**) [$Al(L^1)(Me)_2$] (**1**); (**b**) [$Al(L^2)(Me)_2$] (**2**); (**c**) [$Al(L^3)(Me)_2$] (**3**). Hydrogen atoms are omitted for clarity.

Table 2-2. Selected bond lengths (Å) and angles (°) for the complexes **1-3**, **5-7**

	1	**2**	**3**		**5**	**6**	**7**
Bond length (Å)							
Al(1)-O(1)	1.7650(2)	1.7895(11)	1.8038(8)	Zn(1)-O(1)	1.9077(15)	1.9335(19)	1.9583(17)
Al(1)-C(22)	1.9550(4)	1.9592(17)	1.9626(12)	Zn(1)-O(2)	1.9088(15)	1.9338(18)	1.9573(18)
Al(1)-C(23)	1.9610(3)	1.9614(17)	1.9652(12)	Zn(1)-N(1)	1.9998(18)	2.026(2)	2.027(3)
Al(1)-N(1)	1.9800(3)	1.9570(14)	1.9923(10)	Zn(1)-N(2)	2.0089(18)	2.032(2)	2.026(2)
Bond angles (°)							
O(1)-Al(1)-C(22)	109.08(14)	109.00(6)	107.68(5)	O(1)-Zn(1)-O(2)	122.14(7)	97.45(8)	117.54(8)
O(1)-Al(1)-C(23)	113.48(13)	112.77(6)	105.41(4)	O(1)-Zn(1)-N(1)	96.84(7)	93.54(9)	101.30(8)
C(22)-Al(1)-C(23)	119.12(16)	121.35(7)	123.31(5)	O(2)-Zn(1)-N(1)	111.25(7)	146.25(9)	91.96(9)
O(1)-Al(1)-N(1)	94.59(10)	93.74(5)	91.19(4)	O(1)-Zn(1)-N(2)	111.20(7)	138.49(8)	92.29(8)
C(22)-Al(1)-N(1)	108.91(13)	110.62(7)	111.29(5)	O(2)-Zn(1)-N(2)	95.76(7)	92.70(8)	105.58(9)
C(23)-Al(1)-N(1)	108.81(13)	105.78(7)	112.63(5)	N(1)-Zn(1)-N(2)	121.63(7)	99.93(8)	149.77(9)

2.2.2 Synthesis and characterisation of Schiff-base zinc complexes

The reactions of L^1H, L^2H or L^3H with one equivalent of $ZnEt_2$ in refluxing toluene readily afforded the bis(chelate) complexes **5**, **6** and **7** (Figure 2-1), respectively. Analytically pure yellow prisms were collected, following work-up, from a saturated solution of acetonitrile at 5 °C in 48% (**5**), 40% (**6**) or 60% (**7**) yields, respectively. In the ^{1}H NMR spectra of **5**, **6** or **7**, a resonance is ascribed to the C*H*=N proton at 8.65 ppm for **5**, 8.36 ppm for **6**, or 8.50 ppm for **7** (Figures 2-6, 2-7, 2-8).

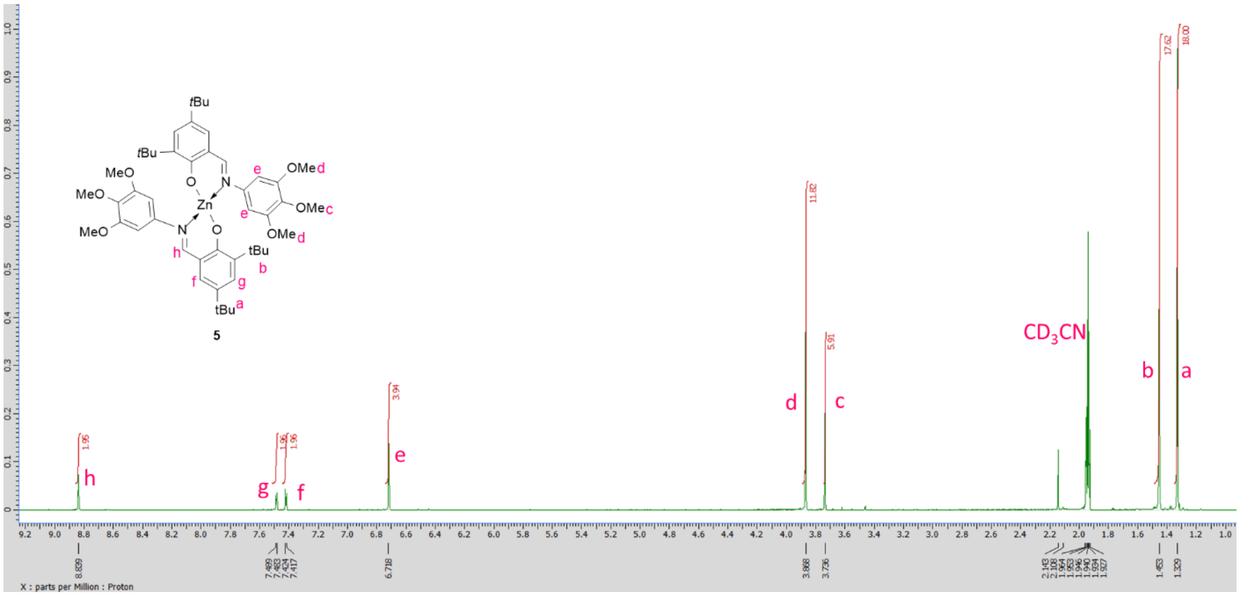

Figure 2-6. ^{1}H NMR spectrum (400 MHz, CD_3CN) of **5**.

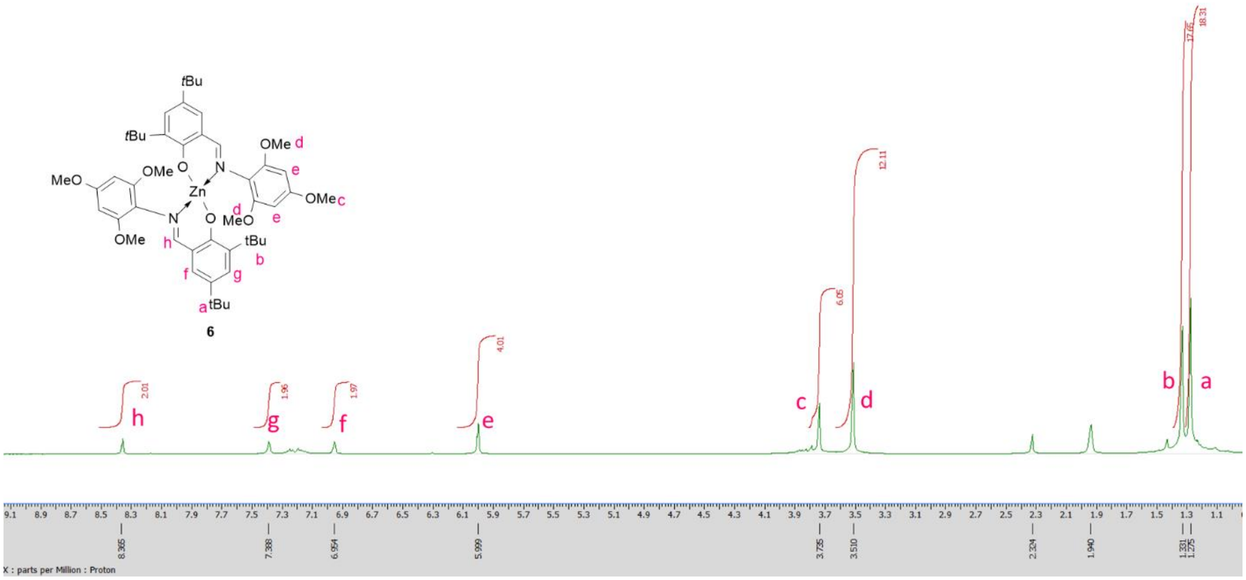

Figure 2-7. ^{1}H NMR spectrum (400 MHz, CD_3CN) of **6**.

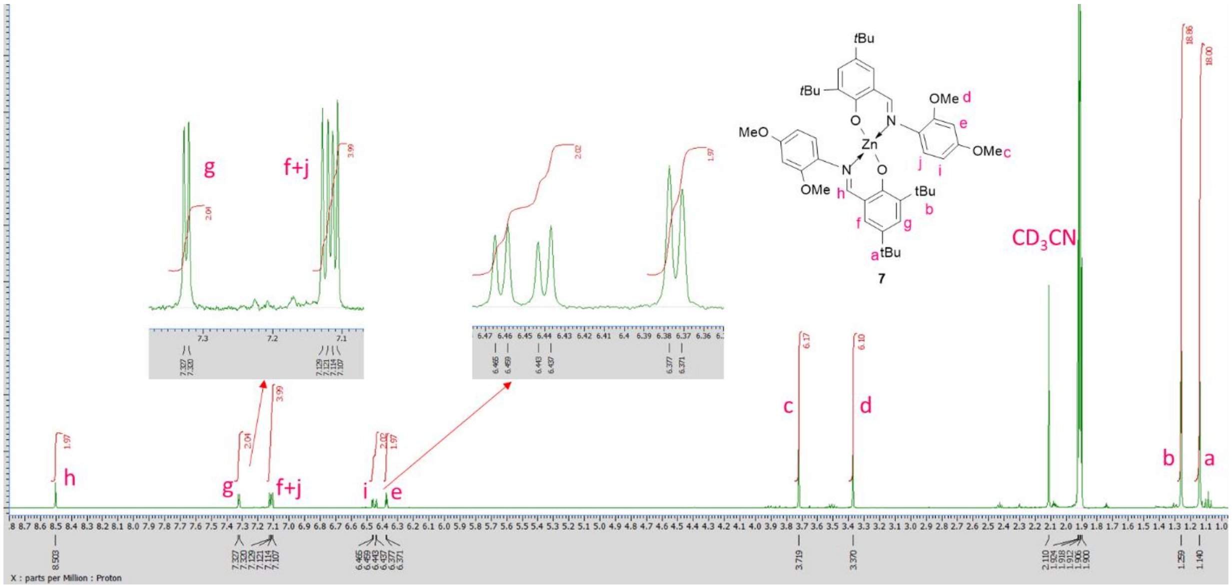

Figure 2-8. ^{1}H NMR spectrum (400 MHz, CD_3CN) of **7**.

The infrared spectra of the complexes **5**, **6** and **7** are collected in Table 2-1 and are compared with that of free ligand to verify the bonding in the complexes. The band in the IR spectrum of L^1 at 1614 cm^{-1} (C=N) is shifted to slightly lower frequencies at 1612 cm^{-1} in **5**, indicating donation of the lone pair of electrons at the azomethine nitrogen to the zinc centre.[20] Moreover, the coordination of the azomethine nitrogen is further supported by the appearance of new band at 598 cm^{-1} assigned to Zn–N. The stretching vibration observed at 1249 cm^{-1} is attributed to the phenolic C–O vibration of L^1.[13] In the complex **5**, the shift to lower frequency at 1237 cm^{-1} indicates the bonding of the ligand to the metal via oxygen. A new band for **5** at 661 cm^{-1} is assigned to Zn–O; the IR spectrums for **6** and **7** are similar to **5**. The structures of the zinc complexes **5**–**7** are consistent with their ^{1}H NMR spectra, elemental analysis and mass spectrometry data.

The molecular structures of **5**, **6** and **7** are presented in Figure 2-9. Selected bond lengths and angles are collated in Table 2-2; crystallographic data are collated in Appendix: Table 1. Complex **5** crystallizes in the orthorhombic space group *Pbca* and each Zn centre in **5** is distorted tetrahedral with two N and two O atoms from two Schiff-base ligands L^1, with angles ranging from 95.76(7)-121.63(7)$^{\circ}$, which are comparable with others reported for analogous square planar Zn(II) species.[21,22] The average bond distances for the Zn(1)–(O) and Zn(1)–(N) bonds are [1.908 Å] and [2.004 Å], respectively, which are comparable with previous reported values.[23-26] The metal ion in **6** (monoclinic space group *I*2/*a*), also adopts a distorted tetrahedral geometry for which the O(1)–Zn(1)–N(1) [93.54(9)$^{\circ}$], O(2)–Zn(1)–N(2) [92.70(8)$^{\circ}$] and O(2)–Zn(1)–O(1) [97.45(8)$^{\circ}$], N(1)–Zn(1)–N(2) [99.93(8)$^{\circ}$] bond angles are smaller than those in **5** [96.84(7)$^{\circ}$, 95.76(7)$^{\circ}$, 122.14(7)$^{\circ}$, 121.63(7)$^{\circ}$, respectively] and **7** [101.30(8), 105.58(9), 117.54(8), 149.77(9)]. Moreover, the O(2)–Zn(1)–N(1) [146.25(9)$^{\circ}$], O(1)–Zn(1)–N(2) [138.49(9)$^{\circ}$] bond angles in **6** are larger than those in **5** [111.25(7)$^{\circ}$ and 111.20(7)$^{\circ}$, respectively] and **7** [91.96(9), 92.29(8)], whilst the Zn(1)–O(2) [1.9573(18) Å] and Zn(1)–N(1) [2.027(3) Å] distances in **7** are longer than in **5** [1.9088(15) Å, 1.9998(18) Å] and **6** [1.9338(18), 2.026(2)]. The observed differences are attributed to the different positions of the methoxy substituents in the aniline derived group.

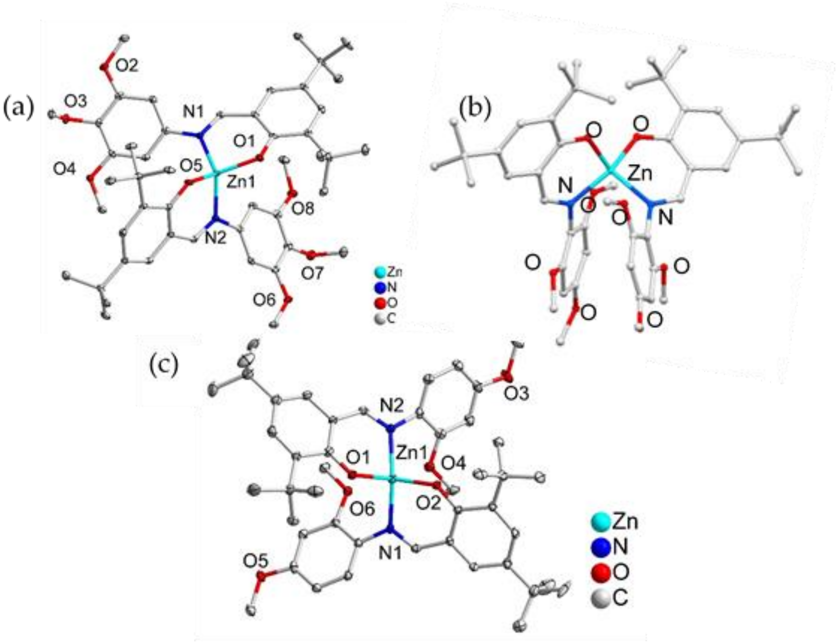

Figure 2-9. ORTEP drawing (20% probability) of complexes (**a**) $[Zn(L^1)_2]$ (**5**); (**b**) $[Zn(L^2)_2]$ (**6**); (**c**) $[Zn(L^3)_2]$ (**7**). Hydrogen atoms are omitted for clarity.

2.2.3 Ring-opening polymerisation studies of ε-CL

Complexes **1**–**8** have been screened for their ability to act as catalysts, in the presence of benzyl alcohol (BnOH), for the ROP of ε-CL and the results are presented in Table 2-3. Results for **1**–**3** and **5**–**7** are compared against the related non-methoxy containing complexes **4**[27] and **8**, respectively. The polymerisation reactions were carried out at 100 °C, using a [CL]:[catalyst]:[BnOH] ratio of 250:1:1. All complexes were found to be active under these polymerisation conditions with similar monomer conversions (>95%) over different times. The aluminium complex **1** can achieve 99% conversion in 40 min., whereas 120, 100 and 120 min. were required for **2**, **3** and **4**, respectively (Table 2-3, entries 1–4). In addition, **1** afforded a larger molecular weight (M_n = 17,000) compared with **2** (M_n = 16,000), **3** (M_n = 16,000) and **4** (M_n = 12,000), and narrow polydispersity indexes **1** (PDI = 1.74) vs. **2** (PDI = 1.87), **3** (PDI = 1.90) and **4** (PDI = 2.41). The results herein indicated that ligands derived from anilines bearing 3,4,5-methoxy substituents favoured the ROP process in terms of rate, molecular weight and control. Looking at the zinc complexes (Table 2-3, entries 5–8), it is evident that **5** bearing Schiff-base ligands with 3,4,5-methoxy substituents is also the most effective catalyst in terms of rate, molecular weight and control. In general, polymers catalysed by the zinc complexes **5**–**8** possessed very narrow distributions (PDI: 1.03–1.18), indicating less transesterification during the polymerisation process.[28] Complex **5** bearing the 3,4,5-methoxy substituents exhibited better activity than did **6** with 2,4,6-methoxy substituents, **7** with 2,4-methoxy substituents and **8** without any methoxy substituents, as was seen for the organoaluminium complexes. These results strongly suggest that the use of 3,4,5-methoxy substituents in complexes of this type favours PCL formation.

During the preliminary experiments, the effect of temperature in the ROP of ε-CL at a fixed ratio of 250:1:1 ([ε-CL]:[catalyst]:[BnOH]) was investigated. At room temperature (25 °C), **1** exhibited no activity for the ROP of ε-CL (Table 2-3, entries 9). When the polymerisation was performed at 50 °C after 18 h, the activity trend followed the order of **1**> **3** > **2** > **4** > **5** > **6** > **7** > **8** (Table 2-3, entries 10–17), which is similar to the trend observed at 100 °C. More specifically, **1** exhibited the best catalytic activity for the ROP of ε-CL, giving 99% conversion. In the case of aluminium, polymer molecular weights were higher at 50 °C and close to the calculated M_n than at 100 °C (e.g., see runs 1 and 10, Table 2-3), which suggests that the active species is approaching its thermal stability level at the higher temperature.[29] At 50 °C, only 18–30% of the monomer was converted to polymer over 18 h using the zinc complexes, *i.e.*, the polymerisation is much slower compared with 100 °C (Table 2-3, entries 14–17).

To gain more insight into the polymerisation mechanism, **1** and **5** with differing amounts of benzyl alcohol were used as catalysts for the ROP of ε-CL. In the absence of BnOH, the polymerisation of ε-CL catalysed by **1** proceeded fastest, reaching 99% conversion in 35 min. at 100 °C (Table 2-3, entry 22). The resultant PCL had a larger M_n (76,000) than the theoretical M_n value, and a broad polydispersity (PDI = 2.75) indicative of a less controlled process likely due to backbiting or transesterification.[30] Increasing the ratio of [BnOH]:[catalyst] from 1 to 2 and 4 decreased the polymerisation rate. For example, in the presence of 4 equiv. of BnOH, a conversion of 99% was achieved over a longer polymerisation time (120 min.). The results indicated that the addition of BnOH led to slower monomer conversion and decreased molecular weight (Table 2-3, entry 22–25). In the presence of 1 equiv. of BnOH, **1** exhibited similar activity to the system used in the absence of BnOH, whereas excess BnOH led to a decrease. This is thought to be due to the decomposition of the catalyst.[31] For complex **5**, the absence of BnOH slowed the monomer conversion and poor control was noted (Table 2-3, entry 26). When the ratio of $[BnOH]_0$:$[catalysts]_0$ is 1, the conversion reached 51% after 2 h which is the best compared with other ratios and the system exhibited good control (PDI = 1.03). The results indicated that BnOH is necessary in the zinc systems for enhanced control and acceleration of the polymerisation process, however increasing the amount of BnOH proved detrimental to conversion, molecular weight and control (Table 2-3, entries 27–29).

Table 2-3. The ROP of ε-CL catalysed by **1-8**[a].

Run	**Complex**	**[CL]:[Cat] :[BnOH]**	**T(°C)**	**Time (min)**	**Conversion (%)**[b]	**M_n,calc (Da)**[c]	**$M_{n,GPC}$ (Da)**[d]	**$M_{W,GPC}$ (Da)**[d]	***PDI***[e]
1	**1**	250:1:1	100	40	99	28358	17000	28000	1.74
2	**2**	250:1:1	100	120	99	28358	16000	30000	1.87
3	**3**	250:1:1	100	100	98	27183	16000	30200	1.90
4	**4**	250:1:1	100	120	99	28358	12000	28100	2.41
5	**5**	250:1:1	100	460	95	27183	14500	15000	1.03
6	**6**	250:1:1	100	720	99	28358	6700	7300	1.10
7	**7**	250:1:1	100	470	98	28072	7100	8300	1.18
8	**8**	250:1:1	100	1560	95	27183	7800	9100	1.18
9	**1**	250:1:1	25	720	4	-	-	-	-
10	**1**	250:1:1	50	1080	99	28358	22100	33000	1.46
11	**2**	250:1:1	50	1080	90	25790	20000	39000	1.96
12	**3**	250:1:1	50	1080	95	27183	21000	34000	1.62
13	**4**	250:1:1	50	1080	85	24363	20237	39000	1.93
14	**5**	250:1:1	50	1080	30	8669	5900	7000	1.20
15	**6**	250:1:1	50	1080	20	5821	3400	4400	1.28
16	**7**	250:1:1	50	1080	19	5530	3300	4300	1.29
17	**8**	250:1:1	50	1080	18	5821	5700	6800	1.20
18	**1**	250:1:1[f]	100	720	99	28358	9200	16000	1.75
19	**5**	250:1:1[f]	100	720	7	-	-	-	-
20	**1**	125:1:1	100	120	99	14233	7300	11300	1.56
21	**1**	500:1:1	100	120	99	56716	24000	49400	2.04
22	**1**	250:1:0	100	35	99	28250	76000	210000	2.75
23	**1**	250:1:1	100	40	99	28358	17000	28000	1.74
24	**1**	250:1:2	100	115	99	14233	6500	14600	2.25
25	**1**	250:1:4	100	120	99	7200	3900	6200	1.60
26	**5**	250:1:0	100	120	40	28250	25500	62500	2.45
27	**5**	250:1:1	100	120	51	27183	14500	15000	1.03
28	**5**	250:1:2	100	120	26	8125	7800	10500	1.34
29	**5**	250:1:4	100	120	13	4959	4000	5300	1.33

---

[a] Polymerisations were carried out in toluene, $[CL]_0$= 2 M. [b] Determined by ^{1}H NMR spectroscopy. [c]M_n, calcd=($[CL]_0/[cat]_0$)×Conv.%×114.14; In the presence of BnOH, $M_{n,cal}$ =114.14 × ($[CL]_0$/($[BnOH]_0$) × conv. (%) + 108.13. [d] Obtained from GPC analysis and calibrated against the polystyrene standard, multiplied by 0.56. [e] Obtained from GPC analysis. [f] Reactions were carried out under air.

On the other hand, the ROP of **1** reached a high conversion (99%) after 120 min. when the catalyst concentration was half ([CL]:[catalyst]:[BnOH] = 500:1:1) (Table 2-3, entry 21). As expected, the M_n values could be controlled by varying the CL:catalyst molar ratio (125:1, 250:1, 500:1) (Table 2-3, run 1, 20–21).

The air stability of these complexes was examined; **1** and **5** were used to initiate the polymerisation of ε-CL at 100 °C with a [CL]:[catalyst]:[BnOH] ratio of 250:1:1 under air. Surprisingly, complex **1** successfully initiated the polymerisation of ε-CL under air after 720 min. with a 99% conversion. However, **5** failed to initiate the polymerisation under the same conditions (Table 2-3, entries 18–19). These results revealed that complex **1** can tolerate moisture during the polymerisation process.

Kinetic studies were performed using **1**–**8**. Plots of $\ln([CL]_0/[CL]_t)$ *versus* time are shown in Figure 2-10 (aluminium complexes **1**–**4**) and Figure 2-11 (zinc complexes **5-8**). Semilogarithmic plots obtained when using aluminium complexes are curves, which implied the polymerisations of ε-CL proceeded in two stages: the first is an induction period then followed by a first-order linear relationship dependence of monomer concentration (Figure 2-10). It is notable that all aluminium catalysts showed different induction periods depending on the type of catalysts. To clarify whether the induction period was caused by the presence of BnOH, the ROP of ε-CL using **1** without BnOH was investigated. This significant induction period (approximately 20 min.) also existed in the absence of BnOH for complex **1** (Figure 2-12, Table 2-3, entry 22). These results suggest that the induction periods in the ROP of ε-CL were not caused by the coordination between aluminium complexes and BnOH when forming the active alkoxide species, but could be caused by the coordination between ε-CL and the aluminium complexes.[32] Specifically, the induction period could be caused by the breakage of the Al-Me bond. The calculated slope of the linear section of the curve is equal to the apparent polymerisation rate constant.[33] The aluminium complex **1** displayed the highest catalytic activity (k_{obs} = 2562 × 10^{-4} min^{-1}, R = 0.9764) compared to **3**, **2** and **4** (k_{obs} = 1253 × 10^{-4} min^{-1}, R = 0.9924; k_{obs} = 903 × 10^{-4} min^{-1}, R = 0.9986; k_{obs} = 729 × 10^{-4} min^{-1}, R = 0.9973, respectively).

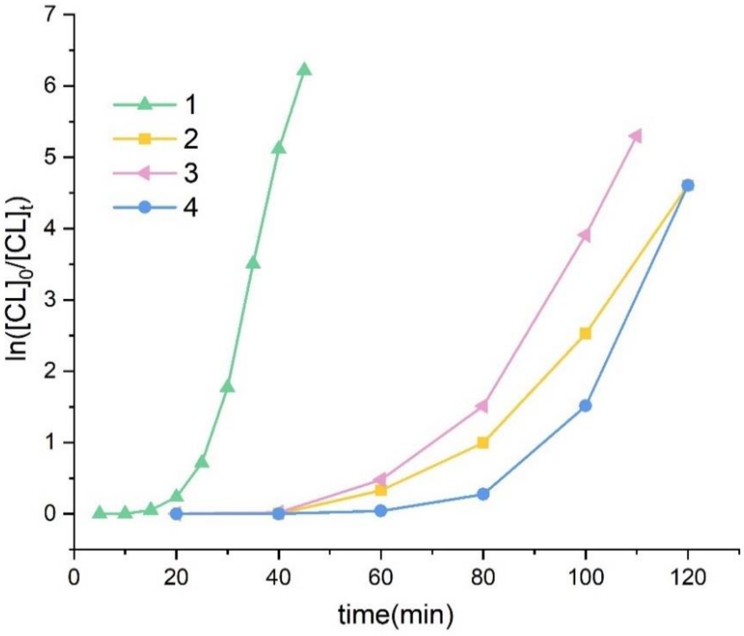

Figure 2-10. Plots of ln([CL]$_0$/[CL]$_t$) *versus* time catalysed by aluminium complexes **1-4**; Reaction conditions: [CL]:[catalyst]:[BnOH] = 250:1:1 at 100 °C.

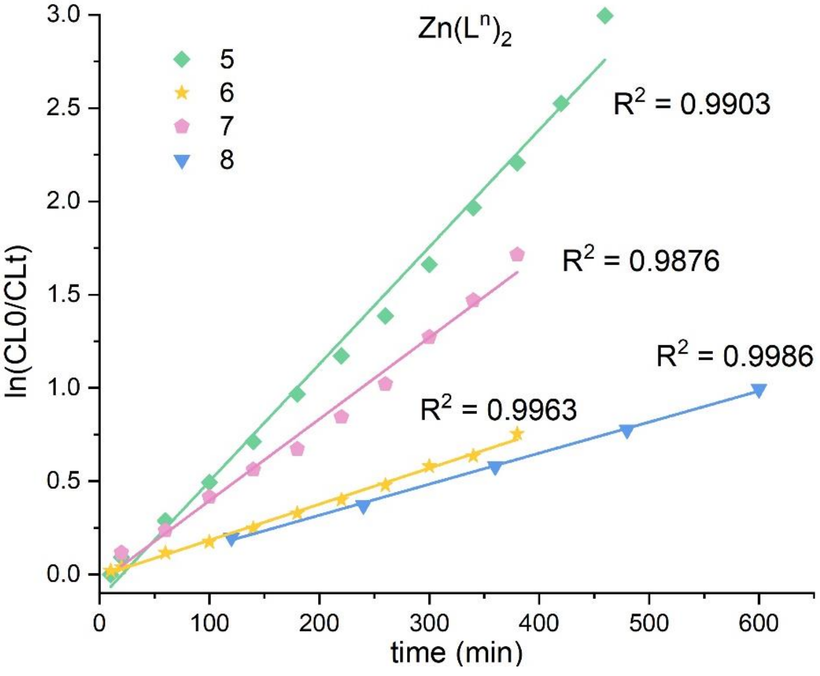

Figure 2-11. Plots of ln([CL]$_0$/[CL]$_t$) *versus* time catalysed by zinc complexes **5-8**; Reaction conditions: [CL]:[catalyst]:[BnOH] = 250:1:1 at 100 °C.

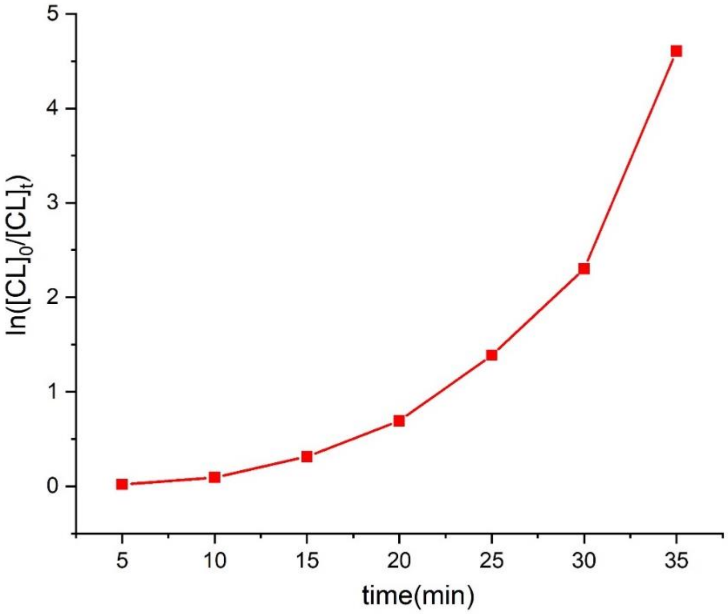

Figure 2-12. Plot of $\ln([CL]_0/[CL]_t)$ *vs* time, [ε-CL]:[**1**]:[BnOH] = 250:1:0 at 100 °C according to the conditions in Table 2-3, entry 22.

The zinc systems (Figure 2-11) exhibited a near linear relationship, which implied that the polymerisation followed a first-order dependence on the monomer concentration and the polymerisation was controllable. Zinc complex **5** exhibited a better catalytic activity ($k_{obs} = 63 \times 10^{-4}$ min^{-1}) compared to **7** ($k_{obs} = 44 \times 10^{-4}$ min^{-1}), **6** ($k_{obs} = 19 \times 10^{-4}$ min^{-1}) and **8** ($k_{obs} = 17 \times 10^{-4}$ min^{-1}). The results showed that the catalytic activity of complexes for ε-CL decreased in the order of **1** (3,4,5-methoxy) > **3** (2,4-methoxy) > **2** (2,4,6-methoxy) > **4** (aniline) > **5** (3,4,5-methoxy) > **7** (2,4-methoxy) > **6** (2,4,6-methoxy) ≥ **8** (aniline). Moreover, the k_{obs} difference between the aluminium complexes and zinc complexes indicates that the metal centre can dramatically affect the catalytic activity of ε-CL. Further, the substituent pattern of the methoxy groups on the Schiff base ligands can strongly influence the polymerisation rate for both the Al and Zn species, as well as the induction period for Al. For example, the k_{obs} value with the sequence of **1** (3,4,5-trimethoxy) > **3** (2,4-trimethoxy) > **2** (2,4,6-trimethoxy). In 'Hammett' terms[34], the presence of two *meta*-methoxy groups (electron withdrawing) and a *para*-methoxy (electron donating) group as in **1** and **5**, enhances the ability of the metal to nucleophilic attack the carbonyl group of the caprolactone *versus* complexes possessing only *para*-/*ortho*-(**2**, **3**, **6** and **7**) or without methoxy substituents (**4** and **8**). The ^{1}H NMR spectroscopic results for the aluminium complexes verified the influence of the methoxy groups. As shown in the ^{1}H NMR spectra, chemical shifts assigned for the $AlCH_3$ group in **1**–**3** are −0.79 (**1**), −1.00 (**2**), −0.95 (**3**), respectively (Figures 2-2, 2-3, 2-4). The chemical shift order of **1** > **3** > **2** revealed that the Lewis acidity of **1** is also larger than **3** and **2**.[35] This supports the polymerisation activity trend. Lastly, the k_{obs} value of complex **4** (aniline) is smaller than **1** (3,4,5-trimethoxy) which suggests that ligands with electron donating groups on the Schiff ligand enhance the catalytic activity, which is in agreement with observations for *ortho*-OMe-substituted (salen)AlCl[36] and $[(L)ZnEt]_2$ (L = 2-[1-[2-(dimethylamino)ethylimino]ethyl]-4-methoxyphenol)[37].

End-group analysis was carried out using ^{1}H NMR spectroscopy and MALDI-TOF mass spectrometry (Figures 2-13 and 2-14). The ^{1}H NMR spectrum of the PCL produced by **1** (Table 2-3, entry 1) indicated the presence of one benzyl group (peaks g and h) (Figure 2-13). The MALDI-TOF results of the same PCL (Table 2-3, entry 1) demonstrated signals ascribed to the end groups with benzyl group (Figure 2-14). The set of peaks is 107.13 + (114.14)n + 1.01 + 22.99 attributed to BnOH + $(CL)_n$ + Na^+. The ^{1}H NMR spectroscopy and MALDI-TOF results suggest the existence of benzyl-capped PCL, which implies that the polymerisation proceeds via a coordination-insertion mechanism, where the monomer coordinates to the metal followed by the acyl oxygen bond cleavage of the monomer and chain propagation.

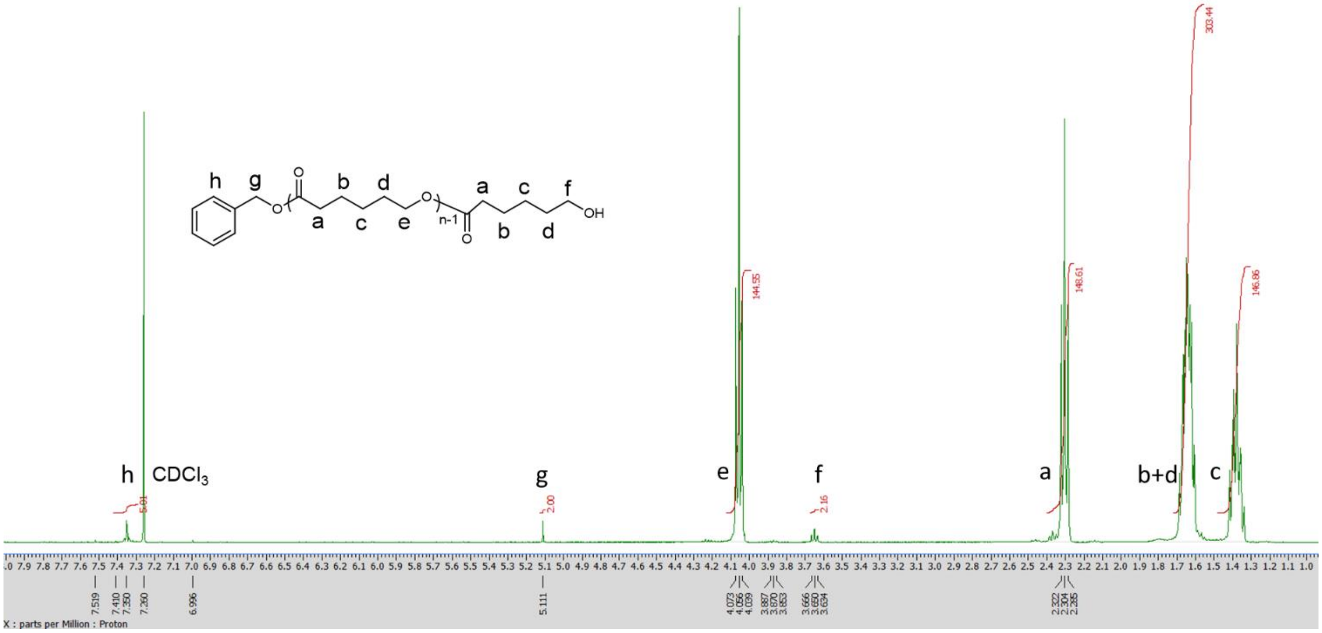

Figure 2-13. ^{1}H NMR spectrum of PCL initiated by complex **1** in the ratio of [CL]:[catalyst]:[BnOH] = 250:1:1 ($CDCl_3$, 25 °C, 400 MHz) (Table 2-3 , entry 1).

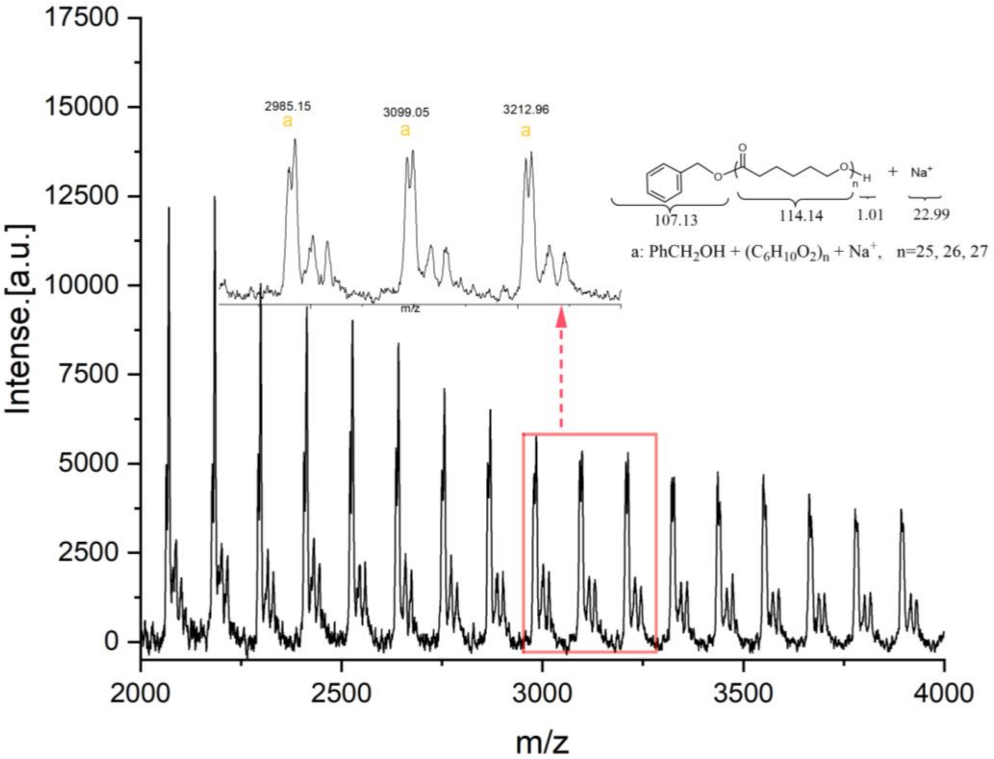

Figure 2-14. MALDI-TOF analysis for the PCL produced by complex **1** ([CL]:[catalyst]:[BnOH] = 250:1:1, 100 °C).

2.2.4 Copolymerisation of ε-CL and GL catalysed by the aluminium complex 1

Given the excellent performance of complex **1**, this catalyst was applied to the copolymerisation of ε-CL and GL, which is a copolymer that is widely used in industry.[38-40] The copolymerisation reactions were conducted at 100 °C by adding the BnOH, ε-CL and GL together in the ratio [CL:GL]:[cat]:[BnOH] = [350:150]:[1]:[1] or [250:250]:[1]:[1]. The reaction was quenched with acidic methanol after 24 h. The microstructure and transesterification of the copolymer chain were demonstrated by ^1H NMR (DMSO-d_6) spectroscopic analysis, as shown in Figure 2-15.

The average lengths of caproyl and glycolidyl blocks (l^eCL and l^eGL) and *R* were calculated from the ^1H NMR spectra, by using reported equations.[41] The average lengths depend on the composition ratio and monomers feed.[42] Ideally, the length of the glycolidyl block can be increased by increasing the feed of GL into the copolymer. However, the limited solubility of the GL derived copolymer in DMSO (100 °C), led to a lower content of glycolide than expected. The coefficient *R* represents the degree of randomness of the chain and if R is equal to 1, this indicates completely random chains, whereas if 0 then this indicates diblock copolymers.[43] The copolymer containing 30% of glycolidyl units is completely random with R close to 1 (Table 2-4, entry 1), and the glycolidyl chain length is shorter than the caproyl one. When the content of glycolidyl is increased to 50% (Table 2-4, entry 2), higher l^eGL, l^eCL and lower *R* values were obtained which indicated a blockier structure and less transesterification. Therefore, **1** is a useful initiator for the copolymerisation of ε-CL and GL, and the randomness of the sequences can be adjusted by the ratio of ε-CL and GL.

Table 2-4. Copolymerisation of glycolide and ε-CL catalysed by **1**^{a}.

Run	*[GL]:[Cl]* (%)	Conversion (%) of GL^b	Conversion (%) of CL^b	$l^e{}_{\mathrm{GL}}{}^c$	$l^e{}_{\mathrm{CL}}{}^c$	R^d	$M_{\mathrm{n,GPC}}$ (Da)^e	$M_{\mathrm{W,GPC}}$ (Da)^e	*PDI*^{f}
1	30:70	97	86	0.79	2.97	0.96	19900	59400	2.99
2	50:50	98	97	1.31	5.73	0.58	8400	24500	2.88

^{a} Polymerisation conditions: catalyst = 0.066 mmol; BnOH = 0.065 (0.01 M in toluene); *T* = 100 °C. ^{b} Obtained by ^{1}H NMR spectroscopy; ^{c} Average length of GL and CL blocks in completely random chains; calculated from ^{1}H NMR spectroscopy (DMSO-d$_6$). ^{d} R, degree of randomness. ^{e} Obtained from GPC analysis and calibrated against the polystyrene standard, multiplied by 0.56. ^{f} Obtained from GPC analysis.

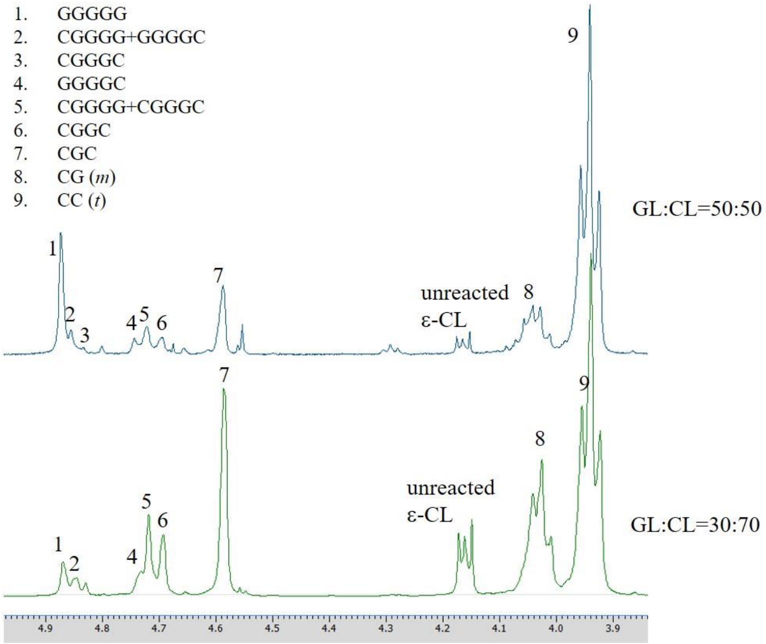

Figure 2-15. ^{1}H NMR spectroscopic analysis of the ε-CL/GL copolymer produced by complex **1**.

2.2.5 Cross-linked PCL catalysed by the aluminium complex 1

Core cross-linked poly(CL-*co*-BOD) polymers (BOD = 4,4’-bioxepane-7,7’-dione) were synthesised via a two-step method (Figure 2-16). In the first step, ε-CL was polymerised in the presence of complex **1** and the initiator benzyl alcohol in the ratio 250:1:1 (100 °C) to produce living linear PCL arms. On completion of the first step (conversion = 99%, 1 h), BOD and **1** in toluene were added to the reaction solution (CL/BOD = 250:25 = 10). The BOD is a cross-linking component, which produces the core structure under ROP conditions. The molecular structure of poly(CL-*co*-BOD) was confirmed by ^{1}H NMR (Figure 2-17). The BnOH end group, BOD and ε-CL peaks in the copolymer were evident in Figure 2-17, however, it proved difficult to calculate the BOD conversion given that peaks due to polyBOD and PCL were indistinguishable.[44] The mole ratio of CL:BOD monomer is 19.55 (verified by the integral peak area) which indicates that nearly half the BOD monomer is either a pendant or unreacted in the poly(CL-*co*-BOD) core. It is assumed here that the conversion of BOD is 51% according to the remaining BOD monomer. Analysis by GPC of the cross-linked polymer showed that the poly(CL-*co*-BOD) (Table 2-5, entry 1 and Figure 2-17) exhibited high M_n = 308,000, which is much larger than PCL (M_n = 17,000) (Table 2-5, entry 2), and narrow PDI = 1.71. The data suggested that complex **1** can be used to synthesise cross-linked PCL with high M_n.

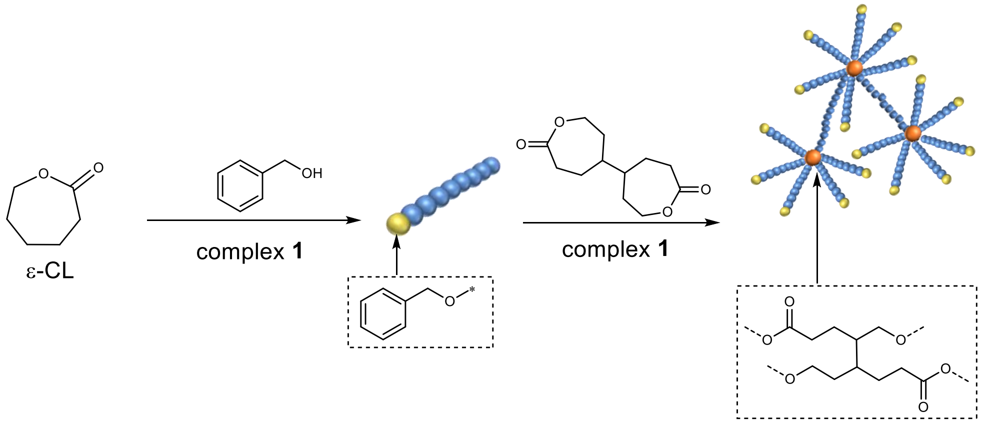

Figure 2-16. Synthesis of core cross–linked polymer via ring-opening polymerisation.

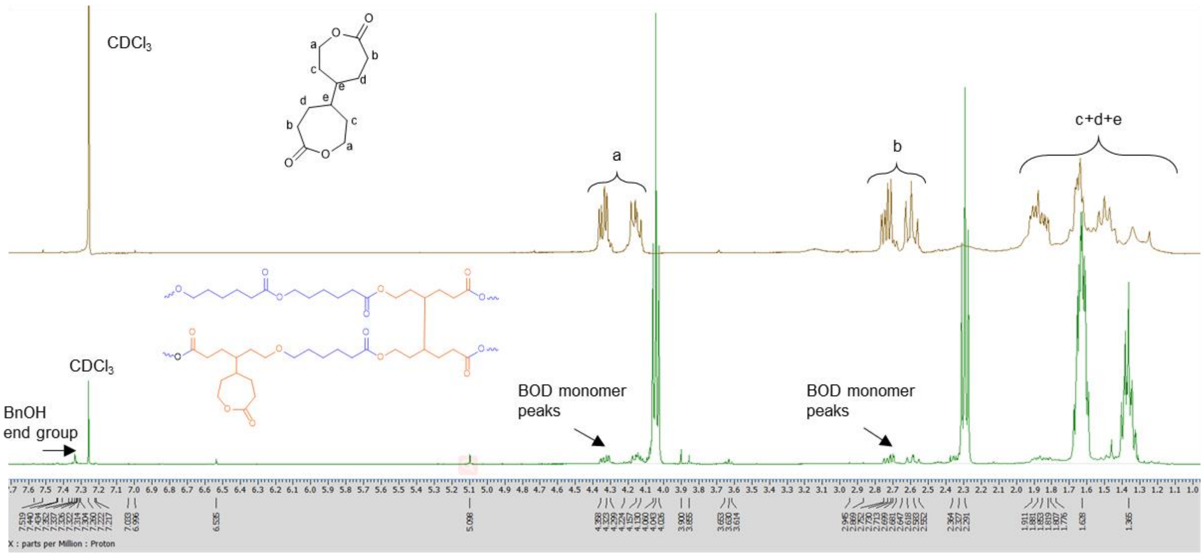

Figure 2-17. ^{1}H NMR spectroscopic (CDCl$_3$, 400 MHz) analysis for BOD monomer (top) and cross-linked poly(CL-*co*-BOD) (bottom) produced by **1** ([CL]:[BOD]:[catalyst]:[BnOH] = 250:25:1:1, 100 °C).

Table 2-5. Polymerisation data for poly(CL-*co*-BOD) catalysed by **1**[a]

Run	[CL]:[BOD]	Conversion (%) of CL[b]	Conversion (%) of BOD[b]	$M_{n,GPC}$ (Da)[c]	$M_{W,GPC}$ (Da)[c]	*PDI*[d]
1	250:250	99	51	308000	526000	1.71
2	250:0	99	-	17000	28000	1.74

[a] Polymerisations were carried out in toluene, $[CL]_0$= 2 M. [b] Determined by ^{1}H NMR spectroscopy. [c] M_n,calcd=($[CL]_0/[cat]_0$)×Conv.%×114.14. [c] Obtained from GPC analysis and calibrated against the polystyrene standard, multiplied by 0.56. [d] Obtained from GPC analysis.

2.3 Conclusion

A comparative study of the effect of methoxy substituents (2,4-, 2,4,6- and 3,4,5-patterns *versus* no methoxy substituents) at the aniline derived ring in a series of Schiff-base organoaluminium and zinc complexes has been carried out. In the series [Al(L^n)(Me)$_2$], for the ROP of ε-CL in the presence (or absence) of BnOH, all complexes exhibited an induction period of up to 20 min., and there after the results indicated that ligands derived from anilines bearing 3,4,5-methoxy substituents favoured the ROP process in terms of rate (with 1st order kinetics), molecular weight and control. The 3,4,5-methoxy containing system was also capable of the efficient ROP of ε-CL under air. The same complex was also capable of the copolymerisation of ε-CL and GL, as well as forming cross-linked PCL in the presence of 4,4’-bioxepane-7,7’-dione. In the case of the [Zn(L^n)$_2$] series, results again indicated that the system bearing the 3,4,5-methoxy moiety most greatly favoured the ROP process. The zinc complexes did not exhibit an induction period and all performed the ROP with 1st order kinetics. The aluminium systems outperformed (in terms of rate) the zinc systems.

References

1. H. Makio, H. Terao, A. Iwashita and T. Fujita, *Chem. Rev.*, 2011, **111**, 2363-2449.
2. C. Redshaw and Y. Tang, *Chem. Soc. Rev.*, 2012, **41**, 4484-4510.
3. T. Fuoco and D. Pappalardo, *Catalysts*, 2017, **7**, 64.
4. J. Wu, T.-L. Yu, C.-T. Chen and C.-C. Lin, *Coord. Chem. Rev.*, 2006, **250**, 602-626.
5. Y. Wei, S. Wang and S. Zhou, *Dalton Trans*, 2016, **45**, 4471-4485.
6. J. Gao, D. Zhu, W. Zhang, G. A. Solan, Y. Ma and W.-H. Sun, *Inorg. Chem. Front.*, 2019, **6**, 2619-2652.
7. O. Santoro, X. Zhang and C. Redshaw, *Catalysts*, 2020, **10**, 800.
8. L. h. Guo, H.y. Gao, L. Zhang, F.m. Zhu and Q. Wu, *Organometallics*, 2010, **29**, 2118-2125.
9. A. Ghaffari, M. Behzad, M. Pooyan, H. A. Rudbari and G. Bruno, *J. Mol. Struct.*, 2014, **1063**, 1-7.
10. A. Arbaoui, C. Redshaw, D. L. Hughes and M. R. J. Elsegood, *Inorg. Chim. Acta*, 2009, **362**, 509-514.
11. W. E. Stewart and T. H. Siddall, *Chem. Rev.*, 1970, **70**, 517-551.
12. B. D. Sarma and J. C. Bailar Jr, *J. Am. Chem. Soc.*, 1955, **77**, 5476-5480.
13. B. K. Singh, A. Prakash, H. K. Rajour, N. Bhojak and D. Adhikari, *Spectrochim. Acta, Part A*, 2010, **76**, 376-383.
14. A. K. Jain, A. Gupta, R. Bohra, I. P. Lorenz and P. Mayer, *Polyhedron*, 2006, **25**, 654-662.
15. P. Å. Bergström and J. Lindgren, *J. Mol. Struct.*, 1990, **239**, 103-111.
16. C. Y. Hsu, H. C. Tseng, J. K. Vandavasi, W. Y. Lu, L. F. Wang, M. Y. Chiang, Y.-C. Lai, H. Y. Chen and H. Y. Chen, *RSC Adv.*, 2017, **7**, 18851-18860.
17. J. Liu, N. Iwasa and K. Nomura, *Dalton Trans*, 2008, **30**, 3978-3988.
18. W. Zhang, Y. Wang, W. H. Sun, L. Wang and C. Redshaw, *Dalton Trans*, 2012, **41**, 11587-11596.
19. S. L. Aeilts, M. P. Coles, D. C. Swenson, R. F. Jordan and V. G. Young, *Organometallics*, 1998, **17**, 3265-3270.
20. A. M. Nassar, A. M. Hassan, M. A. Shoeib and A. N. El kmash, *J. Bio- Tribo-Corros.*, 2015, **1**, 1-16.
21. M. J. Niu, Z. Li, G. L. Chang, X. J. Kong, M. Hong and Q. f. Zhang, *PLoS One*, 2015, **10**, e0130922.
22. W. Chen, Y. Li, Y. Cui, X. Zhang, H. L. Zhu and Q. Zeng, *Eur. J. Med. Chem.*, 2010, **45**, 4473-4478.
23. A. Arbaoui, C. Redshaw, N. M. Sanchez-Ballester, M. R. J. Elsegood and D. L. Hughes, *Inorg. Chim. Acta*, 2011, **365**, 96-102.
24. B. Chakraborty and S. Banerjee, *J. Coord. Chem.*, 2013, **66**, 3619-3628.
25. A. L. Oliveira, L. C. Ferreira, M. L. Dias, R. S. Bitzer and M. A. Nascimento, *Quim. Nova*, 2019, **42**, 505-512.
26. Y. Wang, W. Zhao, D. Liu, S. Li, X. Liu, D. Cui and X. Chen, *Organometallics*, 2012, **31**, 4182-4190.
27. C. L. Lee, Y. F. Lin, M. T. Jiang, W. Y. Lu, J. K. Vandavasi, L. F. Wang, Y. C. Lai, M. Y. Chiang and H. Y. Chen, *Organometallics*, 2017, **36**, 1936-1945.

28. Y. Wei, L. Song, L. Jiang, Z. Huang, S. Wang, Q. Yuan, X. Mu, X. Zhu and S. Zhou, *Dalton Trans.*, 2019, **48**, 15290-15299.
29. N. Ajellal, J.-F. Carpentier, C. Guillaume, S. M. Guillaume, M. Helou, V. Poirier, Y. Sarazin and A. Trifonov, *Dalton Trans.*, 2010, **39**, 8363-8376.
30. L. Qin, Y. Zhang, J. Chao, J. Cheng and X. Chen, *Dalton Trans.*, 2019, **48**, 12315-12325.
31. W. L. Kong, Z. Y. Chai and Z. X. Wang, *Dalton Trans.*, 2014, **43**, 14470-14480.
32. W. A. Munzeiwa, V. O. Nyamori and B. Omondi, *Inorg. Chim. Acta*, 2019, **487**, 264-274.
33. J. L. Mata-Mata, J. A. Gutiérrez, M. A. Paz-Sandoval, A. R. Madrigal and A. Martínez-Richa, *Journal of Polymer Science Part A: Polym. Chem.*, 2006, **44**, 6926-6942.
34. L. P. Hammett, *J. Am. Chem. Soc.*, 1937, **59**, 96-103.
35. W. Zhao, Q. Wang, Y. Cui, J. He and Y. Zhang, *Dalton Trans.*, 2019, **48**, 7167-7178.
36. A. Rae, A. J. Gaston, Z. Greindl and J. A. Garden, *Eur. Polym. J.*, 2020, **138**.
37. W. C. Hung, Y. Huang and C. C. Lin, *J. Polym. Sci., Part A: Polym. Chem.*, 2008, **46**, 6466-6476.
38. J. Wang, L. Wang, Z. Zhou, H. Lai, P. Xu, L. Liao and J. Wei, *Polymers*, 2016, **8**, 115.
39. N. M. Van den Vreken, P. Dubruel and R. M. Verbeeck, *J. Mater. Chem. B*, 2013, **1**, 1584-1594.
40. K. Cooper, A. Nathan and M. Vyakarnam, *Biodegrad. Polym. Clin. Use Clin. Dev.*, 2011, 401-415.
41. J. Kasperczyk, *Macromol. Chem. Phys.*, 1999, **200**, 903-910.
42. A. Meduri, T. Fuoco, M. Lamberti, C. Pellecchia and D. Pappalardo, *Macromolecules*, 2014, **47**, 534-543.
43. S. Li, *Biomacromolecules*, 2005, **6**, 483-488.
44. Y. Zheng, W. Turner, M. Zong, D. J. Irvine, S. M. Howdle and K. J. Thurecht, *Macromolecules*, 2011, **44**, 1347-1354.

Chapter 3. Niobium and tantalum complexes derived from the acids $Ph_2C(X)CO_2H$ (X=OH, NH_2): synthesis, structure and ring-opening polymerisation capability.

3.1 Introduction

On the basis of the successful application of *N,O*-Schiff bases for the ROP of cyclic esters in the previous chapter, the amino acid 2,2′-diphenylglycine ($Ph_2C(NH_2)CO_2H$) which is part of the *N,O*-chelate ligand families seems promising. Furthermore, the use of *O,O*- chelating ligands for coordination complexes is extensive. Benzilic acid ($Ph_2C(OH)CO_2H$) was selected to compare *N,O*- and *O,O*-chelated systems. It should be noted ligands bearing the moiety $Ph_2C(X)$ have proved to own the ability to promote highly crystalline samples.[1] Redshaw's group has been exploring the use of ligands derived from the acids $Ph_2C(X)CO_2H$, where X = OH, or NH_2, and has reported multi-metallic ROP systems based on lithium or zinc as well as rare earth complexes.[2-4] However, the group V metals niobium and tantalum remain underexplored in ROP. One encouraging result involved using niobium and tantalum chelating phenoxide ligation for the ROP of ε-CL. Conversions were >96% at temperatures in excess of 100 °C over either 20 h when conducted in toluene or 1 h when conducted in the absence of solvent.[5] In this chapter, the investigations on such acids are reported through the synthesis and characterisation of new niobium and tantalum complexes bearing ligands derived from 2,2′-diphenylglycine or benzilic acid were extended (see Figure 3-1). The molecular structures are reported together with the catalytic activity of these new niobium and tantalum systems for the ROP of cyclic esters (ε-CL and *r*-LA), and high catalytic efficiency is demonstrated for these ROP systems with low polydispersities (PDIs < 1.9) suggesting reasonable control.

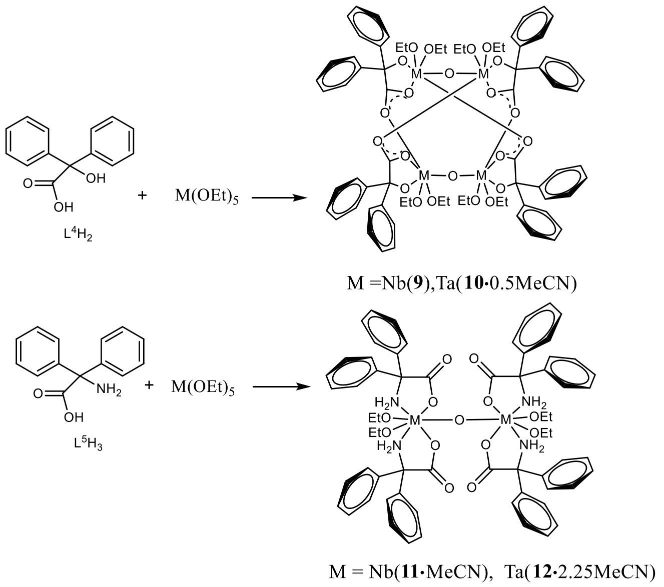

Figure 3-1. Complexes **9** – **12** prepared herein.

3.2 Results and discussion

3.2.1 Synthesis and characterisation of benzilic acid derived niobium or tantalum complexes

Reaction of [Nb(OEt)$_5$] with one equivalent of benzilic acid, Ph$_2$C(OH)CO$_2$H (L^{4}H$_2$) in refluxing toluene afforded, after extraction into acetonitrile, colourless prisms of the complex [Nb$_4$(OEt)$_8$(L^4)$_4$(μ-O)$_2$] (**9**). Crystals suitable for an X-ray diffraction study were grown from a saturated solution of acetonitrile at ambient temperature. The molecular structure is shown in Figure 3-2, with selected bond lengths and angles given in the caption; for alternative views see Figure 3-3. Complex **9** adopts a centrosymmetric structure in the monoclinic space group C2/c. Each Nb(V) ion is six coordinate; one benz^{2-} anion is chelating through the alkoxide and one oxygen of the carboxylate; there are two *cis* ethoxide anions, one μ^2-oxide oxygen atom that forms a bridge between Nb(1) and Nb(1)^i or Nb(2) and Nb(2)^i (where $i = 1-x, y, ½-z$), and the final coordination site is occupied by the carbonyl oxygen of a benz^{2-} bound at the other symmetry-unique metal ion. The five-membered chelate appears to be fairly strained with bond angles of 75.07(6) and 74.41(6)° at Nb(1) and Nb(2) respectively. It is notable that the C···O distances in each carboxylate are rather similar. The C–O bond lengths are 1.271(3) Å for C(1)–O(1) and

1.244(3) Å for C(1)–O(2); for C(15)−O(4) and C(15)–(O5) the lengths are 1.266(2) and 1.250(3) Å respectively. The small difference between the two C···O distances suggests these are best visualised as delocalised carboxylates rather than carbonyl and alkoxide moieties. The bonds Nb(1)−O(5)^{i} (where i = 1−x, y, ½–z) and Nb(2)–O(2) are 2.2460(15) and 2.2401(15) Å are rather longer than all of the other Nb−O bonds suggesting a weaker interaction consistent with significant C=O character. There is a minor disorder in the orientation of the ethoxide alkyl chains, but this was readily modelled using standard procedures.

The space group symmetry assembles pairs of these units into tetranuclear molecules that are non-centrosymmetric and contain four niobium atoms, four benz^{2-}, eight ethoxide ligands and two μ^2-oxide anions bridging between pairs of niobium atoms.

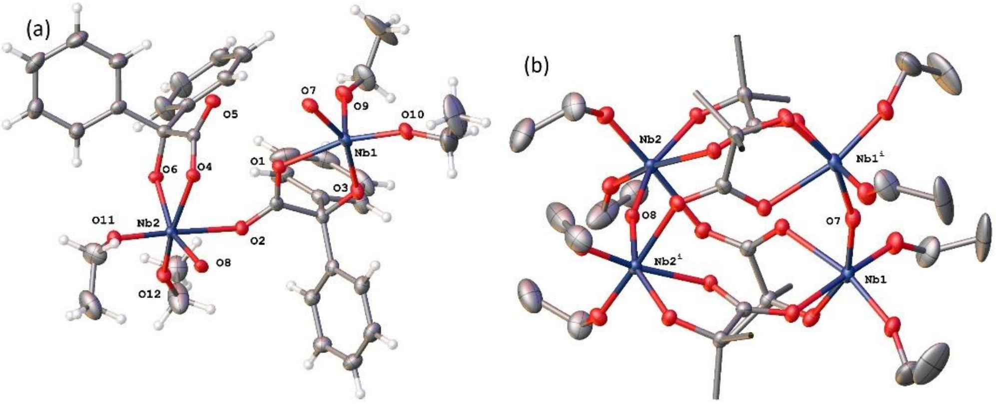

Figure 3-2. (a) Asymmetric unit of **9** with atoms drawn as 50 % probability ellipsoids. (b) Core of **9** (twice the asymmetric unit). Hydrogen atoms and phenyl groups have been omitted for clarity. Small-scale disorder is not represented. Symmetry equivalent atoms are generated by i = 1−x, y, ½ −z. Selected bond lengths (Å) and angles ($^{\circ}$): Nb(1)–O(1) 2.1205(15), Nb(1)–O(3) 1.9517(15), Nb(1)–O(51) 2.2460(15), Nb(1)–O(7) 1.9152(4), Nb(1)–O(9) 1.8572(16), Nb(1)–O(10) 1.8575(16), Nb(2)–O(2) 2.401(15), Nb(2)–O(4) 2.1334(14), Nb(2)–O(6) 1.9442(4), Nb(2)–O(8) 1.9081(14), Nb(2)–O(11) 1.8647(15), Nb(2)–O(12) 1.8502(15); O(1)–Nb(1)–O(3) 75.07(6), O(9)–Nb(1)–O(10) 97.42(7), Nb(1)–O(7)–Nb(1$^{\text{i}}$) 162.09(13), O(4)–Nb(2)–O(6) 74.41(6), O(8)–Nb(2)–O(11) 91.27(6), Nb(2)–O(8)–Nb(2$^{\text{i}}$) 163.46(12).

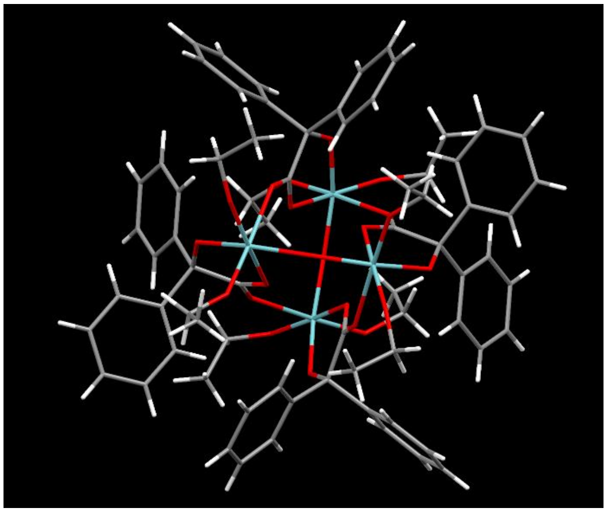

Figure 3-3. Alternative view of four niobium cluster present in **9**.

Similar use of [Ta(OEt)$_5$] led to the isolation of the complex [Ta$_4$(OEt)$_8$(L^4)$_4$(μ-O)$_2$]·0.5MeCN (**10**·0.5MeCN). Crystals suitable for an X-ray diffraction study were grown from a saturated solution of acetonitrile at ambient temperature. The molecular structure is shown in Figure 3-4, with selected bond lengths and angles given in the caption; for alternative views see Figure 3-5. This is isostructural with the Nb compound and differs only in the presence of a small amount of uncoordinated solvent that was modelled using a solvent mask (Squeeze) in Olex2.

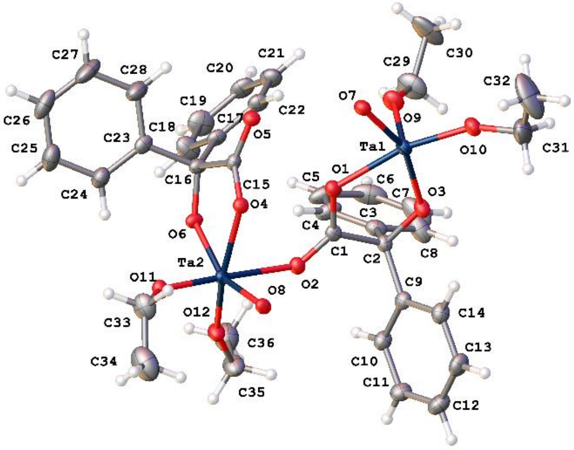

Figure 3-4. Asymmetric unit of **10**·0.5MeCN. Non coordinated solvent molecules have been removed for clarity. Selected bond lengths (Å) and angles (°): Ta(1) – O(1) 2.1135(16), Ta(1) – O(3) 1.9573(17), Ta(1) – O(5) 2.2246(16), Ta(1) – O(7) 1.9175(14), Ta(1) – O(9) 1.8629(18), Ta(1) – O(10) 1.8643(18), Ta(2) – O(2) 2.2139(17), Ta(2) – O(4) 2.1283(16), Ta(2) – O(6) 1.9506(16),

Ta(2) – O(8) 1.9091(4), Ta(2) – O(11) 1.8759(17), Ta(2) – O(12) 1.8547(17); O(1) – Ta(1) – O(3) 75.19(7), O(9) – Ta(1) – O(10) 96.60(8), Ta(1)–O(7)–Ta(1^{i}) 160.74(14), O(4) – Ta(2) – O(6) 74.38(6), O(8) – Ta(2) – O(11) 91.32(7), Ta(2)–O(8)–Ta(2^{i}) 162.86(14).

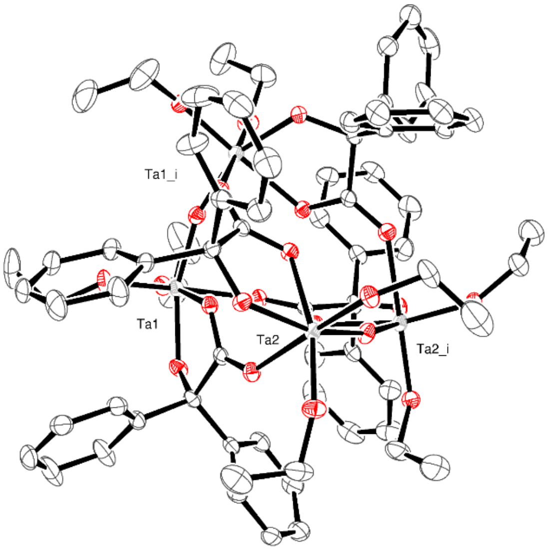

Figure 3-5. Alternative view of four niobium cluster present in **10**·0.5MeCN. Atoms are drawn as 50% probability ellipsoids. Symmetry operation: *i* = 1−x, y, ½ −z.

The ^{1}H NMR spectrums of **9** and **10**·0.5MeCN are consistent with the formulation with peaks assigned to aromatic protons (20H), as well as methylene (8H) and methyl (12H) groups of the ethoxide ligands, respectively. The IR spectrums of **9** and **10**·0.5MeCN do not contain a sharp band at 3394 cm^{-1} corresponding to the –OH stretching vibration of the parent L^{4}H$_2$ acid. The presence of new peaks at 486 and 462 cm^{-1} suggests the formation of M–O bonds (Figure 3-6). In the mass spectrum of **9**, peaks at m/z 1487.40 correspond to the loss of four OEt and H$^+$ from the parent ion (Figure 3-7); the ESI-MS of **10**·0.5MeCN is shown in Figure 3-8.

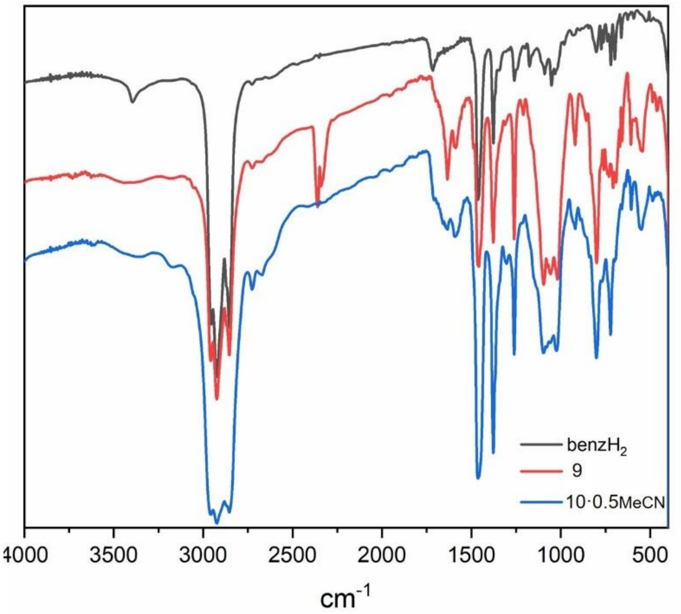

Figure 3-6. IR spectrum of L^4H_2, **9** and **10**·0.5MeCN in Nujol.

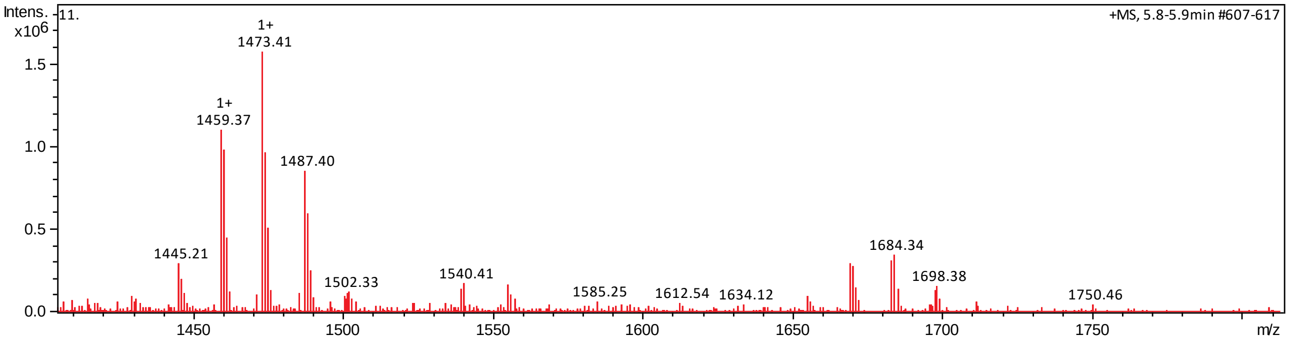

Figure 3-7. ESI-MS spectrum of **9**.

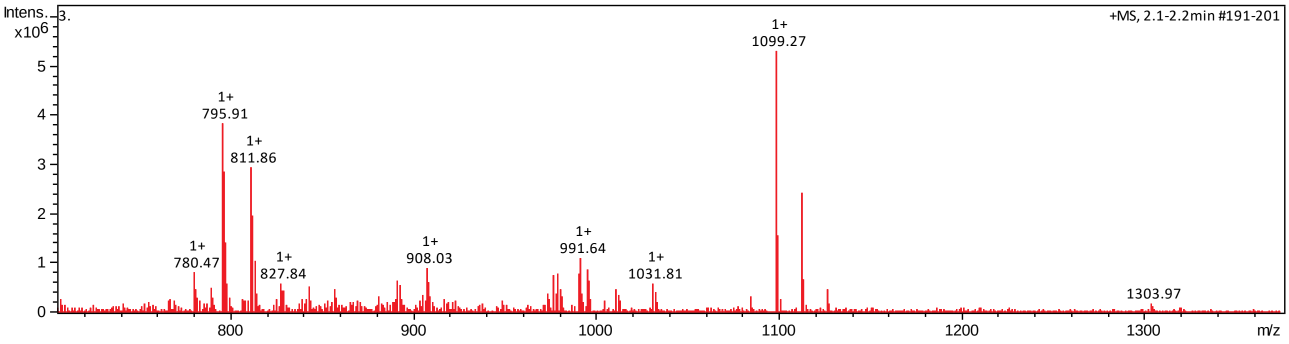

Figure 3-8. ESI-MS spectrum of **10**·0.5MeCN.

3.2.2 Synthesis and characterisation of 2,2’-diphenylglycine derived niobium or tantalum complexes

Reaction of [Nb(OEt)$_5$] with one equivalent of 2,2’-diphenylglycine, $Ph_2C(NH_2)CO_2H$ (L^5H_3), in refluxing toluene afforded, after extraction into acetonitrile, colourless prisms of the complex [$Nb_2(OEt)_4(L^5H_2)_4(\mu$-O)]·2MeCN (**11**·2MeCN). Crystals suitable for an X-ray diffraction study were grown from a saturated solution of acetonitrile at ambient temperature. The molecular structure is shown in Figure 3-9, with selected bond lengths and angles given in the caption; for alternative views see Figure 3-10. Complex **11**·2MeCN crystallises in the centrosymmetric monoclinic space group *C*2/c with two unique Nb atoms in the asymmetric unit that are linked by an oxo bridge. The dinuclear molecules comprise two niobium atoms, four L^5H_3 ligands, two ethoxide ligands and one μ^2-oxide anion. Each Nb(V) ion is seven coordinated in a roughly pentagonal bipyramidal geometry. In the plane around each Nb ion are two cis chelating $L^5H_2^-$ anions and one oxide. Above and below the plane in axial positions lie ethoxide anions. The oxide bridge is close to symmetric (bond lengths are 1.8942(12) and 1.9154(12) Å for Nb(1) and Nb(2) respectively) and the dimer is nearly centrosymmetric. The bound NH_2 group makes hydrogen bonds to the carboxylate bound at the second metal centre in the cluster.

There is a minor disorder in the ethoxide and the orientation of the phenyl groups. This was dealt with satisfactorily using standard techniques within Olex2. A small amount of unbound solvent was modelled using a solvent mask (Squeeze) within Olex2.

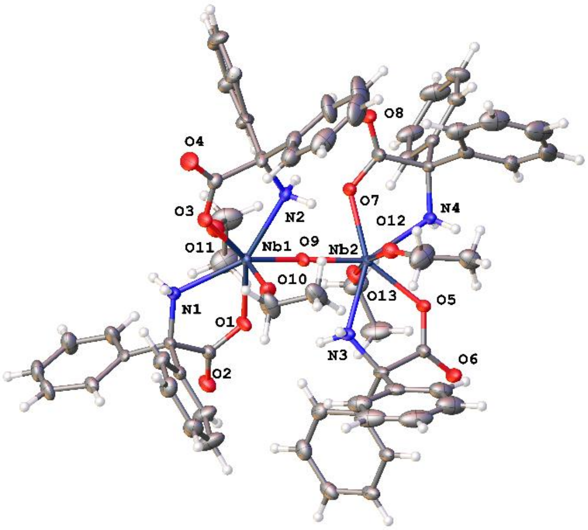

Figure 3-9. Molecular structure of **11**·2MeCN. Non coordinated solvent molecules have been removed for clarity. Selected bond lengths (Å) and angles (^{o}): Nb(1)–O(1) 2.1123(12), Nb(1)–O(3) 2.1060(12), Nb(1)–O(9) 1.8942(12), Nb(1)–O(10) 1.8791(14), Nb(1)–O(11) 1.9022(14), Nb(1)–N(1) 2.3077(15), Nb(1)–N(2) 2.2919(14), Nb(2) – O(5) 2.1093(12), Nb(2)–O(7) 2.1130(12), Nb(2)–O(9) 1.9154(14), Nb(2)–O(12) 1.8907(14), Nb(2) –O(13) 1.8647(14), Nb(2)–N(3) 2.2967(14), Nb(2)–N(4) 2.3068(14); Nb(1)–O(9)–Nb(2) 165.47(9), O(1)–Nb(1)–N(1) 69.92(5), O(9)–Nb(1)–N(2) 69.93(5), O(5)–Nb(2)–N(3) 69.98(5), O(7)–Nb(2)–N(4) 69.84(5), Nb(1)–O(9)–Nb(2) 165.47(9).

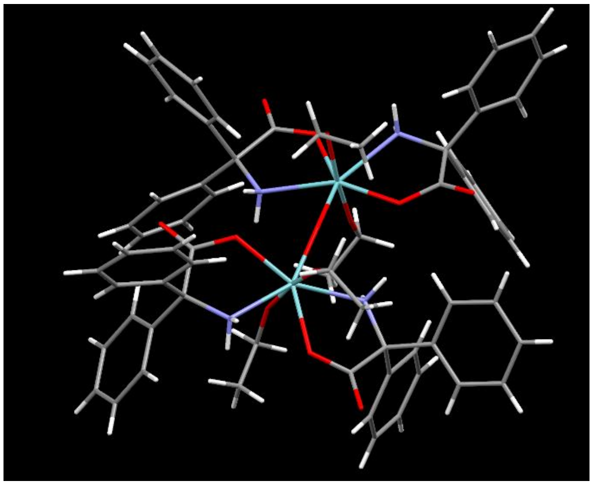

Figure 3-10. Alternative view of the asymmetric unit of **11**·2MeCN.

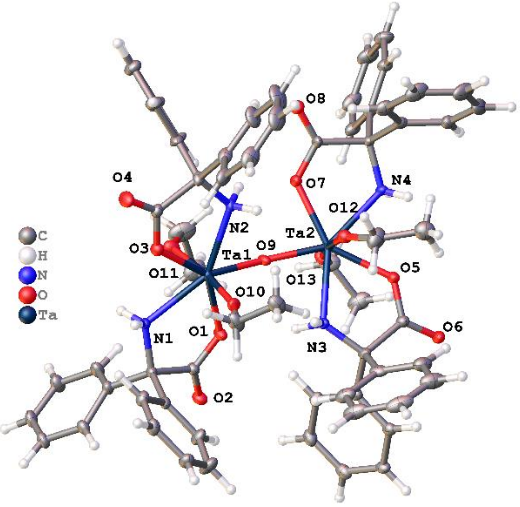

Figure 3-11. Molecular structure of **12**·2.25MeCN. Non coordinated solvent molecules have been removed for clarity. Selected bond lengths (Å) and angles (^{o}): Ta(1)–O(1) 2.101(4), Ta(1)–O(3) 2.094(4), Ta(1)–O(9) 1.899(4), Ta(1)–O(10) 1.895(4), Ta(1)–O(11) 1.904(4), Ta(1)–N(1) 2.298(5), Ta(1)–N(2) 2.283(5), Ta(2)–O(5) 2.101(4), Ta(2)–O(7) 2.109(4), Ta(2)–O(9) 1.920(4), Ta(2)–O(12) 1.894(4), Ta(2)–O(13) 1.891(4), Ta(2)–N(3) 2.299(5), Ta(2)–N(4) 2.297(5); Ta(1)–O(9)–Ta(2) 164.9(3), O(1)–Ta(1)–N(1) 70.25(16), O(9)–Ta(1)–N(2) 70.07(17), O(5)–Ta(2)–N(3) 70.10(16), O(7)–Ta(2)–N(4) 70.26(16), Ta(1)–O(9)–Ta(2) 164.9(3).

Similar use of $[Ta(OEt)_5]$ led to the isolation of the complex $[Ta_2(OEt)_4(L^5H_2)_4(\mu\text{-}O)]\cdot 2.25MeCN$ (**12**·2.25MeCN). Crystals suitable for an X-ray diffraction study were grown from a saturated solution of acetonitrile at ambient temperature. The molecular structure of **12** is shown in Figure 3-11, with selected bond lengths and angles given in the caption; for alternative views see Figure 3-12. The Ta compound is isostructural to **11** and differs only in the amount of solvent present.

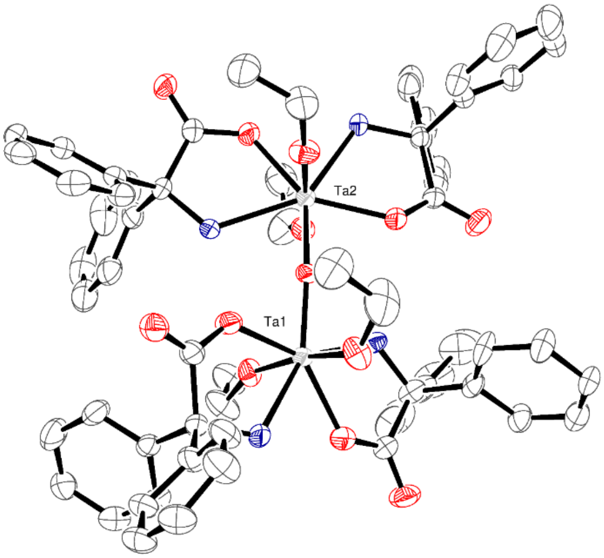

Figure 3-12. Asymmetric unit of **12**·2.25MeCN with atoms drawn as 50% probability ellipsoids.

The ^{1}H NMR spectrum supports the formulation of **11**·2MeCN and **12**·2.25MeCN with the multiple aromatic peaks between 7.03-7.75 ppm, and quartets at 3.50-2.52 ppm and a triplet at 1.06-1.10 ppm assigned to the ethoxide groups; the signal for the NH_2 groups appear as a broad peak at *ca*. 2.2 ppm. In the IR spectrum of the parent acid L^5H_3, there are two absorptions near 3441 and 3267 cm^{-1} (assigned to symmetric and asymmetric N–H stretching), and two weak N–H absorptions are found near 3440 and 3314 cm^{-1} for complexes **11**·2MeCN and **12**·2.25MeCN (Figure 3-13). In the mass spectrum of complex **11**·2MeCN, the peaks at m/z 1366 correspond to loss of 3H$^+$ from the parent ion (Figure 3-14); the ESI-MS of **12**·2.25MeCN is given in Figure 3-15.

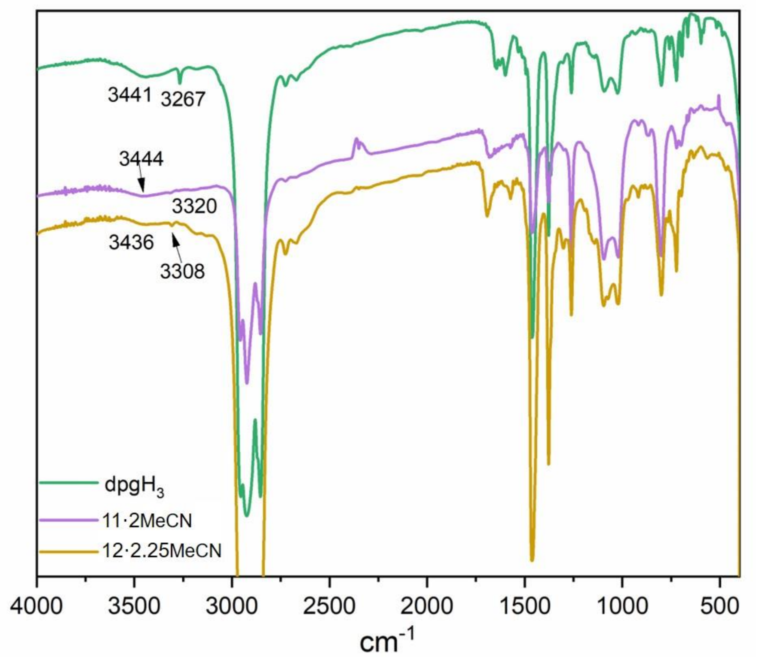

Figure 3-13. IR spectrum of L^{5}H$_3$, **11**·2MeCN and **12**·2.25MeCN in Nujol.

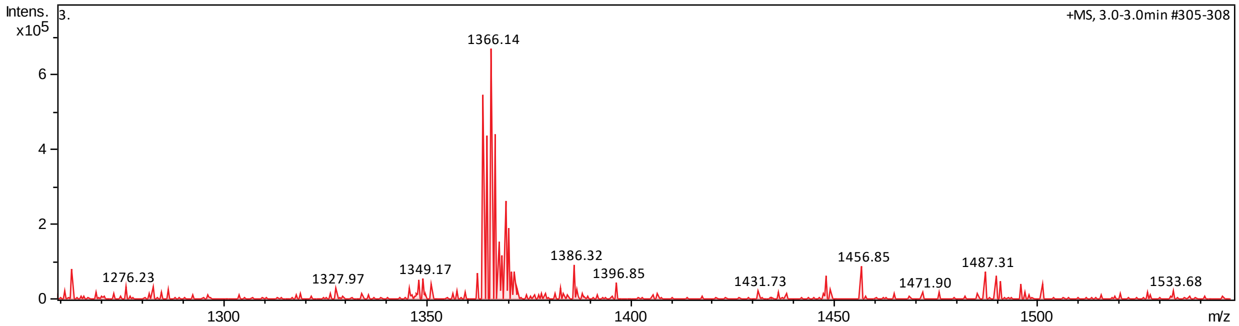

Figure 3-14. ESI-MS spectrum of **11**·2MeCN.

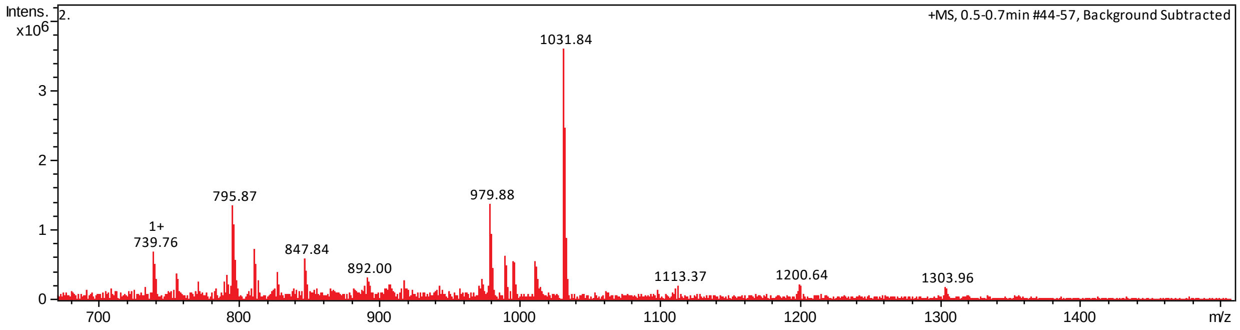

Figure 3-15. ESI-MS spectrum of **12**·2.25MeCN.

3.2.3 Ring-opening polymerisation studies of ε-CL

Complexes **9-12** were screened for the ROP of ε-CL and the results are presented in Table 3-1. The benzilic acid derived complexes **9** and **10**·0.5MeCN exhibited conversions of >99% and 50% at 100 °C within 24 h, respectively (Figure 3-16). By contrast, complexes **11**·2MeCN and **12**·2.25MeCN derived from 2,2'-diphenylglycine were inactive towards the ROP of ε-CL under the same conditions (Table 3-1, entries 1-4). Once increasing the polymerisation temperature to 160 °C, complex **12** reached a conversion of 87%. The results suggest complexes derived from 2,2'-diphenylglycine were only active under higher polymerisation temperature conditions and the presence of the amine-containing $Ph_2C(NH_2)CO_2^-$ moiety is unfavourably in terms of ROP of CL. It is noted that during metal-free studies, a similar trend was also observed, *i.e*. L^4H_2 was active whereas L^5H_3 was not.[4]

Complex **9** adopted PCL with high molecular weight (M_n = 12,000) and narrow molecular distribution (PDI = 1.2). When conducting the polymerisations in the absence of BnOH, the polymerisation activity and molecular weight decreased slightly (Table 3-1, entries 5-8). It implies the initiator of BnOH plays a very important role in generating active metal alkoxides species in the ring-opening polymerisation process and enhances the rate of the reaction. When the mole ratio CL:Nb is increased from 125 to 500, the molecular weight increases from 7000-28,000 (PDI = 1.2-1.4) with the conversion rates and distributions remaining stable. Increasing the ratio to 1000:1 proved to be detrimental to the conversion rate (Table 3-1, entry 12).

Table 3-1. ROP of ε-CL catalysed by the complexes **9-12**.

Run	Cat.	$[CL]_0:[Nb/Ta]_0:[BnOH]^a$	Conv.[b] (%)	M_n[c] (calc.) Da	M_n[d] (obs.) Da	PDI[d]
1	**9**	250:1:1	>99	7170	12000	1.2
2	**10**	250:1:1	50	3675	9000	1.9
3	**11**	250:1:1	2	–	–	–
4	**12**	250:1:1	2	–	–	–
5	**9**	250:1:0	76	5468	9000	1.2
6	**10**	250:1:0	38	2757	6000	1.3
7	**11**	250:1:0	1	–	–	–
8	**12**	250:1:0	1	–	–	–
9	**12**[e]	250:1:0	87	12459	10000	1.3
10	**9**	125:1:1	99	3639	7000	1.4

11	**9**	500:1:1	91	13091	28000	1.3
12	**9**	1000:1:1	20	5815	9000	1.4

[a] [CL] = 10.00 mmol, [catalyst **9** or **10**] = 0.01 mmol, [**11** or **12**] = 0.02 mmol, [BnOH] = 0.04 mmol (0.01M in toluene), 100 °C, 24 h. [b] Determined by ^{1}H NMR spectroscopy. [c] M_n(calc.) = 114.14×$[CL]_0/[Nb/Ta]_0$×%conv + $M_{\text{end group}}$, assuming one propagation chain per metal atom. [d] Mn(obs) and PDI obtained by GPC in THF relative to polystyrene standards corrected by the Mark-Houwink correction factor M_n(obs) = M_{nGPC} raw data × 0.56. [e] Run 9, the reaction was happened at 160 °C

A kinetics study for the polymerisation of ε-CL using **9** and **10**·0.5MeCN in the ratio $[CL]_0:[Nb/Ta]_0:[BnOH]$ = 250:1:1 at 100 °C was performed (Figure 3-16). From the plot, there is an induction period (*ca*. 60 min.) for **9**. The calculated slope of the linear section of the curve is equal to the apparent polymerisation rate constant.[6]

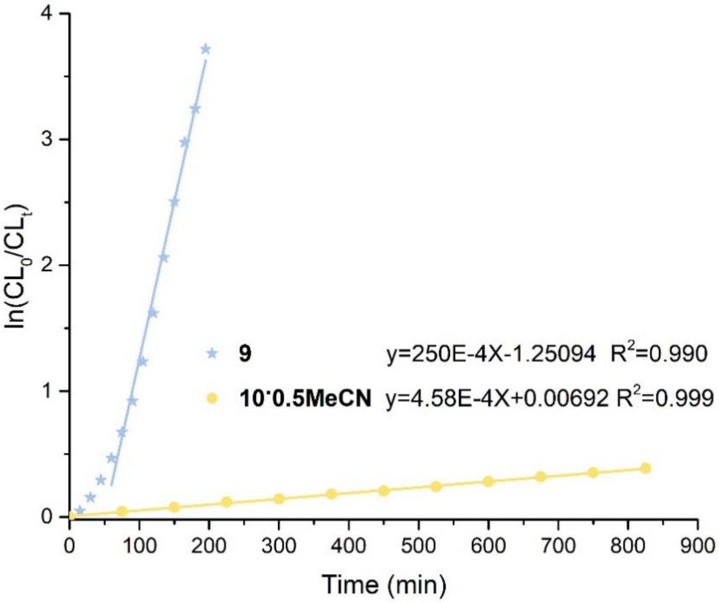

Figure 3-16. Plots of $\ln([CL]_0/[CL]_t)$ *versus* time catalysed by complexes **9** and **10**·0.5MeCN; Reaction conditions: [CL]:[Nb/Ta]:[BnOH] = 250:1:1 at 100 °C.

For complex **10**·0.5MeCN, there is a first-order dependence of the rate of the polymerisation without any induction period. The observed rate constants (k_{obs}) are 250×10^{-4} min^{-1}, R = 0.990 and 4.58×10^{-4} min^{-1}, R =0.999 for **9** and **10**·0.5MeCN, respectively. From the rate constants, it is inferred that the polymerisation rate is significantly faster for Nb complexes than Ta complexes.

In previous work[5], our group has utilized tetraphenolate niobium and tantalum complexes for the ROP of CL. Under the same conditions, such niobium complexes exhibited excellent conversion and high molecular weight compared with tantalum complexes. The better reactivity of niobium complex compared to tantalum in terms of the ROP of CL which possibly assigned to the higher Lewis acidity of niobium.[7] The higher Lewis acidic metal centre benefits the process of carbonyl oxygen from the monomer coordinating to the metal centre.

In the MALDI-TOF spectrum (Figure 3-17), the PCL formed by **9** has two families of peaks. The main peaks are assigned to polymer chains with $PhCH_2O$- end groups, which agree with the ^1H NMR spectra (Figure 3-18). The results suggested the formation of $Nb{-}OCH_2Ph$ species acted as the initiator for the ROP via the coordination-insertion mechanism.[8] Signals at 7.34 and 5.10 ppm indicated a benzyl group and the peak at 3.64 ppm was ascribed to an OH terminal group. A second distribution of peaks is associated with the ethoxy ($-OCH_2CH_3$) and hydroxyl (–OH) end groups, which could also be observed in the ^1H NMR spectrum (Figure 3-18). This result indicated that an ethoxide niobium complex was also present and involved in the ROP process via a coordination-insertion mechanism.[9,10] The successive series showed that there was a m/z difference of 114 between neighbouring peaks, which corresponds to the molecular weight of the monomer. The end group of PCL isolated using **9** in the absence of BnOH was also investigated by MALDI-TOF, and the spectrum (Figure 3-19) confirmed that PCL with an ethoxy and hydroxyl (–OH) end groups was formed.

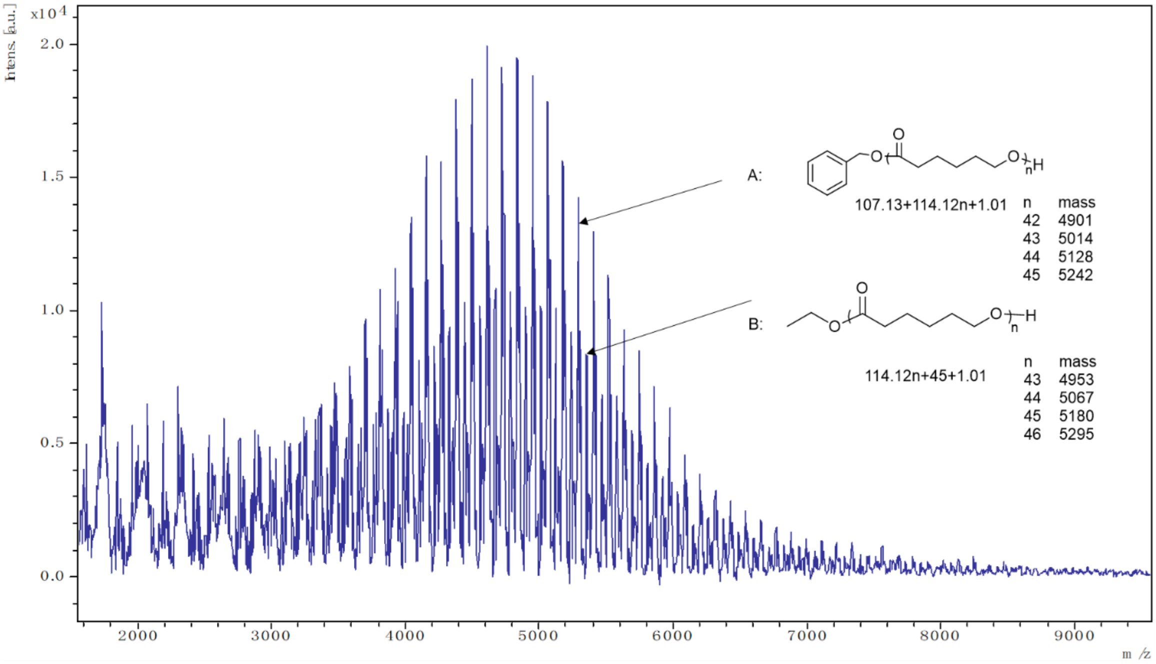

Figure 3-17. MALDI-TOF spectrum of the PCL formed using complex **9** (Table 3-1, entry 1); n is the degree of polymerisation.

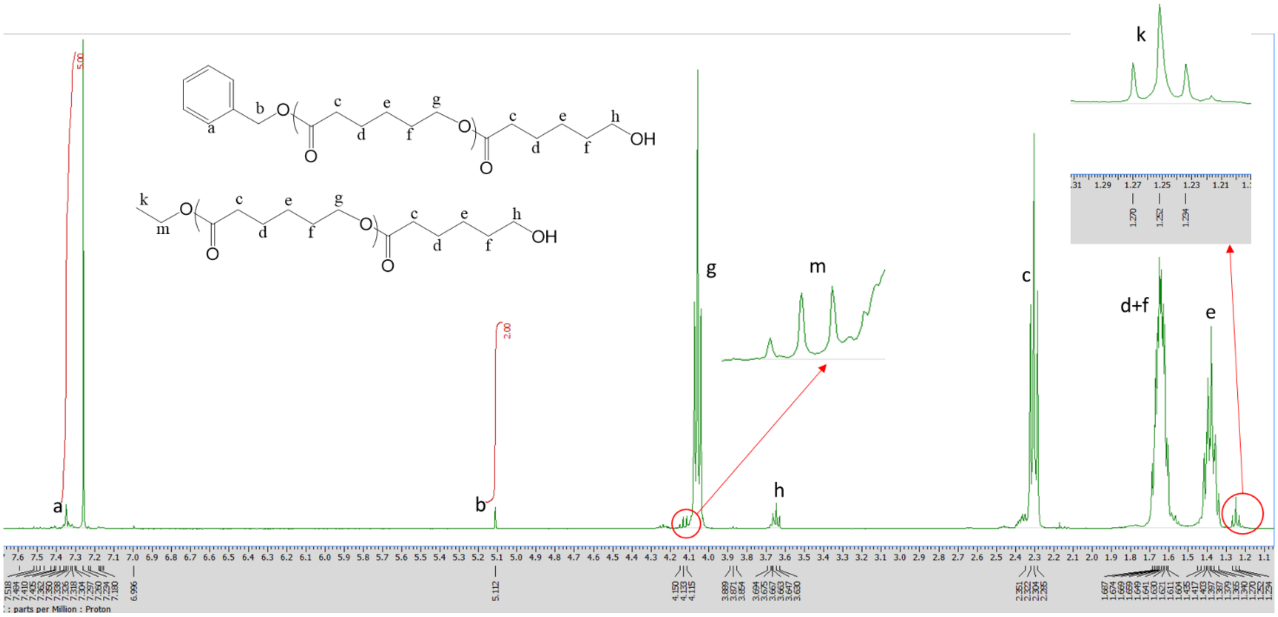

Figure 3-18. ^{1}H NMR spectrum ($CDCl_3$) of PCL formed using complex **9** (Table 3-1, entry 1).

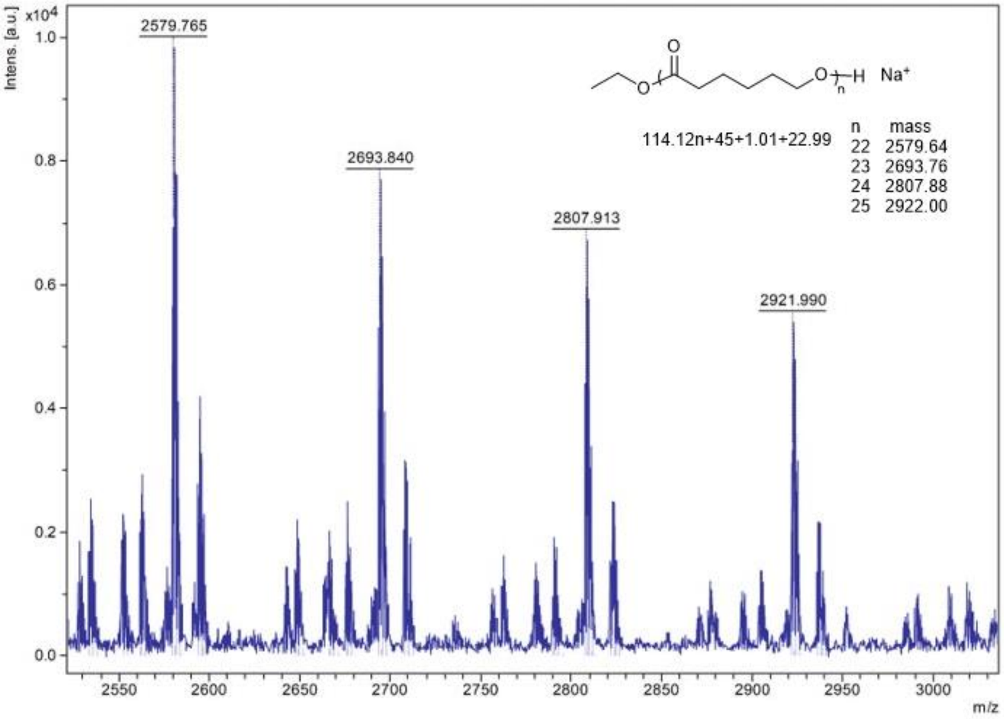

Figure 3-19. MALDI-TOF spectrum of the PCL catalysed by complexes **9** in the absence of BnOH (Table 3-1, entry 5); n is the degree of polymerisation.

3.2.4 Ring-opening polymerisation studies of *r*-LA

Complexes **9**-**12** have also been screened for the ROP of *r*-LA with the [LA]:[Nb/Ta]:[BnOH] ratio of 250:1:1 over 24 h. The results are depicted in Table 3-2. The reaction temperature was first investigated and it was observed that when the temperature was 130 °C, only L^4H_2 derived **9** and **10**·0.5MeCN were active towards the ROP of *r*-LA, and the monomer conversion reached 40% after 24 h for **9**. It was evident that complexes derived from L^5H_3 were inactive at 130 °C even after 24h (Table 3-2, entries 1-4). Results are similar to the polymerisation of ε-CL. When the temperature was increased to 160 °C, the activities substantially increased in all cases (Table 3-2, entries 9-12). For example, a 92% conversion was achieved using **12**·2.25MeCN affording a polymer with a M_n = 9,000 with good control (PDI = 1.0) after 24 h (Table 3-2, entries 12). The catalytic behaviour of complexes **9**-**12** in the absence of BnOH at 130 °C and 160 °C. was tested. Interestingly, the results suggested that the addition of BnOH has a negative effect on the polymerisation rate and molecular weight (Table 3-2, entries 5-8 and 13-16). For a plot of conversion and time (min) for the polymerisation of *r*-LA using **9-12**, see Figure 3-20. The kinetics study of the ROP of *r*-LA using **9-10** is shown in Figure 3-21. The plot exhibited first order dependence on the *r*-LA concentration. The rate order is **12**·2.25MeCN > **9** > **11**·2MeCN > **10**·0.5MeCN. The L^5H_3 derived Ta complex **12**·2.25MeCN showed the highest rate [$k_{obs} = 17\times10^{-4}$ min^{-1}] followed by the L^4H_2 derived Nb complex **9** [$k_{obs} = 11\times10^{-4}$ min^{-1}], L^5H_3 derived Nb complex **11**·2MeCN [$k_{obs} = 8.2\times10^{-4}$ min^{-1}] and the L^4H_2 derived Ta complex **10**·0.5MeCN [$k_{obs} = 5.6\times10^{-4}$ min^{-1}]. Interestingly, for the ROP of *r*-LA, these results show that the Ta-based complex performs best when bound by the L^5H_3 derived ligand set, whereas the Nb system is superior in the case of the L^4H_2 derived ligand.

Table 3-2. ROP of *r*-LA catalysed by complexes **9-12**

Run	Cat	[LA]:[Nb/Ta]:[BnOH] ^{a}	T (°C)	Conv. (%) ^{b}	M_n ^{c}(calc.) $\times10^{-4}$	M_n ^{d}(obs.) $\times10^{-4}$	PDI^d	P_r ^{e}
1	**9**	250:1:1	130	40	0.36	0.12	1.4	-
2	**10**	250:1:1	130	25	0.18	0.09	1.6	-
3	**11**	250:1:1	130	3	-	-	-	-
4	**12**	250:1:1	130	11	-	-	-	-
5	**9**	250:1:0	130	72	0.65	0.27	1.3	-
6	**10**	250:1:0	130	39	0.36	0.20	1.2	-
7	**11**	250:1:0	130	4	-	-	-	-
8	**12**	250:1:0	130	46	0.83	0.23	1.3	-
9	**9**	250:1:1	160	77	0.56	0.45	1.1	0.50
10	**10**	250:1:1	160	55	0.40	0.20	1.2	0.46
11	**11**	250:1:1	160	65	0.93	0.90	1.2	0.61
12	**12**	250:1:1	160	92	1.30	0.90	1.0	0.36
13	**9**	250:1:0	160	93	0.67	0.72	1.3	0.51
14	**10**	250:1:0	160	87	0.62	0.40	1.9	0.50
15	**11**	250:1:0	160	89	1.30	0.80	1.2	0.59
16	**12**	250:1:0	160	99	1.40	1.00	1.4	0.35

[a] [*r*-LA] = 10.00 mmol, [catalyst **9** or **10**] = 0.01 mmol, [**11** or **12**] = 0.02 mmol, [BnOH] = 0.04 mmol (0.01M in toluene), 24 h. [b] Determined by ^{1}H NMR spectroscopy. [c] M_n(calc.) = 144×[LA]$_0$/[Nb/Ta]$_0$×%conv + $M_{\text{end group}}$; [d] M_n(obs) and PDI obtained by GPC in THF relative to polystyrene standards corrected by the Mark-Houwink correction factor M_{nobs} = M_n GPC raw data × 0.58. [e] P_r is the probability of r dyad as determined by ^{1}H NMR spectroscopic analysis.

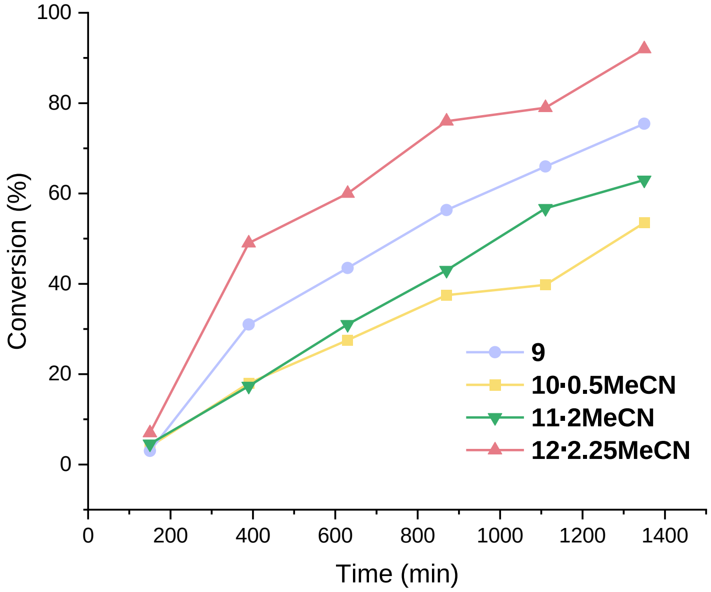

Figure 3-20. Plot of relationship between conversion and time for the polymerisation of *r*-LA at 160 °C. (Table 3-2, entry 13-16).

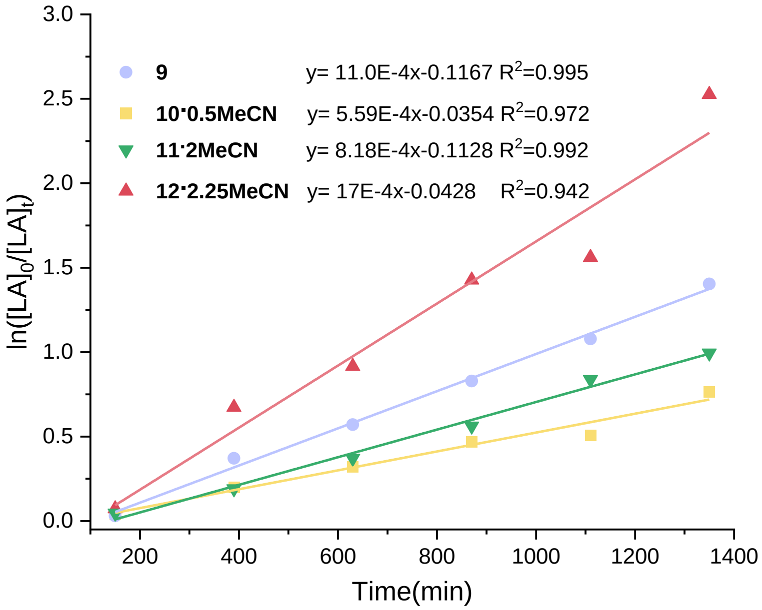

Figure 3-21. Plots of $\ln([LA]_0/[LA]_t)$ *versus* time catalysed by complexes **9-12** at 160 ℃. (Table 3-2, entry 13-16).

To determine the stereo-chemical microstructure of the PLA polymers, 2D homo *J*-resolved NMR spectroscopy was employed and peaks were assigned by reference to the literature.[11,12] For example, complex **12** gives isotactic PLA (Table 3-2, run 12 and 16, P_r = 0.35–0.36), while complex **11** shows a selectivity for heterotactic PLA (Figure 3-22 – 3-29).

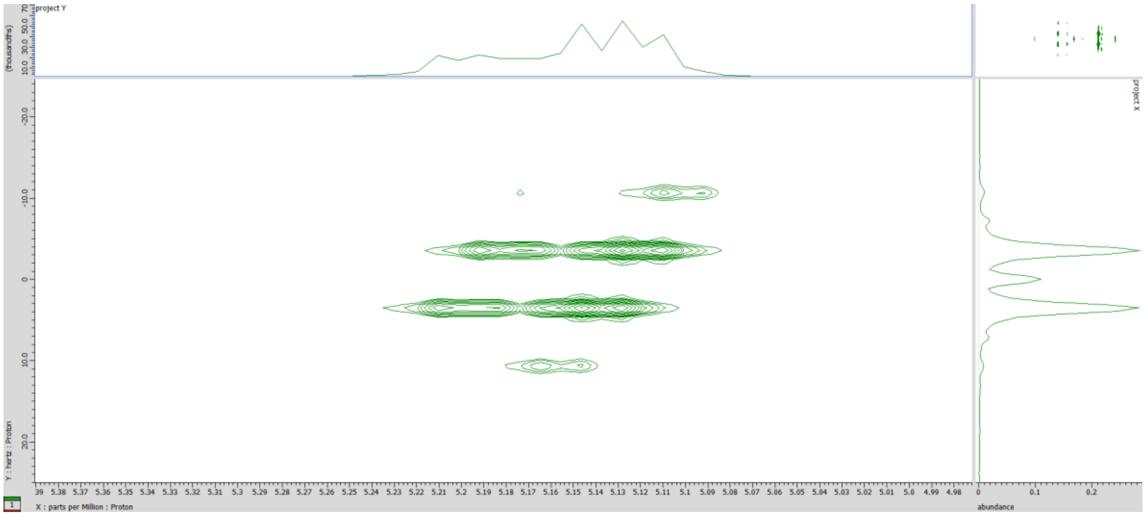

Figure 3-22. 2D homo *J*-resolved NMR spectrum ($CDCl_3$, 400 MHz) of PLA (Table 3-2, entry 5).

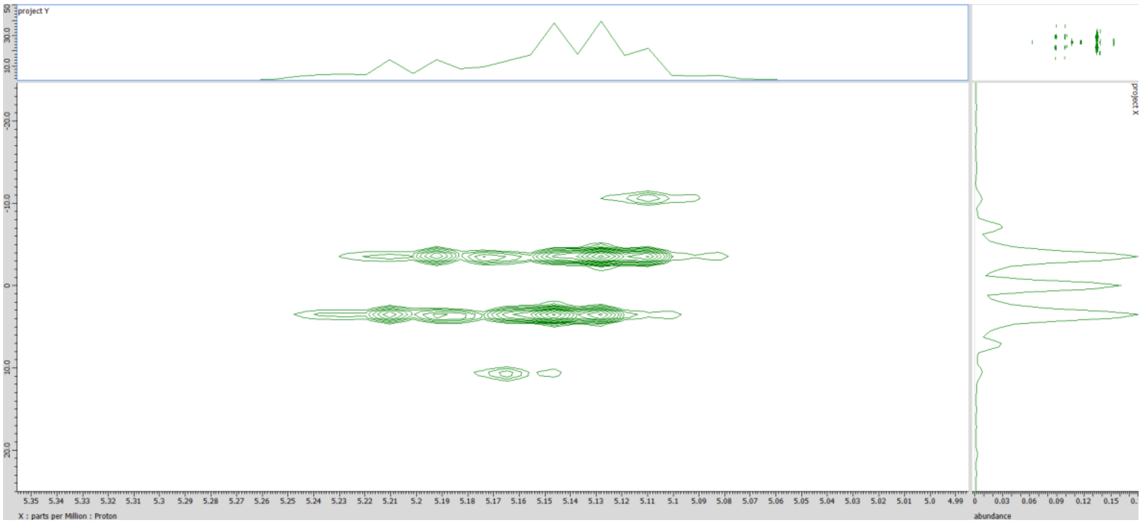

Figure 3-23. 2D homo *J*-resolved NMR spectrum ($CDCl_3$, 400 MHz) of PLA (Table 3-2, entry 6).

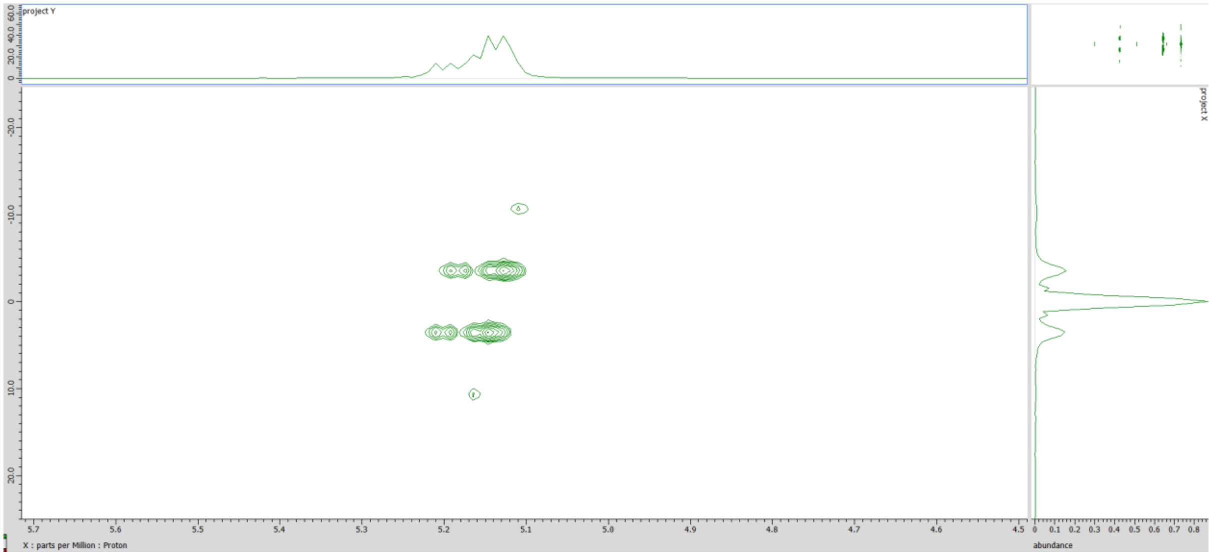

Figure 3-24. 2D homo *J*-resolved NMR spectrum ($CDCl_3$, 400 MHz) of PLA (Table 3-2, entry 7).

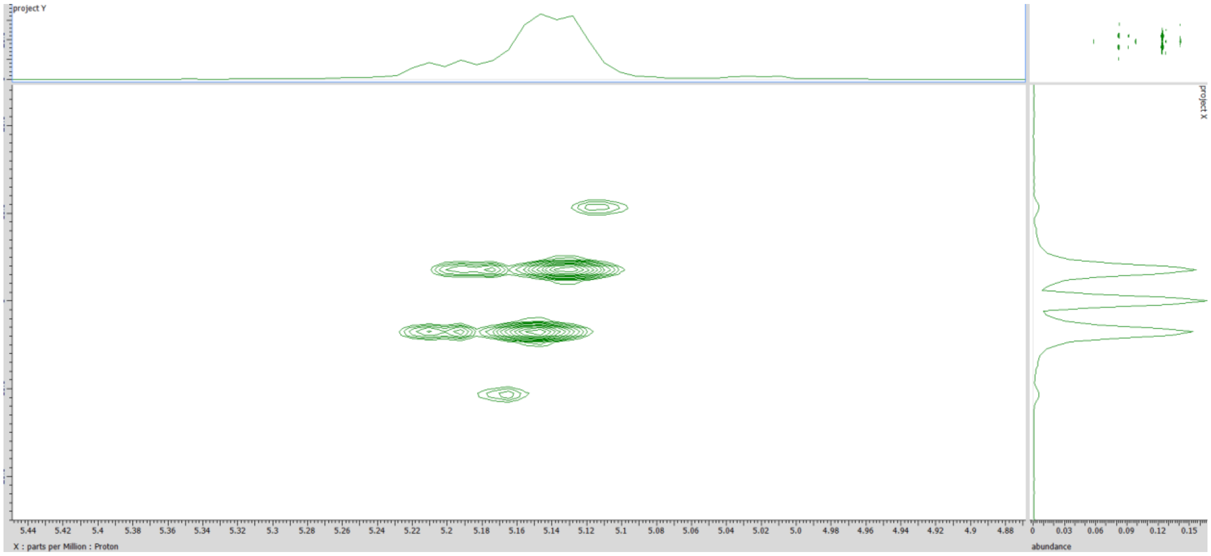

Figure 3-25. 2D homo *J*-resolved NMR spectrum ($CDCl_3$, 400 MHz) of PLA (Table 3-2, entry 8).

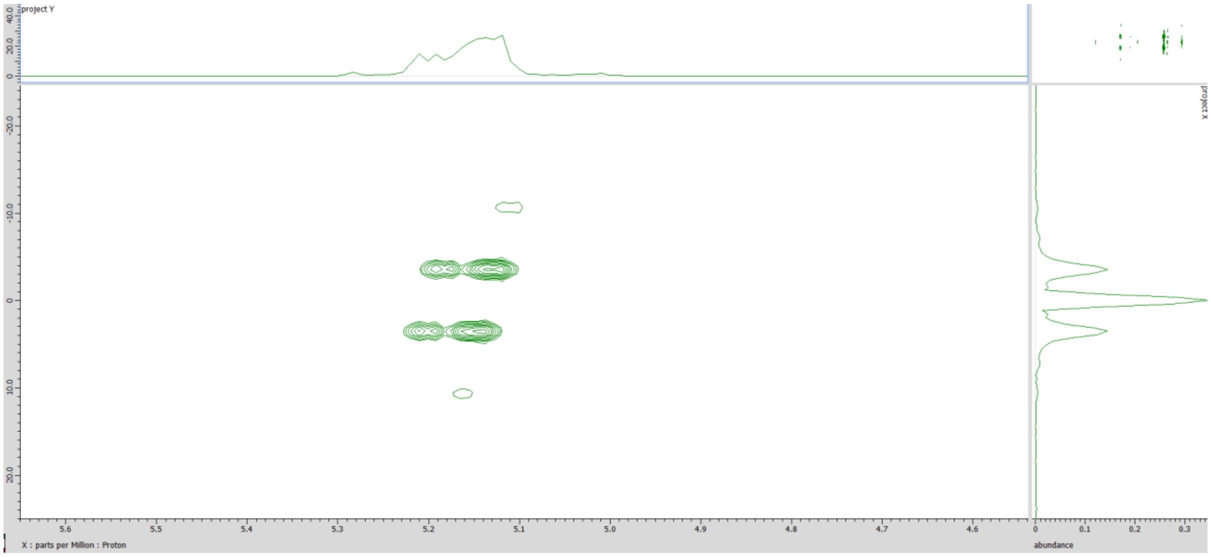

Figure 3-26. 2D homo *J*-resolved NMR spectrum ($CDCl_3$, 400 MHz) of PLA (Table 3-2, entry 9).

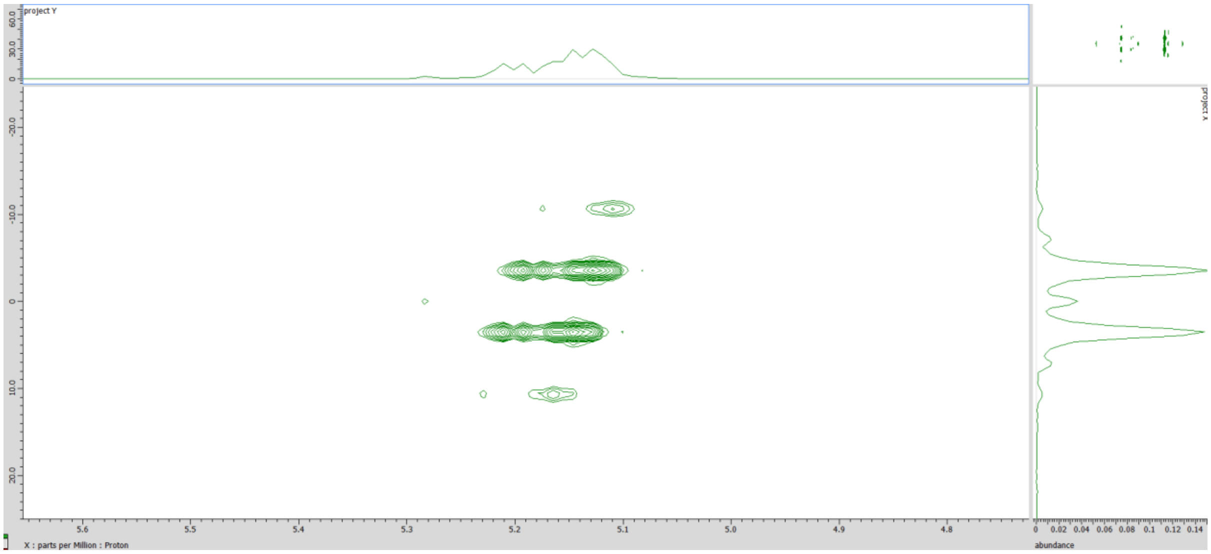

Figure 3-27. 2D homo *J*-resolved NMR spectrum ($CDCl_3$, 400 MHz) of PLA (Table 3-2, entry 10).

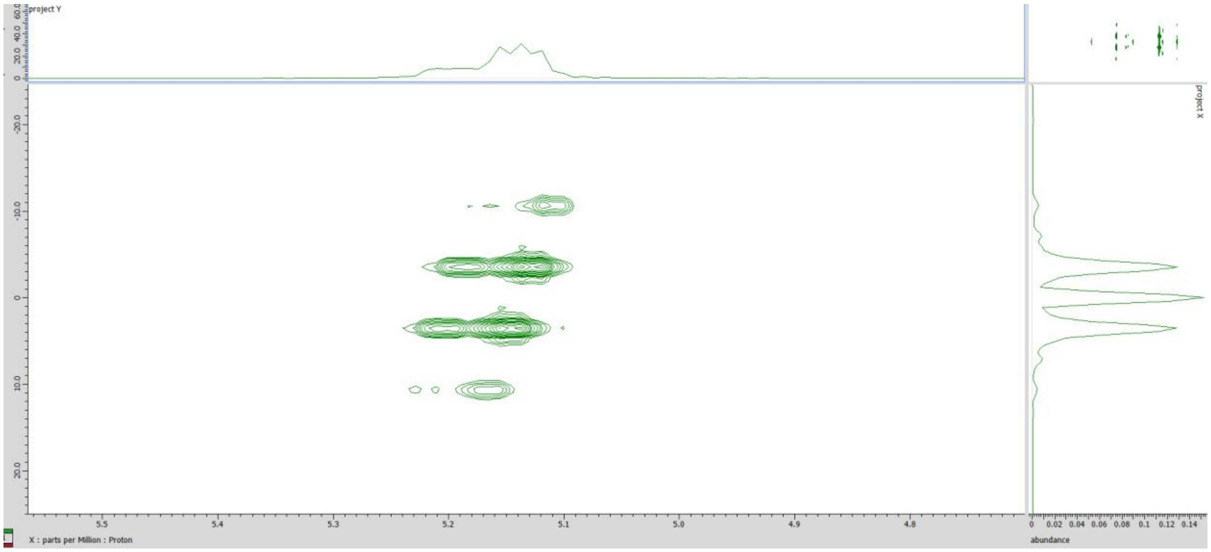

Figure 3-28. 2D homo *J*-resolved NMR spectrum ($CDCl_3$, 400 MHz) of PLA (Table 3-2, entry 11).

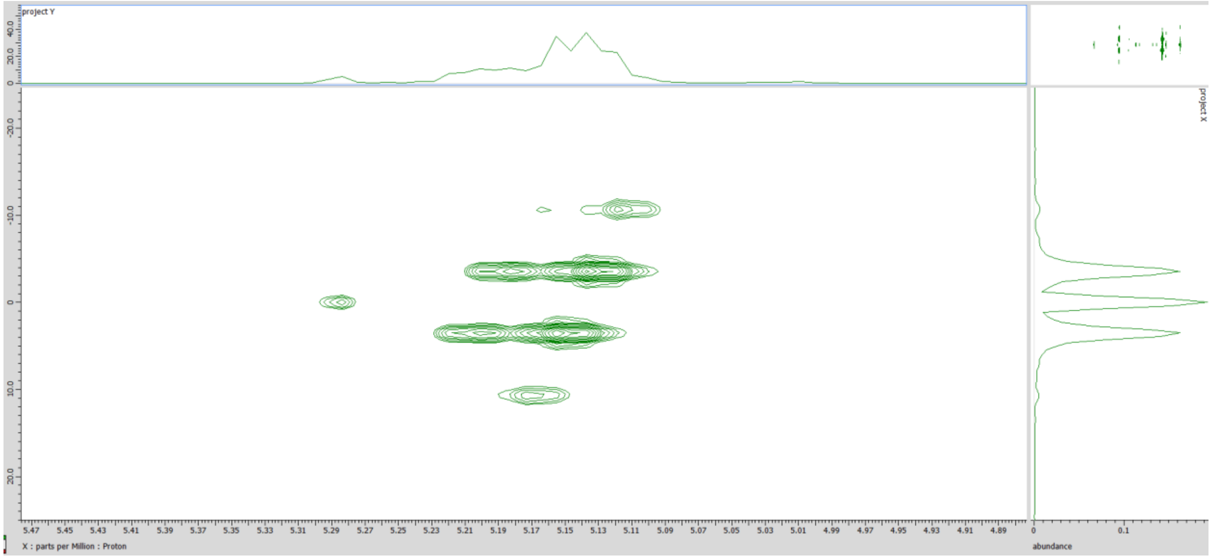

Figure 3-29. 2D homo *J*-resolved NMR spectrum ($CDCl_3$, 400 MHz) of PLA (Table 3-2, entry 12).

Polymer end groups were analysed by ^{1}H NMR spectroscopy and MALDI-TOF mass spectrometry. For example, for the ROP of *r*-LA using **10**·0.5MeCN in the absence of BnOH in a 250:1:0 ratio, a series of peaks were observed with the main peaks identified as CH_3CH_2O– and OH end groups. The set of peaks, namely 114.13 n + 45 + 1.01 + 22.99, is attributed to (LA)n + –

$OCH_2CH_3 + H + Na^+$ (Figure 3-30). From the ^1H NMR spectrum, a quartet peak (e) at 4.15–4.20 ppm and a triplet peak (f) at 1.27 ppm are consistent with the presence of the end group OCH_2CH_3, whilst the quartet peak (a) at 4.32–4.37 is the methine group of the other end group (Figure 3-31).

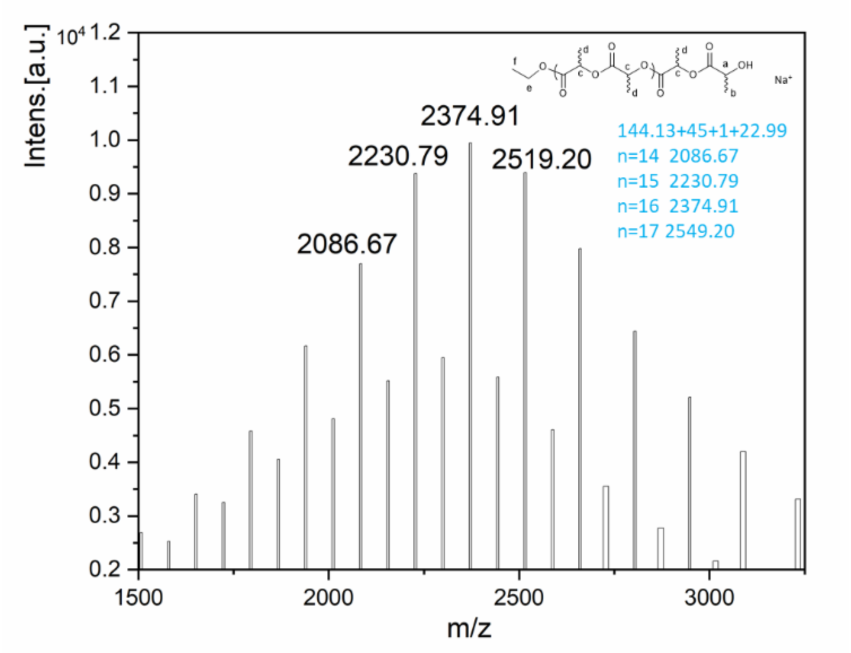

Figure 3-30. MALDI-TOF spectrum of the PLA obtained using **10**·0.5MeCN (Table 3-2, entry 14).

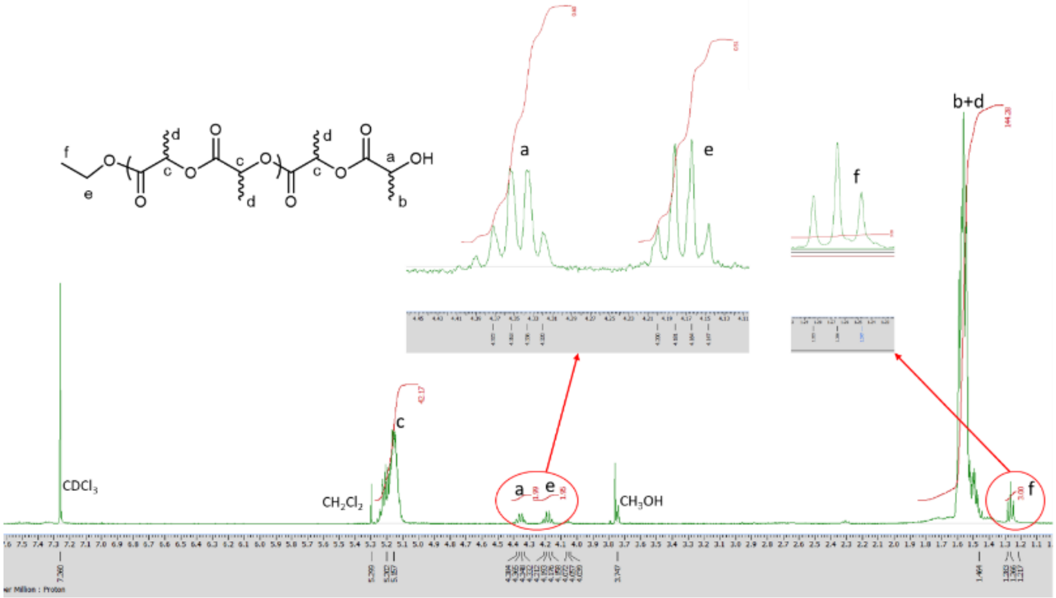

Figure 3-31. ^1H NMR spectrum (400 MHz, $CDCl_3$) of the PLA obtained using **10**·0.5MeCN (Table 3-2, entry 14).

3.2.5 Copolymerisation of ε-CL and *r*-LA using tantalum complex

Based on the results of the homopolymerisation of *r*-LA and ε-CL (Table 3-1, run 9 and Table 3-2, run 16), **12**·2.25MeCN was selected to further explore the ability for the controlled synthesis of diblock PLA-*b*-PCL or PCL-*b*-PLA and random copolymers. The copolymerisation of ε-CL and *r*-LA was studied using **12**·2.25MeCN with different feeding sequences at 160 °C and with a ratio of [CL] : [LA] : [cat] = [125] : [125] : [1] (*i.e.* CL : LA = 50 : 50). Results are summarized in Table 3-3.

Table 3-3. Synthesis of PLA-PCL copolymers catalysed by **12**·2.25MeCN

	First stage polymerisation				Second stage polymerisation					
Run	First monomer	Time (h)	Conversion first monomer	Second monomer	Time (h)	Conv. CL (%)[a]	Conv. LA (%)[a]	M_n (calc.)[c]	M_n (obs.)[b]	PDI[b]
1	CL	12	52	LA	36	68	44	8851	6000	1.1
2	CL	24	88	LA	24	95	59	12079	8000	1.3
3	LA	6	74	CL	42	99	99	16000	11000	1.5
4	LA	12	86	CL	36	37	95	11232	8000	1.5
5	LA	24	94	CL	24	59	99	13160	9000	1.2
6	LA+CL	48	-	-	-	94	95	15294	13000	1.4

[LA] = 3.46 mmol, [CL] = 3.46 mmol, [complex **12**] = 0.028 mmol; solvent: toluene =2 ml; temperature: 160 °C; Reaction time: 48 h. [a] calculated from ^{1}H NMR spectroscopy; [b] M_n(obs) obtained by GPC in THF relative to polystyrene standards corrected by the Mark-Houwink correction factor. [c] M_n(calc.) = $M_{LA}\times[LA]_0/[Ta]\times\%conv + M_{CL}\times[CL]_0/[Ta]\times\%conv + M_{end\ group}$

To find an optimum reaction time for the copolymerisation, the relationship between the conversion of the monomers and the reaction time following the addition of the first monomer was studied. It was found that when ε-CL was the first monomer added (12 h polymerisation time), then following the addition of *r*-LA and an additional 36 h, the conversions of ε-CL and *r*-LA were 68% and 44% respectively. On increasing the first monomer (ε-CL) reaction time to 24 h, the final conversion of ε-CL and *r*-LA reached 95% and 59%, respectively. It was evident that there was always an amount of unreacted *r*-LA when ε-CL was the first monomer added no matter how prolonged was the reaction time. It was evident here that the ROP of ε-CL was somewhat more difficult than that of *r*-LA. This is typified by the homopolymerisation results whereby the activity of complex **12**·2.25MeCN for ε-CL polymerisation is rather low and requires 24 h to convert 250 equiv. of ε-CL to 88% monomer conversion at 160 °C, whilst 18 h was needed to convert 99% of the same amount of *r*-LA. The ^{13}C NMR spectrum of the copolymer when ε-CL was the first monomer added and reacted for 24 h exhibits two carbonyl signals at 173.59 and 169.37 ppm, corresponding to the PCL and PLA block, respectively (Figure 3-32 (b)). The absence of any other peaks between these two carbonyl groups suggests no transesterification occurring in the polymerisation.[13]

In contrast, when *r*-LA was added first and then after 6 h ε-CL was introduced, **12·**2.25MeCN was found to be an efficient initiator and could produce a block copolymer after 48 h with conversions for ε-CL and *r*-LA of 99% and 99%, respectively (Table 3-3, entry 3). Increasing the *r*-LA polymerisation time to 12 h and 24 h reduced the conversion of ε-CL and led to transesterification. In the ^{1}H NMR of PLA-*b*-CL (Figure 3-33), the expected signals for the copolymer were observed; the end groups of CH_3CH_2O– and OH were present. The ^{13}C NMR spectrum of the copolymer exhibits two carbonyl signals at 173.63 and 169.45 ppm, corresponding to the PCL and PLA block, respectively (Figure 3-32 (a)).

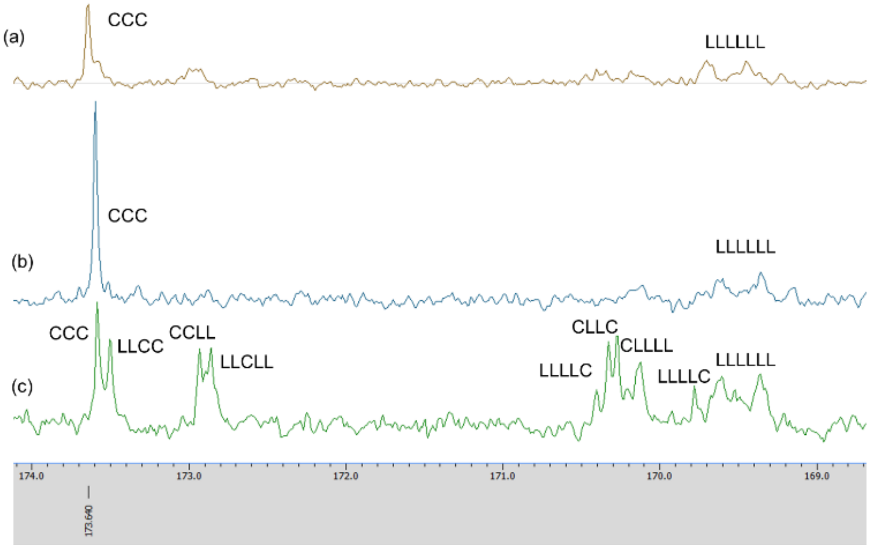

Figure 3-32. Expanded ^{13}C NMR spectra of copolymers prepared in sequential copolymerisation of *r*-LA and ε-CL catalysed by **12·**2.25MeCN. Table 3-3 (a) entry 3; (b) entry 2; (c) entry 6.

For Table 3-3 entry 6, the copolymerisation of *r*-LA and ε-CL was conducted through a one-pot reaction. After 48 h, the two monomers achieved high conversions of 94% for ε-CL and 95% for *r*-LA. The percentage of CL-LA heterodiads could be calculated from the ^{1}H NMR spectrum by comparing the relative intensity of the methylene protons for CL-LA and CL-CL (Figure 3-34), and the percentage of CL-LA heterodiads was 94% suggesting the copolymers had random sequences.[31] The chain microstructure of the copolymer was studied by the ^{13}C NMR spectrum (Figure 3-32 (c)); the carbonyl sequences were assigned according to the literature.[14-18] The average lengths of lactidyl unit L_{LA} and caproyl unit L_{CL} can be calculated according to the equations as described by Kasperczyk.[18] For PCL-*co*-PLA (Table 3-3, entry 6), L_{LA}=2.5 and L_{CL}=1.9, while L_{LA} is slightly longer. The signal at 171 ppm, related to the C-L-C sequence was not detected indicating the absence of a second mode of transesterification.[18] The molecular weights of the copolymers were lower than their theoretical values, with polydispersity in the range of 1.1-1.5.

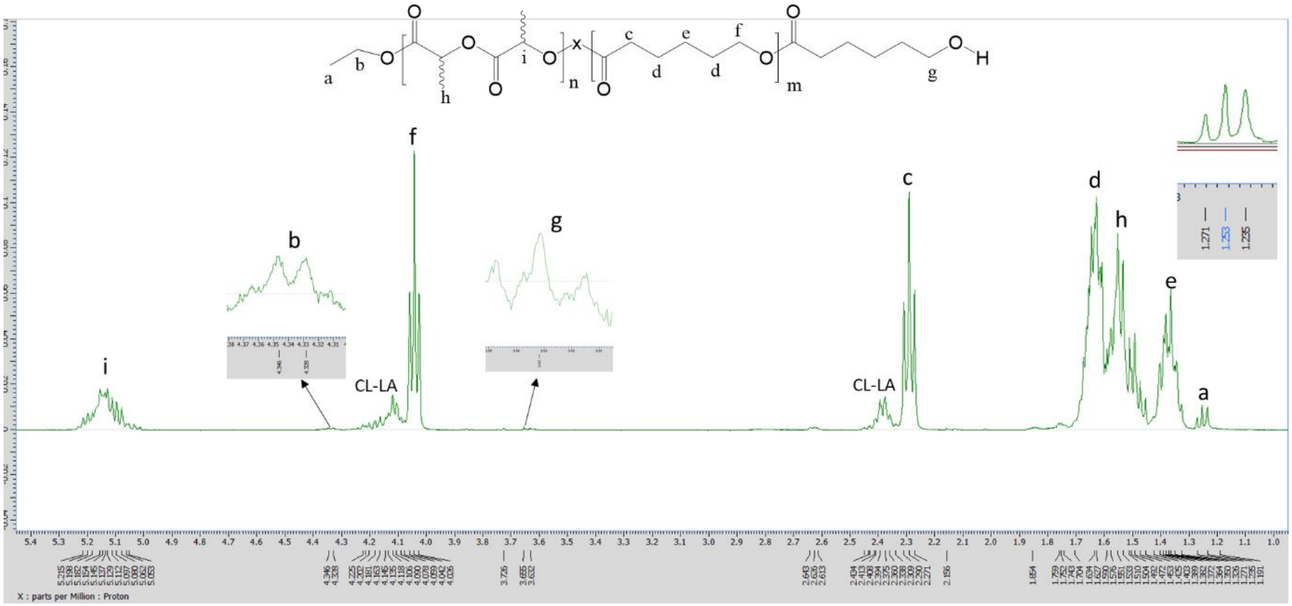

Figure 3-33. ^{1}H NMR spectrum ($CDCl_3$, 400 MHz) of PLA-*b*-CL (Table 3-3, entry 3).

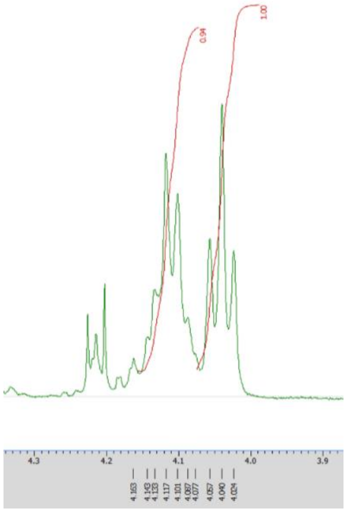

Figure 3-34. ^{1}H NMR spectrum ($CDCl_3$, 400 MHz) of the intensity of methylene protons for CL-LA and CL-CL (Table 3-3, entry 6).

3.3 Conclusion

In this chapter, two different families of complexes on reacting the acids $Ph_2C(X)CO_2H$ (L^4H_2, X = OH; L^5H_3 X = NH_2) with the group V metal alkoxides [$M(OEt)_5$] (M = Nb, Ta) were isolated and structurally characterised. In the case of benzilic acid (L^4H_2), the products were tetranuclear complexes of the form [$M_4(OEt)_8(L^4)_4(\mu\text{-}O)_2$], whereas for 2,2'-diphenylglycine (L^5H_3), dinuclear complexes of the type [$M_2(OEt)_4(L^5H_2)_4(\mu\text{-}O)$] were produced. The benzilic acid derived complexes **9** and **10**·0.5MeCN exhibited good activities in the ROP of ε-CL in the presence of BnOH (conversions were somewhat lower in the absence of BnOH), with the Nb system affording superior conversion. Complexes **9-12** were all active for the ROP of *r*-LA in the absence of BnOH at 160 °C. The Ta-based complex performs best when bound by the L^5H_3 derived ligand set, whereas the Nb system is superior in the case of the L^4H_2 derived ligand. The analysis of the stereoselectivity indicated complex **12**·2.25MeCN affords an isotactic PLA (P_r = 0.35). End group analysis confirmed the alkoxide moiety of the complex initiated the ROP of *ε*-CL or *r*-LA by a coordination-insertion mechanism. Copolymerisations of ε-CL or *r*-LA, in the presence of **12**·2.25MeCN, were conducted using different feed sequences. Block copolymers of PLA-*b*-CL and PCL-*b*-LA and random copolymers PLA-*co*-CL were successfully synthesised by adjusting the feed sequence.

The two new families of niobium and tantalum complexes reported herein, add to the sparse number of examples reported to date that utilize these metals in catalysts for the ring opening polymerisation of cyclic esters.

References

1. M. Braun, *Angew. Chem., Int. Ed. Engl.*, 1996, **35**, 519-522.
2. Y. F. Al-Khafaji, M. R. J. Elsegood, J. W. A. Frese and C. Redshaw, *RSC Adv.*, 2017, **7**, 4510-4517.
3. Y. F. Al-Khafaji, T. J. Prior, L. Horsburgh, M. R. J. Elsegood and C. Redshaw, *ChemistrySelect*, 2017, **2**, 759-768.
4. J. Collins, O. Santoro, T. J. Prior, K. Chen and C. Redshaw, *J. Mol. Struct.*, 2021, **1224**, 129083.
5. Y. Al-Khafaji, X. Sun, T. J. Prior, M. R. Elsegood and C. Redshaw, *Dalton Trans*, 2015, **44**, 12349-12356.
6. J. L. Mata-Mata, J. A. Gutiérrez, M. A. Paz-Sandoval, A. R. Madrigal and A. Martínez-Richa, *J. Polym. Sci., Part A: Polym. Chem.*, 2006, **44**, 6926-6942.
7. R. E. Drumright, P. R. Gruber and D. E. Henton, *Adv. Mater.*, 2000, **12**, 1841-1846.
8. Q. Zhang, W. Zhang, N. M. Rajendran, T. Liang and W. H. Sun, *Dalton Trans*, 2017, **46**, 7833-7843.
9. L. E. Breyfogle, C. K. Williams, V. G. Young, Jr., M. A. Hillmyer and W. B. Tolman, *Dalton Trans*, 2006, DOI: 10.1039/b507014g, 928-936.
10. M. Hayatifar, F. Marchetti, G. Pampaloni and S. Zacchini, *Inorg. Chem.*, 2013, **52**, 4017-4025.
11. M. J. Walton, S. J. Lancaster and C. Redshaw, *ChemCatChem*, 2014, **6**, 1892-1898.
12. C. Ludwig and M. R. Viant, *Phytochem. Anal.*, 2010, **21**, 22-32.
13. D. Dakshinamoorthy and F. Peruch, *J. Polym. Sci., Part A: Polym. Chem.*, 2011, **49**, 5176-5185.
14. D. Pappalardo, L. Annunziata and C. Pellecchia, *Macromolecules*, 2009, **42**, 6056-6062.
15. D. J. Darensbourg and O. Karroonnirun, *Macromolecules*, 2010, **43**, 8880-8886.
16. M. Naddeo, A. Sorrentino and D. Pappalardo, *Polymers*, 2021, **13**, 627.
17. D. J. Gilmour, R. L. Webster, M. R. Perry and L. L. Schafer, *Dalton Trans*, 2015, **44**, 12411-12419.
18. J. Kasperczyk and M. Bero, *Makromol. Chem.*, 1993, **194**, 913-925.

Chapter 4. Ring-opening polymerisation of lactides and lactones by multi-metallic titanium complexes derived from the acids $Ph_2C(X)CO_2H$ (X = OH, NH_2)

4.1 Introduction

In this chapter, the use of titanium alkoxides when combined with these acids was attempted, and some intriguing multi-metallic structural moieties (Figure 4-1) were isolated. These acid/alkoxide products have afforded ROP catalyst systems to exhibit reasonable activities and low PDIs. The use of multi-dentate ligation at titanium in catalytic systems for biopolymer synthesis has been reviewed[1], including a report on the use of amino acid derived ligation.[2] The coordination chemistry of α-hydroxycarboxylic acids has also attracted interest.[3]

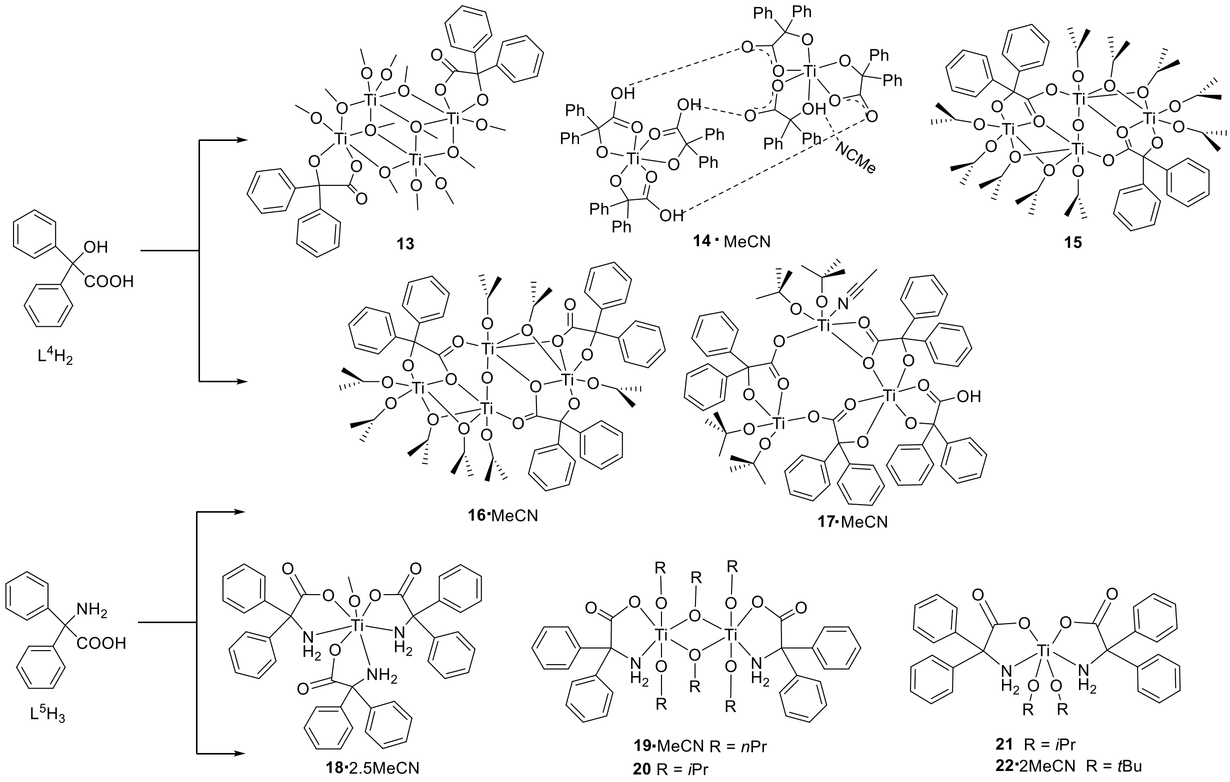

Figure 4-1. Titanium complexes bearing chelate ligands derived from benzilic acid (L^{4}H$_2$) (**13-17**), and 2,2'-diphenylglycine (L^{5}H$_3$) (**18-22**).

4.2 Results and discussion

4.2.1 Synthesis and characterisation of benzilic acid derived titanium complexes

The initial studies focused on the use of benzilic acid, given that it is available in bulk quantities and at relatively low cost.[4] The reactions of L^{4}H$_2$ with differing ratios (see Figure 4-1 and Table 4-1) of the titanium tetra-alkoxides [Ti(OR)$_4$] (R = Me, *n*Pr, *i*Pr, *t*Bu) have been studied, and here only the systems of the products obtained that were suitable for characterisation using X-ray crystallography are presented. The compounds were also characterised by ^{1}H NMR and FTIR spectroscopy, mass spectrometry and elemental analysis. All reactions were conducted in refluxing toluene, followed by workup (extraction) using warm acetonitrile, and recrystallisation on standing (2 – 3 days) at ambient temperature unless stated otherwise (see experimental in chapter 6).

Table 4-1. Summary of molar ratio of ligand:[Ti(OR)$_4$] used to prepare the complexes.

Complex name	ML$_n$(OR)$_m$	Ligand:[Ti(OR)$_4$]	Crystalline products
13	Ti$_4$(L^4)$_2$(OMe)$_2$	L^{4}H$_2$:Ti(OMe)$_4$ = 1:2	✓
14·MeCN	Ti$_2$(L^4)$_2$(L^{4}H)$_4$(O*n*Pr)$_2$·MeCN	L^{4}H$_2$:Ti(O*n*Pr)$_4$ = 2:1	✓
15	Ti$_2$O(L^4)$_2$(O*i*Pr)$_{10}$	L^{4}H$_2$:Ti(O*i*Pr)$_4$ = 1:2	✓
16·MeCN	Ti$_4$O(L^4)$_3$(O*i*Pr)$_8$·MeCN	L^{4}H$_2$:Ti(O*i*Pr)$_4$ = 1:1	✓
		orL^{4}H$_2$:Ti(O*i*Pr)$_4$ = 2:3	
17·MeCN	Ti$_3$(L^4)$_3$(L^{4}H)(O*t*Bu)$_4$(MeCN)·MeCN	L^{4}H$_2$:Ti(O*t*Bu)$_4$ = 1:1	✓
18·2.5MeCN	Ti(L^{5}H$_2$)$_3$(OMe)·2.5MeCN	L^{5}H$_3$:Ti(OMe)$_4$ = 2:1	✓
19·MeCN	Ti$_2$(L^{5}H$_2$)$_2$(O*n*Pr)$_6$·MeCN	L^{5}H$_3$:Ti(O*n*Pr)$_4$ = 1:1	✓
20	Ti$_2$(L^{5}H$_2$)$_2$(O*i*Pr)$_6$	L^{5}H$_3$:Ti(O*i*Pr)$_4$ = 1:1	✓
		orL^{5}H$_3$:Ti(O*i*Pr)$_4$ = 1:2	
21	Ti(L^{5}H$_2$)$_2$(O*i*Pr)$_2$	L^{5}H$_3$:Ti(O*i*Pr)$_4$ = 2:1	✓
22·2MeCN	Ti(L^{5}H$_2$)$_2$(O*t*Bu)$_2$·2MeCN	L^{5}H$_3$:Ti(O*t*Bu)$_4$ = 1:1	✓
-	-	L^{5}H$_3$:Ti(O*t*Bu)$_4$ = 1:4	×

Complex **13** was synthesised by using of a 1:2 mole ratio of L^{4}H$_2$ to [Ti(OMe)$_4$] affording a highly crystalline product **13** in reasonable isolated yield (*ca*. 50%). The molecular structure of [Ti$_4$(L^4)$_2$(OMe)$_{12}$] (**13**) is shown in Figure 4-2, with selected bond lengths and angles given in the caption. Complex **13** crystallizes as centrosymmetric clusters composed of four Ti ions in octahedral coordination that are arranged in a diamond shape. These are bridged by a pair of μ_3-OMe above and below the plane of the four Ti ions. There are four further μ_2-OMe ligands that form the edges of the diamond. For a *trans* pair of Ti ions the coordination is completed by two further terminal OMe ligands. For the two other Ti ions, the coordination is completed by one OMe and chelating benz^{2-}; the benzilic acid plays no part in linking titanium ions. For this structure and others herein, it is possible to classify the coordination mode of the benzilate using the Harris notation[5] and there is further detail in Figure 4-3. Here the coordination of the benzilate can be classified as [1.011]. The asymmetric unit (Figure 4-2) contains two independent half clusters. For a further representation of this structure see Figure 4-4. There are no classical hydrogen bonds present but C–H···O interactions between the clusters.

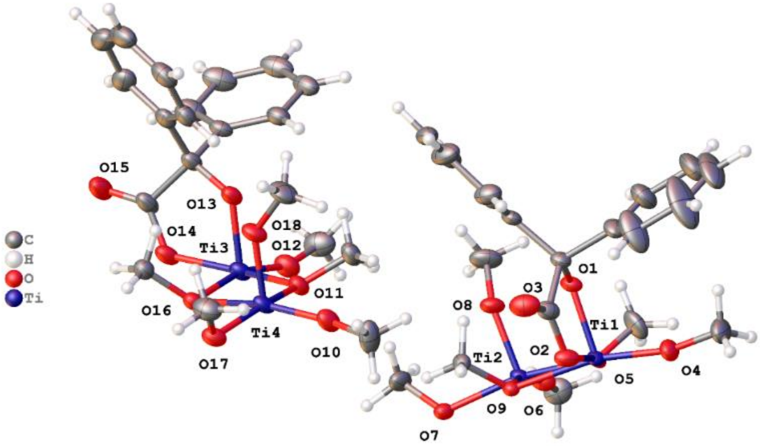

Figure 4-2. Asymmetric unit of **13** with atoms drawn as 50 % probability ellipsoids. Two symmetry-independent half clusters are present. Selected bond lengths (Å) and bond angles (°): Ti(1)-O(4) 1.7660(17), Ti(1)-O(1) 1.8556(16), Ti(1)-O(5) 1.9750(18), Ti(1)-O(2) 1.9800(18), Ti(1)-O(7#1) 2.0173(16), Ti(1)-O(9) 2.2140(15), Ti(2)-O(6) 1.7446(18), Ti(2)-O(8) 1.8031(16), Ti(2)-O(7) 1.9912(16), Ti(2)-O(5) 2.0125(16), Ti(2)-O(9) 2.1424(16), Ti(2)-O(9#1) 2.1847(15); O(4)-Ti(1)-O(1) 101.14(8), O(4)-Ti(1)-O(5) 99.31(8), O(1)-Ti(1)-O(5) 94.61(7), O(4)-Ti(1)-O(2) 100.41(8), O(1)-Ti(1)-O(2) 79.78(7), O(5)-Ti(1)-O(2) 160.19(7), O(4)-Ti(1)-O(7#1) 93.61(7), O(1)-Ti(1)-O(7#1) 162.32(7), O(5)-Ti(1)-O(7#1) 92.56(7), O(2)-Ti(1)-O(7#1) 88.05(7), O(4)-Ti(1)-O(9) 165.98(7), O(1)-Ti(1)-O(9) 92.08(6), O(5)-Ti(1)-O(9) 74.74(6), O(2)-Ti(1)-O(9) 86.41(7), O(6)-Ti(2)-O(8) 101.52(8), O(6)-Ti(2)-O(7) 97.57(8), O(8)-Ti(2)-O(7) 93.87(7), O(6)-Ti(2)-O(5) 94.09(8), O(8)-Ti(2)-O(5) 96.89(7), O(7)-Ti(2)-O(5) 162.23(7), O(6)-Ti(2)-O(9) 163.42(8), O(8)-Ti(2)-O(9) 92.73(7), O(7)-Ti(2)-O(9) 89.79(7), O(5)-Ti(2)-O(9) 75.64(6), O(6)-Ti(2)-O(9#1) 95.55(7), O(8)-Ti(2)-O(9#1) 160.96(7).

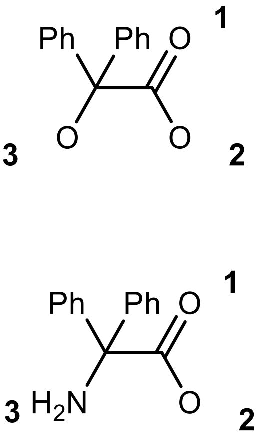

Figure 4-3. Harris notation and its application in describing these ligands.

In line with the method of Harris[5], Figure 4-3 describes the coordination of the benzilic acid in a systematic way. Each of the oxygen atoms has been numbered in a consistent manner as shown above. The order in the Harris symbol reflects the binding of each atom in order. For example, [2.021] signifies the ligand binds to two metals, oxygen #1 does not bind, oxygen #2 binds to both metal ions, and oxygen #3 binds to one metal. It is notable that the same binding occurs for diphenyl glycine in each case, namely [1.011]. That is to say, the dpg is chelating through O#2 and N#3.

In some cases, it is necessary to remove ambiguity about which metal ions are bound and this is done through the use of subscripts to identify the metal ions. For example, $[3.1_{1}1_{2}2_{13}]$ would signify three unique bound metal ions; atom 1 binds M#1, atom 2 binds M#2, and atom 3 binds both M#1 and M#3.

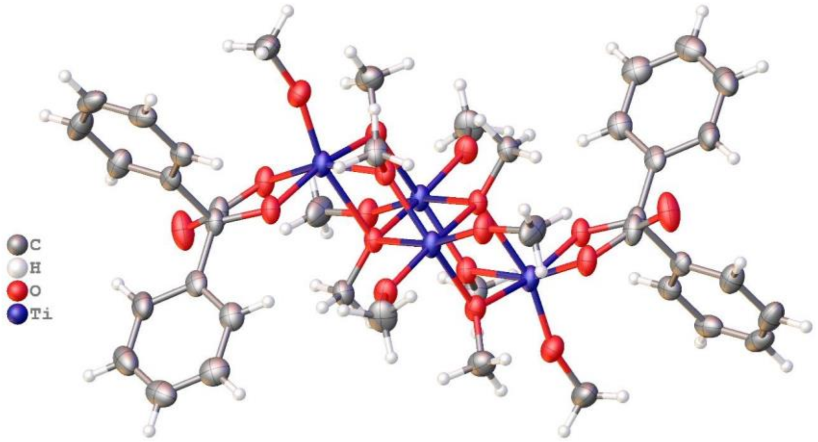

Figure 4-4. Alternative view of **13**.

Similar use of $[\mathrm{Ti}(\mathrm{O}n\mathrm{Pr})_4]$ with L^4H_2 in a ratio of 1:2 led to the isolation of the salt complex $[\mathrm{Ti}(L^4H)_3][\mathrm{Ti}(L^4H)(L^4)_2]$•MeCN (**14**•MeCN). Complex **14**•MeCN crystallizes in the monoclinic space group $P2_1/c$. The asymmetric unit (Figure 4-5) contains two independent six-coordinate titanium ions, each of which is coordinated by three bidentate benzilate ions in a *fac* arrangement. For the first titanium ion, Ti1, each benzilic acid is deprotonated only at the alcohol so that it chelates through the alkoxide and the carbonyl of the carboxylic acid, and formally, the coordination of each benzilate is [1.011]. The OH portion of each carboxylic acid forms a hydrogen bond to the neighbouring cluster centred on Ti2. In this way, there are hydrogen-bonded dimers.

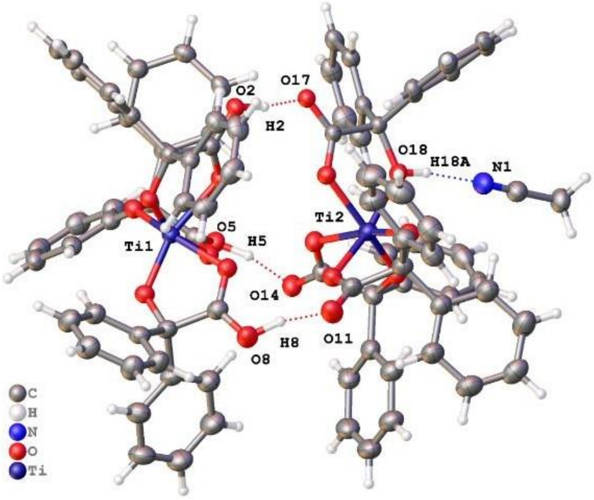

Figure 4-5. Asymmetric unit of **14** with atoms drawn as 50% probability ellipsoids. Dashed lines show classical hydrogen bonds. Selected bond lengths (Å) and bond angles (°): Ti(1)-O(1) 2.0679(18), Ti(1)- O(3) 1.8377(18), Ti(1)-O(4) 2.0880 (19), Ti(1)-O(6) 1.8550 (19), Ti(1)-O(7) 2.097(2), Ti(1)-O(9) 1.8438(19); O(3)-Ti(1)-O(4) 161.49(8), O(3)-Ti(1)-O(6) 100.04(8), O(3)-Ti(1)-O(7) 96.16(8), O(3)-Ti(1)-O(9) 102.00(8), O(4)-Ti(1)-O(7) 84.34(8), O(6)-Ti(1)-O(1) 95.44(8), O(6)-Ti(1)-O(4) 77.91(8), O(6)-Ti(1)-O(7) 162.15(8), O(9)-Ti(1)-O(1) 158.84(8), O(9)-Ti(1)-O(4) 96.24(8), O(9)-Ti(1)-O(6) 105.17(9), O(9)-Ti(1)-O(7) 78.51(8).

The coordination about Ti2 is similar (Figure 4-6); two of the three benzilic acids are twice deprotonated, but the third is deprotonated only at the carboxylic acid. All are chelating in [1.011] mode. The alcohol does bind to Ti2 but also forms a hydrogen bond with an unbound molecule of acetonitrile. The X-ray scattering data were good enough that it was possible to identify the positions of the hydrogen atoms through different Fourier methods.

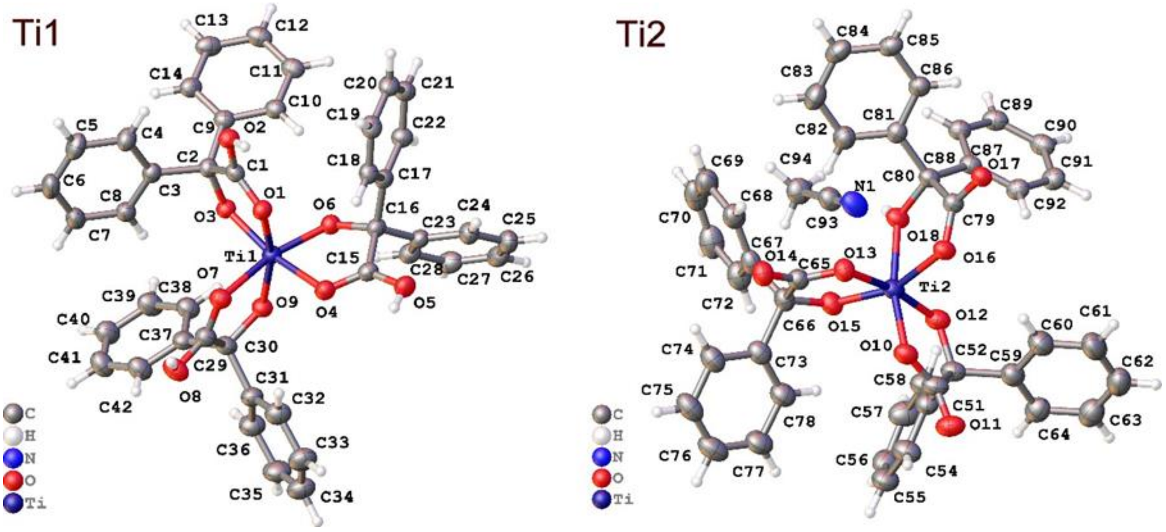

Figure 4-6. Coordination about the two independent Ti ions in **14**.

In the case of [Ti(O*i*Pr)$_4$], varying the reaction stoichiometry led to the isolation of two different products. When using a ratio of 1:2 (L^{4}H$_2$:Ti), the product isolated was found to be [Ti$_4$O(L^4)$_2$(O*i*Pr)$_{10}$] (**15**). The clusters (Figure 4-7) in **15** contain four roughly octahedral Ti ions that are linked by benzilate, each of which has a [3.1$_1$2$_{23}$1$_3$] coordination mode, and by bridging isopropoxide; for an alternative view, see Figure 4-8. The cluster can be described by dividing it into two similar halves. Benzilate is chelated to Ti1, but the carboxylate is also involved in bonding to Ti2 and Ti3. Ti1 and Ti2 are further linked by two μ$_2$-O*i*Pr, and terminal O*i*Pr ligands complete the coordination at Ti1 and Ti2. Ti4 are Ti3 are akin to Ti1 and Ti2, and the two halves are linked by the two Ti–O carboxylate bonds and an oxide bridge. The average Ti···Ti bond distance in the two halves of the cluster is 3.059(4) Å, which is similar to the value of 3.0459 (7) Å in the oxo-bridged tetranuclear titanium compound reported by Kemmitt *et al*.[6], and is indicative of no Ti–Ti bonding.

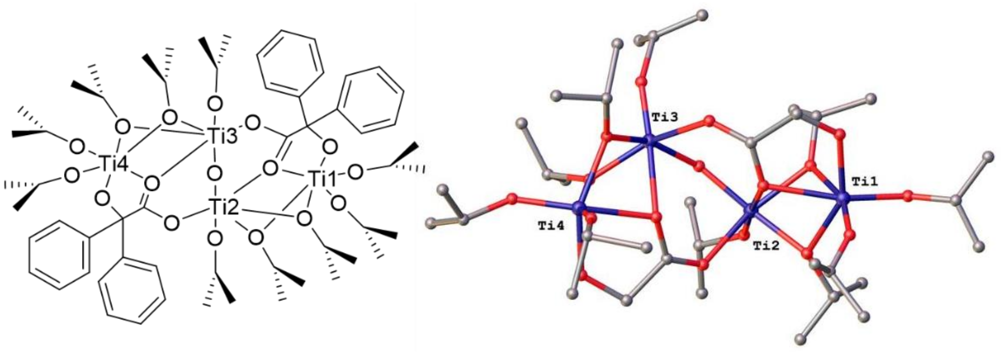

Figure 4-7. Asymmetric unit of **15**.

For clarity, atoms are drawn as spheres of arbitrary radius, minor disorder is not shown, and hydrogen atoms are not shown. Selected bond lengths (Å) and bond angles (°): Ti(1)–O(1) 2.136(8), Ti(1)–O(3) 1.888(9), Ti(1)–O(7) 1.832(9), Ti(1)–O(8) 1.697(10), Ti(1)–O(9) 2.277(9), Ti(1)–O(10) 2.022(8), Ti(2)–O(1) 2.260(7), Ti(2)–O(5) 2.075(8), Ti(2)–O(9) 1.963(9), Ti(2)–O(10) 2.028(8), Ti(2)–O(11) 1.799(7), Ti(2)–O(17) 1.766(8); O(1)–Ti(1)–O(9) 72.1(3), O(3)–Ti(1)–O(1) 76.0(3), O(3)–Ti(1)–O(10) 149.1(3), O(7)–Ti(1)–O(1) 163.5(3), O(7)–Ti(1)–O(10) 106.3(4), O(8)–Ti(1)–O(1) 94.9(4), O(8)–Ti(1)–O(3) 99.6(4), O(8)–Ti(1)–O(7) 101.5(4), O(8)–Ti(1)–O(9) 160.2(4), O(8)–Ti(1)–O(10) 92.1(4), O(10)–Ti(1)–O(1) 74.6(3), O(10)–Ti(1)–O(9) 70.4(3), O(5)–Ti(2)–O(1) 84.7(3), O(9)–Ti(2)–O(1) 75.6(3), O(9)–Ti(2)–O(5) 156.4(3), O(9)–Ti(2)–O(10) 77.1(3), O(10)–Ti(2)–O(1) 71.8(3), O(10)–Ti(2)–O(5) 84.5(3), O(11)–Ti(2)–O(9) 102.6(3), O(11)–Ti(2)–O(10) 155.6(3), O(17)–Ti(2)–O(1) 175.3(3), O(17)–Ti(2)–O(5) 92.9(3), O(17)–Ti(2)–O(9) 105.8(4), O(17)–Ti(2)–O(10) 104.0(3), O(17)–Ti(2)–O(11) 99.5(3).

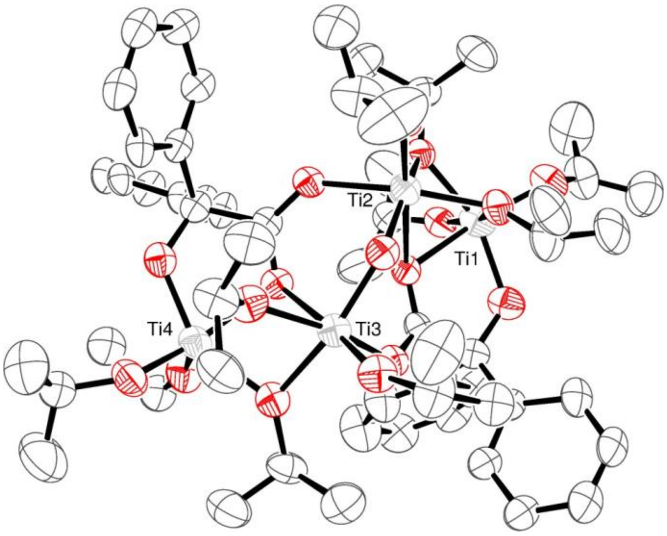

Figure 4-8. Alternate view (ORTEP) of **15** with atoms drawn as 25 % probability ellipsoids. Minor disorder and hydrogen atoms are omitted for clarity.

On changing the ratio to 1:1, the product isolated was [$Ti_4O(L^4)_3(OiPr)_8$] (**16**), which crystallizes in the triclinic system in the space group *P*-1 (Figure 4-9; an alternative view is given in Figure 4-10). Complex **16** is very similar to **15,** but one terminal O*i*Pr ligand and one bridging O*i*Pr ligand on Ti1 are replaced by chelating benzilate, which also bridges to Ti2 in the coordination mode [2.021]. Each of the other two benzilate anions has $[3.1_{1}2_{23}1_{3}]$ coordination mode, being both chelating and bridging. There is substantial disorder in the position and orientation of the ligand set, particularly around Ti4. There is also evidence of a small amount of disordered solvent equating to one acetonitrile per cluster. The Ti···Ti distances are 3.0682(10), 3.2583(12), and 3.3958(11) Å, which are notably longer than observed in **15**.

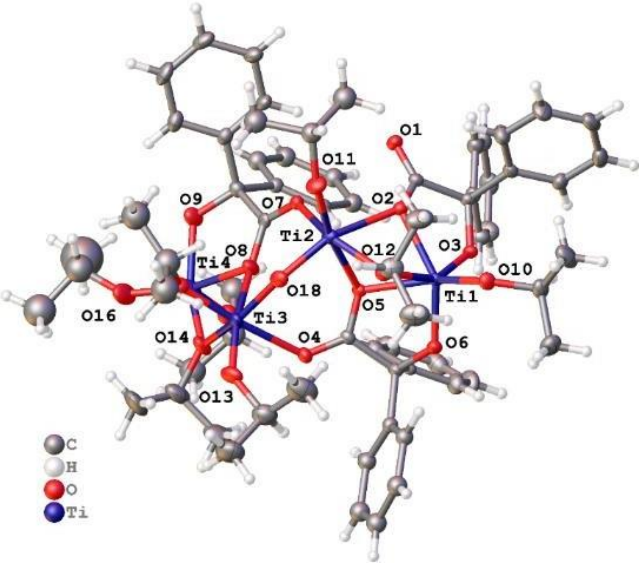

Figure 4-9. Asymmetric unit of **16** with atoms drawn as 50% probability ellipsoids. Disorder is not illustrated. Selected bond lengths (Å) and bond angles (°): Ti(1)-O(5) 2.204(3), Ti(1)-O(3) 1.829(3), Ti(1)-O(2) 2.096(3), Ti(1)-O(6) 1.860(3), Ti(1)-O(10) 1.787(3), Ti(1)-O(12) 2.059(3), Ti(2)-O(5) 2.159(3), Ti(2)-O(7) 2.055(3), Ti(2)-O(2) 2.160(3), Ti(2)-O(12) 1.968(3), Ti(2)-O(18) 1.762(3), Ti(2)-O(11) 1.765(3), Ti(3)-O(4) 2.188(3), Ti(3)-O(18) 1.856(4), Ti(3)-O(8) 2.208(3), Ti(3)-O(14) 2.020(4), Ti(3)-O(13) 1.765(3), Ti(3)-O(17) 1.840(5), Ti(3)-O(17A) 1.907(9), Ti(4)-O(8) 2.098(3), Ti(4)-O(9) 1.884(4), Ti(4)-O(14) 1.957(4), Ti(4)-O(16) 1.757(4), Ti(4)-O(15) 1.830(5), Ti(4)-O(15A) 1.643(10), Ti(4)-O(17A) 2.458(9); O(3)-Ti(1)-O(5) 102.26(11), O(3)-Ti(1)-O(2) 77.55(11), O(3)-Ti(1)-O(6) 99.49(12), O(3)-Ti(1)-O(12) 150.55(12), O(2)-Ti(1)-O(5) 70.52(10), O(6)-Ti(1)-O(5) 75.37(11), O(6)-Ti(1)-O(2) 144.11(12), O(6)-Ti(1)-O(12) 106.64(12),O(10)-Ti(1)-O(5) 159.81(12), O(10)-Ti(1)-O(3) 97.89(13), O(10)-Ti(1)-O(2) 115.59(13), O(10)-Ti(1)-O(6) 100.28(13), O(10)-Ti(1)-O(12) 90.68(13), O(5)-Ti(2)-O(2) 70.24(10), O(7)-Ti(2)-O(5) 84.82(11), O(7)-Ti(2)-O(2) 85.14(10), O(12)-Ti(2)-O(5) 74.96(11), O(12)-Ti(2)-O(7) 154.61(11), O(12)-Ti(2)-O(2) 73.77(11), O(18)-Ti(2)-O(5) 87.37(12), O(18)-Ti(2)-O(7) 93.96(14), O(18)-Ti(2)-O(2) 157.59(13), O(18)-Ti(2)-O(12) 100.18(14), O(18)-Ti(2)-O(11) 103.86(15), O(11)-Ti(2)-O(5) 168.77(13),

O(11)-Ti(2)-O(7) 94.08(14), O(11)-Ti(2)-O(2) 98.54(13), O(9)-Ti(4)-O(8) 75.54(13), O(9)-Ti(4)-O(14) 143.93(16), O(14)-Ti(4)-O(8) 73.34(13).

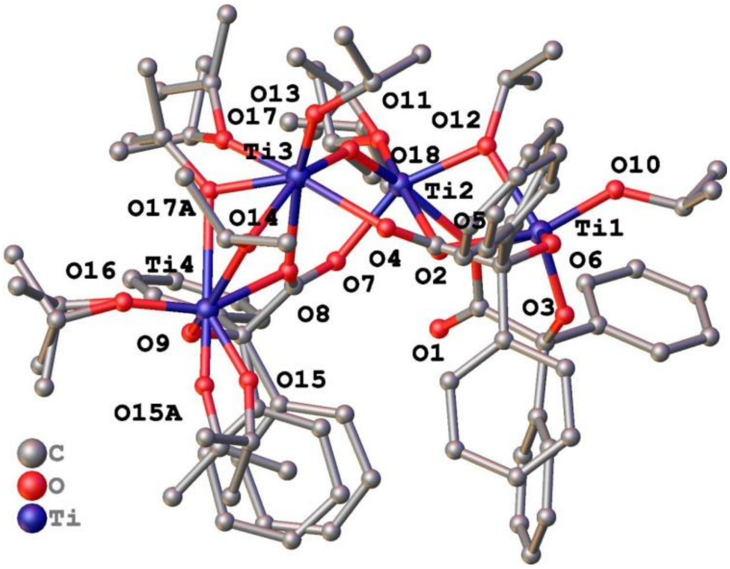

Figure 4-10. Asymmetric unit of **16** with atoms drawn as spheres of arbitrary radius. Each disorder component is illustrated; hydrogen atoms are not shown for clarity.

Finally, the use of $[\mathrm{Ti(O}t\mathrm{Bu)_4}]$ was investigated and found that the use of a 1:1 ratio resulted in the formation of the asymmetric trinuclear titanium complex $[\mathrm{Ti_3(L^4)_4(O}t\mathrm{Bu)_4{\cdot}MeCN}]{\cdot}\mathrm{MeCN}$ (**17**·MeCN) (Figure 4-11; an alternative view is given in Figure 4-12). Complex **17** crystallizes in the triclinic system with the space group *P*-1. This features a cluster composed of Ti ions bridged by benzilate and decorated by two monodentate O*t*Bu ligands as each of Ti2 and Ti3. At Ti1, there is a chelating, but not bridging benzilate. Here there are four unique benzilate anions and these feature three different coordination modes. At Ti1 the alkoxide and carboxylic acid form a 5-membered chelate (benzilate coordination mode [2.011]); one further ion forms a similar chelate but the second oxygen of the carboxylate bonds to Ti2 (coordination mode $[2.1_11_21_2]$); the third chelating anion forms a similar 5-membered chelated but in addition to this the carboxylate forms an unequal bidentate chelate to Ti3 such that one of the oxygen atoms (O4) bridges between Ti1 and Ti3 in coordination mode $[2.1_12_{12}1_2]$. The M−O bond lengths for the bidentate chelating carboxylate are these: Ti3–O4 2.3458(8) Å and Ti3–O5 2.0624(8) Å. Ti2 and Ti3 are joined by a ‘normal’ chelating anion that also bridges through the second oxygen of the carboxylate (coordination mode $[2.1_11_21_2]$).

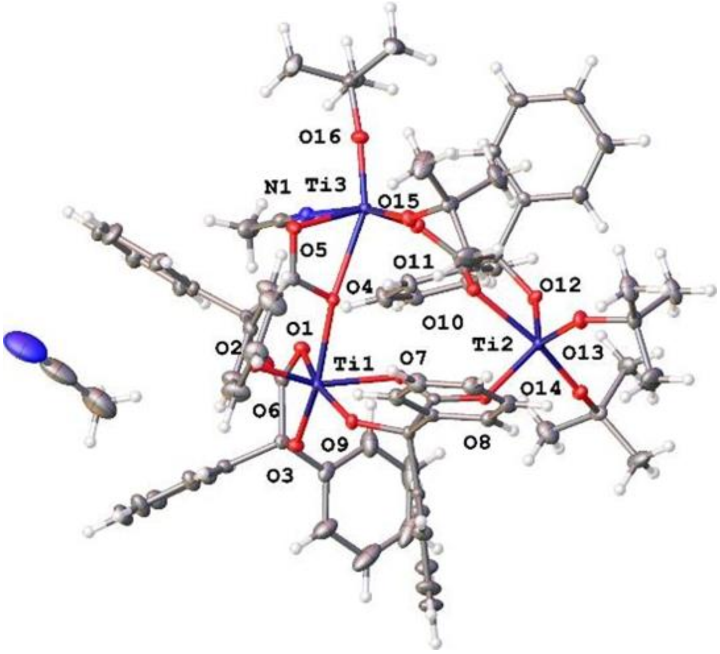

Figure 4-11. Asymmetric unit of **17** with atoms drawn as 50% probability ellipsoids. Selected bond lengths (Å) and bond angles (°): Ti(1)-O(10) 1.7393(10), Ti(1)-O(9) 1.7389(10), Ti(1)-O(6) 1.9703(10), Ti(1)-O(1) 2.0623(10), Ti(1)-N(5) 2.2675(13), Ti(1)-O(2) 2.3456(10), Ti(2)-O(16) 1.8371(10), Ti(2)-O(14) 1.8548(10), Ti(2)-O(15) 1.8580(10), Ti(2)-O(3) 2.0173(10), Ti(2)-O(7) 2.0834(10), Ti(2)-O(2) 2.1848(10), Ti(3)-O(12) 1.7699(10), Ti(3)-O(11) 1.7773(10), Ti(3)-O(13) 1.8650(10), Ti(3)-O(8) 1.9827(10), Ti(3)-O(5) 2.1213(10); O(10)-Ti(1)-O(9) 104.31(5), O(14)-Ti(2)-O(15) 97.49(4), O(11)-Ti(3)-O(8) 108.43(5), O(10)-Ti(1)-O(6) 97.48(4), O(16)-Ti(2)-O(3) 80.13(4), O(13)-Ti(3)-O(8) 131.22(4), O(9)-Ti(1)-O(6) 101.45(4), O(14)-Ti(2)-O(3) 162.34(4), O(12)-Ti(3)-O(5) 161.99(4), O(10)-Ti(1)-O(1) 95.97(4), O(15)-Ti(2)-O(3) 100.09(4), O(11)-Ti(3)-O(5) 92.60(4), O(9)-Ti(1)-O(1) 102.02(4), O(6)-Ti(1)-O(1) 149.05(4), O(8)-Ti(3)-O(5) 80.33(4), O(10)-Ti(1)-N(5) 167.84(5), O(15)-Ti(2)-O(7) 154.51(4), O(9)-Ti(1)-N(5) 87.85(5), O(3)-Ti(2)-O(7) 85.27(4), O(16)-Ti(2)-O(2) 161.52(4), O(1)-Ti(1)-N(5) 81.25(4), O(14)-Ti(2)-O(2) 100.77(4), O(10)-Ti(1)-O(2) 92.13(4), O(15)-Ti(2)-O(2) 77.03(4), O(9)-Ti(1)-O(2) 156.56(4), O(3)-Ti(2)-O(2) 81.60(4), O(6)-Ti(1)-O(2) 92.67(4), O(7)-Ti(2)-O(2) 79.18(4), O(1)-Ti(1)-O(2) 59.04(4), O(12)-Ti(3)-O(11) 105.13(5), N(5)-Ti(1)-O(2) 76.26(4), O(16)-Ti(2)-O(14) 97.48(4), O(11)-Ti(3)-O(13) 115.14(5), O(16)-Ti(2)-O(15) 103.48(4), O(12)-Ti(3)-O(8) 96.65(4), O(11)-Ti(3)-O(8) 108.43(5), O(13)-Ti(3)-O(8) 131.22(4), O(12)-Ti(3)-O(5) 161.99(4), O(11)-Ti(3)-O(5) 92.60(4), O(8)-Ti(3)-O(5) 80.33(4).

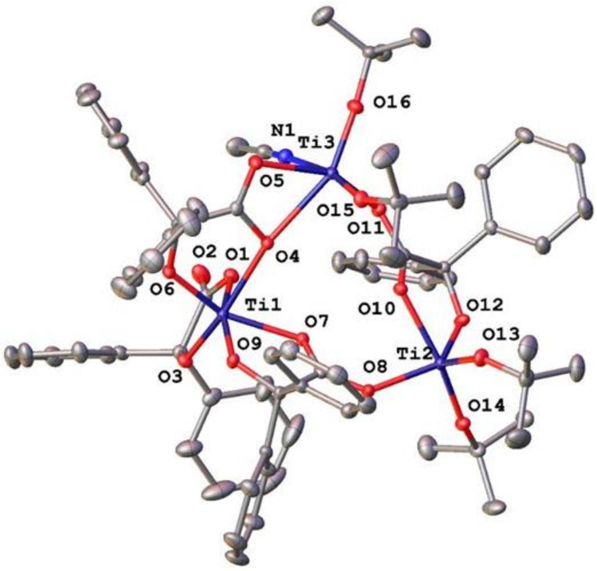

Figure 4-12. Alternative view of **17** with atoms drawn as 50% probability ellipsoids. For clarity hydrogen atoms have been omitted.

Infrared and ^{1}H NMR Spectra of L^4H_2-Derived Complexes

In the FT-IR spectra, for the parent L^4H_2, there is a sharp and intense peak at 3395 cm^{-1}, corresponding to the O-H asymmetric stretching vibration. However, this O-H peak for complexes **13–17** has disappeared, which verifies the participation of the hydroxyl group in the reaction. The C=O stretching vibration in L^4H_2 gives rise to a sharp band at 1716 cm^{-1}, whereas the C=O stretching shifts to 1680 cm^{-1}, 1733 cm^{-1}, 1729 cm^{-1}, 1728 cm^{-1}, 1704 cm^{-1}, for **13–17**, respectively, indicative of bonding between the carboxyl and the titanium centre. A new band appeared for all the complexes in the range 429-466 cm^{-1}, which we assign to Ti-O bonding. The ^{1}H NMR spectra suggest there is alkoxide exchange in solution for the L^4H_2 derived complexes containing bridging and terminal alkoxide ligation. However, variable temperature ^{1}H NMR spectroscopic studies (in CD_3CN) conducted between −40 °C and +50 °C revealed little change; overall integrations were consistent with the solid-state structures, e.g. the integral ratio of the multi-signals for the phenyl groups (δ = 7.83-6.80), the septet for the isopropoxide methine (δ = 3.89-3.83 and 3.32) and the doublet for the methyl (δ = 1.07 and 1.06) are 20:10:60 consistent with the structure of **15**. The structures of the complexes are also consistent with their elemental analysis and mass spectrometry data.

4.2.2 Synthesis and characterisation of 2,2’-diphenylglycine derived titanium complexes

Having established suitable synthetic conditions for the synthesis and isolation of titanium complexes derived from L^4H_2, studies were extended to the somewhat more expensive 2,2′-diphenylglycine, $Ph_2C(NH_2)CO_2H$ (L^5H_3).[7] In every complex, this ligand is deprotonated at the acid and displays a simple 5-membered chelate with Harris notation [1.011]. In the case of $[Ti(OMe)_4]$, the use of a 2:1 ratio (L^5H_3:Ti) resulted in the isolation of the complex $[Ti(L^5H_2)_3OMe]\cdot2.5MeCN$ (**18**·2.5MeCN), which crystallizes in the monoclinic space group *I*2/*a*. The asymmetric unit comprises a discrete seven coordinate Ti complex (Figure 4-13), where the Ti is surrounded by three chelating dpg ligands and one OMe ligand. Two chelating ligands and the NH_2 from another lie approximately in a plane with the carboxylate filling an axial position; the other axial position is filled by methoxide. The ligands are arranged such that two N–H bonds from different bound amines form hydrogen bonds to a carbonyl in an adjacent complex. These interactions generate a hydrogen bonded chain that runs parallel to the crystallographic *b*-axis. Subsidiary C–H···π interactions exist along the direction of these chains and between them (See Figure 4-14).

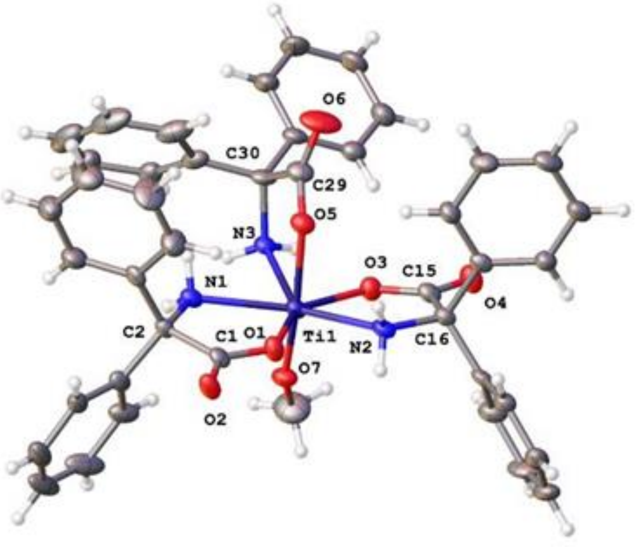

Figure 4-13. Asymmetric unit of **18**·2.5MeCN with atoms drawn as 50 % probability ellipsoids.

Selected bond lengths (Å) and bond angles (°): Ti(1)-O(5) 1.984(2), Ti(1)-O(1) 2.019(2), Ti(1)-O(7) 1.772(2), Ti(1)-O(3) 2.042(2), Ti(1)-N(3) 2.245(3), Ti(1)-N(1) 2.262(3), Ti(1)-N(2) 2.237(3); O(5)-Ti(1)-O(1) 93.65(9), O(5)-Ti(1)-O(3) 88.84(10), O(5)-Ti(1)-N(3) 75.90(9), O(5)-Ti(1)-N(1) 85.75(10), O(5)-Ti(1)-N(2) 85.17(10), O(1)-Ti(1)-O(3) 141.47(9), O(1)-Ti(1)-N(3) 146.56(10), O(1)-Ti(1)-N(1) 72.62(9), O(1)-Ti(1)-N(2) 70.49(9), O(7)-Ti(1)-O(5) 168.79(10), O(7)-Ti(1)-O(1) 95.69(10), O(7)-Ti(1)-O(3) 87.71(10), O(7)-Ti(1)-N(3) 92.89(10), O(7)-Ti(1)-N(1) 91.13(11), O(7)-Ti(1)-N(2) 103.79(11), O(3)-Ti(1)-N(3) 71.00(10), O(3)-Ti(1)-N(1) 145.83(9), O(3)-Ti(1)-N(2) 71.43(9), N(3)-Ti(1)-N(1) 74.96(10), N(2)-Ti(1)-N(3) 137.96(10), N(2)-Ti(1)-N(1) 141.26(10).

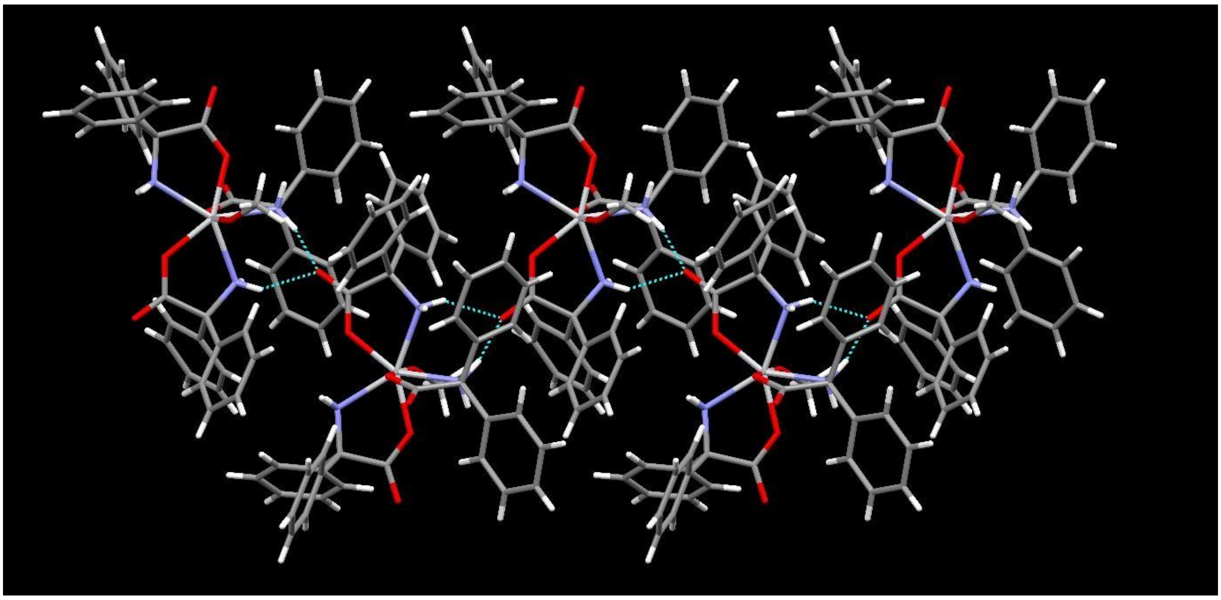

Figure 4-14. Alternative view of the crystal structure of **18**·2.5MeCN down *a*. Dashed lines show hydrogen bonds

The use of [Ti(O*n*Pr)$_4$] in a 1:1 ratio afforded, following work-up, yellow crystals of [Ti$_2$(L^5)$_2$(O*n*Pr)$_6$] (**19**). The structure contains distorted octahedral coordination of titanium; each Ti has two O*n*Pr ligands that bridge to another equivalent Ti to form centrosymmetric dimers. Each Ti bears one chelating dpg, two monodentate alkoxides and two bridging alkoxides. The asymmetric unit contains two symmetry-unique halves of the dimer as shown below (Figure 4-15).

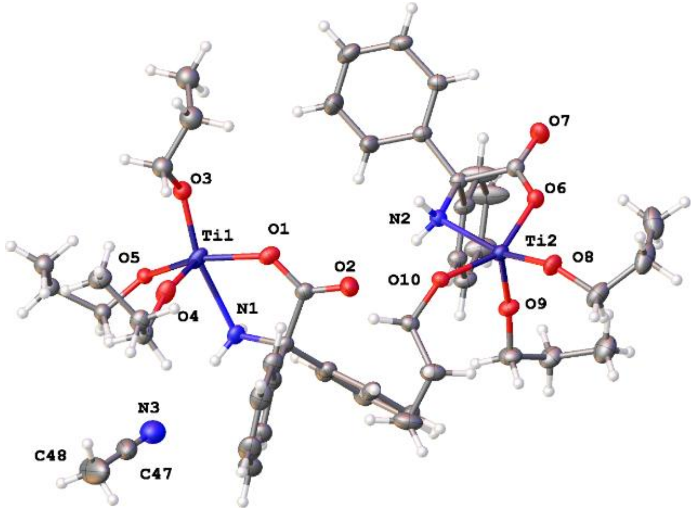

Figure 4-15. Asymmetric unit of **19** with atoms drawn as 50 % probability ellipsoids. For clarity, minor disorder is not shown. Selected bond lengths (Å) and bond angles (^{o}): Ti(1)-Ti(1i) 3.2815(5), Ti(1)-O(1) 1.9868(13), Ti(1)-O(3) 1.8486(17), Ti(1)-O(4) 1.7717(12), Ti(1)-O(5) 2.048 (3), Ti(1)-N(1) 2.2829(14); O(5)-Ti(1)-O(1) 152.78(8), O(5)-Ti(1)-O(4) 96.15(9), O(5)-Ti(1)-N(1) 84.55(8), O(5)-Ti(1)-O(3) 104.04(9), O(4)-Ti(1)-O(1) 100.20(5), O(4)-Ti(1)-O(3) 100.42(7), O(4)-Ti(1)-N(1) 88.62(6), O(3)-Ti(1)-O(1) 94.27(6), O(3)-Ti(1)-N(1) 166.64(7), O(1)-Ti(1)-N(1) 74.31(5), Ti(1)-O(5A)-Ti(1i) 114.10 (18).

The action of the inversion centre generates a dimer from two Ti1 centres and a dimer from two Ti2 centres. There are intramolecular N–H···O (alkoxide) hydrogen bonds that help to stabilise the dimers and N–H···O (carbonyl) hydrogen bonds between adjacent complexes to form 1-D chains that run parallel to the crystallographic [1.1.1] direction. Views of the coordination about Ti1 and Ti2 are shown in Figure 4-16.

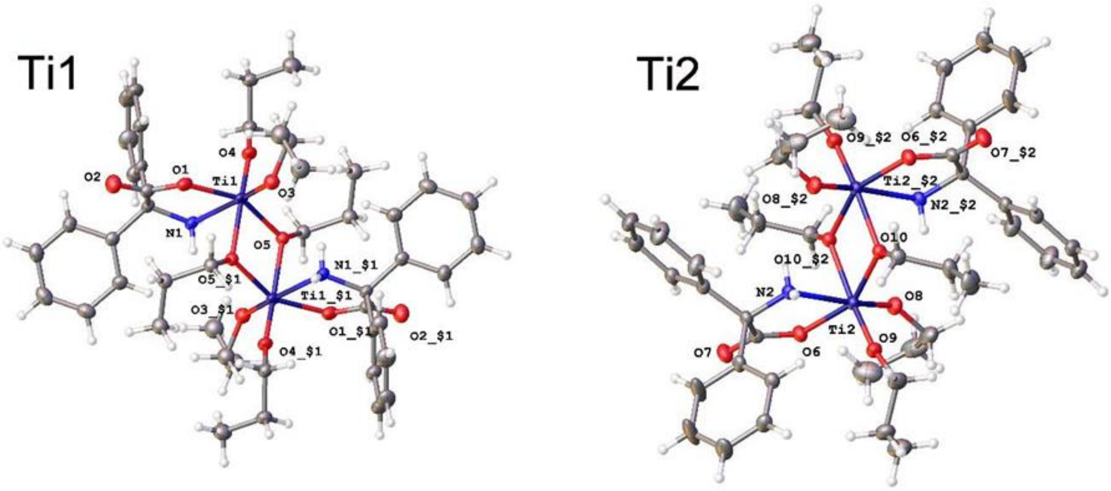

Figure 4-16. The two unique complexes in **19** composed of Ti1 and Ti2. Symmetry-equivalent atoms are generated by the following symmetry operations: $ 1 = 1–x, 2–y, 2–z; $2 = –x, 1–y, 1–z.

The similar use of $[\mathrm{Ti(O}i\mathrm{Pr)_4}]$ also resulted in the formation of a dinuclear complex, namely $[\mathrm{Ti_2(L^5)_2(O}i\mathrm{Pr)_6}]$ (**20**). Although the crystal structure is somewhat different (Figure 4-17; for an alternative view, see Figure 4-18), the basic cluster present in **20** is essentially the same as in **19**; two Ti ions are bridged by a pair of alkoxides and the coordination about each Ti ion is completed by terminal alkoxide ligands and bidentate dpg. The intramolecular hydrogen bonding between NH_2 and alkoxide is also present, but there are no classical hydrogen bonds between the clusters which is the major difference between **19** and **20**. The carbonyl of the carboxylic acid forms C–H···O intermolecular interactions to two different complexes. These interactions extend in 3-D throughout the crystal structure.

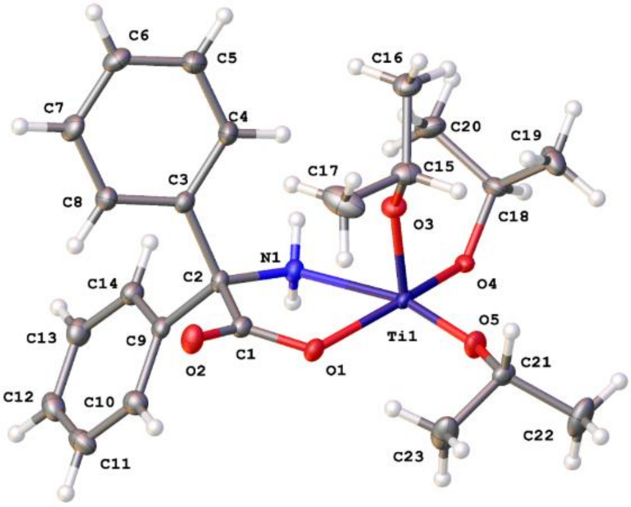

Figure 4-17. Asymmetric unit of **20** with atoms drawn as 50 % probability ellipsoids. For clarity, minor disorder is not shown. Selected bond lengths (Å) and bond angles (°): Ti(1)-Ti(1$^{\mathrm{i}}$) 3.2788(4), Ti(1)-O(4) 1.9618(9), Ti(1)-O(4$^{\mathrm{i}}$) 2.1357(9), Ti(1)-O(1) 1.9945(10), Ti(1)-O(3) 1.7990(9), Ti(1)-O(5) 1.7884(9), Ti(1)-N(1) 2.2901(10), Ti(1)-Ti(1$^{\mathrm{i}}$) 3.2788(4); O(4)-Ti(1)-O(4$^{\mathrm{i}}$) 73.78(4), O(4)-Ti(1)-O(1) 155.56(4), O(4$^{\mathrm{i}}$)-Ti(1)-N(1) 81.69(4), O(4)-Ti(1)-N(1) 87.18(4), O(1)-Ti(1)-O(4$^{\mathrm{i}}$) 89.31(4), O(1)-Ti(1)-N(1) 72.73(4), O(3)-Ti(1)-O(4$^{\mathrm{i}}$) 167.74(4), O(3)-Ti(1)-O(4) 98.25(4), O(3)-Ti(1)-O(1) 95.14(4), O(3)-Ti(1)-N(1) 88.71(4), O(5)-Ti(1)-O(4$^{\mathrm{i}}$) 91.32(4), O(5)-Ti(1)-O(4) 104.07(4), O(5)-Ti(1)-O(1) 93.62(4), O(5)-Ti(1)-O(3) 99.77(5), O(5)-Ti(1)-N(1) 164.63(4), Ti(1)-O(4)-Ti(1$^{\mathrm{i}}$) 106.22(4).

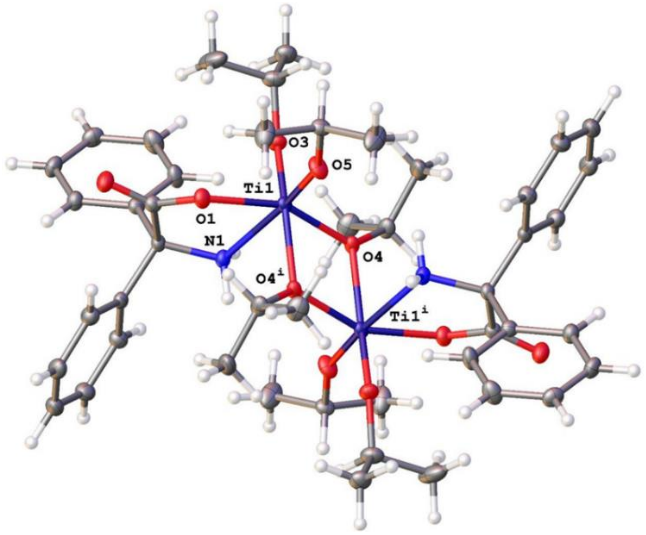

Figure 4-18. Two Ti cluster present in **20**. Symmetry operation used to generate equivalent atoms: i = 1–*x*, 1–*y*, 1–*z*.

Upon changing the ratio to 2:1 (L^5H_3:Ti), the use of [Ti(O*i*Pr)$_4$] led to the isolation of the mononuclear complex [(L^5H_2)$_2$Ti(O*i*Pr)$_2$] (**21**), the molecular structure of which is shown in Figure 4-19 (an alternative view is given in Figure 4-20). This features a rather distorted octahedral coordination about the Ti composed of two *cis* dpg ligands and two terminal isopropoxide ligands such that there is close to the local twofold axis at the metal centre between the two Ti-N bonds. The two nitrogen donor atoms are adjacent but the two oxygen atoms of the chelates are *trans* at the metal. The asymmetric unit has three symmetry-unique complexes that have the same coordination but differ very slightly in the orientation of the methyl groups of the isopropoxide. The three unique complexes are aligned along the crystallographic *a*-axis to form an infinite rank of these complexes in the crystal structure. Between every pair of adjacent complexes there is a pseudo-centrosymmetric pair of N–H···O hydrogen bonds. There is evidence for C–H···O and C–H···π interactions between these ranks.

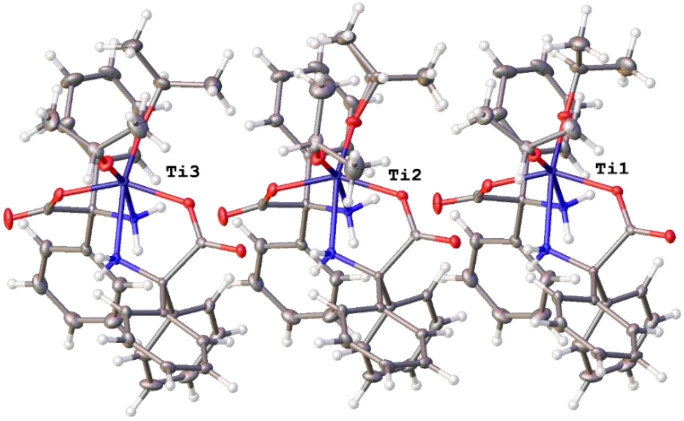

Figure 4-19. Asymmetric unit of **21** with atoms drawn as 50 % probability ellipsoids. For clarity, some minor disorder is not shown. Selected bond lengths (Å) and bond angles (°): Ti(1)-O(3) 1.7658(14), Ti(1)-O(4) 1.7686(14), Ti(1)-O(2) 1.9786(14), Ti(1)-O(5) 1.9847(14), Ti(1)-N(2) 2.2508(16), Ti(1)-N(1) 2.3025(16); O(3)-Ti(1)-O(4) 103.37(7), O(3)-Ti(1)-O(2) 96.33(6), O(4)-Ti(1)-O(2) 98.45(6), O(3)-Ti(1)-O(5) 97.81(6), O(4)-Ti(1)-O(5) 102.24(6), O(2)-Ti(1)-O(5) 151.42(6), O(3)-Ti(1)-N(2) 167.16(7), O(4)-Ti(1)-N(2) 88.06(6), O(2)-Ti(1)-N(2) 87.59(6), O(5)-Ti(1)-N(2) 73.72(5), O(3)-Ti(1)-N(1) 86.36(6), O(4)-Ti(1)-N(1) 168.37(6), O(2)-Ti(1)-N(1) 73.83(6), O(5)-Ti(1)-N(1) 82.42(6), N(2)-Ti(1)-N(1) 83.00(6).

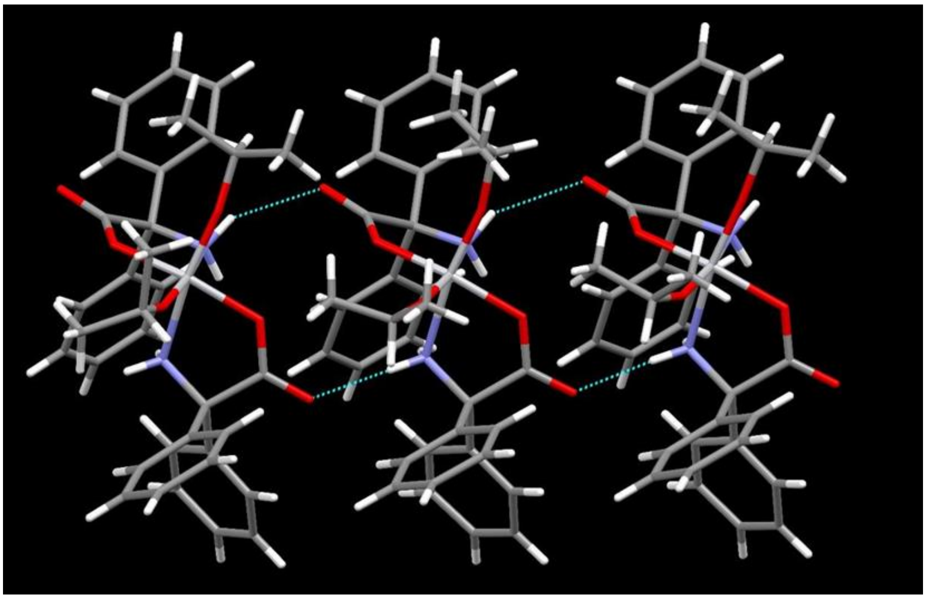

Figure 4-20. Asymmetric unit of **21**. A portion of the infinite hydrogen bonded chain running parallel to the crystallographic *a* direction (left-right on the image) is shown as dashed lines.

Interestingly, the interaction of L^5H_3 with [Ti(O*t*Bu)$_4$] using a ratio of 1:1 resulted in the formation of a similar mononuclear complex [Ti(L^5H_2)$_2$(O*t*Bu)$_2$]·2MeCN (**22**·2MeCN) (as shown in Figure 4-21). The basic complex here is very similar to that in **21**, but the intermolecular interactions present are different which perhaps reflects the inclusion of solvent in the crystal structure. Each discrete complex contains a pair of chelating dpg ligands and two terminal O*t*Bu ligands but there is no local twofold axis. The nitrogen donor atoms are adjacent at the metal centre, but in contrast to **21** so are the two oxygen atoms of the chelating ligand. This close approach of the two NH_2 groups facilitates each of them forming a hydrogen bond to the carboxylate of an adjacent complex, and this forms hydrogen-bonded chains of complexes parallel to the crystallographic *b* direction (see Figure 4-22).

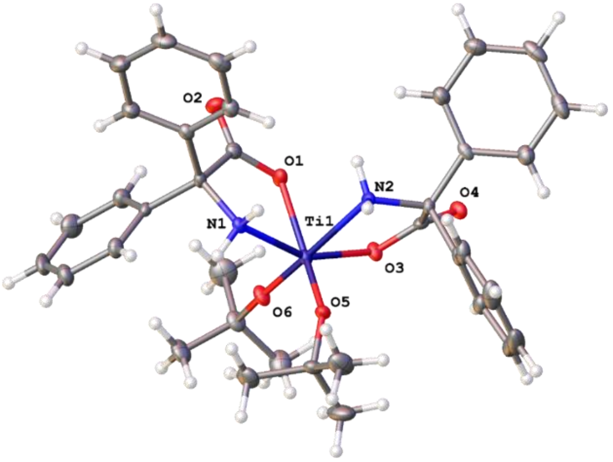

Figure 4-21. Asymmetric unit of **22**·2MeCN with atoms drawn as 50 % probability ellipsoids. For clarity, solvent molecules are not shown. Selected bond lengths (Å) and bond angles (^{o}): Ti(1)-O(6) 1.755(2), Ti(1)-O(5) 1.7747(18), Ti(1)-O(3) 1.9920(18), Ti(1)-O(1) 2.0497(19), Ti(1)-N(1) 2.202(2), Ti(1)-N(2) 2.260(2); O(6)-Ti(1)-O(5) 101.20(9), O(6)-Ti(1)-O(3) 96.38(8), O(5)-Ti(1)-O(3) 105.03(8), O(6)-Ti(1)-O(1) 93.82(9), O(5)-Ti(1)-O(1) 158.53(8), O(3)-Ti(1)-O(1) 88.26(8), O(6)-Ti(1)-N(1) 100.49(9), O(5)-Ti(1)-N(1) 88.48(8), O(3)-Ti(1)-N(1) 155.91(9), O(1)-Ti(1)-N(1) 73.64(7), O(6)-Ti(1)-N(2) 169.12(8), O(5)-Ti(1)-N(2) 87.39(9), O(3)-Ti(1)-N(2) 74.76(8), O(1)-Ti(1)-N(2) 79.81(8), N(1)-Ti(1)-N(2) 86.28(8).

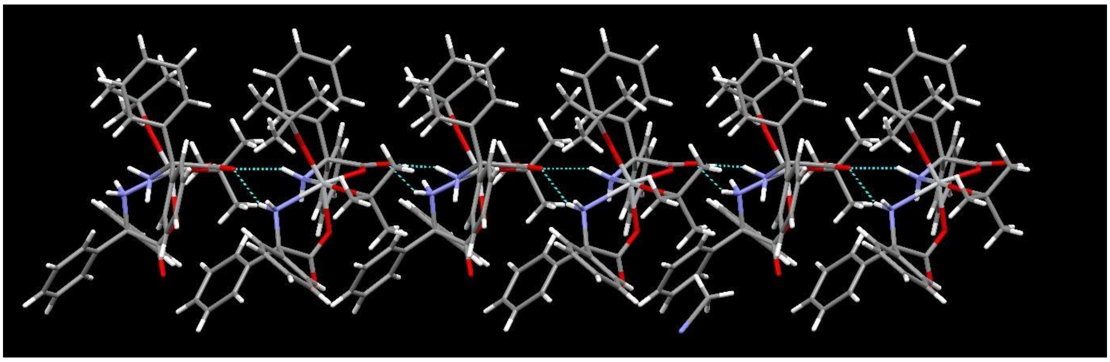

Figure 4-22. Hydrogen-bonded chain within **22**·2MeCN. Dashed lines show hydrogen bonds.

Infrared and ^{1}H NMR spectra of the L^{5}H$_3$ derived complexes

The infrared spectrum of the parent L^{5}H$_3$ contains N-H stretches at 3269 (sharp), 3180, 3052 cm^{-1}. A shift (~90 cm^{-1}) of the N-H was observed for all the dpg derived complexes upon coordinated with titanium. For example, the IR spectrum of **18**·2.5MeCN contains N-H band at 3335, 3245, and 3055 cm^{-1}, which indicates amine-type bonding is retained in the titanium complexes. Several new peaks appeared for all the complexes in the range of 413-465 cm^{-1}, which is due to the formation of new Ti-O and Ti-N bonds. The solid-state structures of the DpgH derived complexes are consistent with their ^{1}H NMR spectra, elemental analysis and mass spectrometry data.

4.2.3 Ring-opening polymerisation studies of ε-CL

Initially, all the complexes were screened for their ability to act as catalysts for the ROP of ε-CL with a monomer to Ti ratio of 250:1 at 100 °C under N_2 (Table 4-2, entries 1 to 10). The complexes **14**, **16** and **17**, which all bear L^4H_2 derived ligands sets, were found to be the most sluggish even after 24 h, allowing for monomer conversions of 20, 31 and 53%, respectively. The poor activity of **14** was tentatively attributed to the absence of OR groups (other than those derived from L^4) as well as to the two acidic protons reducing the complex solubility in the reaction medium. Solubility issues could also explain the rather low conversions achieved with **16** and **17**. By contrast, complexes **13** and **15** allowed for complete monomer conversion within 195 min. and 150 min., respectively. The isopropoxide-containing complex **15** performed slightly better than the methoxide-bearing **13**. Most catalysts afforded polymers with M_n smaller than the calculated values except complexes **15** and **22** albeit with broad polydispersity, allegedly deriving from intramolecular transesterification processes. All complexes bearing L^5H_2 derived ligands (**18-22**) allowed for conversions ≥ 95% within 480 min. An *in-situ* kinetic study was carried out (using Young's tap NMR tube in toluene-d_8) at 100 °C using a monomer to Ti ratio of 250:1. Figure 4-23 (left) shows that the ROP using **13**, **15** and **18-22** proceed rapidly to full conversion but over differing time periods. For the L^5H_3 derived complexes, the *n*-propoxide complex **19** performed best, the k_{obs} is equal to 4743×10^{-4}/min (Table 4-2, entry 7). The linearity indicated that the polymerisation is first-order in monomer with rapid initiation and without induction time, but only at 50 °C (Table 4-2, run 11) did the behaviour approach living-type character. According to the kinetics for **13**, **15**, **18** and **20-22**, the plot of $\ln([CL]_0/[CL]_t)$ *versus* time shows an upward curvature which implies polymerisation rates increased along with reaction time (Figure 4-23, left). This type of acceleration phenomenon for ROP of ε-CL has been reported by Basko. [8] If the basicity of the monomer is significantly higher than the polymer unit, the ratio between the activated monomer concentration and the monomer concentration increases as the monomer is consumed, resulting in an apparent speed up of the polymerisation. A similar acceleration of kinetics has also been reported by Delcroix.[9] Herein, this was observed for complexes **13, 15, 18** and **20-22**, and k_{obs} was calculated after the induction period acceleration in order to compare the activities of the different complexes. By contrast, for complexes **14**, **16**-**17**, there is an obvious induction period (Figure 4-23 (right)); results are listed in Table 4-3. For the L^5H_3 derived complexes **18**-**22**, k_{obs} follow the sequence **19·MeCN** > **20** > **21** > **22·2MeCN** > **18·2.5MeCN.** Cooperative effects between the two Ti centres of dimeric complexes **19** and **20** could explain their superior activity over their monomeric congeners **18**, **21** and **22**. By looking at **19** (O*n*Pr) *versus* **20** (O*i*Pr) with nearly identical structures, O*n*Pr has a remarkable positive effect on polymerisation and also better control of polymerisation (PDI 1.49 *versus* 1.80); for **21** and **22**, the performance of the O*i*Pr exceeds that of the O*t*Bu. These differences can be explained in terms of the steric hindrance of the alkoxide groups. The lower value of k_{obs} for complex **18** is thought to be due to its poor solubility in toluene/ε-Cl. It is noticeable that for **18,** the reaction mixture remains cloudy at 100 °C, and this likely explains the longest observed induction period. Given the better performance of the system **19**, it was selected for further screening. Remarkably, the complex proved able to completely convert up to 2000 equiv. of monomer within minutes at 100 °C (Table 4-2, run 7 and 12-14). In all cases, the polymer exhibited broad dispersity (up to 2.35) and their M_n were lower than the calculated values, suggesting the occurrence of undesired intramolecular transesterification reactions. On varying the temperature, using a CL:Ti ratio of 250:1, high conversion was still achieved at 50 °C over 150 min., whilst at ambient temperature (20 °C), the conversion was only 14% after 24h (Table 4-2, runs 11 and 15, respectively). By conducting the ROP in the absence of the solvent, complex **19** allowed for ≥99% monomer conversion within 6 min., affording a product with a molecular weight of 10.5 kDa (Table 4-2, run 17). Finally, the catalyst was virtually inactive upon carrying out the reaction in the air. To better understand the effect of the presence of the chelate, the ROP behaviour of the titanium alkoxide starting materials $[Ti(OR)_4]$ (R = Me, *n*Pr, *i*Pr, *t*Bu), *i.e.* ROP in the absence of L^4H_2 and L^5H_3 derived ligation, was investigated. The results are presented in Table 4-2 entries 18-21, which revealed that [Ti(O*n*Pr)$_4$] allowed for 92% conversion within 2 min, albeit with far less control compared to **13**-**22** (*i.e.* broader PDI). According to the literature, the complexes $[Ti(OR)_4]$ can adopt varied structures, for example, tetranuclear has been reported for R=Me (X-ray diffraction[10], whilst trimeric was inferred for R = *n*Pr (cryoscopic measurements)[11]. Complex [Ti(O*n*Pr)$_4$] is still active for the ROP of ε-CL at 100 °C in the air, however the M_w distribution is very broad.

Table 4-2. ROP of ε-CL catalysed by the Ti complexes **13-22** and [Ti(OR)$_4$].

Run	**Catalyst**	**L^4/L^5**	**OR group**	**CL:Ti**	**T** (°C)	**Time** (min)	**Conv.**^{a} (%)	$\boldsymbol{M}_{\mathbf{n\ (calc.)}}$^{d} (kDa)	$\boldsymbol{M}_{\mathbf{n\ (obs.)}}$^{b,c} (kDa)	***PDI***^{b}
1	**13**	L^4	OMe	250:1	100	195	99	28.3	7.2	1.87
2	**14**·MeCN		-	250:1	100	1440	20	5.7	4.6	1.25
3	**15**		O*i*Pr	250:1	100	150	99	28.3	30.0	1.93
4	**16**·MeCN		O*i*Pr	250:1	100	1440	31	8.9	6.0	1.53
5	**17**·MeCN		O*t*Bu	250:1	100	1440	53	15.2	4.1	1.25
6	**18**·2.5MeCN	L^5	OMe	250:1	100	480	95	27.1	6.0	1.22
7	**19**·MeCN		O*n*Pr	250:1	100	12	99	28.3	8.4	1.49
8	**20**		O*i*Pr	250:1	100	210	99	28.3	6.7	1.80
9	**21**		O*i*Pr	250:1	100	345	99	28.3	12.0	1.97
10	**22**·2MeCN		O*t*Bu	250:1	100	255	99	28.3	39.0	2.41
11	**19**·MeCN		O*n*Pr	250:1	50	150	99	28.3	4.8	1.20
12	**19**·MeCN		O*n*Pr	500:1	100	6	99	56.6	13.0	2.35
13	**19**·MeCN		O*n*Pr	1000:1	100	9	99	113	8.7	1.45
14	**19**·MeCN		O*n*Pr	2000:1	100	12	99	226	8.6	1.84
15	**19**·MeCN		O*n*Pr	250:1	25	1440	14	-	-	-
16^e	**19**·MeCN		O*n*Pr	250:1	100	1440	6	-	-	-
17^f	**19**·MeCN		O*n*Pr	250:1	100	6	98	28.0	10.5	1.29
18	**[Ti(OR)$_4$]**	-	OMe	250:1	100	195	3	0.9	1.0	1.22
19			O*n*Pr	250:1	100	2	92	26.3	6.7	2.79
20			O*i*Pr	250:1	100	195	94	26.8	7.8	3.01
21			O*t*Bu	250:1	100	195	43	12.3	5.4	2.94
22^e			O*n*Pr	250:1	100	2	96	27.4	5.6	3.21

Reaction conditions: ε-CL 4.5 mmol, toluene 2 mL, N$_2$. ^{a} Determined by ^{1}H NMR spectroscopy on the crude reaction mixture. ^{b} From GPC. ^{c} Values corrected considering Mark–Houwink factor (0.56) from polystyrene standards in THF. ^{d} Calculated from [CL]/[Ti] × Conv. × *M*(CL) + M(end group). ^{e} Reaction conducted under air. ^{f} Conducted under solvent-free conditions.

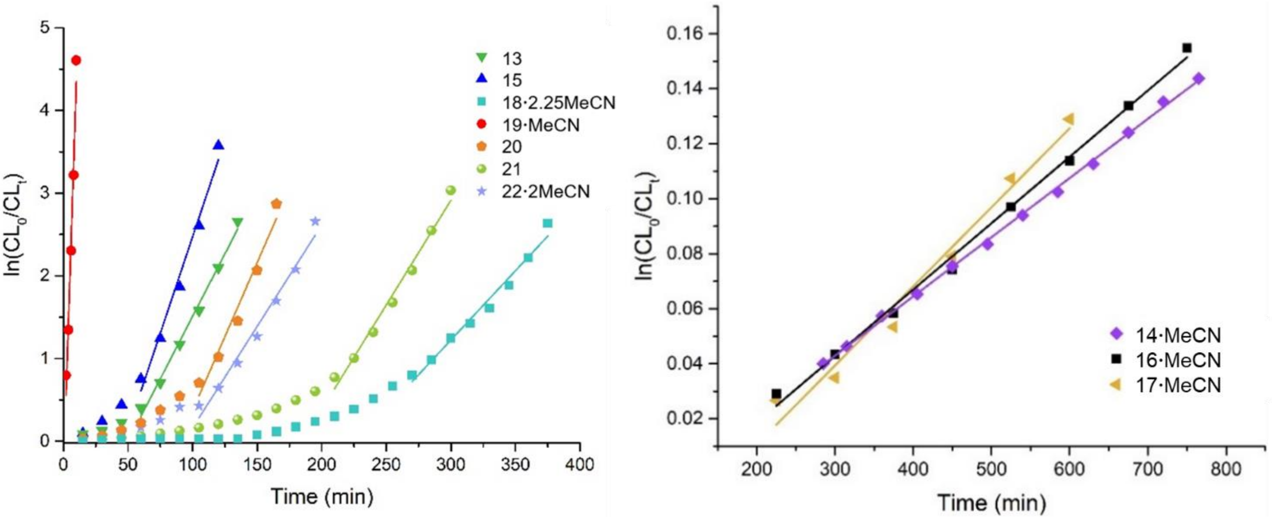

Figure 4-23. Plot of ln([CL]$_0$/[CL]$_t$) *versus* time. Left: complexes **13**, **15** and **18-22**; Right: complexes **14**, **16** and **17** (Table 4-2, entries 1-10).

Table 4-3. Kinetics constants for the ROP of ε-CL catalysed by **13-22** at 100 °C.

Run	**Complex**	k_{obs} (×10^{-4})	**Induction period** (min)
1	**13**	302 (R^2=0.992)	60
2	**14**·MeCN	2.15 (R^2=0.999)	275
3	**15**	416 (R^2=0.969)	60
4	**16**·MeCN	2.57 (R^2=0.994)	215
5	**17**·MeCN	2.87 (R^2=0.977)	300
6	**18**·2.5MeCN	159 (R^2=0.977)	270
7	**19**·MeCN	4743(R^2=0.978)	0
8	**20**	358 (R^2=0.968)	105
9	**21**	253 (R^2=0.986)	210
10	**22**·2.5MeCN	246 (R^2=0.981)	105

End group analysis by ^{1}H NMR spectroscopy indicated that the PCL possessed OR/OH end groups (e.g. Figure 4-24). Furthermore, the MALDI-TOF mass spectrum (e.g. Figure 4-25) revealed the presence of both linear and cyclic products.

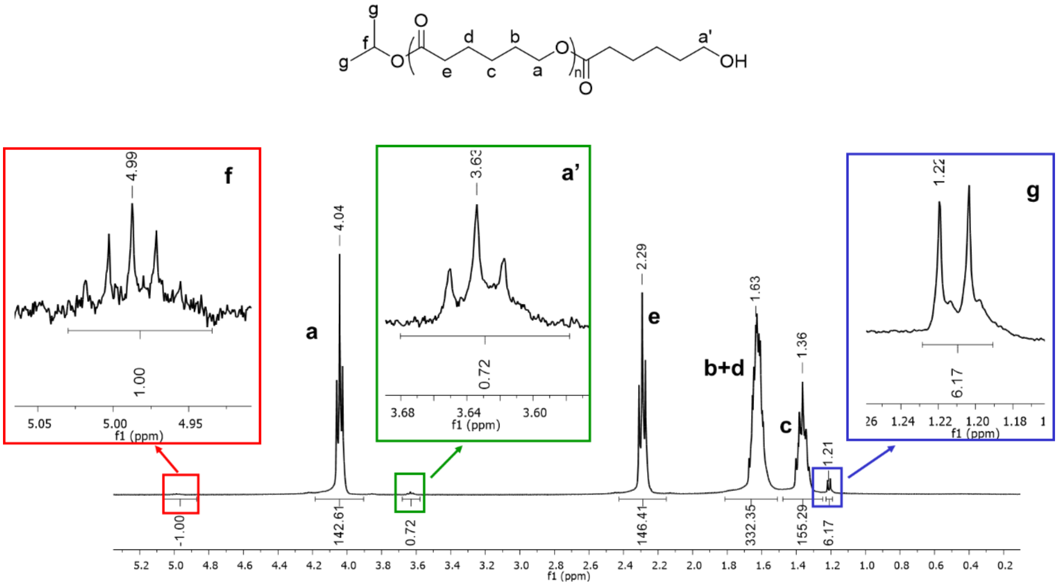

Figure 4-24. ^{1}H NMR spectrum ($CDCl_3$, 400 MHz) of PCL prepared using **20** (Table 4-2, entry 8).

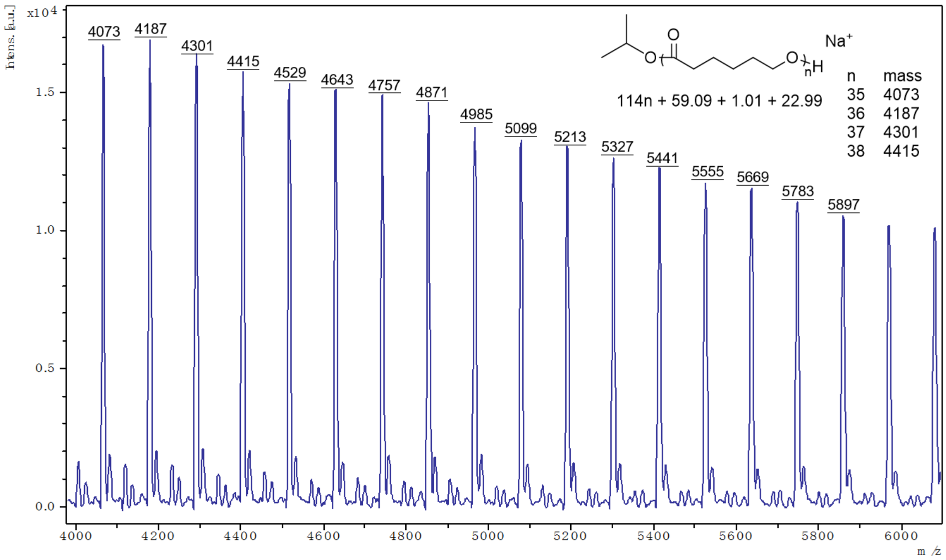

Figure 4-25. MALDI-TOF mass spectrum of PCL prepared using **20** (Table 4-2, entry 8).

4.2.4 Ring-opening polymerisation studies of *r*-LA

Complexes **13-22** were screened as initiators in the ROP of *r*-LA at 130 °C using a monomer to Ti ratio of 250:1 (Table 4-4) under an N_2 atmosphere unless stated otherwise. The L^4H_2 derived complexes **13-17** exhibited good activities (72 – 98% conversion over 24 h at 130 °C; Table 4-4, entries 1-5). Indeed, even complex **14**, which bears only chelate ligands, exhibited a reasonable conversion at 78% (Table 4-4, entry 2). By contrast, the L^5H_3 derived complexes **18**, **20-22** exhibited inferior conversions (8 – 65%; Table 4-4, entries 6, 8-10), suggesting the presence of the L^5H_3 derived ligand set was less beneficial in terms of accessing a high activity system for the ROP of *r*-LA. That said, the L^5H_3 derived complex **19** proved to be the exception, and afforded a conversion of 98% (Table 4-4, entry 7). The alkoxide group effect on the ROP of *r*-LA is best illustrated by looking at the pairs of nearly identical structures, namely **19** (O*n*Pr) *versus* **20** (O*i*Pr) and **21** (O*i*Pr) *versus* **22** (O*t*Bu) (Table 4-4, entries 7-10). For **19** and **20**, the use of O*n*Pr appears to be far more favourably than O*i*Pr, with conversions of 98 and 52% respectively, with **19** (O*n*Pr) also afforded the higher molecular weight product (34 *versus* 19 kDa, respectively); **20** exhibited slightly better control. For **21** and **22**, the performance of the O*i*Pr exceeds that of the O*t*Bu derivative **22**, with **21** affording higher conversion (44 *vs.* 28%), higher molecular weight (16 *vs* 10 kDa, respectively) and better control (1.15 *vs.* 1.37). These results, particularly the induction periods, may well reflect the steric bulk of alkoxide groups present, for example, the bulkier O*t*Bu group may hinder the coordination of *r*-LA to the Ti metal centre. A comparison of complexes **15** and **16**, which bear the same type of alkoxide group, suggests that the number of L^4H^- ligands present may also be an important factor (Table 4-4, entries 3-4). However, the wide variety of structures afforded during these reactions makes further analysis of structure/activity relationships somewhat problematic. With this in mind, the ROP behaviour of the titanium alkoxides $[Ti(OR)_4]$ (R = Me, *n*Pr, *i*Pr, *t*Bu) has been looked at again to investigate the effect of the absence of L^4H_2 and L^5H_3 derived ligands on titanium under the same ROP conditions as employed for **13** – **22**. After 24 h, the sequence of conversion for the $Ti(OR)_4$ complexes was found to be $[Ti(OnPr)_4] \approx [Ti(OMe)_4] > [Ti(OtBu)_4] > [Ti(OiPr)_4]$. Similar to the ROP results for ε-CL, $[Ti(OnPr)_4]$ exhibited superior activity (*vs* **13-22**), but with less control over the polymerisation process (Table 4-4, entry 16). Interestingly, if the ROP of *r*-LA was conducted for only 90 min at 130 °C, then the observed conversions yielded the order $[Ti(OnPr)_4]$ (96%) > $[Ti(OiPr)_4]$ (80%) > $[Ti(OtBu)_4]$ (8%) > $[Ti(OMe)_4]$ (no conversion).

Table 4-4. ROP of *r*-LA catalysed by Ti complexes **13-22** and $[Ti(OR)_4]$

Run	**Catalyst**	**L^4/L^5**	**OR group**	**LA:Ti**	**T** (°C)	**Conv.**[a] (%)	$M_{n\,(calc.)}$[d] (kDa)	$M_{n\,(obs.)}$[b,c] (kDa)	***PDI***[b]	***Pi***[f]
1	**13**	L^4	OMe	250:1	130	90	32.0	22.0	1.34	0.39
2	**14**·MeCN		-	250:1	130	78	28.0	14.0	1.22	0.47
3	**15**		O*i*Pr	250:1	130	92	33.0	13.0	1.15	0.46
4	**16**·MeCN		O*i*Pr	250:1	130	98	35.0	16.0	1.19	0.49
5	**17**·MeCN		O*t*Bu	250:1	130	72	26.0	13.0	1.72	0.48
6	**18**·2.5MeCN	L^5	OMe	250:1	130	65	23.0	11.0	1.21	0.26
7	**19**·MeCN		O*n*Pr	250:1	130	98	35.0	30.0	1.29	0.49
8	**20**		O*i*Pr	250:1	130	52	19.0	14.0	1.19	0.46
9	**21**		O*i*Pr	250:1	130	44	16.0	8.0	1.15	0.51
10	**22**·2MeCN		O*t*Bu	250:1	130	28	10.0	12.0	1.37	0.16
11[e]	**16**·MeCN		O*i*Pr	250:1	130	20	7.3	4.6	1.18	-
12[e]	**19**·MeCN		O*n*Pr	250:1	130	16	5.8	3.6	1.10	-
15	$[Ti(OR)_4]$	-	OMe	250:1	130	99	35.7	0.5	1.24	-
16			O*n*Pr	250:1	130	99	35.7	0.7	3.03	-
17			O*i*Pr	250:1	130	86	31.0	0.5	2.75	-
18			O*t*Bu	250:1	130	98	35.4	1.7	2.60	-

Reaction conditions: *r*-LA 4.5 mmol, toluene 2 mL, 24 h, N_2 atmosphere. [a] Determined by ^1H NMR spectroscopy of the crude reaction mixture. [b] From GPC. [c] Values corrected considering Mark–Houwink factor (0.58) from polystyrene standards in THF [d] Calculated from [*r*-LA]/[Ti] × Conv. × $M_{w\,(LA)} + M_{w\,(end\ group)}$. [e] Reaction conducted under air. [f] $Pi = 1\text{-}2I_{isi}$.

The air stability of complexes **16** and **19** was also examined; they were employed to initiate the polymerisation of *r*-LA at 130 °C with a [LA]:[Ti] ratio of 250:1 under air. Both complexes proved to be less active under air with dramatically decreased conversions (Table 4-4, entries 11-12), and M_n values were found to be lower than the calculated values.

The kinetics for the ROP of *r*-LA using **13**-**22** were investigated by *in situ* ^1H NMR spectroscopy studies, based on the relative areas of the methine signals of PLA and *r*-LA (5.06 and 4.18 ppm, respectively), see Figure 4-26 (displays results using **19**, Table 4-4, entry 7). The corresponding kinetics semi-logarithmic plots for **13**-**21** are shown in Figure 4-27 (data for **22** could not be recorded due to the slow reactivity of the complex). The apparent rate constant of

13-21 follows the trend **16** > **19** > **15** > **13** > **14** > **17** > **18** > **20** > **21**. The first order kinetic plot of *r*-LA polymerisation using **18**, **20** and **21** showed an induction period of 300-400 min suggesting slow insertion of the LA unit because of the different nucleophilicity of the alkoxide groups.[12] The linearity of the plots using **13-17** and **19** indicated the absence of an induction period and the ROP rate exhibits first order dependence on monomer concentration.

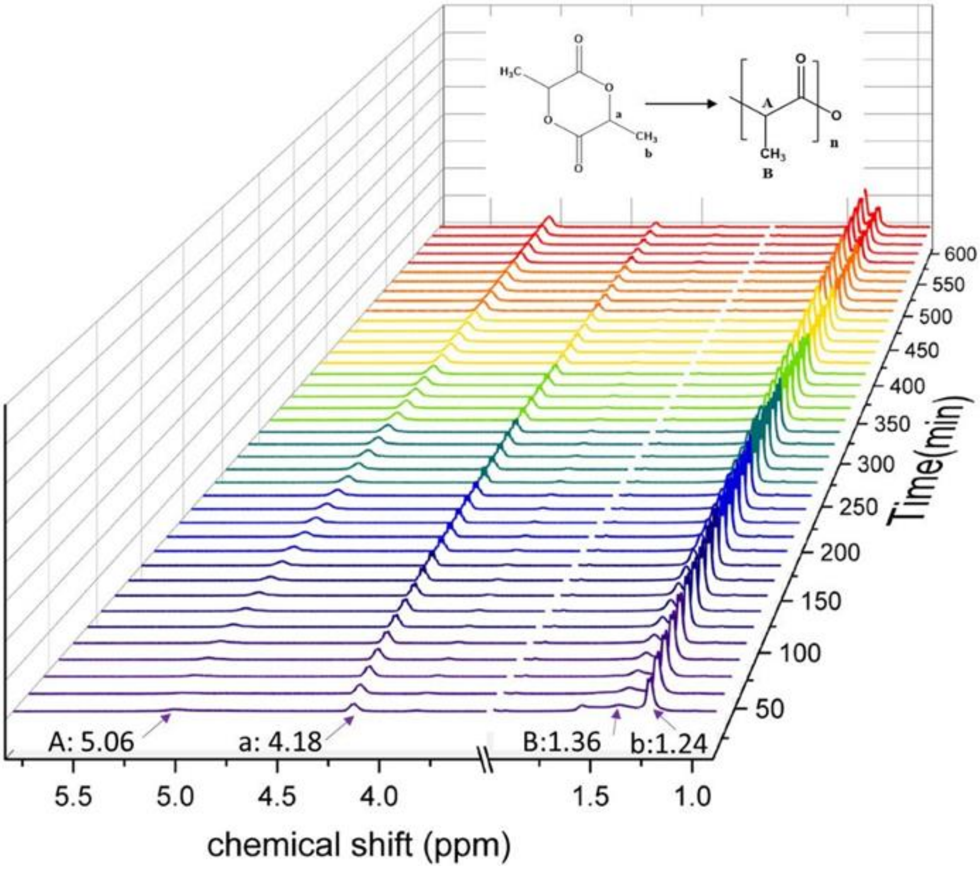

Figure 4-26. 3D time-resolved ^{1}H NMR spectrum (400 MHz, toluene-d$_8$) of kinetics of *r*-LA using complex **19** (Table 4-4, entry 7).

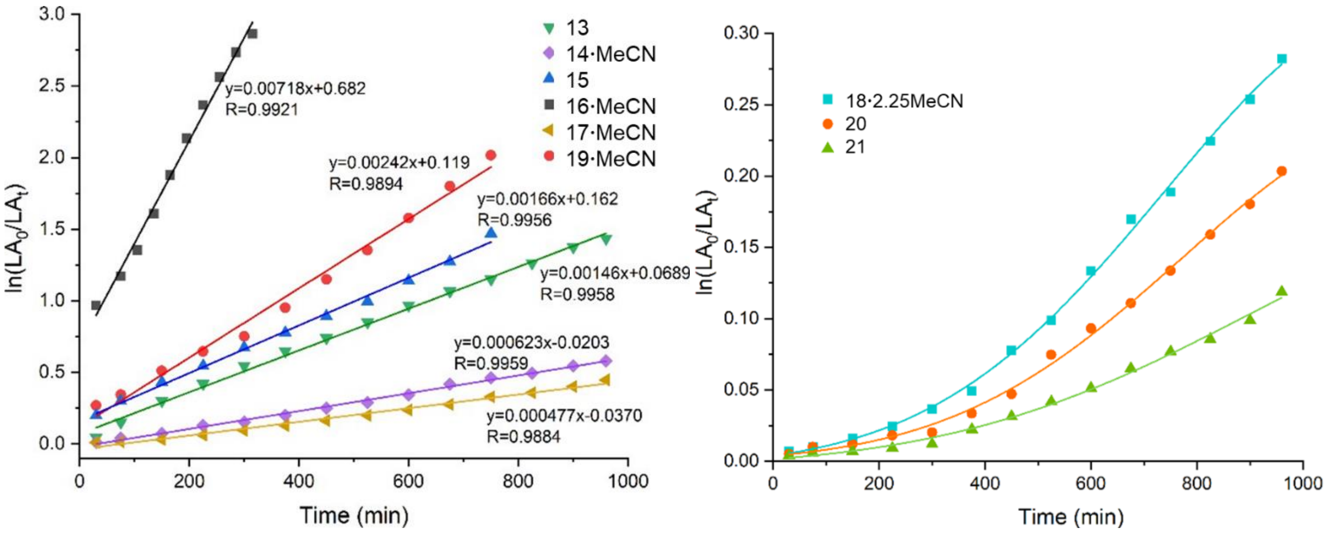

Figure 4-27. Semi-log plot of ln([LA]$_0$/[LA]$_t$) *versus* time for ROP using complexes **13-17**, **19** (Left), **18**, **20-21** (Right) (Table 4-4, entries 1-9).

^{1}H NMR spectroscopic analysis of the end groups of the PLA synthesised with complex **22** indicated the presence of *tert*-butoxy and hydroxyl chain terminus (Figure 4-28), suggesting that polymer initiation occurs through the insertion of lactide into the Ti-O bond via a coordination insertion mechanism. This is further supported by the MALDI-TOF mass spectra (e.g. Figures 4-29). The major set of peaks with a mass difference of m/z = 114 Da corresponds to 144.15n + 72.11 + 1.01, which is attributed to (LA)$_n$ + *t*BuOH. A minor set of peaks corresponds to cyclic polymers separated by 144 Da.

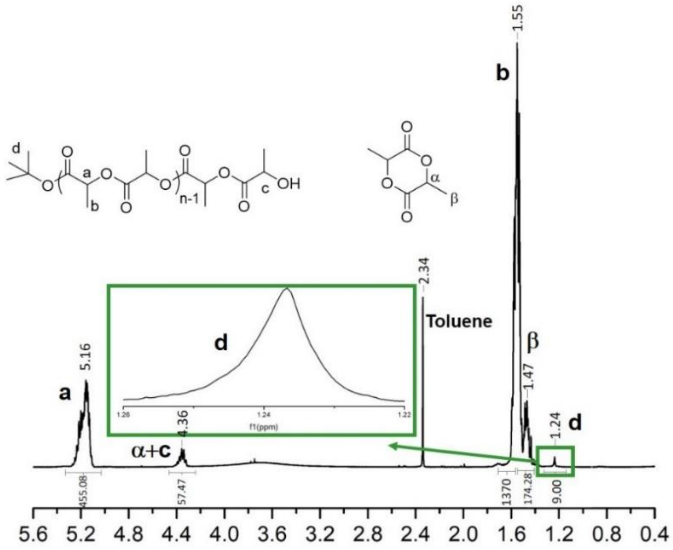

Figure 4-28. ^{1}H NMR spectrum ($CDCl_3$, 400 MHz) of PLA prepared using **22**·2MeCN (Table 4-4, entry 10).

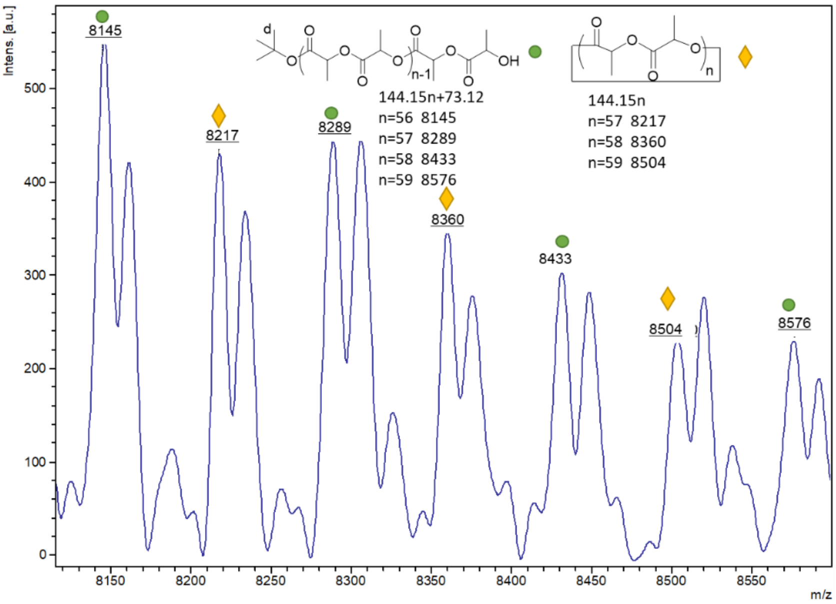

Figure 4-29. MALDI-TOF spectrum of PLA prepared using **22**·2MeCN (Table 4-4, entry 10).

The stereochemical microstructure analysis of PDLLA was verified by the inspection of the methine region of ^{13}C NMR of the polymers (Figures 4-30–4-34 and Table 4-4). The methine carbon signal in the repeat unit of PLA is sensitive to the tetrad. The degree of stereoselectivity is defined by the parameter *Pi*, which is the probability of forming a new *i*-dyad.[13] From Table 4-4, *Pi* is mostly < 0.5, which indicates mostly the formation of an isotactic product.[14] For **21**, the data suggests the formation of an atactic polymer (*Pi* = 0.51).

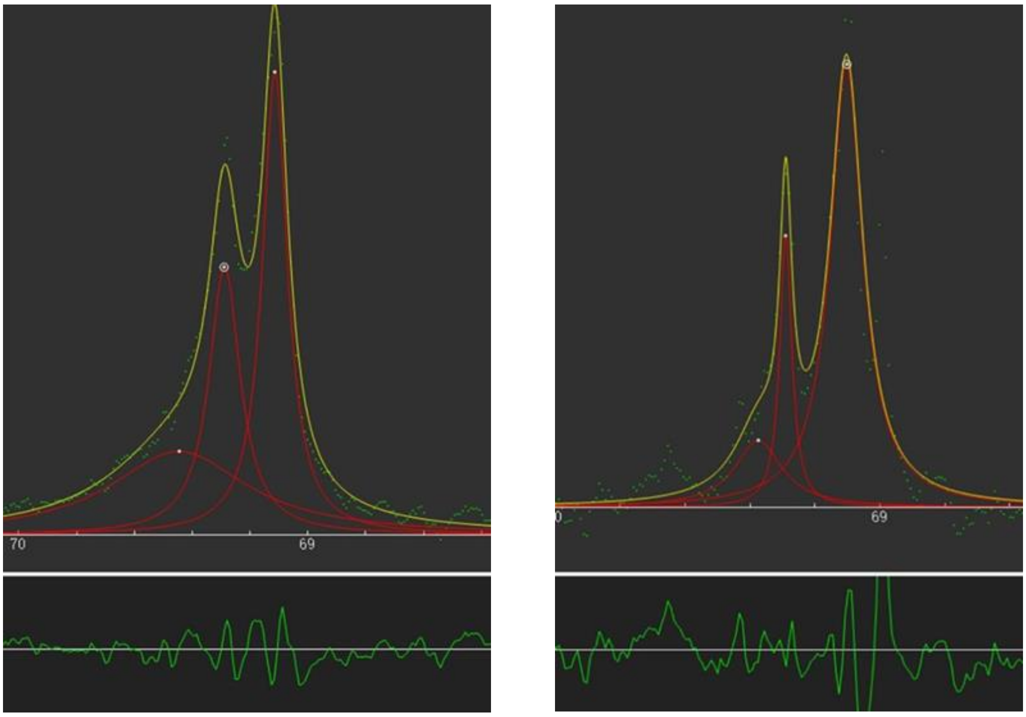

Figure 4-30. ^{13}C NMR spectrum of methine carbon in PLA using **13** (left) and **14** (right) (Table 4-4, entries 1 and 2).

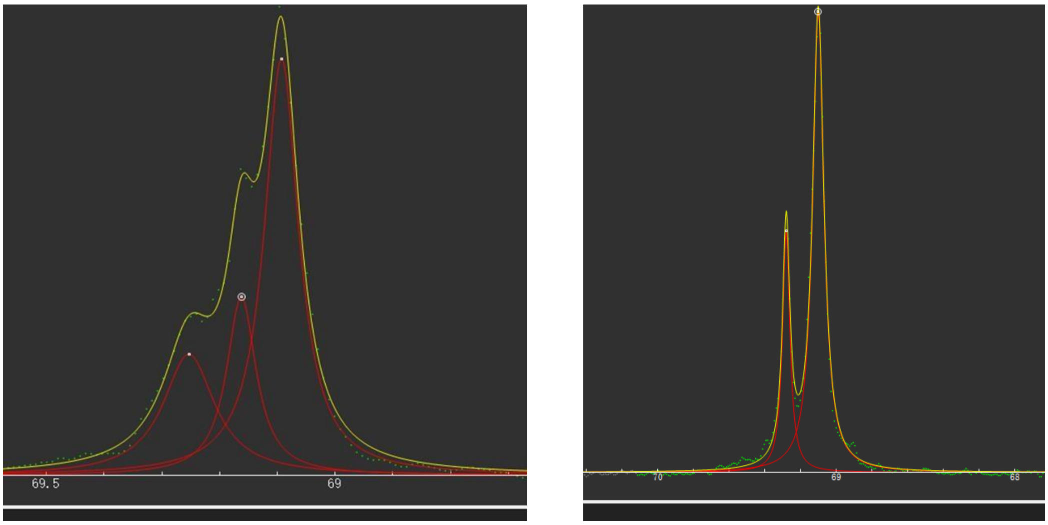

Figure 4-31. ^{13}C NMR spectrum of methine carbon in PLA using **15** (left) and **16** (right) (Table 4-4, entries 3 and 4).

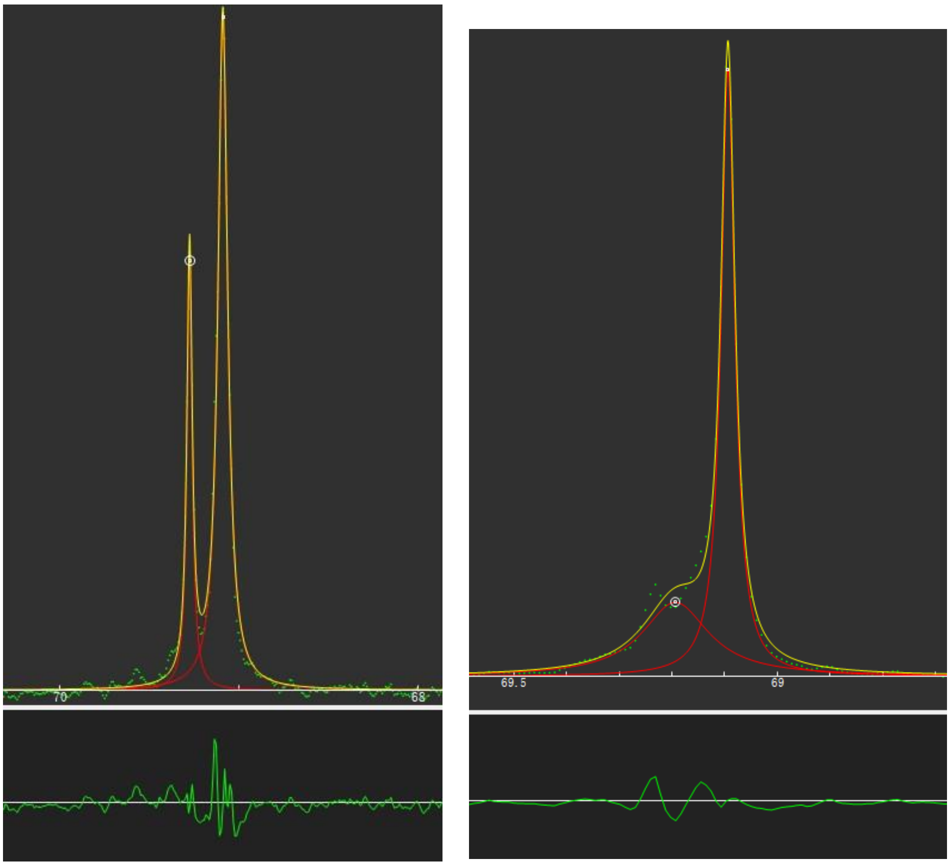

Figure 4-32. ^{13}C NMR spectrum of methine carbon in PLA using **17** (left) and **18** (right) (Table 4-4, entries 5 and 6).

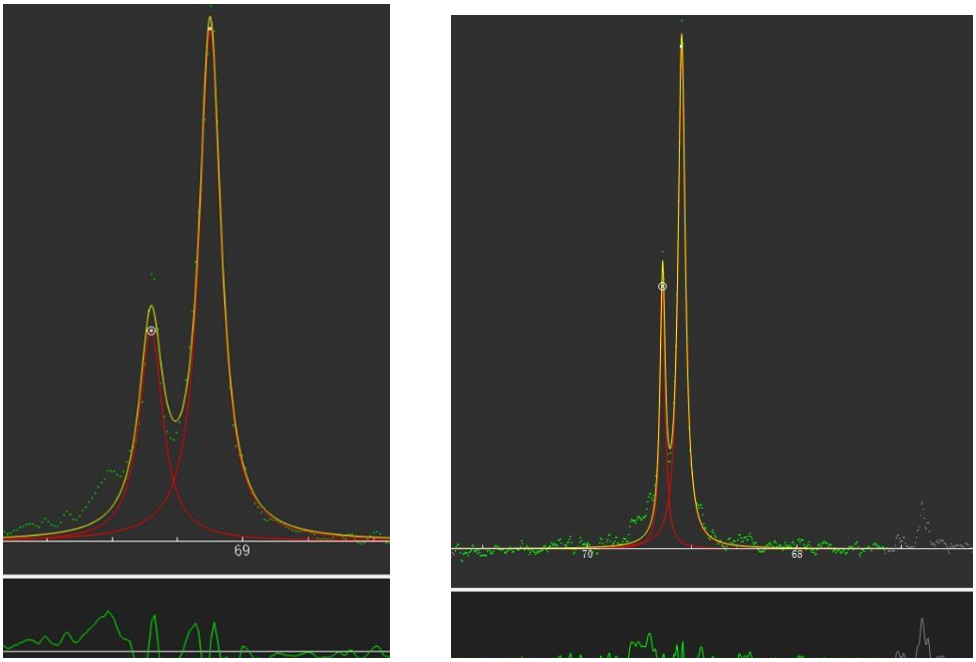

Figure 4-33. ^{13}C NMR spectrum of methine carbon in PLA using **19** (left) and **20** (right) (Table 4-4, entries 7 and 8).

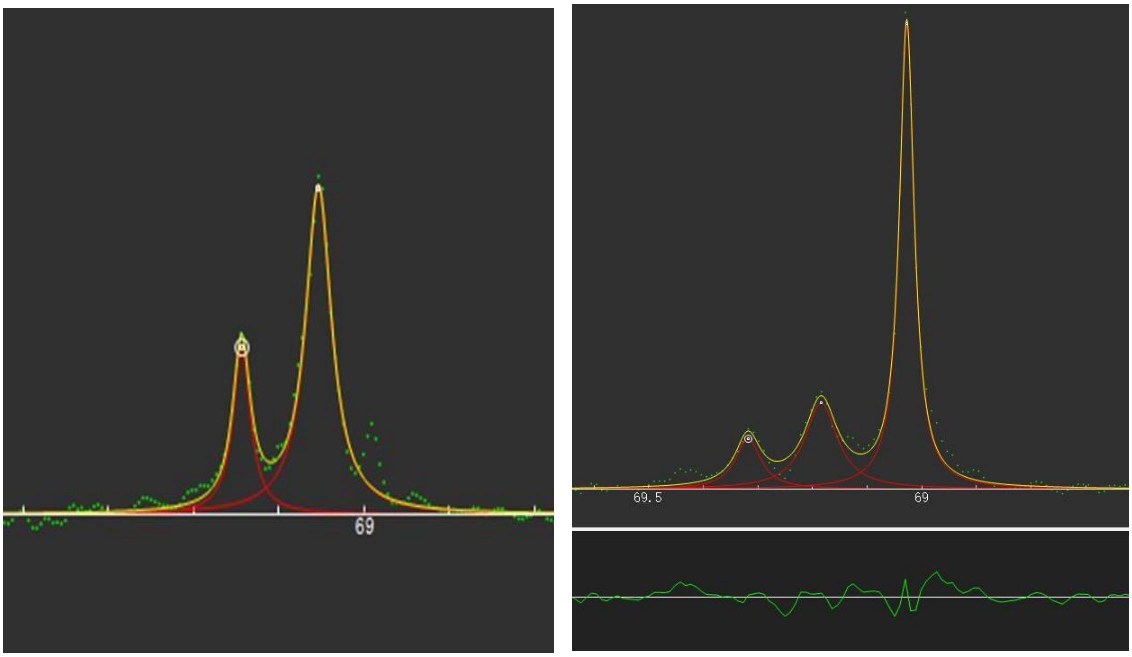

Figure 4-34. ^{13}C NMR spectrum of methine carbon in PLA using **21** (left) and **22** (right) (Table 4-4, entries 9 and 10).

4.3 Conclusions

Summarising findings in this chapter, the investigation of the reaction between acids of the type 2,2′-$Ph_2C(X)(CO_2H)$, where X = OH, NH_2, *i.e.* benzilic acid (L^4H_2) or 2,2′-diphenylglycine (L^5H_3) with the titanium tetraalkoxides [$Ti(OR)_4$] (R = Me, *n*Pr, *i*Pr, *t*Bu) has been conducted. The resulting mono-, bi-, tri or tetra-metallic products have been structurally characterised and employed as catalysts for the ROP of both ε-CL and *r*-LA. For the ROP of ε-CL, the complex [$Ti_2(L^5H_2)_2(OnPr)_6$]·CH_3CN (**19**·CH_3CN) exhibited the best performance achieving a conversion of ≥ 99% conversion within 6 min. at 100 °C. A number of the other systems proved to be quite sluggish and experienced induction periods. For the ROP of *r*-LA, the L^4H_2 derived complexes all exhibited good conversions, whilst most of the L^5H_3 derived species proved to be poorer catalysts. The exception again was complex **19** which achieved high conversion (98%). As well as polymers bearing alkoxide/hydroxy end groups, there was evidence of cyclic polymers.

References

1. E. Le Roux, *Coord. Chem. Rev.*, 2016, **306**, 65-85.
2. R. L. Webster, *RSC Adv*, 2014, **4**, 5254-5260.
3. E. Bermejo, R. Carballo, A. Castiñeiras and A. B. Lago, *Coord. Chem. Rev.*, 2013, **257**, 2639-2651.
4. At the Time of Writing (13.3.23), the Price of 100 g of Benzilic acid Costs £19.30 + VAT (from Merck/Sigma Aldrich). Available online: , https://www.sigmaaldrich.com/GB/en/substance/benzilicacid2282476937).
5. R. A. Coxall, S. G. Harris, D. K. Henderson, S. Parsons, P. A. Tasker and R. E. P. Winpenny, *J. Chem. Soc., Dalton Trans.*, 2000, DOI: 10.1039/B001404O, 2349-2356.
6. T. Kemmitt, G. J. Gainsford and N. I. Al-Salim, *Acta Crystallogr., Sect. C*, 2004, **60**, m42-m43.
7. The Price of 5 g of 2,2'-Diphenylglycine Costs £117.00 + VAT (from Merck/Sigma Aldrich online), https://www.sigmaaldrich.com/GB/en/product/aldrich/161918, (accessed at March 2023).
8. M. Baśko and P. Kubisa, *J. Polym. Sci., Part A: Polym. Chem.*, 2006, **44**, 7071-7081.
9. D. Delcroix, A. Couffin, N. Susperregui, C. Navarro, L. Maron, B. Martin-Vaca and D. Bourissou, *Polym. Chem.*, 2011, **2**, 2249-2256.
10. D. A. Wright and D. A. Williams, *Acta Crystallogr., Sect. B*, 1968, **24**, 1107-1114.
11. R. L. Martin and G. Winter, *Nature*, 1960, **188**, 313-315.
12. Y. Cui, C. Chen, Y. Sun, J. Wu and X. Pan, *Inorg. Chem. Front.*, 2017, **4**, 261-269.
13. Z. Zhong, P. J. Dijkstra and J. Feijen, *J. Am. Chem. Soc.*, 2003, **125**, 11291-11298.
14. H. Li, C. Wang, F. Bai, J. Yue and H. G. Woo, *Organometallics*, 2004, **23**, 1411-1415.

Chapter 5. Summary and outlook

5.1 Summary

From the former three chapters, 22 complexes based on Al(III), Zn(II), Ti(IV), Nb(V) and Ta(V) have been presented. These complexes have been exploited for the ROP of cyclic esters. The effects of substituent groups on the ligand or the alkoxides groups have been discussed at length. In conclusion, the steric bulk of the ligand, in particular the methoxy substituents at the aniline derived ring influences the catalytic activity in ε-CL ROP with the most active catalyst containing 3,4,5-methoxy substituted Schiff-base ligands. Aluminium and zinc catalysts chelated by the same ligand were found to be different between the polymerisation properties. The aluminium systems outperformed (in terms of rate) the zinc systems, indicating the metal centre is key to their performance. A series of Nb and Ta complexes supported by benzilic acid/2,2'-diphenylglycine derived ligation were synthesised and characterised for the ROP of ε-CL and LA. The structure of catalysts depends on the coordinating ligands. In the case of benzilic acid (*O*,*O*'-coordination), the products were tetranuclear complexes of the form, whereas, for 2,2'-diphenylglycine (*O*,*N*-coordination), dinuclear complexes of the type were produced. These different coordination modes influence the catalytic activity in CL and LA ROP. The Nb catalyst chelated by the benzilic acid was found the most active catalyst for CL ROP, whereas the Ta catalyst chelated by 2,2'-diphenylglycine was found the most active catalyst for LA ROP. Block copolymers of PLA-*b*-CL and PCL-*b*-LA and random copolymers PLA-*co*-CL were successfully obtained from catalysts **12**·2.25MeCN by adjusting the feed sequence, which shows that group V complexes of this kind are capable of enchaining both CL and LA in a single reaction pot. By reacting benzilic acid or 2,2′-diphenylglycine with the titanium tetraalkoxides [Ti(OR)$_4$] (R = Me, *n*Pr, *i*Pr, *t*Bu), mono-, bi-, tri or tetra-metallic complexes were obtained and employed as catalysts for the ROP of both ε-CL and *r*-LA. For the ROP of ε-CL, the complex **19**·CH$_3$CN exhibited the best performance achieving a conversion of ⩾ 99% conversion within 6 min. at 100 °C. For the ROP of *r*-LA, the benzilic acid derived complexes all exhibited good conversions, whilst most of the 2,2′-diphenylglycine derived species proved to be poorer catalysts. The exception again was complex **19** which achieved high conversion (98%). The results suggest that both the alkoxide groups and ligands are key to the regulating the catalytic performance.

Importantly, the choice of metals, ligand design, and the structure of the complex play a pivotal role in determining the catalytic activity. [1] The evaluation of the polymerisation catalyst performance depends on various factors, including polymerisation rate, molecular weight and distribution of polymer products, catalyst efficiency, catalyst stability, and catalyst selectivity especially stereo-selective ability. In this chapter, the best performing catalyst in this thesis will be listed and compared with other reported catalysts with similar ligand systems.

When the polymerisation reactions were carried out at 100 °C, using a [CL]:[catalyst]:[BnOH] ratio of 250:1:1, Ti(IV) complex **19** bearing dpg ligand moiety exhibited the highest polymerisation rate compared with Al(III) complex **1** bearing Schiff-base ligand and Nb(V) complex **9** bearing a benzilic acid derived ligand set. The k_{obs} value follows the sequence 4743×10^{-4}/min (**19**) > 2562×10^{-4} min^{-1} (**1**) > 250×10^{-4} min^{-1} (**9**). At lower loading of complex **19**, it proved able to completely convert up to 2000 equiv. of CL within 12 mins at 100 °C. The molecular weight follows the same sequence as k_{obs}, in which M_n = 28,300 Da (**19**) > 17,000 Da (**1**) > 12,000 Da (**9**). As for the control of polymerisation, the PDI follows the sequence 1.20 (**9**) < 1.49 (**19**) < 1.74 (**1**) (Table 5-1, entries 1-3). By conducting the ROP in the absence of the solvent, complex **19** allowed for ⩾99% monomer conversion within 6 min., affording a product with a molecular weight of 105,00 Da (Table 5-1, entry 4). All factors proved Ti(IV) complex **19** is an active and efficient catalyst with good control of polymerisation. However, Al(III) complex **1** can withstand exposure to air and moisture and display better air stability than Ti(IV) complex **19**. Notably, a zinc complex $[(2,4,6\text{-}F_3\text{-}C_6H_2)Zn(dpg)]_4$ (**Zn4**) derived from dpg ligand moiety was found to afford a high activity which the k_{obs} value is 1738×10^{-4} min^{-1} at 110 °C in the absence of BnOH (Table 5-1, entry 5). [2] The [CL]:[catalyst] ratio is 150:1. From the k_{obs}, it is evident that Ti(IV) complex **19** is still the most active (Figure 5-1).

The observed activity differences suggest multiple factors may be at play in combination, including the metal, ancillary ligands and nucleophile (alkoxides groups). Therein, the Lewis acidity of the metal centre is a key catalyst feature in the ROP. However, because of the different ligand systems, it is difficult to estimate the Lewis acidic trend of metal centres from these catalysts. Furthermore, an important factor should be noted is the M–O bond, the length of Ti(1)–O(5) (2.048(3) Å) in complex **19** is longer than the Nb(2)–O(11) (1.8647(15)) one in complex **9** which indicates the Ti complex **19** has a weaker and longer Ti–O*n*Pr bond so that benefits the M–OR bond cleavage step in the ROP.[2]

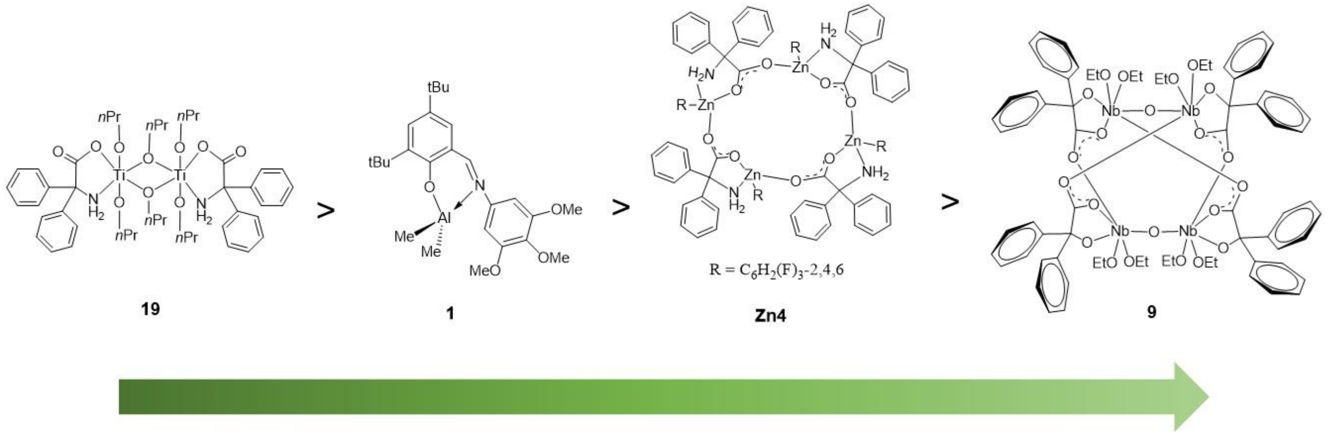

Figure 5-1. The activity sequence of complex **19**, **1**, **Zn4** and **9**.

5.2 Comparative ROP study

For comparative ROP studies, other metal catalysts with similar chelating ligand systems were widely searched. The ROP activity of metal complexes bearing dpg or benzilic acid ligands has been rarely studied except in Redshaw’s research group. Only limited examples were found of metal-amino acid (*O*,*N*-donor) or carboxylate complexes (*O*,*O*-donor) ROP catalysts, as shown in Figures 5-2 (a-h). Besides, two Schiff-base derived complexes with methoxy substituted groups were discussed to compare with complex **1** in this thesis, the structures are shown in Figures 5-2 (i-j).

Comparison between **1**, **9**, **19**, **Zn4** and other catalyst systems is difficult since different authors report catalyst performance under different conditions. For example, He and Zhiyong Wei [3] reported a series of tin complexes consisting of natural amino acids ligands, the results showed that the phenylalanine-tin complex (**Sn(L-Phe)$_2$**) (Figures 5-2(a)) displayed significantly high activity in the ROP of ε-CL and L-LA compared with other amino acid tin-complexes. PCL and PLA were obtained with M_n of 54.5 and 174.9 KDa, respectively. The K_{obs} and M_n were higher than the Sn(Oct)$_2$ under the same conditions (Table 5-1, entries 6-8). The ROP reaction was conducted in bulk at 140 ℃ for 16 h.

In another study, Ruiz and co-workers [4] reported a series of mononuclear cobalt complexes containing 2,2′ -bipyridine and amino acids as mixed ligands. The unsubstituted glycine ligand had a great effect on the catalytic activity of catalysts **Co(gly)$_2$(bipy)** (Figures 5-2(b)). PLA obtained with this cobalt complex, as determined by GPC analysis, M_n is 12.39 KDa and PDI is

1.11 which indicates a good control of the chain growth (Table 5-1, entry 9). The ROP reaction was conducted in the toluene at 130 ℃ for 1 h.

Similarly, a zinc amino acids complex [**Zn(D-Ala)$_2$**] was prepared by reaction of Zn(OAc)$_2$ and D-alanine (Figures 5-2(c)). [5] This complex was applied in the ROP of L-LA at 140 ℃ for 24 h using [LA]/[cat]/[BnOH]=100:1:1, leading to a high conversion (97%) of L-LA to PLA with M_n of 15.5 KDa which is similar to the Sn(Oct)$_2$ performance under the same condition (Table 5-1, entries 10 and 11).

In another carboxylate study, amino acids such as glutamic acid, glycine, and aspartic acid were complexed with samarium salts to give Sm(2,2'-bipyridine)(L^n)$_3$ (L^1= L-aspartic acid, L^2=L-glutamic acid, L^3 = glycine) compounds. [6] Among these, Sm(2,2'-bipyridine)(L^1)$_3$ (**SmC1**), as shown in Figures 5-2 (d), was active toward the ROP of ε-CL and L-LA even if it was used in relatively small amounts (M/I greater than 5000) at 125 ℃. The resultants PCL and PLA were obtained with M_n values of 3.43 and 2.00 KDa and moderate PDI of 1.39 and 1.13, respectively (Table 5-1, entries 12 and 13).

Akintayo and co-workers [7] synthesised nine heteroleptic Zn(II) carboxylate complexes and employed them for the catalytic ROP of ε-CL and L-LA. In particular, complex **ZnL1** with an unsubstituted benzoate anion, as shown in Figures 5-2(e), had the highest k_{obs} (6.97× 10^{-4}/min) and displayed significant activity towards ε-CL and r-LA but afforded low molecular weights PCL and PLA when the [monomer]:[catalyst] ratio is 200:1 at 110 ℃. (Table 5-1, entries 14 and 15).

A zirconium complex (**Zr28**) was synthesised by a reaction of zirconium(IV) propoxide with 5-chlorosalicyclic acid in 1-propanol and its structure was drawn as in Figures 5-2(f). [8] Substituted salicylic acids were bonded to the zirconium atom in a monoanion mode with only the deprotonated carboxylate group. This zirconium complex was used as a catalyst for the ROP of ε-CL and reached complete conversion in 12 h at 100 ℃. As seen from the data in Table 5-1 entry 16, this catalyst produced PCL with M_n = 35.27 KDa and narrow molecular weight distribution (PDI = 1.23), indicating the characteristic of a single-site metal alkoxide catalyst. It was also found that the number of salicylate ligands bonded to the zirconium atom and the presence of substituents on salicylate ligands were effective in the polymerization reactions.

Nikiforov et al. [9] reported a mixed-ligand nickel(II) carboxylate complex with ethylenediamine derivatives as catalysts in the ROP of r-LA. The results showed that the choice of the amino group determines the formation of a complex, for example, only mononuclear complexes were obtained when using *N*,*N*′ -dibenzylethylenediamine. Additionally, the presence of carboxylate ligands, which differ greatly in basicity, will allow a determination of their role (as proton carriers) in the ROP of r-LA. The obtained PLA sample showed the highest values of M_n = 0.75 KDa when using mononuclear mixed-ligand carboxylates containing RCO_2 ligands complex (**Ni2**) as catalyst (Figures 5-2 (g)) at [r-LA]/[Ni] ratio of 250/1. The highest conversion (98%) was also observed for the **Ni2** catalytic system in 72 h (Table 5-1, entry 17).

Balasanthiran and coworkers [10] prepared two five-coordinate magnesium complexes in the form (BDI)Mg(OCMeCOOEt)(L) where BDI = 2-[(2,6-diisopropylphenyl)amino]-4-[(2,6-diisopropylphenyl)imino]pent-2-ene and L = pyridine (py) or 4-dimethylaminopyridine (DMAP). **Mg(py)** and **Mg(DMAP)** are shown in Figure 5-2 (h). A striking result they found was that the chelating ligand has little or no influence on the initiation of the ROP of LA but effectively suppressed the initiation of the polymerisation of CL. Specifically, when conducting the homo polymerisation of CL in CH_2Cl_2 at 25 ℃, neither complexes were active to initiate the ROP of CL (Table 5-1, entries 18 and 20). However, under the same conditions, the conversions of r-LA for **Mg(py)** and **Mg(DMAP)** were both 97% in 3 mins and the GPC obtained polylactides have similar M_n (22.2 and 23.3 KDa) and show relatively narrow PDI (1.21-1.25) (Table 5-1, entries 19 and 21). The ability of **Mg(py)** and **Mg(DMAP)** to initiate the ROP of LA but not CL implicated the role of chelation in the ROP of LA and shut down the ROP of CL. The possible reason for this result could be the greater degree of ring-strain for LA leads to its preferential ring-opening.

Plaman and Durr [11] reported a series of niobium/tantalum alkoxide catalysts, supported by a range of phenoxyimine ligands. The ligands varied on the phenoxy group (^{t}Bu, Cl, and OMe) and the imine group (ph; 2,6-diMePh; 2,6-di^{i}PrPh; and 2,4,6-tri^{t}BuPh). One of the complexes with OMe substituted phenoxy group (**Nb3a**, shown as Figures 5-2 (i)) showed the best catalytic activity to the ROP of CL with the [CL]:[I] ratio of 100:1 at 140 ℃. **Nb3a** was found to reach full conversion in 1 h and showed good control of the polymerisation (PDI = 1.64). To benchmark the catalyst system, $Nb(OEt)_5$ was studied under the same conditions. It reached full conversion in 15 min, which is faster than **Nb3a**, but suffered from poor control (PDI = 2.15). (Table 5-1, entries 22-23) The data suggest the choice of ligand, plays a critical role in catalysis, particularly when polymerising CL.

In a similar ligand system, Durr and Williams [12] reported a detailed study of a series of bis(alkoxy)bis(phenoxyimine)titanium(IV) complexes, coordinated by Schiff-base ligands derived from *o*-vanillin (2-hydroxy-3-methoxybenzaldehyde). The *o*-vanillin derivatives are attractive as they feature an additional *ortho*-methoxy substituent, adjacent to the phenolate, and as such offer different coordination modes: either N-O or O-O chelates should be accessible. A complex **$(L_4)Ti(O^iPr)_2$** (L_4 = 2,6-iPr(C_6H_3)) that adopts the N-O and O-O chelates (Figures 5-2 (j)) completed conversion within 4 h using [CL]:[cat] = 200:1 ratio at 80 ℃. The obtained PCL showed a relatively narrow dispersity value (PDI = 1.27) and M_n is 11.3 KDa. The rate of this titanium complex is generally slower than the homoleptic Ti(OiPr)$_4$ but shows better polymerisation control [13] (Table 5-1, entries 24 and 24).

Although comparisons are complicated by different reaction conditions and uncertainties regarding the number of initiating groups. Overall, based on the M_n data and the narrow to moderate dispersities of the catalyst family, **Sn(L-Phe)$_2$** shows the highest M_n (PLA: 174.9 KDa) and **Co(gly)$_2$(bipy)** shows the narrowest dispersity (PDI = 1.11).

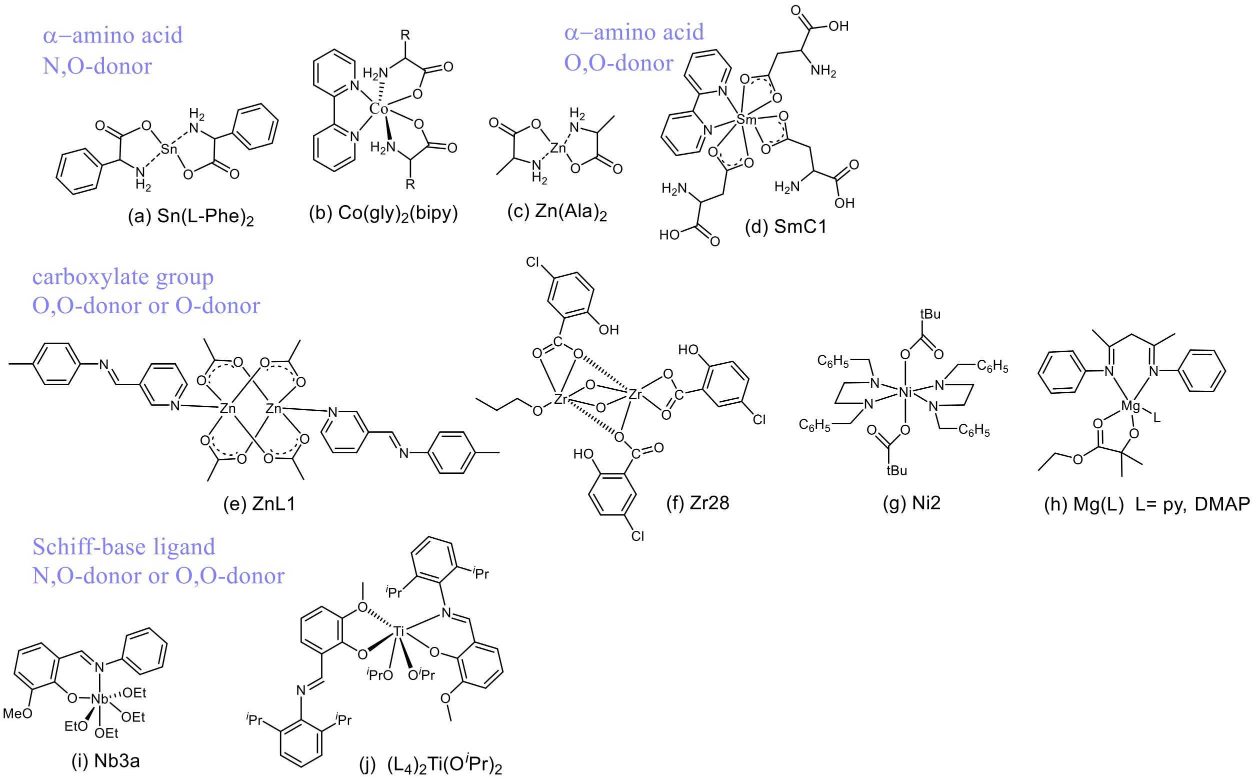

(a) Sn(L-Phe)$_2$ (b) Co(gly)$_2$(bipy) (c) Zn(Ala)$_2$ (d) SmC1

(e) ZnL1 (f) Zr28 (g) Ni2 (h) Mg(L) L= py, DMAP

(i) Nb3a (j) $(L_4)_2Ti(O^iPr)_2$

Figure 5-2. Complexes (a-d) with amino acid derived ligand, coordination mode: N,O-donor or O,O-donor [3-6]; carboxylate complexes e-f, coordination mode: O,O-donor or O-donor [7-10];

Complexes (i and j) with Schiff-base derived ligand, coordination mode: N,O-donor or O,O-donor [11,12].

Table 5-1. Overview of literature catalysts used for the ROP of macrolactones.

Run	catalyst	monomer	[M]:[cat]:[BnOH]	T (°C)	Solvent	t (h)	Conv. (%)	k_{obs} × 10^{-4}/min	M_n (KDa)	PDI	Author
1	**1**	ε-CL	250:1:1	100	toluene	0.67	99	2562	17.0	1.74	This thesis
2	**9**	ε-CL	250:1:1	100	toluene	24	99	250	12.0	1.20	This thesis
3	**19**	ε-CL	250:1:1	100	toluene	0.2	99	4743	28.3	1.49	This thesis
4	**19**	ε-CL	250:1	110	bulk	0.1	99	-	10.5	1.29	This thesis
5	**Zn4**	ε-CL	150:1	110	toluene	1	92	1738	12.9	1.31	Khafaji
6	**Sn(L-Phe)$_2$**	ε-CL	1000:1:1	140	bulk	16	92.7	-	54.5	1.32	He
7		L-LA	2000:1:1	140	bulk	16	95.6	3.85	174.9	1.67	He
8	Sn(Oct)$_2$	L-LA	2000:1:1	140	bulk	16	92.6	2.82	144.6	1.54	He
9	**Co(gly)2(bipy)**	r-LA	100:1	130	toluene	1	94	561	12.39	1.11	Ruiz
10	**Zn(D-Ala)$_2$**	L-LA	100:1:1	130	bulk	24	97	-	15.5	1.40	Liang
11	Sn(Oct)$_2$	L-LA	100:1:1	130	bulk	24	99	-	14.2	1.37	Liang
12	**SmC1**	ε-CL	7982:1	125	bulk	18	10	5.15	3.43	1.39	Medina
13		L-LA	6141:1	125	bulk	18	10	3.95	2.00	1.13	Medina
14	**ZnL1**	ε-CL	200:1	110	bulk	12	99	6.97	1.30	1.80	Akintayo
15		r-LA	200:1	110	bulk	31	97	1.87	1.20	1.72	Akintayo
16	**Zr28**	ε-CL	3:1	100	toluene	12	100	-	35.27	1.23	Kayan
17	**Ni2**	r-LA	250:1	140	bulk	72	98	-	0.75	1.70	Nikiforov
18	**Mg(py)**	ε-CL	100:1	25	CH_2Cl_2	0.05	0	-	-	-	Balasanthiran

19	**Mg(DMAP)**	r-LA	100:1	25	CH_2Cl_2	0.05	97	-	12.9	1.21	Balasanthiran
20		ε-CL	100:1	25	CH_2Cl_2	0.05	0	-	-	-	Balasanthiran
21		r-LA	100:1	25	CH_2Cl_2	0.05	97	-	13.5	1.25	Balasanthiran
22	Nb(OEt)$_5$	ε-CL	100:1	140	Bulk	0.25	99	-	2.85	2.15	Plaman
23	**Nb3a**	ε-CL	100:1	140	Bulk	1	97	-	3.10	1.64	Plaman
24	**(L$_4$)$_2$Ti(O^{i}Pr)$_2$**	ε-CL	200:1	80	toluene	4	99	130.8	11.3	1.27	Durr
25	Ti(O^{i}Pr)$_4$	ε-CL	212:1	100	bulk	0.05	95	-	19.8	2.02	Parssinen

5.3 Outlook

No matter the successful industrial application of tin octoate or the outstanding catalytic performance of Sn(L-Phe)$_2$ reported in the summary, tin compounds exhibit preferred catalytic efficiencies compared with other metal-based catalysts for the production of PCL and PLA. The inherent nature of tin(II) metal along with its lone pair electrons could affect the monomer insertions during the polymerisation.[14] In addition, the ROPs using benzilic acid and dpg tin(II) complexes are still unknown. Therefore, for a 3-month research plan, it is worth to exploring tin benzilic acid/dpg complexes with different structures. An improvement in the catalyst's polymerisation control and air stability may enhance its versatility for use in industry and academia.

For a 6-month research plan, further insight into an interesting question about the difference in catalytic reactivity between mono-, and multimetallic sites is crucial to achieving this. Vanadium complexes can create multiple active metal sites by regulating the coordination environment of metal ions.[15] Thus, this future work could design and construct mono-, di-, multinuclear niobium benzylic/dpg complexes. These complexes can be taken as model catalysts to compare the differences in reactivity between mono- and multimetallic sites for the ROP of lactones and lactides. Besides, density functional theory calculation related to ROP reaction will be conducted to explore the catalytic reaction process and the relationship to the number of active sites.

References

1. E. Fazekas, P. A. Lowy, M. Abdul Rahman, A. Lykkeberg, Y. Zhou, R. Chambenahalli and J. A. Garden, *Chem Soc Rev*, 2022, **51**, 8793-8814.
2. W. Gruszka and J. A. Garden, *Nat. Commun*, 2021, **12**, 3252.
3. M. He, Y. Cheng, Y. Liang, M. Xia, X. Leng, Y. Wang, Z. Wei, W. Zhang and Y. Li, *Polym. J.*, 2020, **52**, 567-574.
4. A. C. Ruiz, K. K. Damodaran and S. G. Suman, *RSC Adv*, 2021, **11**, 16326-16338.
5. Y. Liang, M. Sui, M. He, Z. Wei and W. Zhang, *Polymers (Basel)*, 2019, **11**.
6. D. A. Medina, J. M. Contreras, F. J. López-Carrasquero, E. J. Cardozo and R. R. Contreras, *Polym. Bull.*, 2017, **75**, 1253-1263.
7. D. C. Akintayo, W. A. Munzeiwa, S. B. Jonnalagadda and B. Omondi, *Inorganica Chim. Acta*, 2022, **532**.
8. A. Kayan, *Catal. Surv. Asia*, 2020, **24**, 87-103.
9. A. Nikiforov, N. Panina, D. Blinou, V. Gurzhiy, J. Nashchekina, E. Korzhikova-Vlakh, A. Eremin and M. Stepanova, *Catalysts*, 2023, **13**.
10. V. Balasanthiran, M. H. Chisholm, K. Choojun and C. B. Durr, *Dalton Trans*, 2014, **43**, 2781-2788.
11. A. S. Plaman and C. B. Durr, *ACS Omega*, 2022, **7**, 23995-24003.
12. C. B. Durr and C. K. Williams, *Inorg. Chem.*, 2018, **57**, 14240-14248.
13. C. B. Durr and C. K. Williams, *Inorg. Chem.*, 2018, **57**, 14240-14248.
14. R. H. Platel, L. M. Hodgson and C. K. Williams, *Polym. Rev.*, 2008, **48**, 11-63.
15. R. R. Langeslay, D. M. Kaphan, C. L. Marshall, P. C. Stair, A. P. Sattelberger and M. Delferro, *Chem. Rev.*, 2019, **119**, 2128-2191.

Chapter 6. Experimental section

6.1 Alkoxy-functionalized Schiff-base ligation at aluminium and zinc for ring opening polymerisation

6.1.1 General

The preparation of the aluminium or zinc complexes and the ring opening polymerisation procedures were carried out under an inert atmosphere of dry nitrogen by using Schlenk systems, cannula techniques or a glove box (Saffron scientific equipment). Toluene (Alfa Aesar, Lancashire, UK) was refluxed over sodium/benzophenone (Aldrich, Dorset, UK), acetonitrile (Aldrich, Dorset, UK) was refluxed over calcium hydride (Aldrich, Dorset, UK), whilst benzyl alcohol (Aldrich, Dorset, UK) was dried over molecular sieves. ε-CL (Aldrich, Dorset, UK) and 2,4-dimethoxyaniline (Alfa Aesar, Lancashire, UK) were dried over calcium hydride, and were distilled prior to use. The purity of the monomers ε-CL and GL were determined to be 99.6 and 99.5 %, respectively (determined by ^{1}H NMR spectroscopy. 3,5-Di-*tert*-butyl-2-hydroxybenzaldehyde (Matrix Scientific, Columbia, SC, U.S.A.), 3,4,5-trimethoxyaniline (Alfa Aesar, Tewksbury, MA, U.S.A.), diethylzinc ($ZnEt_2$) (0.9 M in hexane) (Acros Organics, Loughborough, UK), trimethylaluminium ($AlMe_3$) (2.0 M in toluene) (Aldrich, Dorset, UK) were purchased from commercial sources and used directly. 2,4,6-Trimethoxyaniline and complex **5** were prepared by the reported procedures.[1] NMR spectra were recorded at 400.2 MHz on a JEOL ECZ 400S spectrometer (JEOL Ltd., Tokyo, Japan) with TMS δH = 0 as the internal standard or residual protic solvent [CD_3CN, δH = 1.94]. Chemical shifts are given in ppm (δ) and coupling constants (*J*) are given in Hertz (Hz). Elemental analyses were performed by the elemental analysis service at the Department of Chemistry, the University of Hull or OEA labs Ltd. FTIR spectra (Nujol mulls, KBr windows) were recorded on a Nicolet Avatar 360 FT-IR spectrometer (Thermo Nicolet Corporation., Madison, WI, U.S.A.). MALDI-TOF mass spectra (Bruker Daltonics Reflex IV, Bremen, Germany) were acquired by averaging at least 100 laser shots. Matrix Assisted Laser Desorption/Ionization Time of Flight (MALDI-TOF) mass spectrometry was performed in a Bruker autoflex III smart beam in linear mode, and the spectra were acquired by averaging at least 100 laser shots. 2,5-Dihydroxybenzoic acid was used as the matrix and THF as the solvent. Sodium chloride was dissolved in methanol and used as the ionizing agent. Samples were prepared by mixing 20 μl of matrix solution in THF (2 mg·mL^{-1}) with 20 μL of matrix solution (10 mg·mL^{-1})

and 1 μL of a solution of ionizing agent (1 mg·mL^{-1}). Then 1 mL of these mixtures was deposited on a target plate and allowed to dry in air at ambient temperature. Both number average molecular weights and the mass average molecular weight were measured by Viscotek size exclusion chromatography with a refractive index detector (VE 3580 RI detector). Columns were procured from Agilent (plgel, 5 μm, mixed-d) and used for the SEC at 35 °C when extra dry THF was used as the eluent with 1 ml/min flow rate. The light scattering detectors were calibrated with polystyrene standards. Molecular weights were calculated from the experimental traces using the OmniSEC 467.

6.1.2 Synthesis of L^{1}H

L^{1}H was prepared according to a procedure described previously for related Schiff-bases.[2-4] 3,5-Di-*tert*-butyl-2-hydroxybenzaldehyde (3.51 g, 15.00 mmol) was mixed with 3,4,5-trimethyoxyaniline (2.75 g, 15.03 mmol) in refluxing ethanol (200 mL), and the system was refluxed for 12 h. A yellow crystalline solid separated slowly upon stirring. The solid was isolated by filtration then washed with ice-cold methanol (30 mL). The solid was further recrystallized from dichloromethane (10 mL)/methanol (30 mL) then dried under vacuum. Yield: 54% (3.23 g). ^{1}H NMR (400 MHz, CD_3CN, 25 °C): δ: 8.84 (s, 1H, C*H*=N), 7.48–7.49 (d, *J* = 2.4 Hz, 1H, Ar*H*), 7.42–7.43 (d, *J* = 2.4 Hz, 1H, Ar*H*), 6.72 (s, 2H, Ar*H*), 3.87 (s, 6H, CH_3), 3.74 (s, 3H, CH_3), 1.46 (s, 9H, *t*Bu), 1.33 (s, 9H, *t*Bu). IR (KBr disc, Nujol mull, cm^{-1}): 2950(s), 1961(w), 1793(m), 1668(w), 1615 (w), 1575(s), 1503(s), 1455(s), 1376(s), 1329(w), 1276(w), 1249(m), 1228(w), 1171(s), 1154(w), 1130(m), 1043(w), 1023(w), 998(s), 930(w), 922(w), 889(s), 823(s), 773(m), 750(m), 730(s), 678(s), 646(s), 614(w), 577(m), 523(m), 507(m). HR-MS: m/z 400.32 $[L^1+H]^+$.

6.1.3 Synthesis of L^{2}H

L^{2}H was prepared using a procedure similar to that described for L^{1}H. 3,5-Di-*tert*-butyl-2-hydroxybenzaldehyde (3.51 g, 15.00 mmol) was mixed with 2,4,6-trimethyoxyaniline (2.75 g, 15.01 mmol) in refluxing ethanol (200 mL). An orange crystalline solid separated slowly upon stirring. The resulting mixture was stirred for 4 h and the solid was isolated by filtration then washed with ice-cold methanol (30 mL). The solid was further recrystallized from dichloromethane (10 mL)/methanol (30 mL) then dried under vacuum. Yield: 70% (4.19 g). ^{1}H

NMR (400 MHz, CD_3CN, 25 °C): δ: 9.16 (s, 1H, C*H*=N), 7.41-7.40 (d, *J* = 2.5, 1H, Ar*H*), 7.29-7.28 (d, *J* = 1.9 Hz, 1H, Ar*H*), 6.32 (s, 2H, Ar*H*), 3.88 (s, 6H, OCH_3), 3.84 (s, 3H, OCH_3), 1.45 (s, 9H, *t*Bu), 1.32 (s, 9H, *t*Bu). IR (KBr disc, Nujol mull, cm^{-1}): 2955(m), 2924(s), 2854(m), 1611(w), 1596(m), 1460(s), 1377(s), 1337(m), 1337(w), 1311(w), 1260(w), 1230(w), 1195(w), 1108(m), 1061(w), 1041(w), 1021(w), 958(w), 922(w), 893(w), 875(w), 853(w), 808(m), 781(w), 736(w), 686(w), 642(w), 550(w), 523(w), 500(w), 464(w). HR-MS: m/z 400.32 $[L^2+H]^+$.

6.1.4 Synthesis of L^3H

L^3H was prepared using a procedure similar to that described for L^1H. 3,5-Di-*tert*-butyl-2-hydroxybenzaldehyde (5.80 g, 24.78 mmol) was mixed with 2,4-dimethyoxyaniline (3.80 g, 24.78 mmol) in refluxing ethanol (200 mL). An orange crystalline solid separated slowly upon stirring. The resulting mixture was stirred for 4 h and the solid was isolated by filtration then washed with ice cold methanol (30 mL). The solid was further recrystallized from dichloromethane (10 mL)/methanol (30 mL) then dried under vacuum. Yield: 33% (3.00 g). ^1H NMR (400 MHz, CD_3CN, 25 °C): δ: 8.78 (s, 1H, C*H*=N), 7.41-7.42 (d, *J* = 2.4 Hz, 1H, Ar*H*), 7.33-7.34 (d, *J* = 2.4 Hz, 1H, Ar*H*), 7.28-7.29 (d, *J* = 8.8 Hz, 1H, Ar*H*), 6.62-6.63 (d, *J* = 2.8 Hz, 1H, Ar*H*), 6.55-6.58 (dd, J = 8.7, 2.8 Hz, 1H, Ar*H*), 3.87 (s, 3H, OCH_3), 3.80 (s, 3H, OCH_3), 1.42 (s, 9H, *t*Bu), 1.29 (s, 9H, *t*Bu). HR-MS (EI): m/z 370.24 $[L^3]^+$, 233.19 $[L^3 – Ph(OMe)_2]^+$, 154.09. IR (KBr disc, Nujol mull, cm^{-1}): 2955(s), 2923(s), 2854(s), 1616(w), 1590(w), 1502(w), 1463(m), 1377(m), 1362(w), 1306(w), 1264(w), 1250(w), 1206(w), 1169(w), 1125(w), 1047(w), 1025(w), 982(w), 963(w), 871(w), 853(w), 837(w), 821(w), 802(w), 786(w), 773(w), 723(w), 643(w). HR-MS: m/z 370.26 $[L^3+H]^+$.

6.1.5 Synthesis of 2,4-di-*tert*-butyl-6-((phenylimino)methyl)phenol

This ligand was prepared using a procedure similar to that described for L^1H. 3,5-Di-*tert*-butyl-2-hydroxybenzaldehyde (11.71 g, 50.00 mmol) was mixed with aniline (4.65 mL, 50.00 mmol) in refluxing ethanol (200 mL). An orange crystalline solid separated slowly upon stirring. The resulting mixture was stirred for 4 h and the solid was isolated by filtration then washed with ice cold methanol (30 mL). The solid was further recrystallized from dichloromethane (10 mL)/methanol (30 mL). Yield: 80% (12.38 g). ^{1}H NMR (400 MHz, CD_3CN, 25 °C): δ: 8.81 (s, 1H, C*H*=N), 7.50–7.29 (m, 7H, Ar*H*), 1.45 (s, 9H, *t*Bu), 1.33 (s, 9H, *t*Bu). IR (KBr disc, Nujol mull, cm^{-1}): 3174(w), 3062(w), 2923(s), 2853(s), 2726(w), 2670(w), 2351(w), 1946(w), 1867(w), 1790(w), 1757(w), 1731(w), 1696(w), 1618(s), 1581(s), 1455(s), 1377(s), 1319(m), 1374(m), 1250(m), 1197(m), 1170(s), 1131(w), 1075(m).

6.1.6 Synthesis of complex 1

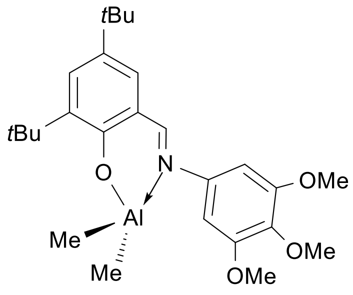

1

In a 25 mL Schlenk tube under nitrogen, L^{1}H (0.27 g, 0.68 mmol) was dissolved in dry toluene (20 mL), and one equivalent of $AlMe_3$ (0.35 mL, 0.68 mmol) was added dropwise into the reaction solution. The system was refluxed for 12 h, and following removal of volatiles *in vacuo,* the residue was extracted into warm MeCN (15 mL), affording on prolonged standing in the refrigerator (5 °C) small, yellow crystals. Yield 52% (0.14 g). Anal. Calcd for $C_{26}H_{38}NO_4Al$ (455.55 g mol^{-1}): C, 68.55; H, 8.41; N, 3.07%; Found: C, 67.79; H, 8.22; N, 3.42%. HR-MS (EI): m/z 457.24 $[Al(L^1)(Me)_2 + H]^+$, 400.31 $[Al(L^1)(Me)_2 - Al(Me)_2 + H]^+$. ^{1}H NMR (400 MHz, CD_3CN, 25 °C): δ: 8.82 (s, 1H, C*H*=N), 7.58–7.59 (d, *J* = 2.8, 1H, Ar*H*), 7.35–7.36 (d, *J* = 2.8, 1H, Ar*H*), 6.70 (s, 2H, Ar*H*), 3.82 (s, 6H, C*H*$_3$), 3.72 (s, 3H, C*H*$_3$), 1.41 (s, 9H, *t*Bu), 1.33 (s, 9H, *t*Bu), -0.79 (s, 6H, Al*Me*$_2$). ^{13}C NMR (400 MHz, CD_3CN, 22 °C) δ (ppm): 170.5, 154.1, 153.3, 147.1, 142.6, 139.8, 139.6, 132.7, 130.4, 120.5, 117.4 (CH_3CN), 99.8, 64.7, 55.9, 34.9, 30.6, 28.7, 27.6. IR (KBr disc, Nujol mull, cm^{-1}): 2922(s), 2583(s), 1614(w), 1591(m), 1540(m), 1509(m), 1462(s), 1378(m), 1360(w), 1332(w), 1256(m), 1237(w), 1198(w), 1186(w), 1177(w), 1125(s), 994(m), 930(w), 920(w), 895(w), 858(m), 835(m), 818(w), 793(w), 786(w), 760(w),721(w), 708(w), 673(w), 609(w), 587(w).

6.1.7 Synthesis of complex 2

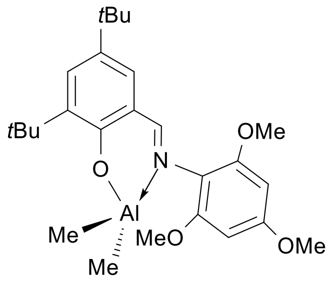

2

The synthesis of **2** was carried out according to the same procedure as for **1** but using L^2H. Yield 34% (0.093 g). Anal. Calcd for $C_{26}H_{38}NO_4Al$ (455.55 g mol^{-1}): C, 68.55; H, 8.41; N, 3.07%; Found: C, 67.94; H, 8.36; N, 3.11%. HR-MS (EI): m/z 400.27 $[Al(L^2)(Me)_2 - Al(Me)_2 + H]^+$. ^1H NMR (400 MHz, CD_3CN, 25 °C): δ: 8.58 (s, 1H, C*H*=N), 7.57–7.58 (d, *J* = 2.4, 1H, Ar*H*), 7.22–7.21 (d, *J* = 2.8, 1H, Ar*H*), 6.34 (s, 2H, Ar*H*), 3.82 (s, 6H, OCH_3), 3.86 (s, 3H, OCH_3), 1.41 (s, 9H, *t*Bu), 1.30 (s, 9H, *t*Bu), –1.00 (s, 6H, Al*Me*$_2$). ^{13}C NMR (400 MHz, CD_3CN, 22 °C) δ (ppm): 160.5, 154.5, 152.3, 140.7, 138.4, 129.4, 125.7, 118.9, 117.4 (CH_3CN), 116.8, 116.0, 94.0, 57.9, 35.5, 32.6, 31.7. IR (KBr disc, Nujol mull, cm^{-1}): 2956 (m), 2923(s), 2853(m), 2728(w), 2360(w), 1614(m), 1598(m), 1555(w), 1540(w), 1502(w), 1458(s), 1382(m), 1344(w), 1301(w), 1259(s), 1230(w), 1207(w), 1173(w), 1173(w), 1157(w), 1134(w), 1059(w), 1028(w), 949(w), 918(w), 872(w), 842(w), 806(s), 757(w), 705(w), 681(w), 641(w), 604(w), 538(w), 518(w).

6.1.8 Synthesis of complex 3

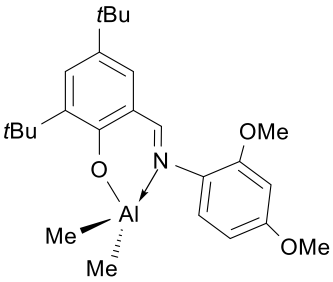

3

The synthesis of **3** was carried out according to the same procedure as for **1** but using L^3H. Yield 40% (0.15 g). Anal. Calcd for $C_{25}H_{36}NO_3Al$ (425.55 g mol^{-1}): C, 70.56; H, 8.53; N, 3.29%; Found: C, 68.83; H, 8.21; N, 3.27 %.* HR-MS (EI): m/z 427.30 $[Al(L^3)(Me)_2 + H]+$, 370.24 $[Al(L^3)(Me)_2 - Al(Me)_2 + H]^+$. ^1H-NMR (400 MHz, CD_3CN, 25 °C): δ: 8.58 (s, 1H, C*H*=N), 7.57 (d, *J* = 2.5 Hz, 1H, Ar*H*), 7.33 (d, *J* = 2.8 Hz, 1H, Ar*H*), 7.28 (d, *J* = 8.7 Hz, 1H, ArH), 6.63 (t, *J* = 8.4 Hz, 2H, Ar*H*), 3.89 (s, 3H, OC*H*3), 3.84 (s, 3H, OC*H*3), 1.41 (s, 9H, *t*Bu), 1.31 (s, 9H, *t*Bu), –0.93(s, 6H, Al*Me*2). ^{13}C NMR (400 MHz, CD_3CN, 22 °C) δ (ppm): 165.0, 160.1, 152.5, 150.4, 137.4, 135.7, 130.9, 127.3, 127.0, 123.3, 122.7, 117.7, 117.4 (CH_3CN), 105.9, 96.7, 56.9, 35.6, 35.2, 31.3, 30.2. IR (KBr disc, Nujol mull, cm^{-1}): 2957(s), 2923(s), 2853(s), 2727(w), 2605(w), 2350(w), 2049(w), 1958(w), 1825(w), 1615(w), 15912(w), 1578(w), 1578(w), 1557(w), 1538(m), 1504(m), 1462(s), 1404(w), 1379(m), 1361(w), 1317(w), 1256(w), 1240(w), 1211(w), 1190(w), 1171(w), 1160(w), 1133(w), 1028(m), 980(w), 926(w), 879(w), 866(w), 846(w), 838(w), 788(m), 755(w), 723(w), 676(w), 640(w), 579(w). * Despite repeated attempts, the %C was always low.

6.1.9 Synthesis of complex 4

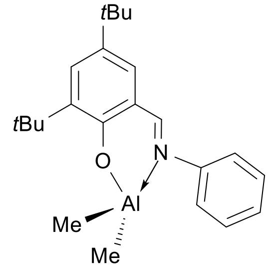

4

The synthesis of **4** was carried out following the previous report.[1] A mixture of 2,4-di-*tert*-butyl-6-((phenylimino)methyl)phenol (3.68 g, 11.89 mmol) and $AlMe_3$ (6 mL, 12.00 mmol) in toluene (20 mL) was stirred for 12 h at 150 °C. Volatile materials were removed under vacuum to give yellow needle crystals, and then acetonitrile (20 mL) was transferred to the suspension. A yellow crystalline solid was obtained after filtering and prolonged standing at 0 °C. Yield 78% (3.37 g). HR-MS (EI): m/z 367.28 $[Al(L)(Me)_2 + H]^+$, 310.22 $[Al(L)(Me)_2 - Al(Me)_2 + H]^+$. ^1H NMR (400 MHz, CD_3CN, 25 °C): δ: 8.52 (s, 1H, C*H*=N), 7.59–7.60 (d, *J* = 2.4 Hz, 1H, Ar*H*), 7.26–7.51 (m, 6H, Ar*H*), 1.43 (s, 9H, *t*Bu), 1.40 (s, 9H, *t*Bu), –1.16 (s, 6H, Al*Me*2). IR (KBr disc, Nujol mull, cm^{-1}): 2955(w), 2924(s), 2854(s), 2670(m), 2359(w), 1866(w), 1744(w), 1616(m), 1589(m), 1555(w), 1540(m), 1463(s), 1410(w), 1377(s), 1363(w), 1324(w), 1277(w), 1258(m), 1230(w), 1194(m), 1175(m), 1136(w), 1027(w), 1002(w), 987(w), 906(w), 875(w), 853(w), 812(w), 785(w), 765(m), 705(w), 604(w), 575(w).

6.1.10 Synthesis of complex 5

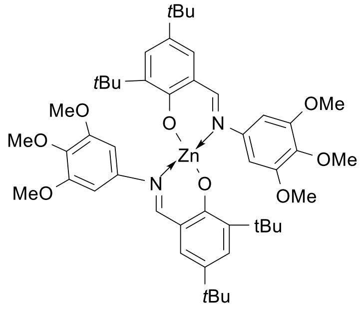

5

In a 25 mL Schlenk tube under nitrogen, L^{1}H (0.50 g, 1.25 mmol) was dissolved in dry toluene (20 mL), and one equivalent of ZnEt$_2$ (1.39 mL, 1.25 mmol) was added dropwise into the reaction solution. The system was refluxed for 12 h, and following removal of volatiles in vacuo, the residue was extracted into warm MeCN (15 mL), affording on prolonged standing in the refrigerator (5 °C) small, yellow crystals. Yield 48% (0.52 g). Anal. Calcd for $C_{52}H_{70}N_4O_8Zn$ (944.53 g mol^{-1}): C, 66.13; H, 7.47; N, 5.93%; Found: C, 66.35; H, 8.05; N, 5.30%. HR-MS (EI): m/z 370.34 [Zn(L^1)$_2$ – Zn(L^1) –(Me)$_2$ + H]$^+$, 400.29 [Zn(L^1)$_2$– (Zn(L^1)) + H]$^+$. ^{1}H NMR (400 MHz, CD_3CN, 25 °C): δ: 8.65 (s, 2H, CH=N), 7.51–7.50 (d, *J* = 2.4, 2H, Ar*H*), 7.26–7.27 (d, *J* = 2.4, 2H, Ar*H*), 6.44 (s, 4H, Ar*H*), 3.62 (s, 6H, OC*H*$_3$), 3.46 (s, 12H, OC*H*$_3$), 1.38 (s, 18H, *t*Bu), 1.32 (s, 18H, *t*Bu). IR (KBr disc, Nujol mull, cm^{-1}): 2956(s), 2923(s), 2853(s), 2727(w), 2360(w), 2340(w), 1612(w), 1598(m), 1584(m), 1551(w), 1530(w), 1462(s), 1377(s), 1303(w), 1260(s), 1237(w), 1166(m), 1130(w), 1093(s), 1019(s), 864(w), 799(s), 722(m), 668(s), 661(w), 598(w), 464(w).

6.1.11 Synthesis of complex 6

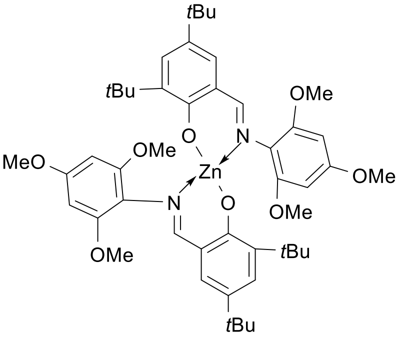

6

The synthesis of **6** was carried out according to the same procedure as **5** but using L^2H as a ligand to react with diethyl zinc. The mole ratio of $ZnEt_2$ and L^2H was 1:1. Yield 40% (0.43 g). Anal. Calcd for $C_{48}H_{64}N_2O_8Zn$ (862.43 g mol^{-1}): C, 66.85; H, 7.48; N, 3.25%. Found: C, 66.61; H, 7.52; N, 3.94%. HR-MS (EI): m/z 400.26 $[Zn(L^2)_2 - Zn(L^2) + H]^+$. ^{1}H NMR (400 MHz, CD_3CN, 25 °C): δ: 8.36 (s, 2H, CH=N), 7.39–7.38 (d, *J* = 2.8 Hz, 2H, Ar*H*), 6.96–6.95 (d, *J* = 2.8, 2H, Ar*H*), 6.00 (s, 4H, Ar*H*), 3.74 (s, 6H, OCH_3), 3.52 (s, 12H, OCH_3), 1.33 (s, 18H, *t*Bu), 1.28 (s, 18H, *t*Bu). IR (KBr disc, Nujol mull, cm^{-1}): 2954(s), 2922(s), 2853(s), 2723(w), 2448(w), 2287(w), 2261(w), 2157(w), 2104(w), 2078(w), 1954(w), 1814(w), 1745(w), 1698(w), 1614(s), 1547(w), 1526(m), 1495(m), 1462(s), 1422(w), 1404(w), 1377(m), 1270(w), 1255(m), 1227(m), 1203(m), 1155(m), 1128(m), 1059(m), 1036(w), 987(w), 950(m), 926(w), 916(w), 873(w), 862(w), 832(w), 806(m), 791(m), 746(m), 727(m), 694(w), 687(w), 635(m), 615(w), 571(w), 524(w), 513(m), 480(m), 463(w), 434(w).

6.1.12 Synthesis of complex 7

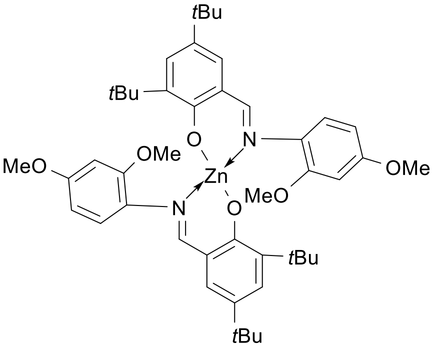

7

The synthesis of **7** was carried out according to the same procedure as **5** but using L^{3}H as a ligand to react with diethyl zinc. The mole ratio of ZnEt$_2$ and L^{3}H was 1:1. Yield 60% (0.60 g). Anal. Calcd for $C_{46}H_{60}N_2O_6Zn$ (802.37 g mol^{-1}): C, 68.86; H, 7.54; N, 3.49%. Found: C, 68.71; H, 7.88; N, 3.75%. HR-MS (EI): m/z 801.41 [Zn(L^3)$_2$ + H]$^+$. ^{1}H NMR (400 MHz, CD$_3$CN, 25 °C): δ: 8.50 (s, 2H, CH=N), 7.11–7.13 (d, *J* = 8.8 Hz, 2H, Ar*H*), 7.11–7.12 (d, *J* = 2.8 Hz, 2H, Ar*H*), 6.44–6.47 (dd, *J* = 8.7 Hz, *J* = 2.4 Hz, 2H, Ar*H*), 6.37–6.38 (d, *J* = 2.4 Hz, 2H, Ar*H*), 3.72 (s, 6H, OC*H*$_3$), 3.37 (s, 6H, OC*H*$_3$), 1.26 (s, 18H, *t*Bu), 1.14 (s, 18H, *t*Bu). IR (KBr disc, Nujol mull, cm^{-1}): 2954(s), 2923(s), 2853(s), 2726(w), 1616(m), 1590(m), 1543(w), 1528(w), 1503(w), 1462(s), 1377(s), 1312(w), 1287(w), 1258(w), 1208(w), 1162(m), 1138(w), 1032(w), 981(w), 926(w), 873(w), 863(w), 843(w), 832(w), 789(w), 722(m).

6.1.13 Synthesis of complex 8

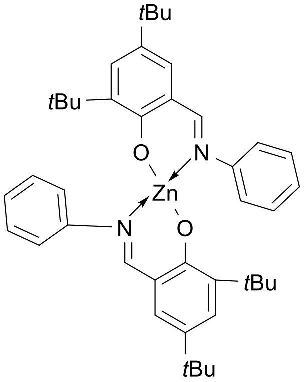

8

The synthesis of **8** was carried out according to the same procedure as **5** but using 2,4-di-*tert*-butyl-6-((phenylimino)methyl)phenol. The mole ratio of $ZnEt_2$ and 2,4-di-*tert*-butyl-6-((phenylimino)methyl)phenol was 1:1.Yield 75% (0.64 g). Anal. Calcd for $C_{42}H_{52}N_2O_2Zn$ (682.27 g mol^{-1}): C, 73.94; H, 7.68; N, 4.11%. Found: C, 73.60; H, 7.62; N, 3.82%. HR-MS (EI): m/z 310.23 $[Zn(L)_2 - Zn(L) + H]^+$. ^{1}H NMR (400 MHz, CD3CN, 25 °C): δ: 8.58 (s, 2H, C*H*=N), 7.49 (d, *J* = 6.4 Hz, 2H, Ar*H*), 7.29–7.15 (m, 12H, Ar*H*), 1.34 (s, 18H, *t*Bu), 1.28 (s, 18H, *t*Bu). IR (KBr disc, cm-1): 2957(s), 2727(w), 2671(w), 2360(w), 1937(W), 1740(w), 1612(w), 1582(m), 1545(w), 1527(m), 1486(w), 1459(s), 1427(w), 1377(s), 1325(w), 1271(w), 1254(m), 1192(w), 1165(m), 1133(w), 1078(w), 1025(w), 1000(w), 986(w), 975(w), 905(w), 871(w), 835(w), 806(w), 789(w), 762(m), 744(w), 728(m), 692(m), 635(w), 565(w), 535(w).

6.1.14 Ring-opening polymerisation of ε-CL

All polymerisations were carried out in Schlenk tubes under a nitrogen atmosphere unless stated otherwise. ε-CL was polymerised using complexes **1**–**8** in the presence of BnOH (0.1 M in toluene) as a co-initiator. Complexes were weighed out in the glove box and the initiator and monomer were added to the flask successively via syringe. The molar ratio of monomer/catalyst/BnOH ([CL]/[Cat]/[BnOH]) is presented in Table 2-3. The reaction mixture was then placed into an oil bath preheated to the required temperature. The reaction was quenched by the addition of an excess of glacial acetic acid (0.2 mL) at the required time, then the reaction solution was poured into cold methanol (20 mL). The reaction conversion was monitored by ^{1}H NMR (400 MHz, $CDCl_3$, 25 °C) spectroscopic studies. The resulting polymer was washed several times with methanol, collected on filter paper and then dried under vacuum to constant weight at 40 °C.

6.1.15 Copolymerisation of ε-CL and GL

Polymerisations were carried out in Schlenk tubes under a nitrogen atmosphere unless stated otherwise. ε-CL and GA were polymerised using complexes **1** (0.03 g) in the presence of BnOH (6.58 mL) (0.1 M in toluene) as a co-initiator. The reaction mixture was then placed into an oil bath preheated to the required temperature of 100 °C. The reaction was quenched by the addition of an excess of glacial acetic acid (0.2 mL), then the reaction solution was poured into cold methanol (20 mL). The precipitated polymers were recovered by filtration, washed with methanol and dried at 60 °C overnight in a vacuum oven.

6.1.16 Polymerisation kinetics method

Kinetic experiments were carried out following the previous polymerisation method. At regular time intervals, 0.05 mL aliquots were removed under the protection of N_2 flow, quenched with wet $CDCl_3$ (1 mL), and analysed by ^{1}H NMR spectroscopy.

6.1.17 Synthesis of 4,4’-bioxepane-7,7’-dione (BOD) cross linker

4,4’-Bioxepane-7,7’-dione (BOD) was synthesised according to the literature.[5] A solution of 20.0 g of urea hydrogen peroxide in 100 mL of formic acid (99%) was stirred at room temperature for 2 h. The flask was immersed in an ice bath to control the exotherm resulting from the former procedure. Then, 10 g of 4,4’-bicyclohexanone was slowly added over 5–10 min with stirring while the ice bath was changed periodically. After 4 h, 200 mL of water was added to the mixture followed by extraction with chloroform (4 times 100 mL), after which the organic fractions were collected, washed with a saturated aqueous of sodium bicarbonate solution and dried overnight with sodium sulfate. The combined organic fractions were concentrated and dried under reduced pressure to yield a white powder (3.07, 27%). ^{1}H NMR (400 MHz, $CDCl_3$, 25 °C): δ: 4.35–4.28 (m, 2H), 4.19–4.11 (m, 2H), 2.75–2.66 (m, 2H), 2.61–2.54 (dd, J = 14.1, 12.5 Hz, 2H), 1.90–1.80 (m, 4H), 1.67–1.66 (m, 4H), 1.54–1.42 (m, 2H).

6.1.18 X-ray Crystallography

In all cases, crystals suitable for an X-ray diffraction study were grown from a saturated MeCN solution at 0 °C. All (except **7**) single crystal X-ray diffraction data were collected at the UK National Crystallography service using Rigaku Oxford Diffraction ultra-high intensity instruments employing modern areas detectors. In all cases, standard procedures were employed for the integration and processing of data. Data for **7** was collected at Hull on a Stoe IPDS2 image plate diffractometer operating with Mo Kα radiation. Data were integrated and reduced using Stoe X-RED software. Crystal structures were solved using dual space methods implemented within SHELXT.[6] Completion of structures was achieved by performing least squares refinement against all unique F^2 values using SHELXL-2018.[7] Cambridge Crystallographic Data Centre (CCDC) numbers -69 and 2,099,692 contain supplementary crystallographic data.

6.2 Niobium and Tantalum complexes derived from the acids $Ph_2C(X)CO_2H$ ($X = OH, NH_2$): synthesis, structure and ROP capability

6.2.1 General

All manipulations were carried out under an atmosphere of dry nitrogen using Schlenk and cannula techniques or in a conventional nitrogen-filled glove box. ε-caprolactone was dried over molecular sieves (3 Å). Toluene was dried over sodium/benzophenone, and acetonitrile from calcium hydride. All solvents were distilled and degassed prior to use. All chemicals were purchased from Sigma Aldrich or TCI UK and used as received. IR spectra (Nujol mulls, KBr windows) were recorded on a Nicolet Avatar 360 FT IR spectrometer. Elemental analyses were performed by the elemental analysis service at the London Metropolitan University, or the Department of Chemistry at the University of Hull. MALDI-TOF mass spectra were acquired by averaging at least 100 laser shots. Molecular weights were calculated from the experimental traces using the OmniSEC software. NMR spectra were recorded at 400 MHz on a JEOL ECZ 400S spectrometer.

6.2.2 Synthesis of complex 9

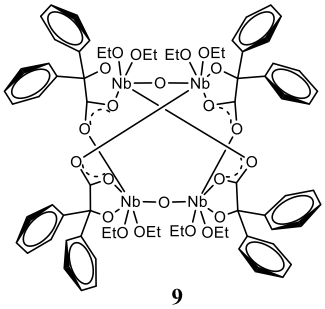

9

To L^4H_2 (1.00 g, 4.38 mmol) in toluene (30 mL) was added $[Nb(OEt)_5]$ (1.11 mL, 4.38 mmol) and the system was refluxed for 12 h. On cooling, volatiles were removed *in vacuo*, and the residue was extracted into MeCN (30 mL). Standing for 2 to 3 days at ambient temperature afforded colourless crystals of **9**. Yield: 0.55 g, 30%. Anal. calcd for $C_{72}H_{80}Nb_4O_{22}$ (1669.00 g mol^{-1}) requires: C 51.81, H 4.83% Found: C 51.75, H 5.09%. HR-MS (EI): m/z 1487.40

$[Nb_4(OEt)_8(L^4)_4(\mu\text{-}O)_2 - 4OEt - 4H]^+$. ^{1}H NMR (400 MHz, CD_3CN, 25 °C) δ: 7.56 (m, 12H, aryl*H*), 7.52 (bm, 6H, aryl*H*), 7.30 (m, 14H, aryl*H*), 7.22 (m, 8H, aryl*H*), 4.76 (m, 2H, OC*H*$_2$), 4.52 (bm, 2H, OC*H*$_2$), 4.39 (q, J = 7.2 Hz, 10H, OC*H*$_2$), 3.51 (bm, 2H, OC*H*$_2$), 1.32 (m, 3H, C*H*$_3$), 1.21 (m, 18H, C*H*$_3$), 1.08 (m, 3H, C*H*$_3$). ^{13}C NMR (400 MHz, CD_3CN, 25 °C) δ (ppm): 153.9, 127.8, 127.4, 126.5, 117.4 (CH_3CN), 94.7, 57.2, 24.7, 17.8. IR: 3442(w), 3179(w), 2957(s), 2923(s), 2853(s), 2726(m), 2341(s), 1958(w), 1806(w), 1771(w), 1749(w), 1733(w), 1694(w), 1683(w), 1634(m), 1588(m), 1558(w), 1540(w), 1520(w), 1505(w), 1488(w), 1458(s), 1377(s), 1312(w), 1260(s), 1210(m), 1096(s), 1057(s), 1019(s), 919(m), 856(w), 800(s), 760(w), 738(w), 730(w), 708(m), 699(w), 668(w), 657(w), 619(w), 608(m), 589(w), 551(m), 542(m), 486(w), 463(w).

6.2.3 Synthesis of complex 10

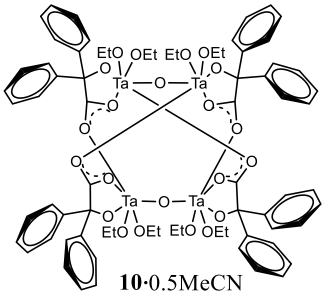

10·0.5MeCN

As for **9**, but using $[Ta(OEt)_5]$ (1.14 mL, 4.38 mmol) and L^5H_2 (1.00 g, 4.38 mmol) affording **10**·0.5MeCN as colourless prisms. Yield: 1.11 g, 50%. Anal. calcd for $C_{72}H_{80}Ta_4O_{22}$ (2021.20 g mol^{-1}) requires: C 42.79, H 3.99% Found: C 42.69, H 4.45%. HR-MS (EI): m/z 1099.27 $[Ta_4(L^4)_4(OEt)_8(\mu\text{-}O)_2 - Ta - 2(L^4) - 4(OEt) - 4(Et) + 8H]^+$. ^{1}H NMR (400 MHz, CD_3CN, 25 °C): δ: 7.56 (m, 12H, aryl*H*), 7.39 (m, 6H, aryl*H*), 7.30(m, 14H, aryl*H*), 7.24 (m, 8H, aryl*H*), 4.60 (m, 2H, OC*H*$_2$), 4.46 (q, J = 6.8 Hz, 10H, OC*H*$_2$), 4.15 (bm, 2H, OC*H*$_2$), 3.51 (q, J = 6.8 Hz, 2H, OC*H*$_2$), 1.32 (m, J = 6.8 Hz, 3H, C*H*$_3$), 1.20 (overlapping t, 18H, C*H*$_3$), 1.09 (t, J = 7.2 Hz, 3H, C*H*$_3$). IR: 3359(w), 3165(w), 2958(s), 2923(s), 2853(s), 2727(m), 2671(m), 1704(w), 1658(w), 1651(m), 1634(m), 1293(m), 1537(w), 1463(s), 1377(s), 1303(m), 1260(s), 1096(s), 1024(s), 919(m), 840(w), 801(s), 722(s), 700(w), 659(w), 638(w), 619(w), 606(m), 551(m), 486(w), 467(w), 448(w).

6.2.4 Synthesis of complex 11

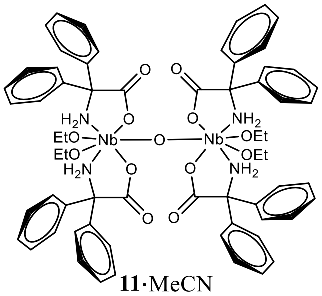

11·MeCN

As for **9**, but using [Nb(OEt)$_5$] (1.11 mL, 4.40 mmol) and L^5H_3 (1.00 g, 4.40 mmol) affording **11**•2MeCN as colourless prisms. Yield 0.60 g, 40%. $C_{64}H_{68}N_4Nb_2O_{13}$ (sample dried *in vacuo* for 2 h, –2MeCN) requires: C 59.72, H 5.33, N 4.35% Found: C 59.34, H 5.21, N 4.11%. HR-MS (EI): m/z 1366.14 [Nb$_2$(OEt)$_4$(L^{5}H$_2$)$_4$(μ-O)•2MeCN – 3H]$^+$. ^{1}H NMR (400 MHz, CD$_3$CN, 25 °C) δ: 7.25 (bm, 40H, aryl*H*), 3.51 (overlapping q, J = 7.2 Hz, 8H, OC*H*$_2$), 2.11 (bs, 8H, N*H*$_2$), 1.10–1.07 (5x s, 3H, 6H, 3H, 3H, 3H, OC*H*$_2$C*H*$_3$ + 2*Me*CN). IR: 3444(w), 2957(s), 2923(s), 2853(s), 2350(w), 2285(w), 1732(w), 1682(m), 1633(w), 1574(w), 1557(w), 1538(w), 1462(s), 1377(s), 1261(s), 1094(s), 1020(s), 917(w), 865(w), 800(s), 722(m), 700(m), 665(w), 633(w), 553(w), 464(w).

6.2.5 Synthesis of complex 12

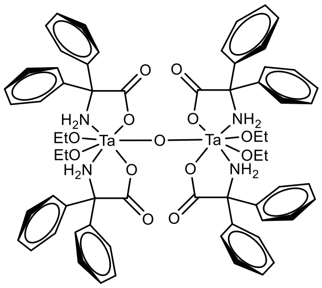

12·2.25MeCN

As for **9**, but using [Ta(OEt)$_5$] (1.14 mL, 4.40 mmol) and L^5H_3 (1.00 g, 4.40 mmol) affording **12**•2MeCN as colourless prisms. Yield 1.03 g, 60%. $C_{68.5}H_{74.75}N_{6.25}Ta_2O_{13}$ requires C 52.89, H 4.84, N 5.63%. Found: C 52.48, H 4.58, N 5.56%. HR-MS (EI): m/z 739.76 [Ta$_2$(OEt)$_4$(L^{5}H$_2$)$_4$(μ-O)–2OEt–2(L^{5}H$_2$)–Ta]$^+$. ^{1}H NMR (400 MHz, CD$_3$CN, 25 °C) δ: 7.74 (m, 2H, aryl*H*), 7.63 (m, 1H, aryl*H*), 7.50 (m, 3H, aryl*H*), 7.26 (bm, 35H, aryl*H*), 3.51 (q, J = 7.2 Hz, 8H, OC*H*$_2$), 2.38 (s, 8H, N*H*$_2$), 1.08 (t, J = 7.2Hz, 12H, C*H*$_3$). ^{13}C NMR (400 MHz, CD$_3$CN, 25 °C) δ (ppm): 176.3, 143.1, 128.5, 128.4, 127.8, 117.4 (CH$_3$CN), 69.7, 69.4, 68.2, 65.8, 65.6, 18.4, 18.0. IR: 3436(w), 3308(w), 2955(s), 2923(s), 2854(s), 2726(w), 2671(w), 1693(m), 1650(w), 1643(w), 1632(w), 1573(w), 1552(w), 1530(w), 1463(s), 1377(s), 1301(w), 1261(m), 1191(w), 1142(w), 1095(m), 1073(m), 1022(m), 918(w), 891(w), 873(w), 800(m), 767(w), 722(m), 697(w), 633(w), 563(w), 468(w).

6.2.6 Polymerisation kinetics method

Kinetic experiments were carried out using a J Young NMR tube at the required temperature. For example, under nitrogen, ε-CL (1.74 mmol, 0.19 mL), toluene-d$_8$ (0.5 mL) and BnOH in toluene (0.01 M, 0.69 mL) were added to the NMR tube containing 0.12 mL of a stock solution of the complex in toluene (0.033mL mg^{-1}). The sample was then analysed at 15 mins intervals.

6.2.7 ROP of ε-CL with catalysts 9-12

All polymerisations were carried out in Schlenk tubes under a nitrogen atmosphere unless stated otherwise. Complexes were weighed out in the glove box and 2 mL of ε-CL was added to the flask via a syringe. The molar ratio of monomer/catalyst/BnOH ([CL]/[Cat]/[BnOH]) is presented in Table 3-1. The reaction mixture was then placed into an oil bath preheated to the required temperature. The reaction was quenched by the addition of an excess of glacial acetic acid (0.2 mL) at the required time, then the reaction solution was then poured into cold methanol (20 mL). The resulting polymer was washed several times with methanol, collected on filter paper and then dried under vacuum to constant weight at 40 °C.

6.2.8 ROP of r-LA with catalysts 9-12

A dried Schlenk flask was charged with a mixture of *r*-LA (3.47 mmol) and the catalyst (1.39e^{-5} mmol) in a glove box. 1.4 ml of BnOH/toluene (0.01 M) solution was added to the flask via a syringe. The flask was then placed into an oil bath preheated to the required temperature. The stirring was continued till nearly complete conversion was observed by ^{1}H NMR spectroscopy. The reaction was quenched by the addition of an excess of glacial acetic acid (0.2 mL), then the reaction solution was then poured into cold methanol (20 mL). The resulting polymer was washed several times with methanol, collected on filter paper and then dried under vacuum to constant weight at 60 °C.

6.2.9 Copolymerisation of r-LA and ε-CL with catalyst 12

A typical example of copolymerisation by using catalyst **12** was as follows. The *r*-LA (3.46 mmol) and catalyst **12** (0.028 mmol) were added into a Schlenk flask in a glove box. Toluene (2 mL) was added via a syringe. The mixture was stirred at 160 ℃ in an oil bath. After 6 hours, ε-CL (3.46 mmol) was added via a syringe under nitrogen protection. The total copolymerisation reaction time was 48 h. The monomer feed sequences and reaction time were changed according to Table 3-3. The reaction was quenched by the addition of an excess of glacial acetic acid (0.2 mL), and then the reaction solution was poured into cold methanol (20 mL). The precipitated polymers were recovered by filtration, washed with methanol and dried at 60 °C overnight in a vacuum oven.

6.3 Ring-opening polymerisation of lactides and lactones by multi-metallic titanium complexes derived from the acids $Ph_2C(X)CO_2H$ (X = OH, NH_2)

All reactions were conducted under an atmosphere of dry nitrogen using standard Schlenk techniques or in a conventional nitrogen-filled glove box unless otherwise specified. The metal alkoxides $[Ti(OR)_4]$ (R = Me, *n*Pr, *i*Pr, *t*Bu) and the acids 2,2′-$Ph_2C(X)(CO_2H)$ (X = OH, NH_2) were purchased from Sigma-Aldrich. All the characterisation equipment and methods employed are the same as in 6.1.

6.3.1 Synthesis of complex 13

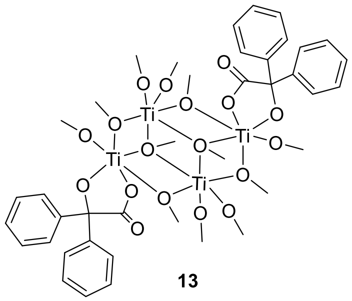

13

In a 25 mL Schlenk tube under nitrogen, 2,2′-$Ph_2C(OH)(CO_2H)$ (L^4H_2) (1.00 g, 4.38 mmol) was dissolved in dry toluene (20 ml), two equivalents of $[Ti(OMe)_4]$ (1.51 g, 8.76 mmol) was added into the reaction solution. The system was refluxed for 12 h, and following removal of volatiles *in vacuo*, the residue was extracted in warm MeCN (12 ml), affording on prolonged standing in the refrigerator (5 °C) small, white crystals. Yield 50% (1.11 g). Anal. Calcd for $C_{40}H_{56}O_{18}Ti_4$ (1016.44 g/mol): C, 47.27; H, 5.55%; Found: C, 47.07; H, 5.42%. HR-MS (EI): $^{m}/_{z}$ 528.64 $[Ti_2(L^4)(OMe)_6 - 3H + Na]^+$. ^1H NMR (400 MHz, Acetone-D_6) δ: 7.76 (m, 8H, Ar*H*), 7.30 (m, 4H, Ar*H*), 7.18 (m, 6H, Ar*H*), 7.09 (m, 2H, Ar*H*), 4.65 (s, 6H, O*Me*), 4.52 – 4.48 (overlapping s, 6H O*Me*), 4.18 (s, 6H, O*Me*), 3.73 (m, 3H, O*Me*), 3.68 (s, 3H, O*Me*), 3.52 (overlapping s, 6H, O*Me*), 3.27 (s, 6H, O*Me*). IR (Nujol mull, cm^{-1}): 2955(s), 2923(s), 2854(s), 2727(w), 2357(w), 1682(s), 1564(s), 1557(s), 1488(m), 1463(s), 1377(s), 1313(w), 1260(m), 1118(s), 1027(s), 916(w), 817(w), 801(w), 758(w), 722(m), 696(m), 666(w), 606(m), 505(m), 455(w).

6.3.2 Synthesis of complex **14**·MeCN

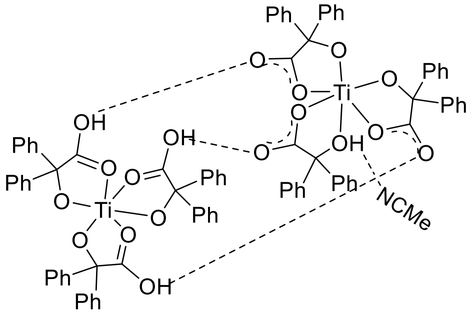

14 · MeCN

The synthesis of **14**·MeCN was carried out according to the same procedure as for **13**, but using L^4H_2 (2.00 g, 8.76 mmol) and $[Ti(OnPr)_4]$ (1.21 ml, 4.38 mmol). Yield 70% (2.24 g). Anal. Calcd for $C_{86}H_{67}NO_{18}Ti_2$ (1498.20 g/mol): C, 68.95; H, 4.51; N, 0.93%; Found: C, 68.66; H, 4.75; N, 0.97%. HR-MS (EI): $^{m}/_{z}$ 729.41$[Ti(L^4H)_3][Ti(L^4H)(L^4H)_2]^+$. ^1H NMR (400 MHz, CD_3CN, 25 °C) δ: 7.74 (m, 2H, Ar*H*), 7.61 (m, 1H, Ar*H*), 7,51 (m, 2H, Ar*H*), 7.40 – 7.20 (overlapping m, 25H, Ar*H*); O*H* not observed. IR (Nujol mull, cm^{-1}): 2957(s), 2923(s), 2953(s), 2359(w), 2340(w), 1596(w), 1457(m), 1376(m), 1260(m), 1090(s), 1020(s), 914(w), 866(w), 799(s), 720(w), 692(w), 668(w), 638(w), 608(w), 552(w), 467(w).

6.3.3 Synthesis of complex 15

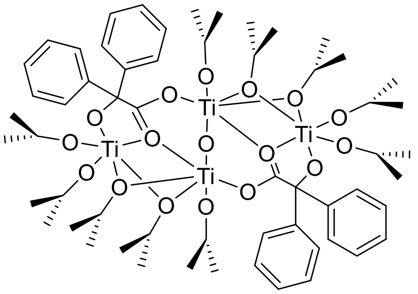

15

The synthesis of **15** was carried out according to the same procedure as for **13**, but using L^4H_2 (2.00 g, 8.76 mmol) and $[Ti(OiPr)_4]$ (3.99 ml, 13.48 mmol). Yield 30% (1.26 g). Anal. Calcd for $C_{58}H_{90}O_{17}Ti_4$ (1250.89 g/mol): C, 55.69; H, 7.25%; Found: C, 56.10; H, 7.22%. HR-MS (E/I): $^{m}/_{z}$ 1256.84 $[Ti_4O(L^4)_2(OiPr)_{10} + 6H]^+$. ^1H NMR (400 MHz, Acetone-D_6 25 °C) δ: 7.83-6.80 (bm, 20H, Ar*H*), 3.86 (sept, *J* = 6.0 Hz, 10H, C*H*Me$_2$), 1.07 (d, *J* = 6.0 Hz, 60H, CH*Me*$_2$). IR (Nujol mull, cm^{-1}): 2956(s), 2923(s), 2853(s), 1729(m), 1634(s), 1597(s), 1460(s), 1377(s), 1261(s), 1212(m), 1165(s), 1113(s), 1089(m), 1055(s), 1019(s), 1006(m), 941(m), 914(w), 854(m), 803(s), 777 (m). 757(m), 738(w), 722(s), 694(m), 661(w), 623(s), 612(s), 550(m), 527(w), 484(w), 467(w), 430(w).

6.3.4 Synthesis of complex **16**·MeCN

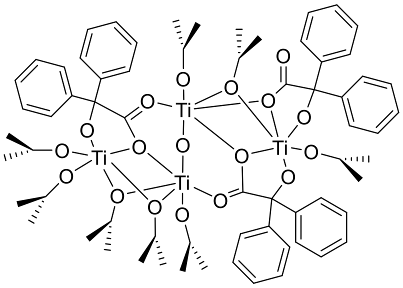

16·MeCN

The synthesis of **16**·MeCN was carried out according to the same procedure as for **13**, but using L^4H_2 (2.00 g, 8.76 mmol) and $[Ti(OiPr)_4]$ (2.66 ml, 8.98 mmol). Yield 45% (1.42 g). Anal. Calcd for $C_{66}H_{86}O_{18}Ti_4$ (1358.94 g/mol): C, 58.34; H, 6.38%; Found: C, 57.89; H, 6.16%. HR-MS (EI): $^m/_z$ 1272.71 $[Ti_2O(L^4)_3(OiPr)_7–2(iPr)]^+$, 1256.80 $[Ti_2O(L^4)_3(OiPr)_7 – (OiPr) – (iPr)]^+$. ^1H NMR (400 MHz, Acetone-D_6, 25 °C) δ: 7.83-6.67 (bm, 30H, Ar*H*), 3.86 (sept, *J* = 6.4 Hz, 8H, C*H*Me_2), 1.07 (d, *J* = 6.4 Hz, 48H, CHMe_2). IR (KBr disc, cm^{-1}): 2955(s), 2923(s), 2853(s), 1961(w), 1887(w), 1821(w), 1728(m), 1633(m), 1957(m), 1491(m), 1462(s), 1377(s), 1261(m), 1211(m), 1165(m), 1110(s), 1088(m), 1045(s), 1025(s), 1006(m), 941(w), 913(w), 854(m), 803(s), 757(m), 738(w), 722(m), 694(m), 661(w), 622(w), 607(m), 538(m), 526(m), 485(w), 429(w).

6.3.5 Synthesis of complex **17**·MeCN

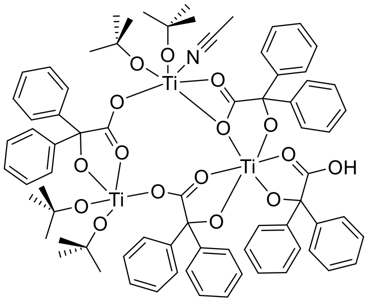

17·MeCN

The synthesis of **17**·CH_3CN was carried out according to the same procedure as for **13**, but using L^4H_2 (2.00 g, 8.76 mmol) and [Ti(O*t*Bu)$_4$] (3.38 ml, 8.75 mmol). Yield 10% (0.42 g). Anal. Calcd for $C_{74}H_{79}NO_{16}Ti_3$ (1382.04 g/mol): C, 64.31; H, 5.76; N, 1.01%; Found: C, 63.94; H, 5.77; N, 0.94 %. HR-MS (EI): $^{m}/_{z}$ 1468.42 $[Ti_3(L^4)_4(OtBu)_4(CH_3CN)\cdot CH_3CN + 2Na]^+$. ^{1}H-NMR (400 MHz, Acetone-D_6) δ: 7.77-7.10 (bm, 40H, Ar*H*), 2.28 (s, 3H, *Me*CN), 1.15 (s, 36H, *t*Bu). IR (Nujol mull, cm^{-1}): 2958(s), 2853(s), 2727(w), 2671(w), 1704(w), 1660(w), 1644(w), 1568(w), 1463(s), 1377(s), 1310(m), 1261(s), 1236(s), 1170(s), 1088(s), 1026(s), 941(w), 915(w), 795(s), 722(s), 694(m), 666(w), 638(w), 621(w), 607(m), 587(w), 545(m), 490(m), 456(w).

6.3.6 Synthesis of complex **18**·2.5CH$_3$CN

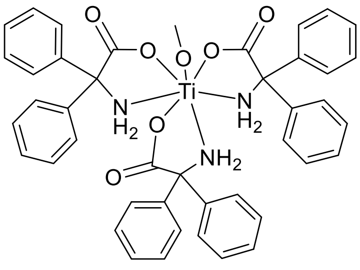

18·2.5MeCN

As for **13**, but using L^5H_3 (1.00 g, 4.40 mmol) and [Ti(OMe)$_4$] (0.38 g, 2.21 mmol), affording **18**·2.5CH_3CN as colourless prisms formed. Yield 24% (0.46 g). Anal. Calcd for $C_{43}H_{39}N_3O_7Ti$ (860.30 g/mol): C, 68.17; H, 5.19; N, 5.55%; Found: C, 67.98; H, 4.99; N, 5.46%. HR-MS (EI): $^{m}/_{z}$ 1031.87 $[2\times Ti(L^5H_2)_6(OMe)_2 - OMe - 2(L^5H_2)]$. ^{1}H NMR (400 MHz, Acetone-D_6) δ: 7.77-7.15 (bm, 30H, Ar*H*), 3.27 (s, 3H, O*Me*), 2.95 (bs, 6H, N*H*$_2$). IR (KBr disc, cm^{-1}): 3336(w), 3246(w), 3056(m), 2958(s), 2923(s), 2854(s), 2360(w), 2342(w), 2250(w), 1682(s), 1651(w), 1589(m), 1494(m), 1463(s), 1448(s), 1377(s), 1261(s), 1191(w), 1101(s), 1019(s), 800(s), 764(m), 698(s), 677(w), 614(w), 583(w), 502(w), 455(w).

6.3.7 Synthesis of complex **19**·CH_3CN

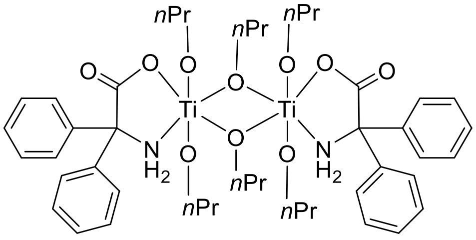

19·MeCN

As for **13**, but using L^5H_3 (2.00 g, 8.80 mmol) and $[Ti(OnPr)_4]$ (2.61 ml, 8.80 mmol), affording **19**·CH_3CN as colourless prisms. Yield 80% (3.17 g). Anal. Calcd for $C_{46}H_{66}N_2O_{10}Ti_2$ (902.77 g/mol): C, 61.20; H, 7.37; N, 3.10%; Found: C, 60.93; H, 7.02; N, 2.98%. HR-MS (EI): $^m/_z$ 811.76 $[Ti_2(L^5H_2)_2(OnPr)_6 - 2nPr - 3H^+]$. ^1H NMR (400 MHz, CD_3CN, 25 °C) δ: 7.40 (overlapping m, 5H, Ar*H*), 7.33 (overlapping m, 13H, Ar*H*), 7.23 (overlapping m, 2H, Ar*H*), 4.45-3.99 (overlapping bm, 12H, NH_2 + 5x $OCH_2CH_2CH_3$), 3.43 (m, *J* =6.4 Hz, 2H, $OCH_2CH_2CH_3$), 2.31 (bs, 2H, NH_2), 1.46 (overlapping m, 12H, $OCH_2CH_2CH_3$), 0.89-0.62 (overlapping m, 18H, $OCH_2CH_2CH_3$). ^{13}C NMR (400 MHz, CD_3CN, 25 °C) δ (ppm): 188.7, 142.9, 129.8, 128.5, 127.8, 127.3, 117.4 (CH_3CN), 96.3, 64.7, 40.6, 29.2, 12.8. IR (KBr disc, cm^{-1}): 3336(w), 3246(w), 3056(m), 2958(s), 2923(s), 2854(s), 2360(w), 2342(w), 2250(w), 1682(s), 1651(w), 1589(m), 1494(m), 1463(s), 1448(s), 1377(s), 1261(s), 1191(w), 1101(s), 1019(s), 800(s), 764(m), 698(s), 677(w), 614(w), 583(w), 502(w), 455(w).

6.3.8 Synthesis of complex 20

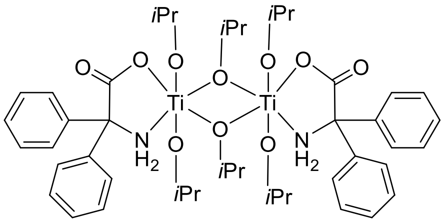

20

As for **13**, but using L^5H_3 (2.00 g, 8.76 mmol) and [Ti(O*i*Pr)$_4$] (2.61 ml, 8.80 mmol), affording **20** as colourless prisms. Yield 30% (0.40 g). Anal. Calcd for $C_{46}H_{66}N_2O_{10}Ti_2$ (902.88 g/mol): C, 61.20; H, 7.37; N, 3.10%; Found: C, 60.12; H, 6.92; N, 3.38%%. HR-MS (EI): $^m/_z$ 1080.09 = 2[$Ti_2(L^5H_2)_2(OiPr)_6$] – 3(L^5H_2) – *i*Pr – 3H$^+$]. ^{1}H-NMR (400 MHz, Acetone-D_6) δ: 7.31 (overlapping m, 8H, Ar*H*), 7.26 (overlapping m, 12H, Ar*H*), 5.01 (sept, *J* = 6.4 Hz, 2H, C*H*(CH_3)$_2$), 3.86 (sept, *J* = 6.4 Hz, 4H, C*H*(CH_3)$_2$), 3.27 (bs, 2H, NH_2), 2.86 (bs, 2H, N*H*$_2$), 1.16 (d, *J* = 6.4 Hz, 12H, CH(C*H*$_3$)$_2$), 1.08 (d, *J* = 6.4 Hz, 24H, CH(C*H*$_3$)$_2$). IR (KBr disc, cm^{-1}): 3366(m), 3296(m), 2955(s), 2923(s), 2853(s), 2724(w), 2613(w), 2355(w), 1986(w), 1960(w), 1900(w), 1682(s), 1651(m), 1633(m), 1574(m), 1495(m), 1463(s), 1378(s), 1365(m), 1322(m), 1261(s), 1192(w), 1160(m), 1105 (s), 1073(m), 1014(s), 980(m), 948(w), 932(m), 916(w), 851(m), 801(s), 775(w), 758(w), 732(w), 700(m), 674(w), 624(m), 606(m), 553(m), 524(w), 499(m), 472(m), 458(m), 426(w).

6.3.9 Synthesis of complex 21

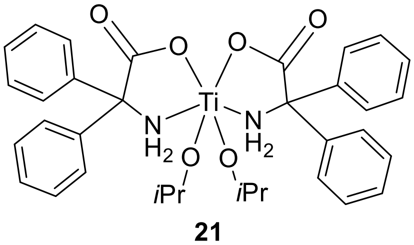

21

As for **13**, but using L^5H_3 (2.00 g, 8.76 mmol) and [Ti(O*i*Pr)$_4$] (1.31 ml, 4.4 mmol), affording **21** as colourless prisms. Yield 30% (0.82 g). Anal. Calcd for 3×[$C_{34}H_{38}N_2O_6Ti$] (1855.69 g/mol): C, 66.02; H, 6.19; N, 4.53%; Found: C, 65.88; H, 6.07; N, 4.42%. HR-MS (EI): $^m/_z$ 770.16 = 2× [$Ti(L^5H_2)_2(OiPr)_2$] – $2L^5H_2$–CH_3]. ^{1}H-NMR (400 MHz, $CDCl_3$) δ: 7.31-6.87 (2x bm, 20H, Ar*H*), 4.65 (sept, *J* = 6.4 Hz, 2H, C*H*Me$_2$), 3.70 (bs, 4H, N*H*$_2$), 1.19 (d, *J* = 6.4 Hz, 12H, CH*Me*$_2$). IR (Nujol mull, cm^{-1}): 3356(w), 3316(w), 3280(w), 3202(w), 3134(w), 2955(s), 2923(s), 2853(s), 1667(s), 1573(m), 1494(w), 1463(s), 1377(s), 1344(w), 1307(m), 1261(m), 1192(w), 1165(w), 1117(m), 1066(w), 1050(w), 1017(m), 967(w), 922(w), 911(w), 892(w), 857(m), 819(s), 802(s), 763(w), 747(m), 723(m), 696(m), 676(w), 631(w), 617(w), 561(w), 540(w), 517(w), 492(w), 458(m), 405(m).

6.3.10 Synthesis of complex 22·2CH$_3$CN

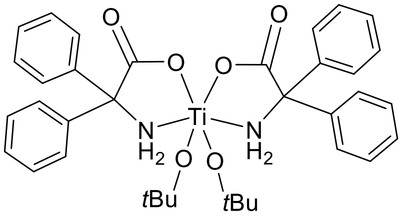

22·2MeCN

As for **13**, but using L^{5}H$_3$ (2.00 g, 8.76 mmol) and [Ti(O*t*Bu)$_4$] (3.00 ml, 8.80 mmol), affording **22**·2MeCN as colourless prisms. Yield 60% (3.85 g). Anal. Calcd for $C_{36}H_{42}N_2O_6Ti\cdot2[CH_3CN]$ (728.72 g/mol): C, 65.93; H, 6.64; N, 7.69%; Found: C, 65.40; H, 6.74; N, 6.98 %. HR-MS (EI): $^m/_z$ 589.781 [Ti(L^{5}H$_2$)$_2$(O*t*Bu)$_2$ – *t*Bu]. ^{1}H-NMR (400 MHz, Acetone-D$_6$) δ: 7.54 (bm, 2H, Ar*H*), 7.47 (bm, 2H, Ar*H*), 7.36 (bm, 4H, Ar*H*), 7.29 (overlapping m, 8H, Ar*H*), 7.18 (bm, 4H, Ar*H*), 4.43 (bs, 2H, N*H*$_2$), 1.16 (s, 18H, C(C*H*$_3$)$_3$), 1.03 (bs, 2H, N*H*$_2$). IR (Nujol mull, cm^{-1}): 3347(m), 3244(m), 3057(w), 2955(s), 2922(s), 2853(s), 2727(w), 2671(w), 1684(s), 1651(s), 1572(s), 1494(m), 1463(s), 1377(s), 1362(m), 1327(m), 1296(s), 1261(m), 1234(m), 1182(s), 1124(s), 1078(m), 1032(w), 1015(s), 990(s), 861(w), 821(m), 793(m), 767(m), 758(m), 737(w), 723(w), 699(s), 677(m), 624(m), 609(m), 579(m), 544(w), 522(w), 489(m), 466(m), 447(w), 421(w).

6.3.11 Ring-opening polymerisation of ε-CL or *r*-LA

All polymerisations were carried out in Schlenk tubes under a nitrogen atmosphere unless stated otherwise. ε-CL or *r*-LA were polymerised using the respective Ti complexes and toluene as solvent (2 ml). The reaction mixture was then placed into a preheated oil bath to the required temperature (shown in Table 4-2 or 4-4). The reaction was quenched by the addition of an excess of glacial acetic acid (0.2 mL), then the reaction solution was then poured into cold methanol (20 mL). The precipitated polymers were recovered by filtration, washed with methanol and dried at 60 °C overnight in a vacuum oven.

6.3.12 Polymerisation kinetics method

Kinetic experiments were carried out using a J Young NMR tube at the required temperature. All complexes were prepared as stock solutions (dry toluene) in a Schlenk flask because of the small amount of catalysts needed for each kinetics test in the NMR tube. The stock solution concentration for complexes **13-22** were 75 ml/g, 40 ml/g, 44 ml/g, 50 ml/g, 100 ml/g, 25 ml/g, 30 ml/g, 48 ml/g, 30 ml/g, and 40 ml/g, respectively. Then under nitrogen, the complex from the stock solution (0.12 - 0.4ml), ε-CL (1.74 mmol, 0.19 mL) and toluene-d_8 (0.75 ml) were added via syringe to J Young NMR tube. For the kinetics of PLA, *r*-LA (0.4 g) was weighted in the dry box first then the stock solution was added together with toluene-d_8 via syringe. The sample was then analysed by ^{1}H NMR spectroscopy at 15 minutes intervals.

6.3.13 X-ray Crystallography

Full sets of X-ray diffraction intensity data were collected using modern X-ray diffractometers at the National Crystallography Service in Southampton, UK. Routine processing of raw intensity data and multi-scan absorption corrections were applied. The structures were solved using dual-space methods within SHELXT and full-matrix least squares refinement was carried out using SHELXL-2018[7] via program Olex2[8]. All non-hydrogen positions were located in the direct and difference Fourier maps and refined using anisotropic displacement parameters. Disorder was modelled conservatively using standard techniques.

References

1. C. L. Lee, Y. F. Lin, M. T. Jiang, W. Y. Lu, J. K. Vandavasi, L. F. Wang, Y. C. Lai, M. Y. Chiang and H.-Y. Chen, *Organometallics*, 2017, **36**, 1936-1945.
2. B. Chakraborty and S. Banerjee, *J.. Coord. Chem.*, 2013, **66**, 3619-3628.
3. A. Oliveira, L. Ferreira, M. Dias, R. Bitzer and M. Nascimento, *Química Nova*, 2019, **42**, 505-512.
4. W. Yang, K. Q. Zhao, B. Q. Wang, C. Redshaw, M. R. J. Elsegood, J. L. Zhao and T. Yamato, *Dalton Trans*, 2016, **45**, 226-236.
5. J. T. Wiltshire and G. G. Qiao, *Macromolecules*, 2006, **39**, 4282-4285.
6. G. Sheldrick, *Acta Crystallogr., Sect. A*, 2015, **71**, 3-8.
7. G. Sheldrick, *Acta Crystallogr., Sect. C*, 2015, **71**, 3-8.
8. O. V. Dolomanov, L. J. Bourhis, R. J. Gildea, J. A. K. Howard and H. Puschmann, *J. Appl. Crystallogr.*, 2009, **42**, 339-341.

Appendix

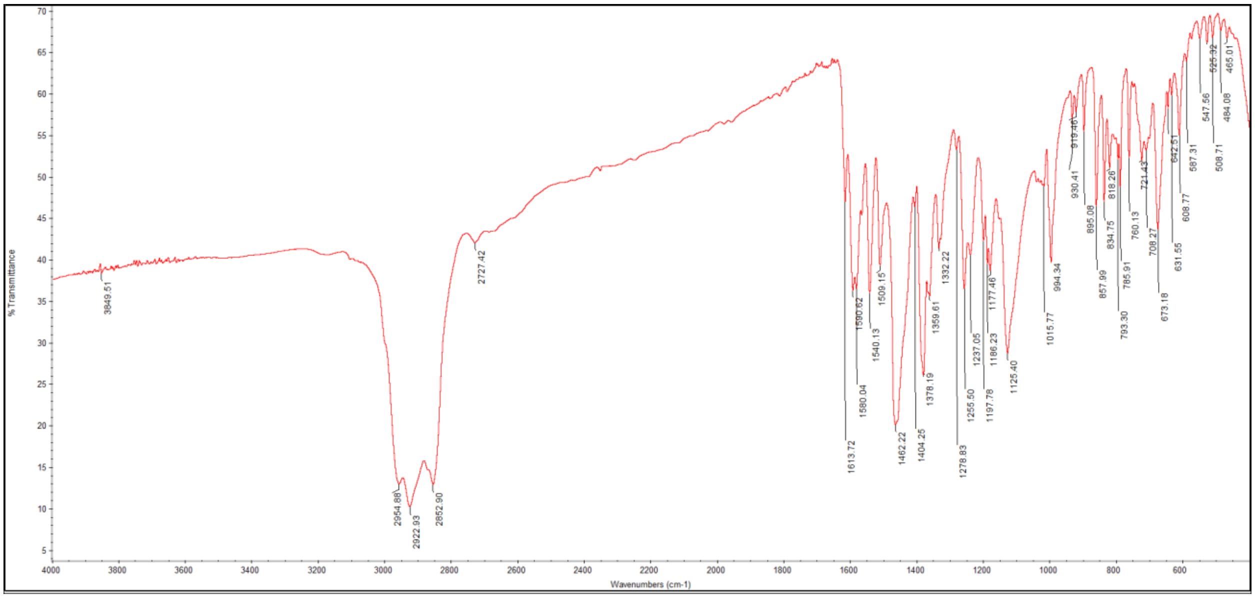

Figure S1. FTIR spectrum of complex **1**.

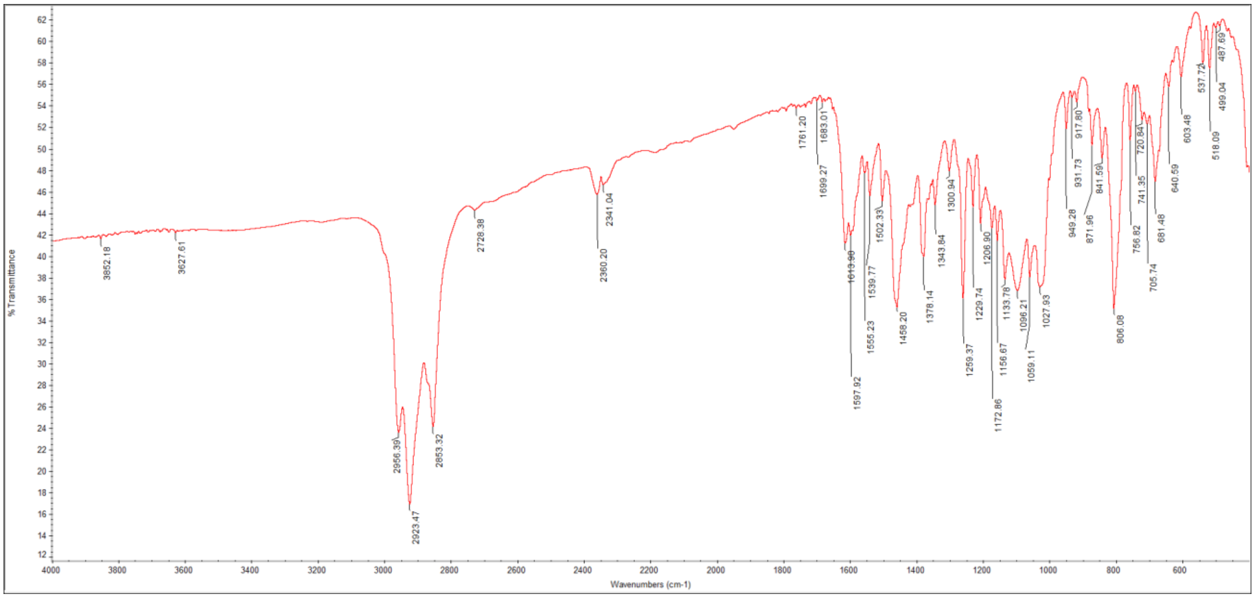

Figure S2. FTIR spectrum of complex **2**.

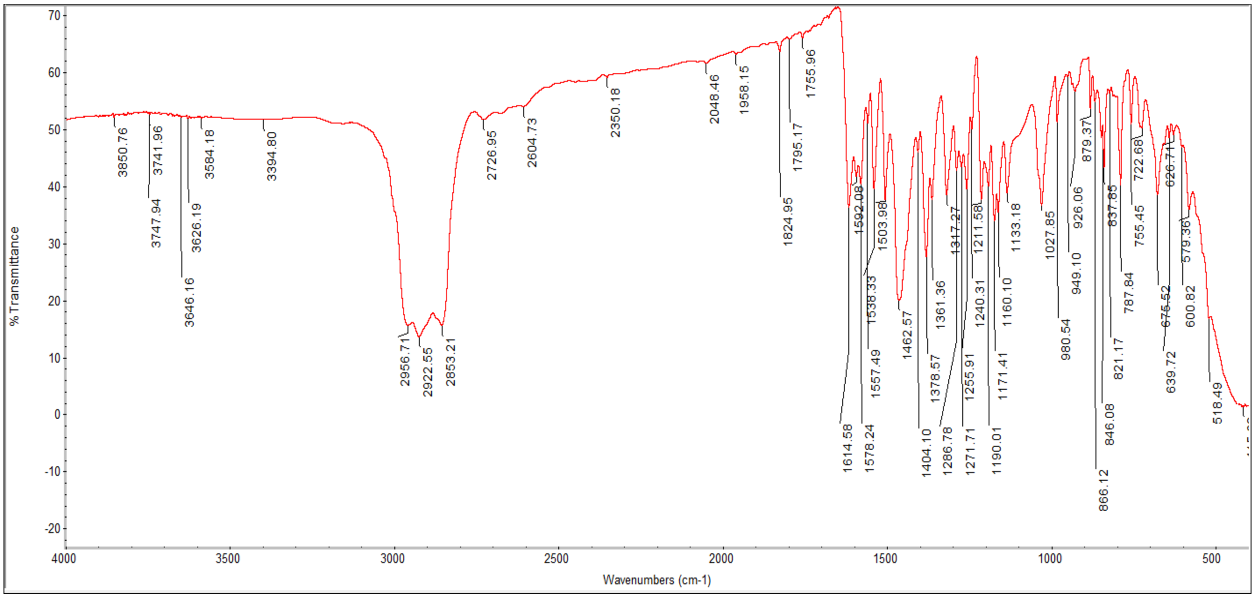

Figure S3. FTIR spectrum of complex **3**.

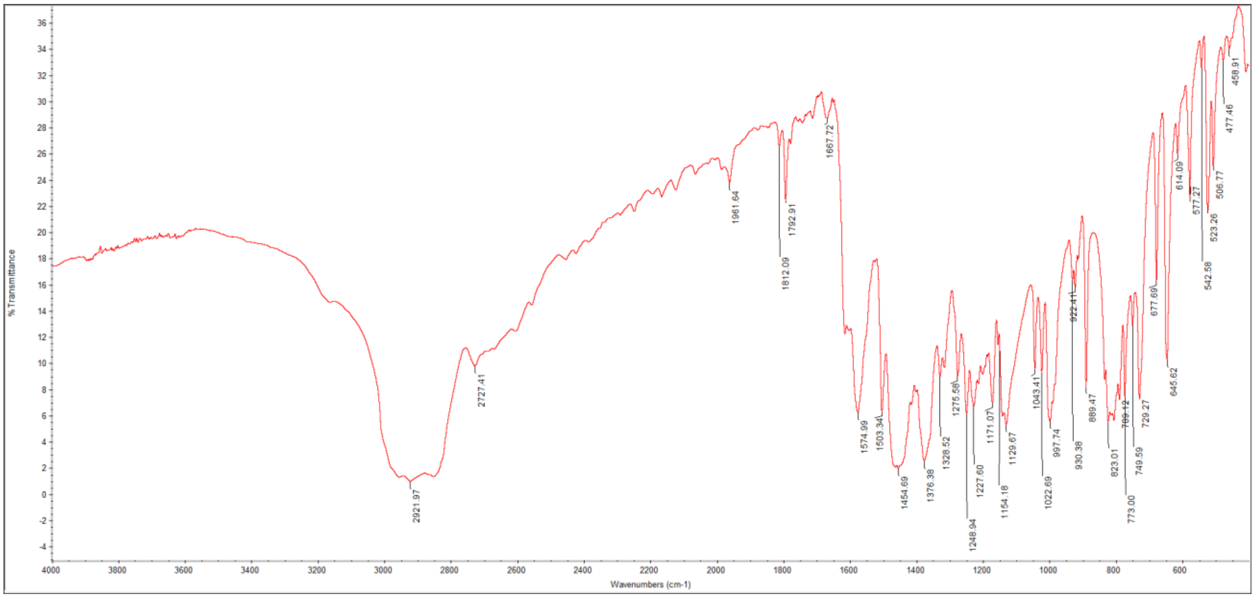

Figure S4. FTIR spectrum of L^{1}H.

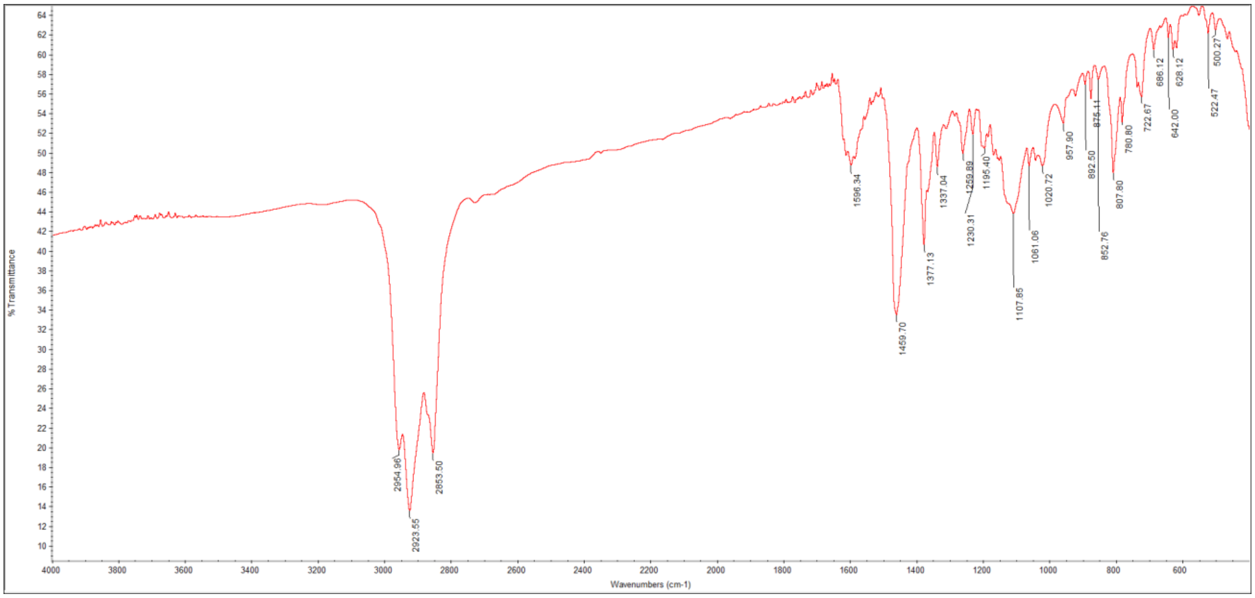

Figure S5. FTIR spectrum of L^2H.

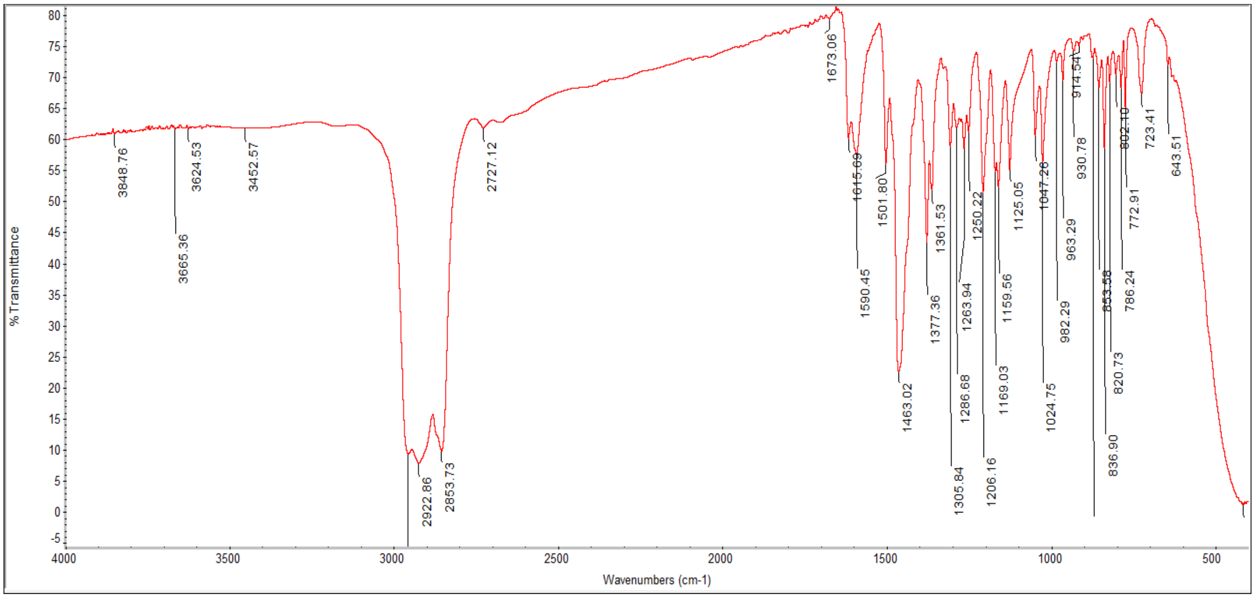

Figure S6. FTIR spectrum of L^3H.

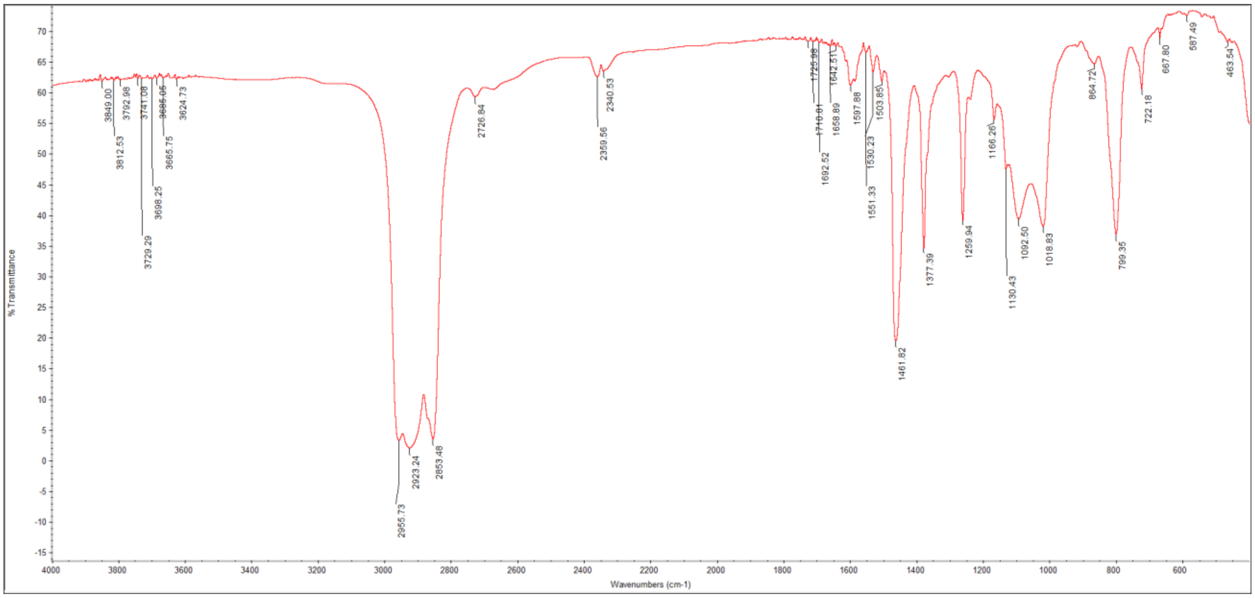

Figure S7. FTIR spectrum of complex **5**.

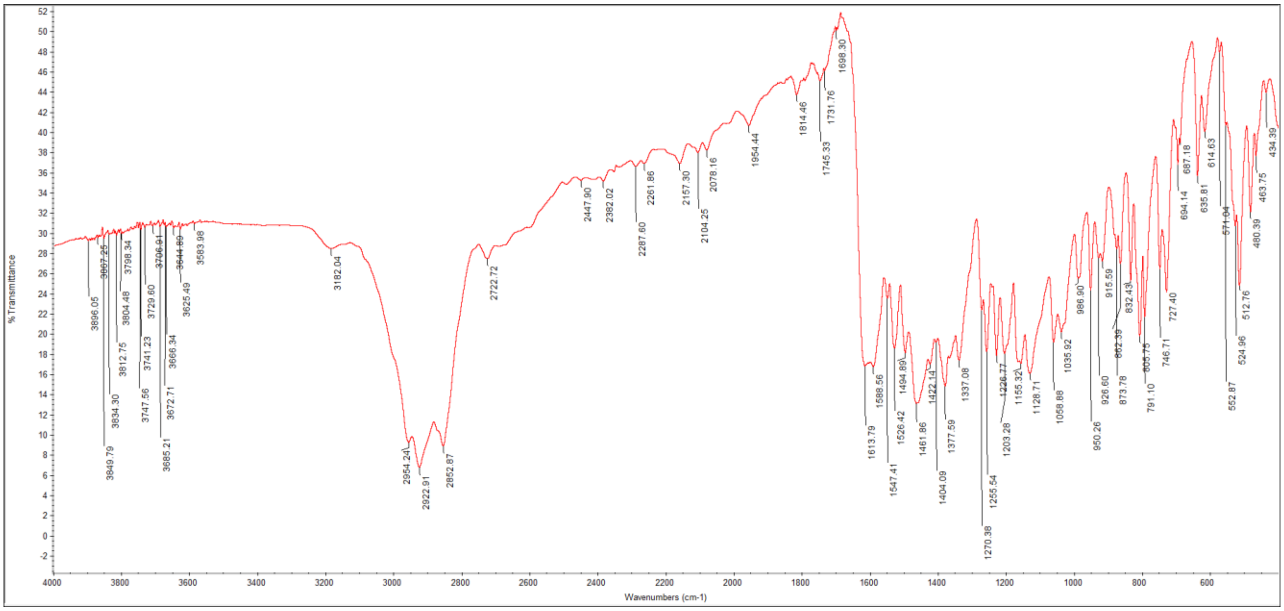

Figure S8. FTIR spectrum of complex **6**.

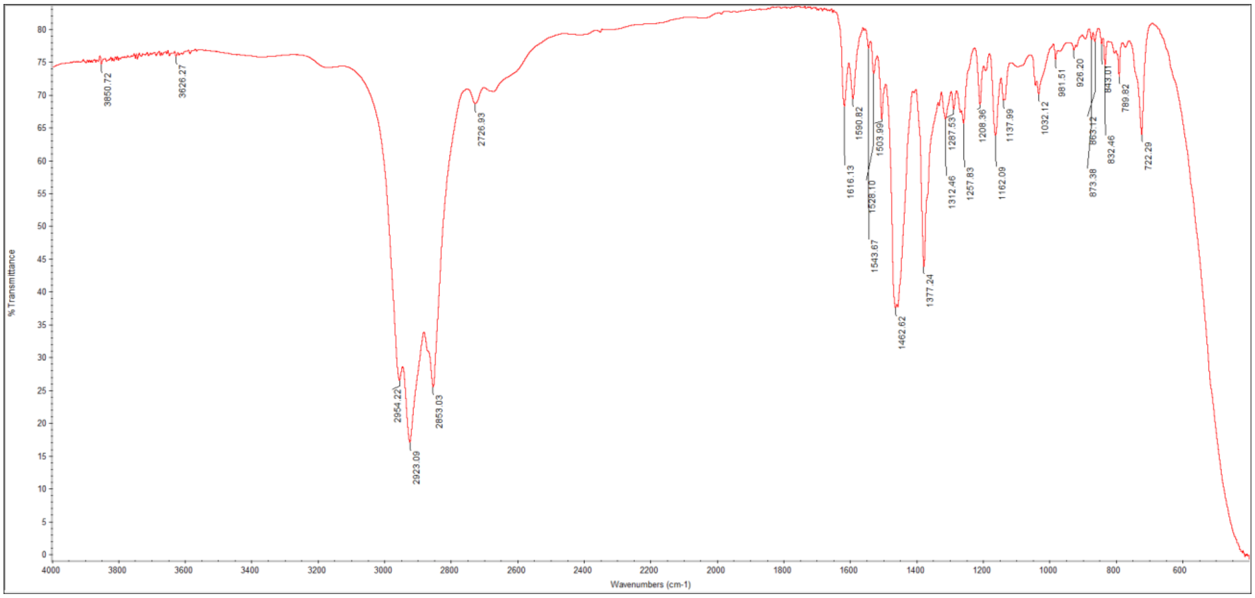

Figure S9. FTIR spectrum of complex **7**.

Table S1. Crystallographic data and refinement details for compounds **1-3, 5-7**

Compound	**1**	**2**	**3**	**5**	**6**	**7**
Empirical formula	$C_{26}H_{38}NO_4Al$	$C_{26}H_{38}NO_4Al$	$C_{25}H_{36}NO_3Al$	$C_{52}H_{70}N_4O_8Zn$	$C_{48}H_{64}N_2O_8Zn$	$C_{46}H_{60}N_2O_6Zn$
Formula weight	455.55	455.55	425.53	944.49	862.40	802.33
Crystal system	Tetragonal	Triclinic	Monoclinic	Orthorhombic	Monoclinic	Monoclinic
Temp (K)	100(2)	100(2)	100(2)	100(2)	100(2)	150(2)
Wavelength/Å	1.54178	0.71075	1.54178	0.71075	1.54178	0.71073
Space group	$P4_2/n$	$P-1$	$P2_1/c$	$Pbca$	$I2/a$	$P2_1$/n
a /Å	28.9022(5)	8.77450(10)	10.49237(5)	16.8034(4)	13.0291(4)	13.3203(9)
b /Å	28.9022(5)	11.85330(10)	20.94049(12)	20.9651(5)	27.0249(8)	10.1701(4)
c /Å	6.0320(2)	12.71810(10)	11.23374(5)	28.4430(7)	27.2058(8)	32.869(2)
α /°	90	101.2730(10)	90	90	90	90
β /°	90	94.7670(10)	94.2834(4)	90	90.472(3)	92.384(5)
γ /°	90	93.6800(10)	90	90	90	90
V /Å^3	5038.8(2)	1288.38(2)	2461.33(2)	10020.0(4)	9579.1(5)	4448.9(4)
Z	8	2	4	8	8	4
D_{calc}/g cm^{-3}	1.201	1.174	1.148	1.252	1.196	1.198
F (000)	1968	492	920	4032	3680	1712
μ /mm^{-1}	0.948	0.109	0.906	0.546	1.121	0.599
θ range	2.162−64.995	2.337−24.998	3.896−75.379	2.071−25.000	2.3040−68.480	1.240−26.215
Crystal size/mm	0.300 × 0.200 × 0.200	0.340 × 0.300 × 0.200	0.150×0.1200 × 0.110	0.080 × 0.050 × 0.030	0.320 × 0.040 × 0.040	0.400 × 0.320 × 0.240
Reflns collected	66,305	9350	8,5197	50,096	8821	20,791
Reflns unique	4278	9350	4659	8814	8821	8877
R_{int}	0.1663	0.0234	0.0468	0.0650	0.1309	0.0551
R_1;wR_2 [$I > 2\sigma(I)$]	0.0691; 0.1785	0.0420; 0.1202	0.0327;0.0319	0.0434; 0.0925	0.0441; 0.1179	0.0386;0.0644
R_1; wR_2 (all data)	0.0828; 0.1879	0.0445; 0.1226	0.0856;0.0850	0.0620; 0.1003	0.0510;0.1212	0.0868; 0.0709
Parameters	300	301	281	606	551	490
GOF (F^2)	1.050	1.030	1.036	1.061	1.058	0.765
Largest diff. peak and hole/ e.Å^{-3}	0.348 and -0.367	0.579 and -0.339	0.268 and -0.267	0.298 and -0.412	1.063 and -0.566	0.396 and -0.358

Table S2. Crystallographic data and refinement details for compounds **9-14**

Compound	**9**	**10**	**11**	**12**	**13**	**14**
Empirical formula	$C_{72}H_{80}Nb_4O_{22}$	$C_{73}H_{81.5}N_{0.5}O_{22}Ta_4$	$C_{68}H_{74}N_6Nb_2O_{13}$	$C_{68.5}H_{74.75}N_{6.25}O_{13}Ta_2$	$C_{40}H_{56}O_{18}Ti_4$	$C_{86}H_{67}NO_{18}Ti_2$
Formula weight	1669	2041.68 (includes MeCN)	1369.15 (includes 2MeCN)	1555.49	1016.44	1498.20
Crystal system	Monoclinic	Monoclinic	Monoclinic	Monoclinic	Monoclinic	Monoclinic
Temp (K)	100(2)	100.00(10)	100.00(2)	100.00(10)	293(2)	100.00(10)
Wavelength/Å	0.71075	0.71075	0.71075	0.71075	0.71075	1.54178
Space group	$C2/c$	$C2/c$	$C2/c$	$C2/c$	$P2_1/c$	$P2_1/c$
a /Å	22.2498(4)	22.2617(4)	54.0723(4)	54.1856(8)	15.0818(2)	13.56971(15)
b /Å	14.4513(2)	14.3187(2)	10.74623(10)	10.7080(2)	10.3772(2)	22.7268(2)
c /Å	25.8064(5)	25.8451(8)	22.47203(18)	22.4972(4)	29.5766(3)	24.3573(3)
α /°	90	90	90.0	90.0	90	90.0
β /°	114.086(2)	114.593(2)	92.8757(7)	92.7533(14)	94.4760(10)	99.4529(12)
γ /°	90	90	90.0	90	90	90.0
V /Å^3	7575.3(3)	7491.0(3)	13041.45(19)	13038.2(4)	4614.82(12)	7409.69(14)
Z	4	4	8	8	4	4
D_{calc}/g cm^{-3}	1.463	1.810	1.395	1.585	1.463	1.343
F (000)	3408	3964.0	5680.0	6236.0	2112	3112.0
μ /mm^{-1}	0.661	5.896	0.413	3.416	0.738	2.441
θ range	3.458 − 57.396	3.466 − 57.4	3.86 − 57.4	3.626 − 58.702	2.009 − 25.000	5.352 − 134.8
Crystal size/mm	0.16 × 0.08 × 0.04	0.32 × 0.16 × 0.09	0.2 × 0.14 × 0.08	0.25 × 0.06 × 0.05	0.200 x 0.100 x 0.040	0.1 × 0.09 × 0.08
Reflns collected	60080	104958	202219	84692	48068	108438
Reflns unique	9774	9677	16857	17841	8130	13303
R_{int}	0.0344	0.0431	0.0502	0.0681	0.0386	0.0621
R_1;wR_2 [$I > 2\sigma(I)$]	0.0317; 0.0831	0.0194; 0.0464	0.0340; 0.0858	0.0561; 0.1420	0.0385; 0.1035	0.0577; 0.1607
R_1; wR_2 (all data)	0.0374; 0.0856	0.0226; 0.0475	0.0387; 0.0881	0.0694; 0.1510	0.0461; 0.1083	0.0663; 0.1729
Parameters	471	480	934	940	571	1042
GOF (F^2)	1.060	1.030	1.034	1.039	1.080	1.110
Largest diff. peak and hole/ e.Å^{-3}	1.42 and -0.57	1.27 and -1.13	1.28 and -0.49	5.35 and -3.28	0.650 and -0.277	0.80 and -0.55

Table S3. Crystallographic data and refinement details for compounds **15-20**

Compound	**15**	**16**	**17**	**18**	**19**	**20**
Empirical formula	$C_{58}H_{90}O_{17}Ti_4$	$C_{66}H_{86}O_{18}Ti_4$	$C_{76}H_{82}N_2O_{16}Ti_3$	$C_{48}H_{46.5}N_{5.5}O_7Ti$	$C_{48}H_{69}N_3O_{10}Ti_2$	$C_{46}H_{66}N_2O_{10}Ti_2$
Formula weight	1250.89	1358.94	1423.14	860.30	943.86	902.80
Crystal system	Monoclinic	Triclinic	Triclinic	Monoclinic	Triclinic	Monoclinic
Temp (K)	100.01(10)	100	293(2)	100	100.0(6)	100.0(2)
Wavelength/Å	1.54178	0.71075	0.71075	0.71075	0.71075	0.71075
Space group	$P2_1/n$	$P\text{-}1$	$P\text{-}1$	$I2/a$	$P\text{-}1$	$P2_1/n$
a /Å	12.6108(4)	12.8781(2)	13.33000(10)	21.9587(7)	13.0035(2)	10.3162(2)
b /Å	23.6288(15)	13.2342(2)	13.9101(2)	11.9009(4)	13.3151(3)	9.5070(2)
c /Å	21.6816(10)	21.9004(4)	20.0787(2)	33.0123(11)	15.4551(2)	23.1620(4)
α /°	90.0	74.6984(15)	85.2790(10)	90	99.7910(10)	90
β /°	97.745(4)	84.0184(15)	85.0040(10)	100.491(4)	95.9380(10)	96.2240(10)
γ /°	90.0	89.8909(14)	77.9540(10)	90	111.156(2)	90
V /Å^3	6401.7(5)	3579.33(11)	3619.35(7)	8482.8(5)	2419.36(8)	2258.25(8)
Z	4	2	2	8	2	2
D_{calc}/g cm^{-3}	1.298	1.261	1.306	1.347	1.296	1.328
F (000)	2648.0	1428.0	1492	3608.0	1004.0	960.0
μ /mm^{-1}	4.626	0.494	0.390	0.262	0.388	0.412
θ range	5.56 − 88.978	4.472 − 51.364	2.29 − 25.00	3.908 - 51.356	4.554 - 63.722	5.558 - 63.454
Crystal size/mm	0.11 × 0.1 × 0.02	0.15 × 0.08 × 0.05	0.22 x 0.16 x 0.11	0.35 × 0.05 × 0.02	0.2 × 0.1 × 0.05	0.22 × 0.13 × 0.12
Reflns collected	29511	80493	68109	39805	95900	30148
Reflns unique	5042	13590	12745	8053	15274	6471
R_{int}	0.1119	0.0505	0.0347	0.1211	0.0395	0.0456
R_1;wR_2 [$I > 2\sigma(I)$]	0.1045; 0.2866	0.0848; 0.2232	0.0284; 0.0793	0.0675; 0.1692	0.0501; 0.1185	0.0369; 0.0886
R_1; wR_2 (all data)	0.1324; 0.3173	0.0958; 0.2338	0.0303; 0.0817	0.0947; 0.1872	0.0658; 0.1280	0.0416; 0.0917
Parameters	705	761	888	538	577	309
GOF (F^2)	1.209	1.024	0.732	1.026	1.044	1.031
Largest diff. peak and hole/ e.Å^{-3}	0.79 and -0.36	1.88 and -1.46	0.315 and -0.350	0.45 and -0.58	1.09 and -0.63	0.50 and -0.49

Table S4. Crystallographic data and refinement details for compounds **21-22**

Compound	**21**	**22**
Empirical formula	$C_{102}H_{114}N_6O_{18}Ti_3$	$C_{40}H_{48}N_4O_6Ti$
Formula weight	1855.69	728.72
Crystal system	Monoclinic	Orthorhombic
Temp (K)	293(2)	293(2)
Wavelength/Å	0.71075	0.71073
Space group	$P2_1/n$	*Pbcn*
a /Å	18.3904(3)	26.4812(14)
b /Å	15.5778(2)	12.2434(4)
c /Å	33.2787(6)	23.8635(12)
α /°	90	90
β /°	100.423(2)	90
γ /°	90	90
V /Å^3	9376.4(3)	7737.0(6)
Z	4	8
D_{calc}/g cm^{-3}	1.315	1.251
F (000)	3912	3088
μ /mm^{-1}	0.321	0.271
θ range	1.805 - 25.000	2.022 - 24.998
Crystal size/mm	0.180 × 0.120 × 0.100	0.260 × 0.040 × 0.020
Reflns collected	88643	24612
Reflns unique	16515	6815
R_{int}	0.0495	0.0709
R_1;wR_2 [$I > 2\sigma(I)$]	0.0490; 0.1370	0.0567; 0.1021
R_1; wR_2 (all data)	0.0681; 0.1511	0.0567; 0.1021
Parameters	1174	468
GOF (F^2)	1.047	1.080
Largest diff. peak and hole/ e.Å^{-3}	0.765 and -0.737	0.377 and -0.420